DESIGN OF SEISMIC ISOLATED STRUCTURES

Design of Seismic Isolated Structures: From Theory to Practice. F. Naeim and J. M. Kelly

DESIGN OF SEISMIC ISOLATED STRUCTURES

From Theory to Practice

Farzad Naeim, Ph.D., S.E.
Director of Research and Development
John A. Martin and Associates, Inc.
Los Angeles, California

James M. Kelly, Ph.D.
Professor in the Graduate School
University of California at Berkeley
Berkeley, California

JOHN WILEY & SONS, INC.
New York / Chichester / Weinheim / Brisbane / Singapore / Toronto

This book is printed on acid-free paper. ♾

Published simultaneously in Canada.

Library of Congress Cataloging-in-Publication Data

Naeim, Farzad.
Design of seismic isolated structures : from theory to practice / Farzad Naeim, James M. Kelly.
p. cm.
Includes bibliographical references and index.
ISBN 0-471-14921-7 (alk. paper)
1. Earthquake resistant design. I. Kelly, James M. II. Title.
TA658.44.N34 1999
624.1′762—dc21 98-51588

Printed in the United States of America.
10 9 8 7 6 5

To the memory of precious lives
lost to earthquakes worldwide

CONTENTS

PREFACE xiii

CHAPTER 1. DEVELOPMENT OF SEISMIC ISOLATION WORLDWIDE 1

1.1 Introduction / 1
1.2 Base Isolation in the United States / 6
1.3 Base Isolation in Japan / 18
1.4 Base Isolation in Europe / 20
1.5 Base Isolation in New Zealand / 21
1.6 State of Isolation Technology Today / 23

CHAPTER 2. THEORETICAL BASIS OF SEISMIC ISOLATION 25

2.1 Linear Theory / 25
2.2 Extension of Theory to Buildings / 31
2.2.1 M-Degree-of-Freedom Equations of Motion / 31
2.2.2 Modal Analysis of M-DOF System / 33
2.3 Analysis of Coupled Dynamic Equations / 36

CHAPTER 3. ISOLATION SYSTEM COMPONENTS 47

3.1 Introduction / 47
3.2 Elastomeric-Based Systems / 47

3.2.1 Low-Damping Natural and Synthetic Rubber Bearings / 48
3.2.2 Lead-Plug Bearings / 49
3.2.3 High-Damping Natural Rubber Systems (HDNR) / 50

3.3 Isolation Systems Based on Sliding / 52
3.3.1 Electricité-de-France System / 55
3.3.2 EERC Combined System / 55
3.3.3 The TASS System / 56
3.3.4 Resilient-Friction Base Isolation System / 56
3.3.5 Friction Pendulum System / 57

3.4 Spring-Type Systems / 58
3.5 Sleeved-Pile Isolation System / 58
3.6 Rocking Systems / 61

CHAPTER 4. CODE PROVISIONS FOR SEISMIC ISOLATION 63

4.1 Introduction / 63
4.2 Seismic Hazard Level / 64
4.3 Design Methods / 65
4.4 Static Analysis / 65
4.4.1 Seismic Zone Factor Z / 67
4.4.2 Site Soil Profile Type / 68
4.4.3 Seismic Source Types: A, B, and C / 68
4.4.4 Near-Source Factors: N_A and N_V / 68
4.4.5 MCE Response Coefficient M_M / 70
4.4.6 Spectral Seismic Coefficients: C_{VD}, C_{VM} and C_{AD}, C_{AM} / 70
4.4.7 Damping Coefficients: B_D and B_M / 71
4.4.8 Effective System Vibration Periods: T_D and T_M / 73
4.4.9 Total Design Displacements: D_{TD} and D_{TM} / 74
4.4.10 Design Forces / 75
4.4.11 Vertical Distribution of Force / 76
4.4.12 Drift Limits / 77

4.5 Dynamic Analysis / 78
4.5.1 Time History Analysis / 78
4.5.2 Scaling / 78

4.6 Other Requirements for Nonstructural Components / 80
4.7 Peer Review / 80

4.8 Design and Testing Requirements for Isolators / 81
4.9 OSHPD-96 Requirements / 82
4.10 Other Considerations / 84
4.11 Step-by-Step Procedure for UBC-97 Compliant Design / 85
4.11.1 Preliminary Design Steps / 85
4.11.2 Final Design Steps / 87
4.11.3 Design Example / 89

CHAPTER 5. MECHANICAL CHARACTERISTICS AND MODELING OF ISOLATORS 93

5.1 Introduction / 93
5.2 Mechanical Characteristics of Elastomeric Bearings / 93
5.3 Mechanical Characteristics of Lead-Plug Bearings / 100
5.4 Mechanical Characteristics of Friction Pendulum System / 101
5.5 Modeling of Isolation Bearings by Bilinear Modeling / 104
5.6 Implications of Bilinear Modeling / 107
5.6.1 Energy Dissipation in High-Damping Natural Rubber Bearings / 111
5.6.2 Adjustments to the Model to Account for High-Strain Stiffening / 115
5.6.3 Comparisons with Experimental Data / 117

CHAPTER 6. BUCKLING AND STABILITY OF ELASTOMERIC ISOLATORS 121

6.1 Introduction / 121
6.2 Stability under Large Lateral Displacement / 126
6.3 Rollout Stability / 133

CHAPTER 7. DESIGN EARTHQUAKE GROUND MOTIONS 137

7.1 Introduction / 137
7.2 Characteristics of Earthquake Ground Motions / 139
7.3 From Response Spectra to Design Spectra / 143
7.4 Earthquake Energy Content and Energy Spectra / 149
7.5 Various Ground Motion Predictive Formulations / 150
7.5.1 Source Characterizations / 150
7.5.2 Attenuation Relations / 155
7.6 Deterministic and Probabilistic Approaches / 158
7.6.1 Deterministic Seismic Hazard Evaluation / 158

7.6.2 Probabilistic Seismic Hazard Evaluation / 159
7.6.3 Limitations of Deterministic and Probabilistic Seismic Hazard Analysis / 166
7.6.4 Seismic Hazard Maps / 170
7.7 Code Interpretations of Design Ground Motions / 172
7.8 Application of Earthquake Time Histories / 174
7.8.1 UBC-94 Provisions / 174
7.8.2 UBC-97 Provisions / 175
7.8.3 OSHPD-91 Provisions / 176
7.8.4 OSHPD-96 Provisions / 176
7.8.5 Time-Domain Scaling of Time Histories / 176
7.8.6 Frequency-Domain Scaling of Time Histories / 180
7.8.7 Analytic Dilemma of Designing by Time History Analysis / 183

CHAPTER 8. DESIGN EXAMPLES **185**

8.1 Design Example for a High-Damping Rubber Bearing / 185
8.1.1 Bearing Stiffnesses / 186
8.1.2 First Estimate of Design Displacement D_D / 187
8.1.3 Actual Bearing Stiffness / 188
8.1.4 Composite Stiffness / 188
8.1.5 Composite Damping / 188
8.1.6 Allowance for Torsion / 189
8.1.7 Elastic Base Shear from Code / 190
8.1.8 Bearing Detail / 191
8.1.9 Buckling Loads: Safety Factor / 193
8.1.10 Calculation of MCE Displacement D_M / 195
8.1.11 Rollout Displacement / 196
8.2 Design Example for a Lead-Plug Bearing / 196

CHAPTER 9. COMPUTER APPLICATIONS **203**

9.1 Introduction / 203
9.2 Preliminary Selection of Design Loads and Isolator Sizes / 203
9.2.1 Overview / 203
9.2.2 Selection of Design Loads by Linear Regression and Least-Squares Analysis Techniques / 204

9.2.3 The ISOSEL Solution Strategy / 206
9.2.4 Application of the ISOSEL Computer Program / 207

9.3 Computer Programs for Analysis of Seismically Isolated Structures / 216
9.3.1 N-PAD / 217
9.3.2 3D-BASIS / 217
9.3.3 ETABS / 218
9.3.4 SAP-2000 Nonlinear / 218
9.3.5 General Nonlinear Three-Dimensional Analysis Programs / 220

9.4 Nonlinear Dynamic Time History Analysis / 220

CHAPTER 10. SPECIFICATIONS FOR DESIGN, MANUFACTURING, AND TESTING OF ISOLATION DEVICES **233**

10.1 Introduction / 233
10.2 Sample Specifications / 234

APPENDIX. COMPANION SOFTWARE AND EARTHQUAKE DATA FILES **255**

REFERENCES **273**

INDEX **282**

PREFACE

Seismic isolation is a simple structural design approach to mitigate or reduce earthquake damage potential. Seismic isolated structures are currently difficult to analyze, design, and implement, however, due to complex code requirements. This book serves as a guide to help the reader navigate and understand the concepts and procedures involved in analysis, design, and development of specifications for seismic isolated structures. The book is intended as a reference for practicing engineers and architects as well as a text for graduate-level courses on seismic isolation.

It provides a complete and up-to-date coverage of the subject and numerical examples and systematic development of the concepts in theory and practical application. The book is partially developed from lecture notes generated over the period of two decades of teaching graduate classes at the University of California at Berkeley. The material is complemented by practical insights obtained from many years of involvement in analysis, design, and review of major seismic isolated projects in the United States.

In response to the damage generated by recent earthquakes in densely populated areas, seismic design codes for the design of buildings, bridges, and industrial facilities changed with the intention of leading to better seismic performance. This process has been repeated in response to all recent damaging earthquakes, such as the 1989 Loma Prieta, 1994 Northridge, and 1995 Kobe events. In addition, damaging earthquakes in Mexico, Australia, Armenia, Iran, and India have all caused changes in the seismic design codes and procedures. Consequently, all structural engineers designing earthquake-resistant structures have had to contend with increasingly complex code requirements.

Seismic isolation is an approach to earthquake-resistant design that is based

on the concept of reducing the seismic demand rather than increasing the earthquake resistance capacity of the structure. Proper application of this technology leads to better performing structures that will remain essentially elastic during large earthquakes. Surprisingly, the basics of this approach are rather simple.

Unfortunately, however, the seismic design code provisions for design of seismic isolated structures are complicated and difficult for the engineer to apply. This textbook is intended to clarify for the practicing engineer, as well as engineering student, the basic concepts of seismic isolation and the fundamental principles of seismic isolation design. It provides a framework for the design professional to satisfy the code requirements while retaining the favorable, cost-effective, damage control aspects of this new technology. It is the authors' contention that, once the intimidating barriers of code application are bypassed, the use of seismic isolation will become a routine procedure for many types of structures.

The theoretical underpinning of seismic isolation has been firmly established and the technology has been verified by extensive experimental work over the past quarter century. The relevant material is covered in many technical reports, archived publications, and journal articles. But no general collection of this research in a form accessible to the practicing engineer has been available until this time. This textbook will bring much of this information to the engineering profession and will compliment it with knowledge gained by the authors from years of experience as designers, consultants, and reviewers of many seismic isolated projects.

The authors would like to express their gratitude to the following individuals and institutions: Ashraf Habibullah and Computers and Structures, Inc., for kindly permitting the educational version of the SAP2000 computer program to be used as a companion to this book; Syed Hasanain and Iqbal Suharwardy for their valuable assistance in this regard; Claire Johnson for her expert typing of the manuscript; Roy Lobo for coding the optimization algorithm for the companion ISOSEL computer program; Ian Aiken and Fredrick Tajirian of Seismic Isolation Engineering, Inc., for providing the sample specification included in Chapter 10 of the book; and last but not least, Mark Day, Andrew Besirof, Evita Oseguera, and Nicki Hyde for their valuable assistance with the artwork and logistics during the course of preparation of the manuscript.

FARZAD NAEIM
Los Angeles, California

JAMES M. KELLY
Berkeley, California

CHAPTER 1

DEVELOPMENT OF SEISMIC ISOLATION WORLDWIDE

1.1 INTRODUCTION

In August 1909 J. A. Calantarients, a medical doctor from the northern English city of Scarborough, wrote a letter to the Director of the Seismological Service of Chile in Santiago calling his attention to a method of building construction that he had developed whereby "substantial buildings can be put up in earthquake countries on this principle with perfect safety since the degree of severity of an earthquake loses its significance through the existence of the lubricated free joint." Calantarients had submitted a patent application to the British patent office for his construction method, which proposed that the building be built on his "free joint" and a layer of fine sand, mica, or talc that would allow the building to slide in an earthquake, thereby reducing the force transmitted to the building itself.

What the doctor was prescribing was an early example of an earthquake-resistant design strategy known as *base isolation* or *seismic isolation*. Many mechanisms have been invented over the last century to try to achieve the goal of uncoupling the building from the damaging action of an earthquake, for example, rollers, balls, cables, rocking columns, as well as sand. Buildings have been built on balls, including a building in Sevastopol, Ukraine, and a five-story school in Mexico City. At least one building, a four-story dormitory for the State Seismological Observatory in Beijing, has been built on a sand layer between the building and the foundation specifically designed to slip in the event of an earthquake.

Dr. Calantarients mentions in his letter that, "I made the experiment with balls many years before it was done in Japan, or at any event before any amount

Design of Seismic Isolated Structures: From Theory to Practice. F. Naeim and J. M. Kelly

of it appeared in the papers about 25 years ago." The reference is almost certainly to the Englishman John Milne, who was a Professor of Mining Engineering in Tokyo in the years 1876 through 1895. During this period Milne became very interested in earthquake phenomena, and he devised and improved a number of seismoscopes and seismographs. Milne carried out pioneering research on seismology, so much so that he is often referred to as the "Father of Modern Seismology." He also gave much thought to the design of buildings in seismically active areas and published rules for earthquake-resistant construction that are still valid today.

While at the University of Tokyo, he built an example of an isolated building. The structure was built on balls in "cast-iron plates with saucer-like edges on the heads of piles. Above the balls and attached to the buildings are cast-iron plates slightly concave but otherwise similar to those below." The building was instrumented and apparently experienced earthquake movement. In 1885 he described this experiment in a report to the British Association for the Advancement of Science. Apparently he was not completely satisfied with the performance of his building under wind load, so he changed the isolation system, and in 1886 he described the new version in a follow-up report to the association. The first balls had been 10 inches in diameter; 8-inch balls were tried, then 1-inch balls. Finally the house was rested at each of its piers on a handful of cast-iron shot, each 1/4 inch in diameter. By this means the building became stable against wind loads. The final design was evidently successful under actual earthquake action.

The concept of seismic isolation has become a practical reality within the last 20 years with the development of multilayer elastomeric bearings, which are made by vulcanization bonding of sheets of rubber to thin steel reinforcing plates. These bearings are very stiff in the vertical direction and can carry the vertical load of the building but are very flexible horizontally, thereby enabling the building to move laterally under strong ground motion. Their development was an extension of the use of elastomeric bridge bearings and bearings for the vibration isolation of buildings. In recent years other systems have been developed that are modifications of the sliding approach. The concept of base isolation is now widely accepted in earthquake-prone regions of the world for protecting important structures from strong ground motion, and there are now many examples in the United States and Japan. A smaller number of base-isolated buildings have been built in New Zealand and in Italy, mainly for large and important buildings. Demonstration projects that apply low-cost base isolation systems for public housing in developing countries have been completed in Chile, the People's Republic of China, Indonesia, and Armenia.

It is not surprising that most applications are for important buildings that house sensitive internal equipment. The basic dilemma facing a structural engineer charged with providing superior seismic resistance of a building is how to minimize interstory drift and floor accelerations. Large interstory drifts cause damage to nonstructural components and to equipment that interconnects stories. Interstory drifts can be minimized by stiffening the structure, but this

leads to amplification of the ground motion, which leads to high floor accelerations, which can damage sensitive internal equipment. Floor accelerations can be reduced by making the system more flexible, but this leads to large interstory drifts. The only practical way of reducing simultaneously interstory drift and floor accelerations is to use base isolation; the isolation system provides the necessary flexibility, with the displacements concentrated at the isolation level.

The concept of base isolation is quite simple. The system decouples the building or structure from the horizontal components of the ground motion by interposing structural elements with low horizontal stiffness between the structure and the foundation. This gives the structure a fundamental frequency that is much lower than both its fixed-base frequency and the predominant frequencies of the ground motion. The first dynamic mode of the isolated structure involves deformation only in the isolation system, the structure above being to all intents and purposes rigid. The higher modes that produce deformation in the structure are orthogonal to the first mode and, consequently, to the ground motion. These higher modes do not participate in the motion, so that the high energy in the ground motion at these higher frequencies cannot be transmitted into the structure. The isolation system does not absorb the earthquake energy, but rather deflects it through the dynamics of the system; this effect does not depend on damping, but a certain level of damping is beneficial to suppress possible resonance at the isolation frequency.

The first use of a rubber isolation system to protect a structure from earthquakes was in 1969 for an elementary school in Skopje, Yugoslavia. The Pestalozzi School, a three-story concrete structure designed and built by Swiss engineers (Fig. 1.1), is isolated by a system known as the Swiss Full Base Isolation-3D (FBI-3D) System [116]. Unlike more recently developed rubber bearings, the rubber blocks used here (Fig. 1.2) are completely unreinforced so that the weight of the building causes them to bulge sideways. Glass blocks (Fig. 1.3) acting as seismic fuzes are intended to break when the seismic loading exceeds a certain threshold. Because the vertical and horizontal stiffness of the system is about the same, the building will bounce and rock backward and forward in an earthquake. These bearings were designed when the technology for reinforcing rubber blocks with steel plates—as in bridge bearings—was not highly developed or widely known, and it is unlikely that this approach will be used again.

Most recent examples of isolated buildings use multilayered laminated rubber bearings with steel reinforcing layers as the load-carrying component of the system. Because of the reinforcing steel plates, these bearings are very stiff in the vertical direction but are very soft in the horizontal direction, thereby producing the isolation effect. Easy to manufacture, these bearings have no moving parts, are unaffected by time, and are very resistant to environmental degradation.

Many isolation systems, particularly those used in New Zealand and Japan, combine low-damping natural rubber bearings with some form of mechanical

Fig. 1.1 Pestalozzi School, Skopje, Macedonia.

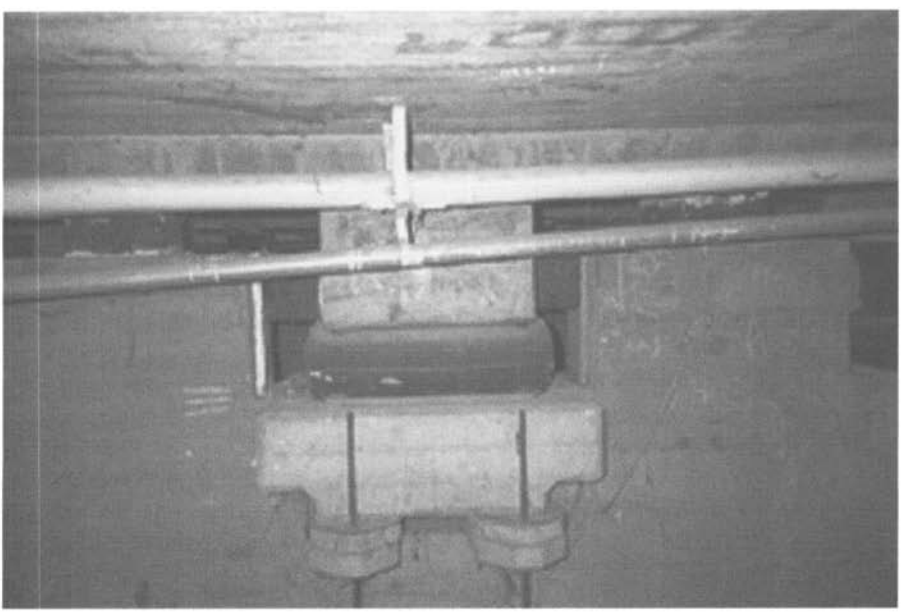

Fig. 1.2 Bearings used in the Pestalozzi School.

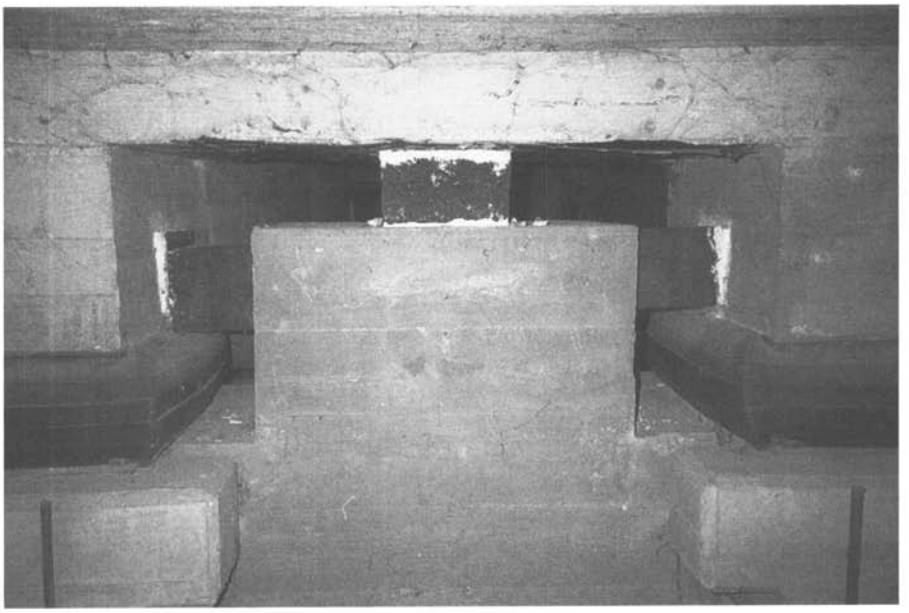

Fig. 1.3 Seismic fuzes used in the Pestalozzi School.

damper. These include hydraulic dampers, steel bars, steel coils, or lead plugs within the bearing itself. There are several drawbacks to using dampers for isolating structures: Every type of damper—except the internal lead plug—requires mechanical connectors and routine maintenance, the yielding of metallic dampers introduces a nonlinearity into the response that complicates the analysis of the dynamic response of the isolated building, and they reduce the degree of isolation by causing response in higher modes.

In the United States the most commonly used isolation system is the lead-plug rubber bearing. These bearings are multilayered, laminated elastomeric bearings that have one or more circular holes. Lead plugs are inserted into these holes to add damping to the isolation system. Although some projects are isolated solely with lead-plug rubber bearings, they are generally used in combination with multilayered elastomeric bearings without lead plugs.

It is also possible to incorporate damping into an isolation system by including damping in the elastomer itself. Buildings in the United States, Italy, Japan, the Peoples's Republic of China, and Indonesia have been isolated using these high-damping natural rubber bearings, and the simplicity of this approach is such that its use can be expected to spread rapidly. The first base-isolated building to be built in the United States used this type of isolator: the Foothill Communities Law and Justice Center (FCLJC).

Both before and after the beginning of implementation of base isolation in structures in the United States, there was an extensive program of research on the subject at a number of universities. Much of this research work was

sponsored by the U.S. National Science Foundation (NSF), with other funding from agencies such as the U.S. Department of Energy and the Electric Power Research Institute.

This research included several shake table experiments at the large earthquake simulator at the Earthquake Engineering Research Center (EERC) at the University of California at Berkeley. The test programs used a series of increasingly larger building models, ranging from a 20-ton, three-story model to a 60-ton, nine-story model, with increasingly realistic models of isolation bearings of several types. In parallel with shake table tests, which generally used small models of isolators with scale factors between 3 and 8, static tests were carried out on a wide range of isolators at sizes closer to full size. These tests have permitted users of isolators to study failure mechanisms and the influence of various parameters on the mechanical characteristics of the isolators. The results of these test programs have been reported in a series of EERC reports.

The concept of base isolation has also provided a rich source of theoretical work, both in the dynamics of the isolated structural system and in the mechanics of the isolators themselves. This theoretical work, widely published in structural engineering and earthquake engineering journals, has led to design guidelines for isolated structures and design rules for isolators. Several countries are now formulating design codes for isolated structures.

In the United States design codes have been in use since 1986. The code-writing process has undergone a steady evolution through a code series that began with a simple regulation titled "Tentative Seismic Isolation Design Requirements" based mainly on equivalent static design methods [121], which was considerably modified and became the 1991 version of the Uniform Building Code (UBC), "Earthquake Regulations for Seismic-Isolated Structures" [53]. The 1994 and finally the 1997 version of the UBC are even more elaborate. The 1997 UBC [55] is an extremely complex code based mainly on dynamic methods of design. The 1986 Structural Engineers Association of Northern California (SEAONC) code was deliberately straightforward and simple, with the intent of encouraging the use of this new technology. As the code has evolved, it has become increasingly difficult to use, and it now constitutes a considerable impediment to the implementing base isolation technology in the United States.

1.2 BASE ISOLATION IN THE UNITED STATES

The first base-isolated building to be built in the United States was the Foothill Communities Law and Justice Center (FCLJC) (Fig. 1.4), a legal services center for the County of San Bernardino, located in the city of Rancho Cucamonga, about 97 km (60 miles) east of downtown Los Angeles. Not only was it the first base-isolated building in the United States, it was also the first building in the world to use isolation bearings made from high-damping natural rubber. The FCLJC was designed with rubber isolators at the request of the County of San Bernardino. The building is only 21 km (13 miles) from the San Andreas Fault,

Fig. 1.4 Foothill Communities Law and Justice Center, Rancho Cucamonga, California.

which is capable of generating very large earthquakes on its southern branch. As a result, the county has had for many years one of the most thorough earthquake preparedness programs in the United States.

The building, approximately 15,794 m^2 (170,000 ft^2) and four stories high with a full basement, was designed to withstand an 8.3 magnitude earthquake. Located in a special subbasement, a total of 98 bearings were used to isolate the building. The construction of the building began in early 1984 and was completed in mid-1985 at a cost of $38 million.

Four high-damping natural rubber compounds were developed by the Malaysian Rubber Producers' Research Association (MRPRA) of the United Kingdom for this building [123]. The isolators are made from a highly filled natural rubber with mechanical properties that make it ideal for a base isolation system. The shear stiffness of this rubber is high at small strains but decreases by a factor of about 4 or 5 as the strain increases, reaching a minimum value at 50% shear strain. For strains greater than 100%, the stiffness begins to increase again. Thus, for small loading caused by wind or low-intensity earthquakes, the system has high horizontal stiffness and a short period; as the load intensity increases, the stiffness drops and the period is lengthened. For very high loads, for example, above maximum capable earthquake (MCE) loads, the stiffness increases again, providing a fail-safe action. The damping follows a similar but

less dramatic pattern, decreasing from an initial value of about 20% to a minimum of around 10% and then increasing again. The system is designed so that the minimum values of stiffness and damping are assumed, and the response is taken to be linear. The high initial stiffness is used only for wind load resistance and the large strain response only for fail-safe action.

The same high-damping rubber system was adopted for a building commissioned by Los Angeles County, the Fire Command and Control Facility (FCCF) [11] (Fig. 1.5). The FCCF houses the computer and communications systems for the fire emergency services program of the county and is required to remain functional during and after an extreme earthquake. This building was isolated based on a comparison of conventional and isolation schemes designed to provide the same degree of protection. On this basis the isolated design was estimated to cost 6% less than the conventional design. For most projects an isolated design generally costs around 5% more when compared with a conventional code design; however, the design code provides a minimum level of protection against strong ground shaking, guaranteeing only that the building will not collapse. It does not protect the building from structural damage. When equivalent levels of design performance are compared, an isolated building is always more cost-effective. Additionally, these are the primary costs when contemplating a structural system and do not address the life-cycle costs, which are also more favorable when an isolation system is used as compared to conventional construction.

A second base-isolated building has recently been completed for the County of Los Angeles at the same location as the FCCF. The Emergency Operations Center (EOC) (Fig. 1.6) is a two-story steel braced frame structure isolated

Fig. 1.5 Fire Command and Control Facility, Los Angeles, California.

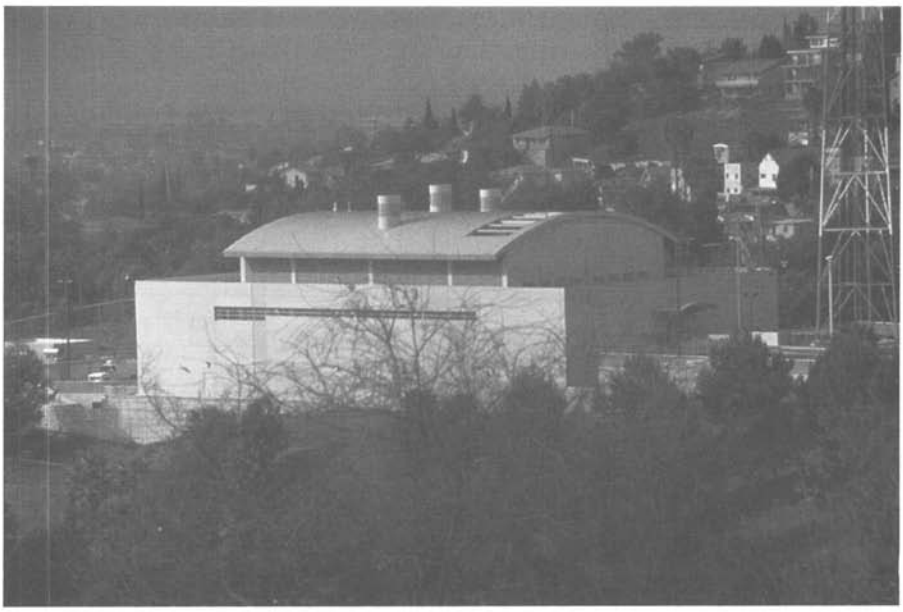

Fig. 1.6 Emergency Operations Center, Los Angeles, California.

using 28 high-damping natural rubber bearings provided by the Bridgestone Engineered Products Company.

A recent example of an isolated emergency center is the construction of the two-story Traffic Management Center for Caltrans in Kearny Mesa, California, near San Diego [131]. The superstructure has a steel frame with concentrically braced panels at the perimeter. The isolation system consists of forty 600-mm-(24-in.-) diameter high-damping natural rubber isolators provided by Bridgestone Engineered Products Rubber Company. The nominal isolation period is around 2.5 sec, and the MCE isolator displacement is around 254 mm (10 in.). The design base shear for the superstructure is around 15% of the structural weight. This design is quite conservative and the structure is very stiff. The expected interstory drift at the MCE is not expected to exceed 0.1%, implying that there will be very little nonstructural damage, even at the MCE.

Other new base-isolated building projects in California include a number of hospitals. The M. L. King/C. R. Drew Diagnostics Trauma Center (Fig. 1.7) in Willowbrook is a five-story, 13,000-m^2 (140,000-ft^2) structure supported on 70 high-damping natural rubber bearings and 12 sliding bearings with lead-bronze plates that slide on stainless steel surface. Built for the County of Los Angeles and completed in 1995, the building is located within 5 km (3 miles) of the Newport-Inglewood Fault, which is capable of generating 7.5 magnitude earthquakes. The isolators are 1.0 m (40 in.) in diameter, and at the time of their manufacture were the largest isolation bearings fabricated in the United States.

Fig. 1.7 M. L. King/C. R. Drew Diagnostics Trauma Center, Willowbrook, California.

There are several base isolation projects for new construction in the United States outside of California. One very early example was a flight simulator manufacturing facility in Salt Lake City completed in 1988 [7, 108] (Fig. 1.8). The purpose of the isolation system was to protect the inventory of computer systems in the facility (potentially over $100 million worth of inventory at any one time). The building is located very close to the Wastach Fault, which has been assessed as being capable of generating 7.0–7.5 magnitude earthquakes with a long return period. This four-story, 10,800-m^2 (116,000-ft^2) building is a steel moment-resisting frame structure. There are a total of 98 isolators in the structure: 50 of the bearings are 460 mm (18 in.) square with a 90-mm- (3.5-in.-) diameter lead plug and are located under the moment-resisting frame columns. The other isolators are 380 mm (15 in.) square, plain elastomeric bearings, which are located under gravity columns. The estimated displacement requirement for the system was 230 mm (9 in.) at a nominal period of 2.0 sec.

A large office building was recently completed in Memphis, Tennessee, for the automobile parts retailing company AutoZone [79]. This eight-story, 23,226-m^2 (250,000-ft^2) building houses the company's computer equipment. The isolation system is composed of 24 lead-plug rubber isolators and 19 high-damping natural rubber isolators. Including the isolation system, the total cost

Fig. 1.8 Flight Simulator Manufacturing Facility, Salt Lake City, Utah.

of construction of the building was $27 million. Other recently completed base-isolated projects include two buildings in Oregon: a new laboratory for the Portland Water Bureau and the retrofit of Campbell Hall, a building on the campus of the Western Oregon State College in Monmouth, Oregon.

In addition to the new buildings described above, there are a number of very large buildings in California that were retrofitted using base isolation. The retrofit of the Oakland City Hall was completed in 1995 and the retrofit of the San Francisco City Hall began in 1995. Both buildings were damaged in the 1989 Loma Prieta earthquake.

Built in 1914, Oakland City Hall (Fig. 1.9) was the tallest building on the west coast at the time of its construction. Its height was surpassed by the Los Angeles City Hall, which was built in 1928. The seismic rehabilitation of Oakland City Hall using base isolation was recently completed, and it is now the tallest seismically isolated building in the world. When the seismic rehabilitation of the Los Angeles City Hall is completed, it will be the tallest seismically isolated building in the world.

The Oakland City Hall isolation system uses 110 lead-plug rubber bearings ranging from 737 mm (29 in.) to 940 mm (37 in.) in diameter [131]. A moat was constructed around the building to provide a seismic gap of 508 mm (20 in.). Installation of the isolators proved to be very complicated and required shoring up the columns, cutting the columns, and transferring the column loads to temporary supports. In order to protect the interior, the columns were raised not more than 2.5 mm (0.1 in.) during the jacking process. The cost of the retrofit

Fig. 1.9 Oakland City Hall, Oakland, California. (Photo courtesy of SIE, Inc.)

was very substantial—about $84 million—with the isolators around 2.5% of that figure.

The San Francisco City Hall (Fig. 1.10) was designed in 1912 to replace the previous structure that was destroyed in the 1906 San Francisco earthquake. An outstanding example of classical architecture, it occupies two city blocks and is listed in the National Register of Historic Places. Substantial damage sustained from 1989 Loma Prieta earthquake necessitated extensive repair and seismic strengthening. The retrofit strategy adopted for the building was a base isolation scheme with superstructure strengthening using concrete shear walls. This five-story building has a 91-m (300-ft) dome and an exterior facade clad with Sierra granite. The structural system is a steel frame with unreinforced brick masonry integral with the granite cladding. There are hollow clay tile infill walls, and many of the interior spaces are lined with limestone and marble panels.

Fig. 1.10 San Francisco City Hall, San Francisco, California.

An interesting aspect of the original structural system is that the main floor level is a flexible soft story and appears to have been intended by the structural engineer to concentrate the seismic displacement at this level. The flexible first-story approach to seismic design was first proposed in the 1930s and again as the soft first story in the 1960s—to a certain extent it is a precursor of the base isolation approach.

The primary goal of the retrofit strategy was to preserve the historic fabric of the building [90]. Many options were considered and base isolation was selected. The plane of isolation is just above the existing foundation. The building was isolated with 530 lead-plug rubber bearings (Fig. 1.11) and, as in the Oakland City Hall retrofit project, the installation of the isolation system proved to be a complicated process of cutting, shoring, and installation. Many of the columns are supported on four isolators under a cruciform steel structure. Construction began in 1994 and is scheduled to be completed in 1998.

The Los Angeles City Hall is a 28-story steel frame building completed in 1928, with a total floor area close to 83,000 m^2 (890,000 ft^2) (Fig. 1.12). The lateral resistance is provided by several different elements, including steel cross-bracing, reinforced concrete walls, and interior clay hollow-core tile walls; most of the superstructure stiffness is provided by masonry infill perimeter walls. The building was damaged in the 1994 Northridge earthquake, with the most severe damage occurring on the twenty-fifth and twenty-sixth floors, which are characteristically soft stories. The base isolation retrofit scheme [138] will use about 475 high-damping rubber isolators in combination with about 60 slid-

Fig. 1.11 Isolators under supports at San Francisco City Hall.

ers and is to be supplemented by about 52 mechanical viscous dampers at the isolation level. In addition, 12 viscous dampers will be installed between the twenty-fourth and twenty-sixth floors to control interstory drifts at the soft-story levels. The total cost of this retrofit is estimated to be around $150 million, with the isolators comprising $3.5 million of that figure.

The second most common type of isolation system uses sliding elements. This approach assumes that a low level of friction will limit the transfer of shear across the isolation interface—the lower the coefficient friction, the less the shear transmitted. The earliest and most simple of all the proposed systems, it is not without its drawbacks. To provide adequate resistance to wind load and avoid unnecessary movement under small earthquakes or other disturbances, a fairly high value of frictional coefficient is needed. Many frictional surfaces have sliding characteristics that are sensitive to pressure and to the relative velocity of slip, and because the slip process is intrinsically nonlinear, a proper dynamic analysis must also be nonlinear. Furthermore, any sudden change in the stiffness of the overall structure when slipping or sticking occurs has the effect of generating high-frequency vibrations in the structure, vibrations at frequencies that might not be present in the ground motion. The system responds by transforming low-frequency energy in the ground motion into high-frequency energy in the structure.

Another problem with using sliders—and only sliders—in an isolation system is that there is no effective restoring force; thus, the code requirements for the displacement become extremely large. Since this displacement can be

Fig. 1.12 Los Angeles City Hall.

in any horizontal direction, the diameter of the bearing plates and the support system must be very large. In addition, the superstructure components bearing on the isolators must be designed for large moments caused by these large displacements.

It is possible to introduce a restoring force capability in several ways; for example, sliding bearings can be combined with elastomeric bearings. Kelly [61] proposed combining sliders and elastomeric bearings, thereby taking advantage of the best features of both types of isolator. Using sliders produces a system with a long period: the rubber bearings control the displacement by providing a centering action; they control torsion, and, if the displacements exceed the design level, they produce a stiffening action. This slider/elastomer combination was used in the 1992 seismic rehabilitation of the Mackay School of Mines at the University of Nevada at Reno (Fig. 1.13) [133]

Fig. 1.13 Mackay School of Mines, Reno, Nevada.

and for the MLK/Drew Hospital, which uses high-damping rubber isolators and lead-bronze sliders.

Another strategy to produce a restoring force capability in a sliding isolator is to curve the sliding surface. The friction pendulum system (FPS) is a sliding isolation system whereby the weight of the structure is carried on spherical sliding surfaces that slide relative to each other when the ground motion exceeds a threshold level. The recentering action is generated by raising the building when sliding occurs on the spherical surface. This system was developed in 1986 and was first used to retrofit a four-story apartment building (Fig. 1.14) in San Francisco that was badly damaged in the 1989 Loma Prieta earthquake. The retrofit involved installing a steel moment-resisting frame at ground level that supports the upper three floors of a wood-framed structure. Isolators were placed under the columns of the steel frame.

A more recent application of the FPS isolators is the seismic retrofit of the U.S. Court of Appeals building (Fig. 1.15) in San Francisco [8]. This five-story, 32,516-m^2 (350,000-ft^2) building was built in 1905 and survived the 1906 San Francisco earthquake. The original structure is a steel gravity frame with unreinforced granite and brick masonry walls. The FPS isolators were installed under the existing steel columns with new concrete for each column and a new rigid diaphragm system above the isolation level. Two buildings currently under construction that are to be isolated using the FPS are the International Terminal at San Francisco Airport and the new Hayward City Hall.

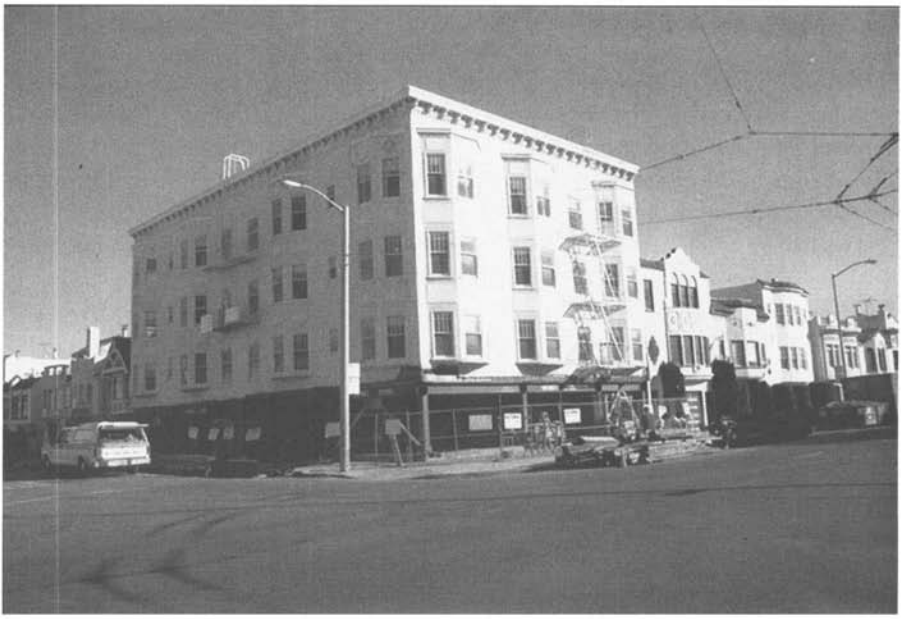

Fig. 1.14 Marina Apartments, San Francisco, California.

Fig. 1.15 U.S. Court of Appeals, San Francisco, California.

1.3 BASE ISOLATION IN JAPAN

Earthquake-resistant design has always been a high priority in Japan, and many mechanisms for the seismic protection of structures, including forms of seismic isolation, have been developed there. Japanese structural engineers generally design buildings with more seismic resistance than do U.S. or European engineers and are willing to consider more costly designs.

The use of isolation for earthquake-resistant design is also very actively pursued in Japan, with the completion of the first large modern base-isolated building in 1986 and increased to a level of around 10 isolated buildings per year in 1990 and 1991. The rate of construction of isolated buildings had dropped to around 4 or 5 per year due to the economic turndown, and at the time of the January 1995 Kobe earthquake the number stood at around 80.

All base isolation projects in Japan are approved by a standing committee of the Ministry of Construction. As many of the completed buildings have experienced earthquakes, in some cases it has been possible to compare their response with adjacent conventionally designed structures. In every case where such a comparison has been made, the response of the isolated building has been highly favorable, particularly for ground motions with high levels of acceleration. The system most commonly used in the past has been natural rubber bearings with mechanical dampers or lead-plug rubber bearings, and recently there has been an increasing use of high-damping natural rubber isolators.

Currently the largest base-isolated building in the world is the West Japan Postal Computer Center (Fig. 1.16), which is located in Sanda, Kobe Prefecture. This six-story, 47,000-m^2 (506,000-ft^2) structure is supported on 120 elastomeric isolators, with a number of additional steel and lead dampers. This building, which has an isolated period of 3.9 sec and is located approximately 30 km (17 miles) from the epicenter of the 1995 Hyogo-Ken Nanbu (Kobe) earthquake, experienced severe ground motion in that earthquake. The square root of the sum of squares (SRSS) peak ground acceleration under the isolators was 400 cm/s^2 (0.41 g) and was reduced by the isolation system to 127 cm/s^2 (0.31 g) (SRSS) at the sixth floor. The estimate of the displacement of the isolators is around 12 cm (4.7 in.). There was no damage to the isolated building, but a fixed-based building adjacent to the computer center reportedly experienced some damage [81]. A smaller base-isolated office building on high-damping rubber bearings (the Matsumura-Gumi Technical Research Institute (Fig. 1.17) was also affected by the Kobe earthquake and exhibited similar satisfactory performance.

As a result of the superior performance of the West Japan Postal Computer Center, there has been a rapid increase in the number of applications for permits for base-isolated buildings, especially for apartment buildings and condominiums. The total number of isolated buildings reviewed by the special Ministry of Construction committee as of March 1997 stands at 393, and the projected rate for the next few years is estimated to be around 200 per year. Of the 393 projects, 228 are for residential buildings and 84 are for office buildings. Other

Fig. 1.16 West Japan Postal Center, Sanda, Japan.

Fig. 1.17 Matsumura-Gumi Technical Research Institute.

projects include hospitals (31) and local government buildings (22). At this time there are few retrofit projects.

1.4 BASE ISOLATION IN EUROPE

In Europe, base isolation is being studied most actively in Italy under the auspices of the National Working Group on Seismic Isolation [Gruppo de Lavoro Isolamento Sismico (GLIS)]. GLIS has a wide membership comprising researchers and practitioners; it has organized several workshops and is preparing design guidelines for isolation systems.

Several buildings have been built in Italy using base isolation. One of these is the new Administration Center of the National Telephone Company (SIP), a complex of five seven-story buildings in Ancona (Fig. 1.18). As part of a demonstration project, a four-story apartment house was recently completed in Squillace, Calabria [130], with an identical, conventionally designed building next to it. A second base-isolated building is under construction in Ancona for the Ministry of Defense. A design for base-isolated standardized prefabricated switch houses, also for SIP, has been developed by Giuliani [46]; a number of these are to be located in highly seismic areas. A pilot project on the retrofit of a historic building has recently been completed in the village of Frigento in southern Italy. In addition to other structural strengthening, the simple

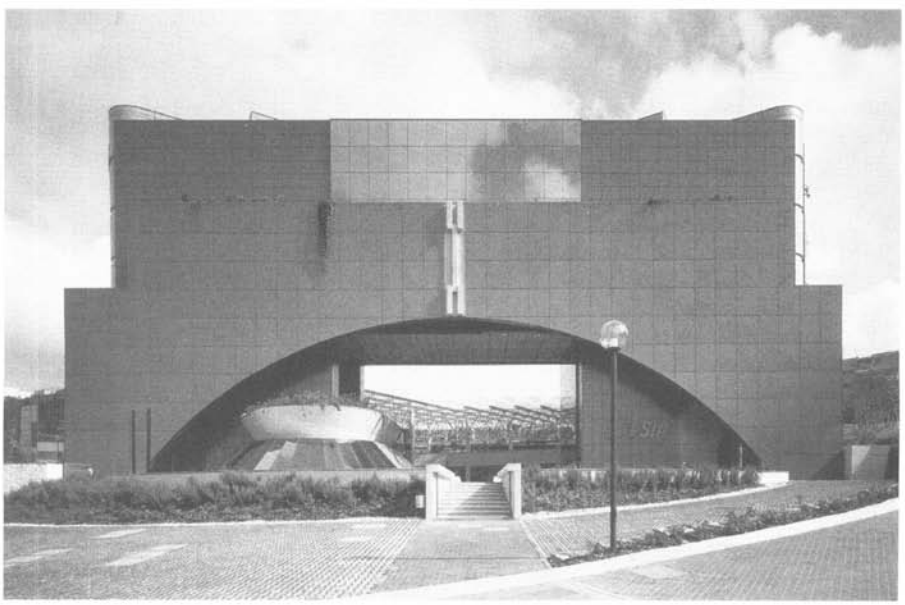

Fig. 1.18 The SIP Complex, Ancona, Italy.

masonry church of St. Peter was restored using high-damping rubber bearings [114].

1.5 BASE ISOLATION IN NEW ZEALAND

The first base-isolated building in New Zealand was the William Clayton building in Wellington [31]. Completed in 1981, it was the first building in the world to be isolated on lead-rubber bearings. Since its completion, three other base-isolated buildings have been built in New Zealand; two of these structures (Union House, Auckland, and Wellington Central Police Station) are isolated using the sleeved-pile approach. The Union House (Fig. 1.19) is a 12-story reinforced concrete braced frame. Displacement control is provided by an addi-

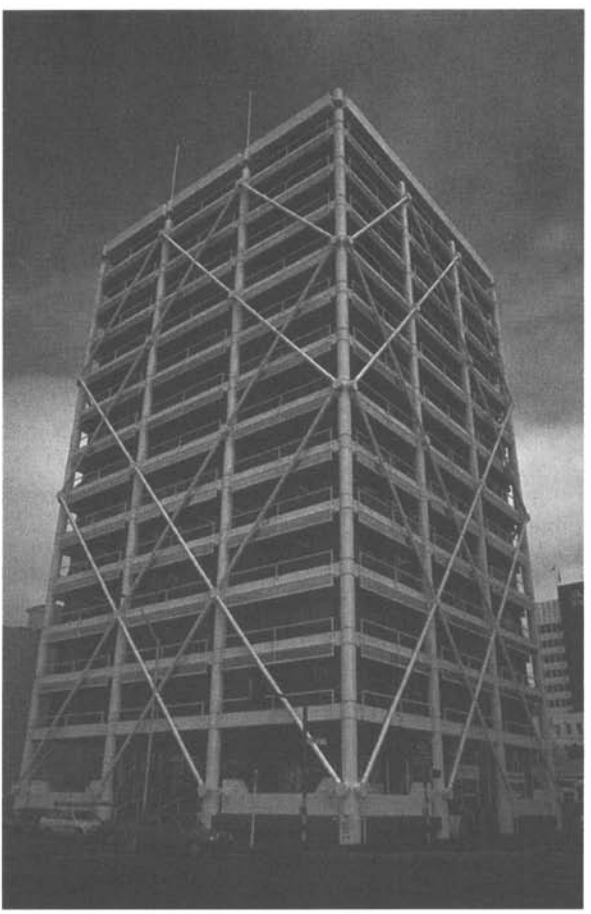

Fig. 1.19 Union House, Auckland, New Zealand.

tional damping system based on the elastic–plastic deformation of mild steel-tapered plates. The Wellington Central Police Station is a 10-story reinforced concrete braced frame structure, and displacement control is effected by lead-extrusion dampers [24]. The National Museum of New Zealand in Wellington has recently been completed; it is isolated with 142 lead-rubber bearings and 36 Teflon pads under the shear walls.

Another notable isolated building is the New Zealand Parliament House. Recently retrofitted using isolation, the Parliament House is a masonry bearing wall structure originally completed in 1922; this building and one other building were isolated using more than 514 lead-rubber bearings [107].

An unusual isolation project is a printing press building located in Petone near Wellington. This building was built on lead-rubber isolators [40], where the purpose of the isolation system is to protect the printing presses, which are very large and brittle pieces of equipment. The presses are made of cast iron and are equivalent in height to a four-story building. The building structure surrounds and is connected to the press, and the entire system is isolated at the base.

1.6 STATE OF ISOLATION TECHNOLOGY TODAY

Despite recent advances in base isolation research, the widespread application of this technology is still impeded by overconservative attitudes. For example, in the United States, the number of bureaucratic mandates (i.e., feasibility studies, peer reviews, and plant and site inspections) that an engineer must satisfy in order to isolate a structure make it remarkable that anyone does a base-isolated project. Unless bearings become a catalog commodity with certified characteristics and allied to reasonably simple design and analysis procedures that promote the benefits of base isolation, this technology will remain difficult to implement and restricted to a few projects a year. More importantly, while base isolation provisions are now in the UBC, the requirements are so conservative that the potential advantages of using base isolation (reduced-design requirements in the superstructure) are lost.

Many of the completed base-isolated buildings have experienced earthquakes and their performance has been as predicted. With the exception of the USC University Hospital in the 1994 Northridge earthquake [18], these earthquakes have been either nearby and small or have been moderate and distant, so that the accelerations experienced by isolated structures have not been large. As more isolated buildings are built in earthquake-prone regions of the world, engineers can anticipate learning more about the behavior of such structures and it will be possible to reduce the degree of conservatism that is currently present in the design of these structures. Once there is sufficient data detailing the response of base-isolated buildings to major earthquakes, the next step is an alignment of the codes for fixed-base and isolated structures with a common code based on a specified level of seismic hazard and structural performance, paving the way

for cost-effective application of this new technology for those building types for which it is appropriate.

For all systems, the most important area for future research is that of the long-term stability of the mechanical characteristics of the isolator and its constituent materials. The long-term performance of isolators can best be developed from inspection and retesting of examples that have been in service for many years. Elastomeric systems in the form of nonseismic bridge bearings have been used for upward of 30 years and a record of satisfactory performance has been established [118, 124].

CHAPTER 2

THEORETICAL BASIS OF SEISMIC ISOLATION

2.1 LINEAR THEORY

The linear theory of seismic isolation has been given in detail by Kelly [65]. A concise outline of the analysis will be given in this section. The theory is based on a two-mass structural model, as shown in Fig. 2.1. The mass m is intended to represent the superstructure of the building and m_b the mass of the base floor above the isolation system. The structure stiffness and damping are represented by k_s, c_s and the stiffness and damping of the isolation by k_b, c_b. Absolute displacements of the two masses are denoted by u_s and u_b, but it is convenient to use relative displacements and accordingly define

$$v_b = u_b - u_g \qquad v_s = u_s - u_b$$

where u_g is the ground displacement. This choice of relative displacements is particularly convenient for this analysis because the two important results will be the isolation system displacement, represented here by v_b, and the interstory drift, represented by v_s.

In terms of these quantities, the basic equations of motion of the two-degree-of-freedom model are

$$(m + m_b)\ddot{v}_b + m\ddot{v}_s + c_b\dot{v}_b + k_b v_b = -(m + m_b)\ddot{u}_g \tag{2.1}$$

$$m\ddot{v}_b + m\ddot{v}_s + c_s\dot{v}_s + k_s v_b = -m\ddot{u}_g \tag{2.2}$$

which can be written in matrix notation as

Design of Seismic Isolated Structures: From Theory to Practice. F. Naeim and J. M. Kelly

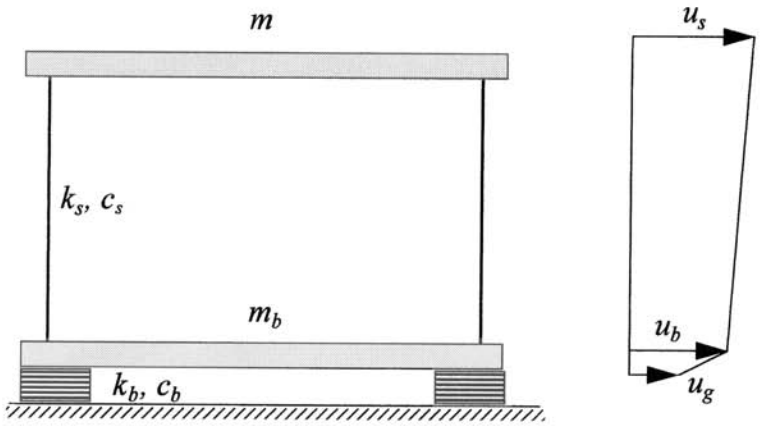

Fig. 2.1 Parameters of two-degree-of-freedom isolated system [63].

$$\begin{bmatrix} M & m \\ m & m \end{bmatrix} \begin{Bmatrix} \ddot{v}_b \\ \ddot{v}_s \end{Bmatrix} + \begin{bmatrix} c_b & 0 \\ 0 & c_s \end{bmatrix} \begin{Bmatrix} \dot{v}_b \\ \dot{v}_s \end{Bmatrix} + \begin{bmatrix} k_b & 0 \\ 0 & k_s \end{bmatrix} \begin{Bmatrix} v_b \\ v_s \end{Bmatrix} = \begin{bmatrix} M & m \\ m & m \end{bmatrix} \begin{Bmatrix} 1 \\ 0 \end{Bmatrix} \ddot{u}_g \tag{2.3}$$

where $M = m + m_b$, that is, in matrix notation

$$\mathbf{M}\ddot{\mathbf{v}} + \mathbf{C}\dot{\mathbf{v}} + \mathbf{K}\mathbf{v} = -\mathbf{M}\mathbf{r}\ddot{u}_g$$

We define a mass ratio γ as

$$\gamma = \frac{m}{m + m_b} = \frac{m}{M} \tag{2.4}$$

and nominal frequencies ω_b and ω_s given by

$$\omega_b^2 = \frac{k_b}{m + m_b} \qquad \omega_s^2 = \frac{k_s}{m} \tag{2.5}$$

and assume that $\omega_b^2/\omega_s^2 = \epsilon$ and $\epsilon = O(10^{-2})$.

The damping factors β_b and β_s are given by

$$2\omega_b\beta_b = \frac{c_b}{m + m_b} \qquad 2\omega_s\beta_s = \frac{c_s}{m} \tag{2.6}$$

In terms of these quantities, the basic equations of motion [Eqs. (2.1) and (2.2)]

become

$$\gamma\ddot{v}_s + \ddot{v}_b + 2\omega_b\beta_b\dot{v}_b + \omega_b^2 v_b = -\ddot{u}_g \tag{2.7a}$$

$$\ddot{v}_s + \ddot{v}_b + 2\omega_s\beta_s\dot{v}_s + \omega_s^2 v_s = -\ddot{u}_g \tag{2.7b}$$

The classical modes of the combined system will be denoted by $\boldsymbol{\phi}^1$ and $\boldsymbol{\phi}^2$, where

$$\boldsymbol{\phi}^{i\mathrm{T}} = (\phi_b^i, \phi_s^i) \qquad i = 1, 2$$

with frequencies ω_1 and ω_2. The characteristic equation for the frequencies is

$$(1-\gamma)\omega^4 - (\omega_s^2 + \omega_b^2)\omega^2 + \omega_b^2\omega_s^2 = 0 \tag{2.8}$$

the solutions of which are

$$\omega_1^2 = \frac{1}{2(1-\gamma)}\{\omega_b^2 + \omega_s^2 - [(\omega_b^2 - \omega_s^2)^2 + 4\gamma\omega_b^2\omega_s^2]^{1/2}\}$$

$$\omega_2^2 = \frac{1}{2(1-\gamma)}\{\omega_b^2 + \omega_s^2 + [(\omega_b^2 - \omega_s^2)^2 + 4\gamma\omega_b^2\omega_s^2]^{1/2}\} \tag{2.9}$$

and to first order in ϵ are given by

$$\omega_1^2 = \omega_b^2(1-\gamma\epsilon) \qquad \omega_2^2 = \frac{\omega_s^2}{1-\gamma}(1+\gamma\epsilon) \tag{2.10}$$

and the mode shapes with $(\phi_b^i = 1)$, $i = 1, 2$, are

$$\boldsymbol{\phi}^{1\mathrm{T}} = (1, \epsilon) \qquad \boldsymbol{\phi}^{2\mathrm{T}} = \left\{1, -\frac{1}{\gamma}[1-(1-\gamma)\epsilon]\right\} \tag{2.11}$$

To express the original displacements in modal coordinates, we write

$$v_b = q_1\phi_b^1 + q_2\phi_b^2 \qquad v_s = q_1\phi_s^1 + q_2\phi_s^2$$

where q_1, q_2 are time-dependent modal coefficients.

We note that modal quantities M_i, L_i are given by

$$M_i = \boldsymbol{\phi}^{i\mathrm{T}}\mathbf{M}\boldsymbol{\phi}^i \qquad M_iL_i = \boldsymbol{\phi}^{i\mathrm{T}}\mathbf{M}\mathbf{r}$$

To first order in ϵ, those are

$$M_1 = M(1 + 2\gamma\epsilon) \qquad M_2 = M\,\frac{(1-\gamma)[1-2(1-\gamma)\epsilon]}{\gamma} \tag{2.12}$$

and

$$L_1 = 1 - \gamma\epsilon \qquad L_2 = \gamma\epsilon \tag{2.13}$$

When (v_b, v_s) in Eqs. (2.1) and (2.2) are expressed in terms of $\boldsymbol{\phi}^1$ and $\boldsymbol{\phi}^2$, we have two equations in the modal coefficients (q_1, q_2) of the form

$$\ddot{q}_1 + 2\omega_1\beta_1\dot{q}_1 + \lambda_1\dot{q}_2 + \omega_1^2 q_1 = -L_1\ddot{u}_g \tag{2.14}$$

$$\ddot{q}_2 + \lambda_2\dot{q}_1 + 2\omega_2\beta_2 + \omega_2^2 q_2 = -L_2\ddot{u}_g \tag{2.15}$$

The terms $2\omega_1\beta_1$ and $2\omega_2\beta_2$ are computed from

$$M_i 2\omega_i\beta_i = \boldsymbol{\phi}^{i\mathrm{T}} \begin{bmatrix} c_b & 0 \\ 0 & c_s \end{bmatrix} \boldsymbol{\phi}^i$$

from which we obtain

$$2\omega_1\beta_1 = 2\omega_b\beta_b(1 - 2\gamma\epsilon)$$

$$2\omega_2\beta_2 = \frac{1}{1-\gamma}\,(2\omega_s\beta_s + 2\gamma\omega_b\beta_b)$$

leading to

$$\beta_1 = \beta_b(1 - \tfrac{3}{2}\gamma\epsilon) \tag{2.16}$$

$$\beta_2 = \frac{\beta_s + \gamma\beta_2\epsilon^{1/2}}{(1-\gamma)^{1/2}}\left(1 - \frac{\gamma\epsilon}{2}\right) \tag{2.17}$$

The coupling coefficients λ_1 and λ_2 are computed from

$$\lambda_1 M_1 = \boldsymbol{\phi}^{i\mathrm{T}} \begin{bmatrix} c_b & 0 \\ 0 & c_s \end{bmatrix} \boldsymbol{\phi}^2$$

$$\lambda_2 M_2 = \boldsymbol{\phi}^{2\mathrm{T}} \begin{bmatrix} c_b & 0 \\ 0 & c_s \end{bmatrix} \boldsymbol{\phi}^1 = \lambda_1 M_1$$

Thus

$$\lambda_1 M_1 = (1, \epsilon)\begin{bmatrix} c_b & 0 \\ 0 & c_s \end{bmatrix}\begin{pmatrix} 1 \\ -a \end{pmatrix} = c_b - \epsilon a c_s \qquad a = \frac{1}{\gamma}\,[1 - (1-\gamma)\epsilon]$$

Using (M_1, M_2) from Eq. (2.12), we have

$$\begin{aligned}\lambda_1 &= \frac{2\omega_b\beta_b M - \epsilon\{(1/\gamma)[1-(1-\gamma)\epsilon]\}2\omega_s\beta_s m}{M(1+2\gamma\epsilon)} \\ &= 2\omega_b\beta_b(1-2\gamma\epsilon) - \epsilon 2\omega_s\beta_s(1-2\gamma\epsilon) \\ &= 2\omega_b[\beta_b(1-2\gamma\epsilon) - \epsilon^{1/2}\beta_s] \end{aligned} \tag{2.18}$$

and

$$\begin{aligned}\lambda_2 &= \frac{2\omega_b\beta_b M - \epsilon\{(1/\gamma)[1-(1-\gamma)\epsilon]\}2\omega_s\beta_s m}{[M(1-\gamma)/\gamma][1-2(1-\gamma)\epsilon]} \\ &= (2\omega_b\beta_b - \epsilon 2\omega_s\beta_s)[1+2(1-\gamma)\epsilon]\,\frac{\gamma}{1-\gamma} \\ &= 2\omega_b\{\beta_b[1+2(1-\gamma)\epsilon] - \epsilon^{1/2}\beta_s\}\,\frac{\gamma}{1-\gamma} \end{aligned} \tag{2.19}$$

In most structural applications it is assumed that the damping is small enough that the effect of the off-diagonal components (here λ_1 and λ_2) are negligible and that the required solution can be obtained from the uncoupled modal equations of motions, namely,

$$\begin{aligned}\ddot{q}_1 + 2\omega_1\beta_1\dot{q}_1 + \omega_1^2 q_1 &= -L_1\ddot{u}_g \\ \ddot{q}_2 + 2\omega_2\beta_2\dot{q}_2 + \omega_2^2 q_2 &= -L_2\ddot{u}_g \end{aligned}$$

If the time history of the ground motion, $\ddot{u}_g(t)$, is known, then modal components $q_1(t)$, $q_2(t)$ can be computed from

$$q_1 = \frac{L_1}{\omega_1}\int_0^t \ddot{u}_g(t-\tau)e^{-\omega_1\beta_1\tau}\sin\,\omega_1\tau\,d\tau \tag{2.20a}$$

$$q_2 = -\frac{L_2}{\omega_2}\int_0^t \ddot{u}_g(t-\tau)e^{-\omega_2\beta_2\tau}\sin\,\omega_2\tau\,d\tau \tag{2.20b}$$

and estimates of the maximum values of q_1 and q_2 can be given by

$$|q_1|_{\max} = L_1 S_D(\omega_1, \beta_1) \tag{2.21a}$$

$$|q_2|_{\max} = L_2 S_D(\omega_2, \beta_2) \tag{2.21b}$$

where $S_D(\omega, \beta)$ is the displacement response spectrum for the ground motion, $\ddot{u}_g(t)$, at frequency ω and damping factor β.

In order to estimate the various response quantities from the peak spectral values, it is necessary to use the SRSS method. The values of the maximum isolation system displacement and structural deformation are given by

$$|v_s|_{\max} = [(\phi_2^1 |q_1|_{\max})^2 + (\phi_2^2 |q_2|_{\max})^2]^{1/2} \tag{2.22a}$$

$$|v_b|_{\max} = [(\phi_1^1 |q_1|_{\max})^2 + (\phi_1^2 |q_2|_{\max})^2]^{1/2} \tag{2.22b}$$

Inserting the results obtained from Eqs. (2.12), (2.13), (2.22a), and (2.22b), we get

$$\begin{aligned} |v_b|_{\max} &= \{[L_1 S_D(\omega_1, \beta_1)]^2 + [L_2 S_D(\omega_2, \beta_2)]^2\}^{1/2} \\ &= \{(1 - \gamma\epsilon)^2 [S_D(\omega_1, \beta_1)]^2 + \gamma^2 \epsilon^2 [S_D(\omega_2, \beta_2)]^2\}^{1/2} \end{aligned} \tag{2.23}$$

and

$$\begin{aligned} |v_s|_{\max} &= \left\{\epsilon^2 (1 - \gamma\epsilon)^2 [S_D(\omega_1, \beta_1)]^2 + \gamma^2 \epsilon^2 \frac{1}{\gamma^2} [1 - (1 - \gamma)\epsilon]^2 [S_D(\omega_2, \beta_2)]^2\right\}^{1/2} \\ &= \epsilon\{(1 - 2\gamma\epsilon)^2 [S_D(\omega_1, \beta_1)]^2 + [1 - 2(1 - \gamma)\epsilon]^2 [S_D(\omega_2, \beta_2)]^2\}^{1/2} \end{aligned} \tag{2.24}$$

Generally, the term $\epsilon^2 S_D(\omega_1, \beta_2)$ can be neglected with earthquake spectra where the displacement at high frequencies (i.e., ω_2) is much smaller than at lower frequencies (i.e., ω_1). This gives

$$|v_b|_{\max} = (1 - \gamma\epsilon) S_D(\omega_1 \beta_1) \tag{2.25}$$

If we neglect any terms that are higher than ϵ^2, then the estimate for the structural deformation or interstory drift, v_s, is given as

$$|v_s|_{\max} = \epsilon [S_D(\omega_1 \beta_1)^2 + S_D(\omega_2, \beta_2)^2]^{1/2} \tag{2.26}$$

Similarly, the base shear coefficient C_S given by

$$C_S = \left| \frac{k_s v_s}{m} \right|_{\max} = \omega_s^2 |v_s|_{\max}$$

becomes

$$\begin{aligned} C_S &= \omega_s^2 \epsilon [S_D(\omega_1, \beta_1)^2 + S_D(\omega_2, \beta_2)^2]^{1/2} \\ &= [\omega_b^4 S_D(\omega_1, \beta_1)^2 + \epsilon^2 \omega_s^4 S_D(\omega_2, \beta_2)^2]^{1/2} \\ &= [S_A(\omega_1, \beta_1)^2 + \epsilon^2 S_A(\omega_2, \beta_2)^2]^{1/2} \end{aligned} \tag{2.27}$$

Thus if we retain only the first terms, we get

$$|v_s|_{\max} = \frac{\epsilon S_V}{\omega_b} = \epsilon S_D(\omega_b, \beta_b) \tag{2.28a}$$

$$|v_b|_{\max} = \frac{S_V}{\omega_b} = S_D(\omega_b, \beta_b) \tag{2.28b}$$

and the design base shear coefficient C_S defined by

$$C_S = \frac{k_s v_s}{m} = \omega_s^2 v_s$$

becomes

$$\begin{aligned} C_S = \omega_b S_V \left[1 + \epsilon^2 \frac{\omega_2^2}{\omega_1^2}\right]^{1/2} &= S_A(\omega_b, \beta_b)\left(1 + \frac{\epsilon}{1-\gamma}\right)^{1/2} \\ &\approx S_A(\omega_b, \beta_b) \end{aligned} \tag{2.29}$$

indicating that for small ϵ and a typical design spectrum, the isolation system can be designed, at least in the initial phase, for a relative base displacement of $S_D(\omega_b, \beta_b)$ and the building for a base shear coefficient of $S_A(\omega_b, \beta_b)$. The reduction in base shear as compared with a fixed-base structure, where $C_S = S_A(\omega_s, \beta_s)$, is given by $S_A(\omega_b, \beta_b)/S_A(\omega_s, \beta_s)$, which for a constant-velocity spectrum is ω_b/ω_s, or roughly of order $\epsilon^{1/2}$; this underestimates the reduction in base shear because, in general, β_b will be larger than β_s.

2.2 EXTENSION OF THEORY TO BUILDINGS

2.2.1 *M*-Degree-of-Freedom Equations of Motion

The two-degree-of-freedom (2-DOF)-analysis of the simple linear model developed earlier can be applied to the case of a multistoried building. Let us represent the structural system of this building by mass matrix **M**, damping matrix **C**, and stiffness matrix **K**. For a conventionally based structure, the relative

displacement $\mathbf{u}$ of each degree of freedom with respect to the ground is given by

$$\mathbf{M}\ddot{\mathbf{u}} + \mathbf{C}\dot{\mathbf{u}} + \mathbf{K}\mathbf{u} = -\mathbf{M}\mathbf{r}\ddot{u}_g \tag{2.30}$$

where $\mathbf{r}$ is a vector that couples each degree of freedom to the ground motion. When this structural model is superimposed on a base isolation system with base mass m_b, stiffness k_b, and damping, c_b, Eq. (2.30) becomes

$$\mathbf{M}\ddot{\mathbf{v}} + \mathbf{C}\dot{\mathbf{v}} + \mathbf{K}\mathbf{v} = -\mathbf{M}\mathbf{r}(\ddot{u}_g + \ddot{v}_b) \tag{2.31}$$

where $\mathbf{v}$ is the displacement relative to the base slab and v_b is the relative displacement of the base slab to the ground. The overall equation of motion for the combined building and base slab is

$$\mathbf{r}^{\mathrm{T}}\mathbf{M}(\ddot{\mathbf{v}} + \mathbf{r}\ddot{v}_b + \mathbf{r}\ddot{u}_g) + m_b(\ddot{v}_b + \ddot{u}_g) + c_b\dot{v}_b + k_b v_b = 0 \tag{2.32}$$

which can be written in the form

$$\mathbf{r}^{\mathrm{T}}\mathbf{M}\ddot{\mathbf{v}} + (m + m_b)\ddot{v}_b + c_b\dot{v}_b + k_b v_b = -(m + m_b)\ddot{u}_g \tag{2.33}$$

Equation (2.33) identifies $\mathbf{r}^{\mathrm{T}}\mathbf{M}\mathbf{r}$ as the total mass m of the building; therefore, $m + m_b$ is the total mass carried on the isolation system. The matrix form of these equations is

$$\mathbf{M}^*\ddot{\mathbf{v}}^* + \mathbf{C}^*\dot{\mathbf{v}}^* + \mathbf{K}^*\mathbf{v}^* = -\mathbf{M}^*\mathbf{r}^*\ddot{u}_g \tag{2.34}$$

where

$$\mathbf{M}^* = \begin{bmatrix} m + m_b & \mathbf{r}^{\mathrm{T}}\mathbf{M} \\ \mathbf{M}\mathbf{r} & \mathbf{M} \end{bmatrix} \qquad \mathbf{C}^* = \begin{bmatrix} c_b & 0 \\ \mathbf{0} & \mathbf{C} \end{bmatrix}$$

and

$$\mathbf{K}^* = \begin{bmatrix} k_b & 0 \\ \mathbf{0} & \mathbf{K} \end{bmatrix} \qquad \mathbf{r}^* = \begin{bmatrix} 1 \\ \mathbf{0} \end{bmatrix}$$

with

$$\mathbf{v}^* = \begin{bmatrix} v_b \\ \mathbf{v} \end{bmatrix}$$

2.2.2 Modal Analysis of *M*-DOF System

The natural modes of the fixed-base structure are assumed known and denoted by $\boldsymbol{\phi}^i$, where $i = 1, \ldots, N$. In terms of these mode shapes, the displacement of each degree of freedom of the structure can be represented as

$$\mathbf{v} = \sum_{i=1}^{N} q_i \boldsymbol{\phi}^i \tag{2.35}$$

The natural frequencies ω_i^2 are given by

$$\mathbf{M}\boldsymbol{\phi}^i \omega_i^2 = \mathbf{K}\boldsymbol{\phi}^i$$

and we assume that $\boldsymbol{\phi}^i \mathbf{C} \boldsymbol{\phi}^j = 0$ if $i \neq j$.

The matrix equations of motion reduce to the $N + 1$ equations

$$\sum_{i=1}^{N} \mathbf{r}^{\mathrm{T}} \mathbf{M}\boldsymbol{\phi}^i \ddot{q}_i + (m + m_b)\ddot{v}_b + c_b \dot{v}_b + k_b v_b = -(m + m_b)\ddot{u}_g \tag{2.36a}$$

and

$$\ddot{q}_i + 2\omega_i \beta_i \dot{q}_i + \omega_i^2 q_i = -L_i(\ddot{v}_b + \ddot{u}_g) \qquad i = 1, \ldots, N \tag{2.36b}$$

where L_i are the participation factors of the fixed-base modes, that is,

$$L_i = \frac{\boldsymbol{\phi}^{i\mathrm{T}} \mathbf{M}\mathbf{r}}{\boldsymbol{\phi}^{i\mathrm{T}} \mathbf{M}\boldsymbol{\phi}^i}$$

The fixed-base modal masses are given by

$$M_i = \boldsymbol{\phi}^{i\mathrm{T}} \mathbf{M}\boldsymbol{\phi}^i$$

We can write these equations in the form

$$\sum_{i=1}^{N} \frac{L_i M_i}{m + m_b} \ddot{q}_i + \ddot{v}_b + 2\omega_b \beta_b \dot{v}_b + \omega_b^2 v_b = -\ddot{u}_g \tag{2.37a}$$

and

$$L_i\ddot{v}_b + \ddot{q}_i + 2\omega_i\beta_i\dot{q}_i + \omega_i^2 q_i = -L_i\ddot{u}_g \qquad i = 1, \ldots, N \tag{2.37b}$$

The complete modal analysis of these $N + 1$ equations is given in Kelly [65], where the procedure for the frequencies and mode shapes of the composite system is described. In most cases the modes higher than the first mode play no role in the design of the structure or the isolation system; therefore only the first mode needs to be included.

Comparing the equations of motion [Eqs. (2.37a) and (2.37b)] with the previous set for the isolated 1-DOF structure [Eqs. (2.7a) and (2.7b)], the equations can be made to correspond if we replace v_b in the elementary analysis with $L_1 v_b$, $\ddot{u}_g$ with $L_1\ddot{u}_g$, and

$$\gamma = \frac{m}{m + m_b} = \frac{m}{M}$$

with

$$\gamma_1 = \frac{L_1^2 M_1}{m + m_b}$$

giving

$$\frac{L_1^2 M_1}{m + m_b}\ddot{q}_1 + (L_1\ddot{v}_b) + 2\omega_b\beta_b(L_1\dot{v}_b) + \omega_b^2(L_{1v_b}) = -L_1\ddot{u}_g$$

$$(L_1\ddot{v}_b) + \ddot{q}_1 + 2\omega_1\beta_1\ddot{q}_1 = -L_1\ddot{u}_g$$

In the solution of these equations, the result for q_1 follows that for v_s in the simple 1-DOF system.

The basic results for the 1-DOF structure, namely, that

$$|v_b|_{\max} = \frac{1}{\omega_b^2} S_A(\omega_b, \beta_b) \tag{2.38}$$

and

$$C_S = [S_A(\omega_b^*, \beta_b^*) + \epsilon^2(1 - \gamma)^2 S_A^2(\omega_s^*, \beta_s^*)]^{1/2} \tag{2.39}$$

are replaced as follows. The maximum relative base displacement is given by

$$|L_1 v_b|_{\max} = \frac{1}{\omega_b^2} L_1 S_A(\omega_b, \beta_b) \tag{2.40}$$

and because L_1 appears on both sides, the result is the same as before.

To obtain the base shear, we have

$$|q_1|_{\max} = \left[\frac{\epsilon^2 L_1^2 S_A^2(\omega_b^*, \beta_b^*)}{\omega_b^{*4}} + \frac{\epsilon^2 L_1^2 S_A^2(\omega_s^*, \beta_s^*)}{\omega_s^{*4}} \right]^{1/2} \tag{2.41}$$

with ω_s^*, β_s^* calculated as before and ϵ replaced by $\epsilon_1 = \omega_b^2/\omega_1^2$. The relative displacement vector $\mathbf{v}$ is given by

$$\mathbf{v} = q_1 \boldsymbol{\phi}^1 \tag{2.42}$$

and if we neglect the damping contributions, the inertial force on each element is

$$\mathbf{F} = \mathbf{K}\mathbf{v} = q_1 \mathbf{K}\boldsymbol{\phi}^1 = q_1 \mathbf{M}\boldsymbol{\phi}^1 \omega_1^2 \tag{2.43}$$

The total horizontal force on the superstructure is

$$\mathbf{r}^{\mathrm{T}}\mathbf{F} = q_1 \omega_1^2 L_1 M_1 \tag{2.44}$$

and this is expressed in terms of the base shear coefficient C_S through

$$C_S m = \mathbf{r}^{\mathrm{T}}\mathbf{F} \tag{2.45}$$

Thus

$$\begin{aligned} C_S &= \frac{L_1 M_1}{m} [L_1^2 S_A^2(\omega_b, \beta_b) + (1 - \gamma_1)^2 \epsilon^2 L_1^2 S_A^2(\omega_s^*, \beta_s^*)]^{1/2} \\ &= \frac{L_1^2 M_1}{m} [S_A^2(\omega_b, \beta_b) + (1 - \gamma_1)^2 \epsilon^2 S_A^2(\omega_s^*, \beta_s^*)]^{1/2} \end{aligned} \tag{2.46}$$

with $\epsilon = \omega_b^2/\omega_1^2$ as established previously.

2.3 ANALYSIS OF COUPLED DYNAMIC EQUATIONS

In most structural applications it is assumed that the damping is small enough that the effect of the off-diagonal components is negligible and the required solution can be obtained from the uncoupled modal equations of motions. The previous analysis neglects the off-diagonal components, leading to very simple results for base displacement, base shear, and interstory drift.

In many isolated structures designed according to the most recent California design codes, the code requirements are so conservative that the designers are using additional viscous dampers in an attempt to control the large design displacements, and damping factors for the isolation system of the order of 0.50 are obtained. Clearly, at this level of damping the equations cannot remain uncoupled and a complex modal analysis should be used. In complex modal analysis, however, we lose the physical insight that led to the simple results of the uncoupled solution [65]. For this reason a similar approximation to that employed there will be used in this section to demonstrate the effect of high levels of damping in the isolation system on the response of the structure.

It is interesting to note that to zero order in ϵ, the four damping terms are

$$2\omega_1\beta_1 = 2\omega_b\beta_b \qquad 2\omega_2\beta_2 = \frac{1}{1-\gamma}\,2\omega_s\beta_s$$

$$\lambda_1 = 2\omega_b\beta_b \qquad \lambda_2 = 2\omega_b\beta_b\,\frac{\gamma}{1-\gamma}$$

so that the off-diagonal components are of the same order as the diagonal terms. Recalling that $L_1 \approx O(1)$ and $L_2 \approx O(\epsilon)$, we assume that the influence of $\lambda_1\dot{q}_2$ on the result for q_1 is negligible but the influence of $\lambda_2\dot{q}_1$ on q_2 could be significant. Thus, we assume that Eqs. (2.14) and (2.15) are modified, so that $q_1(t)$ is given by the solution of

$$\ddot{q}_1 + 2\omega_1\beta_1\dot{q}_1 + \omega_1^2 q_1 = -L_1\ddot{u}_g$$

and $q_2(t)$ by

$$\ddot{q}_2(t) + 2\omega_2\beta_2\dot{q}_2 + \omega_2^2 q_2 = -L_2\ddot{u}_g - \lambda_2\dot{q}_1$$

To aid in simplifying the solution, it is useful to take the Laplace transform of these equations using

$$\mathrm{LT}[f(t)] = \int_0^\infty e^{-st} f(t)\,dt = \bar{f}(s)$$

In terms of the Laplace transform, we have

$$\bar{q}_1(s) = -\frac{L_1\bar{a}(s)}{s^2 + 2\omega_1\beta_1 s + \omega_1^2}$$

$$\bar{q}_2(s) = -\frac{L_2\bar{a}(s)}{s^2 + 2\omega_2\beta_2 s + \omega_2^2} + \frac{\lambda_2 L_1 s\bar{a}(s)}{(s^2 + 2\omega_2\beta_2 s + \omega_2^2)(s^2 + 2\omega_1\beta_1 s + \omega_1^2)}$$

$$= -L_2 A_1(s)\bar{a}(s) + \lambda_2 L_1 A_2(s)\bar{a}(s)$$

where $\bar{a}(s) = \mathrm{LT}[\ddot{u}_g]$. The term $A_2(s)$ can be reduced by partial fractions to

$$A_2(s) = \frac{a + bs}{s^2 + 2\omega_1\beta_1 s + \omega_1^2} + \frac{c + ds}{s^2 + 2\omega_2\beta_2 s + \omega_2^2}$$

where after considerable manipulation we find

$$a = \frac{\omega_1^2(2\omega_2\beta_2 - 2\omega_1\beta_1)}{D} \qquad b = \frac{\omega_2^2 - \omega_1^2}{D}$$

$$c = \frac{\omega_2^2(2\omega_2\beta_2 - 2\omega_1\beta_1)}{D} \qquad d = -\frac{\omega_2^2 - \omega_1^2}{D} \tag{2.47}$$

and

$$D = (\omega_2^2 - \omega_1^2)^2 + (2\omega_2\beta_2 - 2\omega_1\beta_1)(\omega_1^2 2\omega_2\beta_2 - \omega_2^2 2\omega_1\beta_1) \tag{2.48}$$

The inversion of the two terms of $A_2(s)$ follows from

$$\mathrm{LT}^{-1}\left[\frac{s - \alpha}{(s - \alpha)^2 + \gamma^2}\right] = e^{\alpha t}\cos\,\gamma t$$

and

$$\mathrm{LT}^{-1}\left[\frac{1}{(s - \alpha)^2 + \gamma^2}\right] = \frac{1}{\gamma}\,e^{\alpha t}\sin\,\gamma t$$

so that the inversion of $(a + bs)/(s^2 + 2\omega_1\beta_1 s + \omega_1^2)$ is

$$be^{-\omega_1\beta_1 t}\cos\ \bar{\omega}_1 t + (a - b\bar{\omega}_1\beta_1)\ \frac{e^{-\omega_1\beta_1 t}\sin\ \bar{\omega}_1 t}{\bar{\omega}_1}$$

and that of $(c + ds)/s^2 + 2\omega_2\beta_2 s + \omega_2^2$ is

$$de^{-\omega_2\beta_2 t}\cos\ \bar{\omega}_2 t + (c - d\omega_2\ \beta_2)\ \frac{e^{-\omega_2\beta_2 t}\sin\ \bar{\omega}_2 t}{\bar{\omega}_2}$$

where

$$\bar{\omega}_1 = \omega_1(1 - \beta_1^2)^{1/2} \qquad \bar{\omega}_2 = \omega_2(1 - \beta_2^2)^{1/2}$$

The final result of $q_1(t)$ and $q_2(t)$ is obtained by convolution and substitution of a, b, c, and d from Eq. (2.47) as

$$q_1(t) = -\frac{L_1}{\bar{\omega}_1}\int_0^t \ddot{u}_g(t-\tau)e^{-\omega_1\beta_1\tau}\sin\ \bar{\omega}_1\tau\ d\tau \tag{2.49}$$

$$\begin{aligned} q_2(t) = {} & -L_2\ \frac{1}{\bar{\omega}_2}\int_0^t e^{-\omega_2\beta_2(t-\tau)}\sin\ \bar{\omega}_2(t-\tau)\ddot{u}_g(\tau)\ d\tau \\ & + \lambda_2 L_1\left\{\frac{\omega_2^2 - \omega_1^2}{D}\int_0^t e^{-\omega_1\beta_1(t-\tau)}\cos\ \bar{\omega}_1(t-\tau)\ddot{u}_g(\tau)\ d\tau\right. \\ & + \frac{\omega_1^2(2\omega_2\beta_2) - (\omega_1^2 + \omega_2^2)\omega_1\beta_1}{D}\ \frac{1}{\omega_1}\int_0^t e^{-\omega_1\beta_1(t-\tau)}\sin\ \bar{\omega}_1(t-\tau)\ddot{u}_g(\tau)\ d\tau \\ & - \frac{\omega_2^2 - \omega_1^2}{D}\int_0^t e^{-\omega_2\beta_2(t-\tau)}\cos\ \bar{\omega}_2(t-\tau)\ddot{u}_g(\tau)\ d\tau \\ & \left. - \frac{(\omega_1^2 + \omega_2^2)\omega_2\beta_2 - \omega_2^2 2\omega_1\beta_1}{D}\ \frac{1}{\bar{\omega}_2}\int_0^t e^{-\omega_2\beta_2(t-\tau)}\sin\ \bar{\omega}_2(t-\tau)\ddot{u}_g(\tau)\ d\tau\right\} \end{aligned} \tag{2.50}$$

These convolution integrals can be computed for any choice of $\ddot{u}_g(t)$, but for the purpose of this demonstration, it is necessary only to have a sense of the order of magnitude of the results.

Terms in ω_1, ω_2 can be expressed in terms of the nominal frequencies ω_b, ω_s by use of Eq. (2.9), from which we have

$$\omega_2^2 - \omega_1^2 = \frac{1}{1-\gamma}\,[(\omega_s^2 - \omega_b^2)^2 - 4\gamma\omega_b^2\omega_s^2]^{1/2}$$

$$\omega_2^2 + \omega_1^2 = \frac{\omega_s^2 + \omega_b^2}{1-\gamma}$$

$$\omega_1^2\omega_2^2 = \frac{\omega_s^2\omega_b^2}{1-\gamma}$$

The denominator D of each term in Eq. (2.50) can be written as

$$D = (\omega_2^2 - \omega_1^2)^2 - 4\omega_1^2\omega_2^2(\beta_1^2 + \beta_2^2) + 4\omega_1\omega_2(\omega_1^2 + \omega_2^2)\beta_1\beta_2$$

which reduces to

$$D = \frac{1}{(1-\gamma)^2}\,[(\omega_s^2 - \omega_b^2)^2 + 4\gamma\omega_s^2\omega_b^2 - 4(1-\gamma)\omega_s^2\omega_b^2\beta_1^2\beta_2^2 + 4(1-\gamma)^{1/2}\omega_s\omega_b(\omega_s^2 + \omega_b^2)\beta_1\beta_2] \tag{2.51}$$

A further reduction of each term is possible if we assume the following orders of magnitude:

$$\gamma = O(1) \qquad \frac{\omega_b^2}{\omega_s^2} = \epsilon \ll 1$$

To the first order in ϵ, we have

$$D = \frac{\omega_s^4}{(1-\gamma)^2}\,[1 - 2(1-2\gamma)\epsilon]$$

and the multipliers of each integral become

$$\frac{\omega_2^2 - \omega_1^2}{D} = \frac{\omega_s^2}{1-\gamma}\,[1-(1-2\gamma)\epsilon]\,\frac{1}{D}$$

$$= \frac{1-\gamma}{\omega_s^2}\,[1+(1-2\gamma)\epsilon]$$

$$\frac{\omega_1^2(2\omega_2\beta_2) - (\omega_1^2 - \omega_2^2)\omega_1\beta_1}{D\omega_1} = \frac{1-\gamma}{\omega_s^2}\,\beta_1$$

$$\frac{(\omega_1^2 + \omega_2^2)\omega_2\beta_2 - \omega_2^2 2\omega_1\beta_1}{D\omega_2} = \frac{1-\gamma}{\omega_s^2}\,\beta_2$$

giving for the four terms in parentheses in Eq. (2.50)

$$\frac{1-\gamma}{\omega_s^2}\left\{[1+(1-2\gamma)\epsilon]\left[\int_0^t e^{-\omega_1\beta_1(t-\tau)}\cos\bar{\omega}_1(t-\tau)\ddot{u}_g(\tau)\,d\tau - \int_0^t e^{-\omega_2\beta_2(t-\tau)}\cos\bar{\omega}_2(t-\tau)\ddot{u}_g(\tau)\,d\tau\right]\right.$$
$$- \beta_1\int_0^t e^{-\omega_1\beta_1(t-\tau)}\sin\bar{\omega}_1(t-\tau)\ddot{u}_g(\tau)\,d\tau$$
$$\left. + \beta_2\int_0^t e^{-\omega_2\beta_2(t-\tau)}\sin\bar{\omega}_2(t-\tau)\ddot{u}_g(\tau)\,d\tau\right\}$$

The results for q_1 and q_2 to first order in ϵ are thus

$$q_1(t) = -\frac{L_1}{\bar{\omega}_1}\int_0^t e^{-\omega_1\beta_1(t-\tau)}\sin\bar{\omega}_1(t-\tau)\ddot{u}_g(\tau)\,d\tau \tag{2.52}$$

$$q_2(t) = -\frac{L_2}{\bar{\omega}_2}\int_0^t e^{-\omega_2\beta_2(t-\tau)}\sin\bar{\omega}_2(t-\tau)\ddot{u}_g(\tau)\,d\tau$$
$$+\lambda_2 L_1\,\frac{1-\gamma}{\omega_s^2}\left\{[1+(1-2\gamma\epsilon)]\left[\int_0^t e^{-\omega_1\beta_1(t-\tau)}\cos\bar{\omega}_1(t-\tau)\ddot{u}_g(\tau)\,d\tau - \int_0^t e^{-\omega_2\beta_2(t-\tau)}\cos\bar{\omega}_2(t-\tau)\ddot{u}_g(\tau)\,d\tau\right]\right.$$
$$- \beta_1\int_0^t e^{-\omega_1\beta_1(t-\tau)}\sin\bar{\omega}_1(t-\tau)\ddot{u}_g(\tau)\,d\tau$$
$$\left. + \beta_2\int_0^t e^{-\omega_2\beta_2(t-\tau)}\sin\bar{\omega}_2(t-\tau)\ddot{u}_g(\tau)\,d\tau\right\} \tag{2.53}$$

It is convenient to denote the convolution integrals in Eqs. (2.52) and (2.53) by I_1, I_2, I_3, and I_4, where

$$I_1 = \int_0^t e^{-\omega_1\beta_1(t-\tau)} \sin \bar{\omega}_1(t-\tau)\ddot{u}_g(\tau)\, d\tau$$

$$I_2 = \int_0^t e^{-\omega_2\beta_2(t-\tau)} \sin \bar{\omega}_2(t-\tau)\ddot{u}_g(\tau)\, d\tau$$

$$I_3 = \int_0^t e^{-\omega_1\beta_1(t-\tau)} \cos \bar{\omega}_1(t-\tau)\ddot{u}_g(\tau)\, d\tau$$

$$I_4 = \int_0^t e^{-\omega_2\beta_2(t-\tau)} \cos \bar{\omega}_2(t-\tau)\ddot{u}_g(\tau)\, d\tau$$

In this analysis the quantities of interest are the interstory drift and the floor accelerations, which are represented in this simple model by v_s and $\ddot{u}_s$. In this simple model they are related by

$$|\ddot{u}_s|_{\max} = \frac{k_s|v_s|_{\max}}{m}$$

so that the evaluation of v_s will also provide the floor acceleration. The interstory drift v_s is given by

$$v_s = q_1\phi_s^1 + q_2\phi_s^2$$

leading to

$$v_s = -\epsilon \frac{L_1}{\bar{\omega}_1} I_1 + \frac{1}{\gamma}[1-(1-\gamma)\epsilon] \frac{L_2}{\bar{\omega}_2} I_2$$

$$- \frac{1}{\gamma}[1-(1-\gamma)\epsilon]\lambda_2 L_1 \frac{1-\gamma}{\omega_s^2}\{[1+(1-2\gamma\epsilon)](I_3 - I_4) - \beta_1 I_1 + \beta_2 I_2\} \tag{2.54}$$

It is useful here to separate the three contributions to the drift as follows:

(i) that produced by the base shear generated by the isolation system

$$v_s^{(1)} = -\epsilon \frac{L_1}{\bar{\omega}_1} I_1 \tag{2.55}$$

(ii) that from the uncoupled modal equations

$$v_s^{(2)} = \frac{1}{\gamma}\,[1-(1-\gamma)\epsilon]\,\frac{L_2}{\bar{\omega}_2}\,I_2 \tag{2.56}$$

and

(iii) that from the coupling terms, which is generally neglected in most analyses,

$$v_s^{(3)} = -\frac{1}{\gamma}\,[1-(1-\gamma)\epsilon]\lambda_2 L_2\,\frac{1-\gamma}{\omega_s^2}\,\{[1+(1-2\gamma\epsilon)](I_3-I_4)-\beta_1 I_1+\beta_2 I_2\} \tag{2.57}$$

The convolution integrals I_1, I_2, I_3, and I_4 can be estimated for the purpose of this demonstrative analysis by response spectrum methods. We recognize that

$$\frac{1}{\bar{\omega}_1}\,|I_1|_{\max} = S_D(\omega_1,\beta_1) \qquad \frac{1}{\bar{\omega}_2}\,|I_2|_{\max} = S_D(\omega_2,\beta_2)$$

where S_D is the displacement response spectrum.

The expression

$$\left|\int_0^t e^{-\omega\beta(t-\tau)}\cos\,\omega(t-\tau)\ddot{u}_g(\tau)\,d\tau\right|_{\max}$$

is the relative velocity response spectrum $S_{RV}(\omega,\beta)$ for a single-degree-of-freedom oscillator of frequency ω and damping factor β. This we approximate by the pseudo–velocity response spectrum $S_V(\omega,\beta)$ given by $\omega S_D(\omega,\beta)$. The peak values of the four convolution integrals in parentheses in Eq. (2.53) will occur at different times and should be added by the SRSS method, leading estimates of the maxima of the three contributions to v_s.

We have

$$|v_s^{(1)}|_{\max} = \epsilon L_1 S_D(\omega_1,\beta_1)$$

$$|v_s^{(2)}|_{\max} = \frac{1}{\gamma}\,[1-(1-\gamma)\epsilon]L_2 S_D(\omega_2,\beta_2)$$

$$|v_s^{(3)}|_{\max} = \frac{1}{\gamma}\,[1-(1-\gamma)\epsilon]\lambda_2 L_1\,\frac{1-\gamma}{\omega_s^2}$$

$$\{[1+(1-2\gamma\epsilon)]^2[\omega_1^2 S_D^2(\omega_1,\beta_1)+\omega_2^2 S_D^2(\omega_2,\beta_2)]$$

$$+\beta_1^2\omega_1^2 S_D^2(\omega_1,\beta_1)+\beta_2^2\omega_2^2 S_D^2(\omega_2,\beta_2)\}^{1/2} \tag{2.58}$$

All design codes for seismically isolated structures are based on constant-velocity spectra, so that the various terms in the above can be related through

$$S_V(\omega, \beta) = S_V H(\beta)$$

where S_V is constant and $H(\beta)$ is a suitable damping modification function that decreases with increasing β and is unity at $\beta = 0.05$. Many such functions have been used, either as tables in code documents or as continuous functions. A particularly simple form is the Kawashima–Aizawa function [60]

$$H(\beta) = \frac{1.5}{1 + 40\beta} + 0.5 \tag{2.59}$$

where $H(0) = 2$, $H(0.05) = 1$, and $H \to 0.5$ as $\beta \to \infty$. Using a constant-velocity spectrum of this form and the results for the modal quantities L_1, L_2, ω_1, ω_2, ... from the earlier section (after considerable manipulation), we obtain the following results:

$$\begin{aligned}
|v_s^{(1)}|_{\max} &= \epsilon \frac{S_V}{\omega_b} H(\beta_1) \\
|v_s^{(2)}|_{\max} &= \epsilon^{2/3}(1-\gamma)^{1/2} \frac{S_V}{\omega_b} H(\beta_2) \\
|v_s^{(3)}|_{\max} &= 2\epsilon\beta_b \left\{[1 + 2(1-2\gamma)\epsilon + \beta_1^2]H^2(\beta_1)\right. \\
&\quad \left. +[1 + 2(1-2\gamma)\epsilon + \beta_2^2]H^2(\beta_2)\right\}^{1/2} \frac{S_V}{\omega_b}
\end{aligned} \tag{2.60}$$

Clearly, for small values of β_b, say $\beta \approx 0.10$, the first term, $|v_s^{(1)}|_{\max}$, is the dominant term. For all values of β_b the second term, $|v_s^{(2)}|_{\max}$, is always much less than the first term and is neglected. The significance of the third term, $|v_s^{(3)}|_{\max}$, depends on the value of β_b. For the usual values of β_s, the value of β_2^2 is small compared to unity, so the ratio between them becomes

$$\frac{v_s^{(3)}}{v_s^{(1)}} = R = \frac{2\beta_b\{(1+\beta_1^2)H^2(\beta_1) + H^2(\beta_2)\}^{1/2}}{H(\beta_1)} \tag{2.61}$$

Now $\beta_1 \approx \beta_b$ and

$$\beta_2 \approx \frac{1}{(1-\gamma)^{1/2}} (\beta_s + \gamma\epsilon^{1/2}\beta_b)$$

Suppose we adopt the Kawashima–Aizawa formula for $H(\beta)$ and take $\epsilon = \frac{1}{25}$, $\gamma = \frac{1}{2}$, and $\beta_s = 0.02$; then the ratio of the two terms is 0.33 when $\beta_b = 0.10$ and increases to 1.80 when $\beta_b = 0.50$. To put this into numbers appropriate for an example project, suppose that the code-mandated displacement at the MCE is 76 cm (30 in.) for 5% damping and a period of 2.5 sec. To reduce this to a more acceptable level, suppose that linear viscous dampers are added to bring the damping to around 50%, at which point the reduction factor is 0.57. The displacement is now acceptable, and in code notation the elastic base shear becomes $F_s = KD$, which before was

$$F_s = \frac{K}{M} D \frac{W}{g} = 0.50W$$

and is now reduced to $0.285W$, which, again, seems quite reasonable; however, the viscous force

$$F_v = 2\omega\beta M\dot{D}$$

which is out of phase with F_s, is, for $\beta = 0.50$ and $\dot{D} = \omega D$, exactly the same as F_s, and the maximum base shear is

$$\sqrt{2}F_s = 0.40W$$

The corresponding maximum floor accelerations given by

$$|\ddot{u}_s|_{\max} = \omega_s^2 |v_s|_{\max}$$

are

$$|\ddot{u}_s|^{(1)}_{\max} = \epsilon \frac{S_V}{\omega_b} H(\beta)\omega_s^2 = \omega_b S_V H(\beta_1)$$

and

$$\begin{aligned} |\ddot{u}_s|^{(3)}_{\max} - \omega_s^2 \cdot 2\epsilon\beta_b \{&[1 + 2(1 - 2\gamma)\epsilon + \beta_1^2]H^2(\beta_1) \\ &+ [1 + 2(1 - 2\gamma)\epsilon + \beta_2^2]H^2(\beta_2)\}^{1/2} \frac{S_V}{\omega_b} \\ = 2\omega_b\beta_b \{&[1 + 2(1 - 2\gamma)\epsilon + \beta_1^2]H^2(\beta_1) \\ &+ [1 + 2(1 - 2\gamma)\epsilon + \beta_2^2]H^2(\beta_2)\}^{1/2} S_V \end{aligned}$$

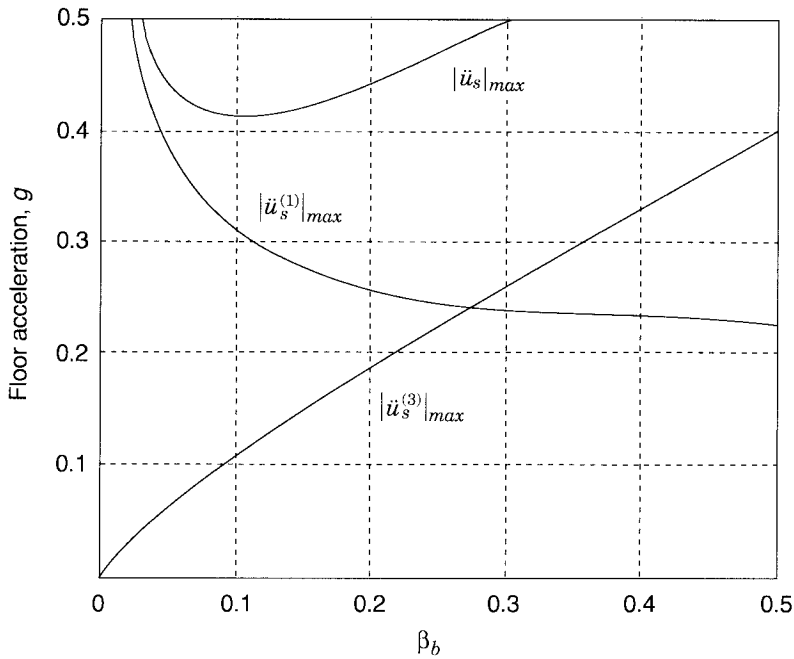

Fig. 2.2 Influence of damping on floor accelerations.

For the same example the these two components and their sum as a function of β_b are shown in Fig. 2.2. We see that $|\ddot{u}_s|_{\max}$ becomes equal to $|\ddot{u}_s|_{\max}$ when β_b is around 0.26, but their sum has a minimum value at about 0.12.

This result implies that the addition of dampers (leading to large values of β_b), while controlling the isolator displacement by reducing v_b, has the countereffect of increasing the interstory drift and the floor accelerations. For a constant-velocity design spectrum the accelerations generated by the coupling terms become the dominant term. It is not widely appreciated that in base-isolated structures the higher modes, which carry both the floor accelerations and the interstory drift, are almost orthogonal to the base shear, so that a low base shear is not a guarantee of an effective isolation system. In this respect the effort to improve the performance of the system by adding excessive damping is a misplaced effort and inevitably self-defeating.

CHAPTER 3

ISOLATION SYSTEM COMPONENTS

3.1 INTRODUCTION

Base isolation is now a mature technology and is used in many countries, and there are a number of acceptable isolation systems, the construction of which is well understood. Nevertheless, the concept appears to have an irresistible attraction to inventors, and many new and different systems of isolators are proposed and patented each year. Many of these new systems will prove to be impractical and some might actually be lethal, but the number continues to increase year by year.

Most systems used today incorporate either elastomeric bearings, with the elastomer being either natural rubber or neoprene, or sliding bearings, with the sliding surface being Teflon and stainless steel (although other sliding surfaces have been used). Systems that combine elastomeric bearings and sliding bearings have also been proposed and implemented.

This chapter will discuss as many of the available systems as possible within the constraints of space and time. With the increasing number of new systems and modifications of existing systems, it is possible that some may be overlooked. We apologize in advance to inventors or vendors of isolation systems that have been inadvertently excluded.

3.2 ELASTOMERIC-BASED SYSTEMS

Natural rubber bearings were first used for the earthquake protection of buildings in 1969 for the Pestalozzi School in Skopje, Macedonia (see Chapter 1).

Design of Seismic Isolated Structures: From Theory to Practice. F. Naeim and J. M. Kelly

The bearings are large rubber blocks without the steel reinforcing plates used today and compress by about 25% under the weight of the building. The bearings have a vertical stiffness that is only a few times the horizontal stiffness and the rubber is relatively undamped. This system was tested on the shake table at the EERC in 1982 [117]. Characteristic of isolation systems of this kind, the horizontal motion is strongly coupled to a rocking motion, so that purely horizontal ground motion induces vertical accelerations in the rocking mode. The system also has foam–glass blocks on either side of a rubber bearing that are intended to act as fuses to prevent movement in the building under wind, internal foot traffic, or low seismic input. The system is still in place and is monitored from time to time.

Since this building was completed, many other buildings have been built on natural rubber bearings but with internal steel reinforcing plates that reduce the lateral bulging of the bearings and increase the vertical stiffness. The internal steel plates, referred to as shims, provide a vertical stiffness that is several hundred times the horizontal stiffness. These multilayered elastomer bearings provide vibration isolation for apartment blocks, hospitals, and concert halls built over subway lines or mainline railroads. In 1975 Derham et al. [38] suggested that this approach could be used to protect buildings from earthquake ground motion, and an intensive experimental and theoretical research program was begun at the EERC to develop this concept. Laminated elastomeric bearings can be differentiated into low-damping or high-damping types.

3.2.1 Low-Damping Natural and Synthetic Rubber Bearings

Low-damping natural rubber bearings and synthetic rubber bearings have been widely used in Japan in conjunction with supplementary damping devices, such as viscous dampers, steel bars, lead bars, frictional devices, and so on. The elastomer used in Japan comprises natural rubber, while in France neoprene has been used in several projects. The isolators have two thick steel endplates and many thin steel shims, as shown in Fig. 3.1. The rubber is vulcanized and bonded to the steel in a single operation under heat and pressure in a mold. The steel shims prevent bulging of the rubber and provide a high vertical stiffness but have no effect on the horizontal stiffness, which is controlled by the low shear modulus of the elastomer. The material behavior in shear is quite linear up to shear strains above 100%, with the damping in the range of 2–3% of critical. The material is not subject to creep, and the long-term stability of the modulus is good.

It is possible to manufacture an isolator with no damping and exactly linear shear behavior. Such bearings were made for an isolation system proposed for nuclear power plant application by the Central Electricity Generating Board in the United Kingdom. These bearings were intended to be used in conjunction with a viscous damper developed by the GERB Corp. in Germany [68]. The combined system was tested at the EERC, and the tests confirmed that the bearings were completely linear to 150% shear strain and completely without

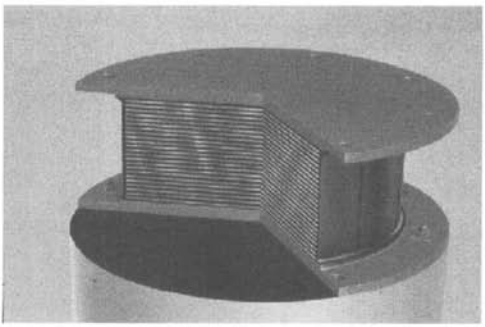

Fig. 3.1 Low-damping natural rubber bearing.

damping. The intent of the design was to provide an isolation system that could exactly correspond to the linear viscous dynamic model. While the rubber fitted the model, the tests showed that the response of the damper was not exactly that of a linear viscous element.

The advantages of the low-damping elastomeric laminated bearings are many: They are simple to manufacture (the compounding and bonding process to steel is well understood), easy to model, and their mechanical response is unaffected by rate, temperature, history, or aging. The single disadvantage is that a supplementary damping system is generally needed. These supplementary systems require elaborate connections and, in the case of metallic dampers, are prone to low-cycle fatigue.

Many applications of this type of system have been used in Japan. The energy dissipation elements consist of a variety of steel-yielding devices, including tapered rods, coiled yielding springs, lead bars, and frictional elements. A variant of this approach is the lead-plug bearing. Developed in New Zealand in the 1970s, the lead-plug bearing is now the most frequently used isolation system.

3.2.2 Lead-Plug Bearings

The lead-plug bearing was invented in New Zealand in 1975 [110, 111] and has been used extensively in New Zealand, Japan, and the United States. Lead-plug bearings are laminated rubber bearings similar to low-damping rubber bearings but contain one or more lead plugs that are inserted into holes, as shown in Fig. 3.2. The steel plates in the bearing force the lead plug to deform in shear. The lead in the bearing deforms physically at a flow stress of around 10 MPa (1500 psi), providing the bearing with a bilinear response [129]. The lead must fit tightly in the elastomeric bearing, and this is achieved by making the lead plug slightly larger than the hole and forcing it in. Because the effective stiffness and effective damping of the lead-plug bearing is dependent on the displacement, it is important to state the displacement at which a specific damping value is required. Lead-plug bearings have been extensively tested in New Zealand [27], and there are very complete guidelines on their design and model-

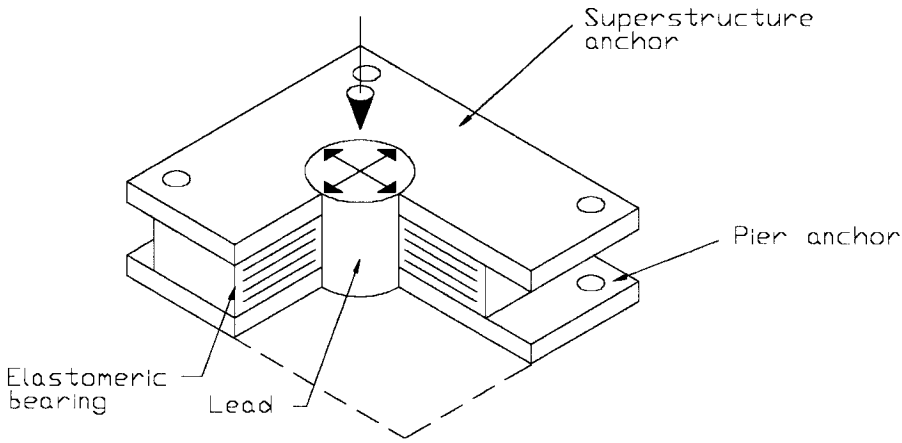

Fig. 3.2 Lead-plug isolator.

ing [23, 80]. Buildings isolated with these bearings performed well during the 1994 Northridge and 1995 Kobe earthquakes.

3.2.3 High-Damping Natural Rubber Systems (HDNR)

The development of a natural rubber compound with enough inherent damping to eliminate the need for supplementary damping elements was achieved in 1982 by the Malaysian Rubber Producers' Research Association (MRPRA) of the United Kingdom [39]. The damping is increased by adding extrafine carbon block, oils or resins, and other proprietary fillers. The damping is increased to levels between 10 and 20% at 100% shear strains, with the lower levels corresponding to low hardness (50–55 durometer) and a shear modulus around 0.34 MPa (50 psi) and the high levels to high hardness (70–75 durometer) and a high shear modulus [1.40 MPa (200 psi)]. The methods of vulcanization, bonding, and construction of the isolators are unchanged.

The material is nonlinear at shear strains less than 20% (Fig. 3.3) and is characterized by higher stiffness and damping, which tends to minimize response under wind load and low-level seismic load. Over the range of 20–120% shear strain, the modulus is low and constant. At large strains the modulus increases due to a strain crystallization process in the rubber that is accompanied by an increase in the energy dissipation. This increase in stiffness and damping at large strains can be exploited to produce a system that is stiff for small input, is fairly linear and flexible at design level input, and can limit displacements under unanticipated input levels that exceed design levels.

The damping in the isolators is neither viscous nor hysteretic, but somewhat in between. In a purely linear viscous element the energy dissipation is quadratic in the displacement; in a hysteretic system it tends to be linear in displacement. Tests on a large number of different rubber isolators at the EERC (Fig. 3.4)

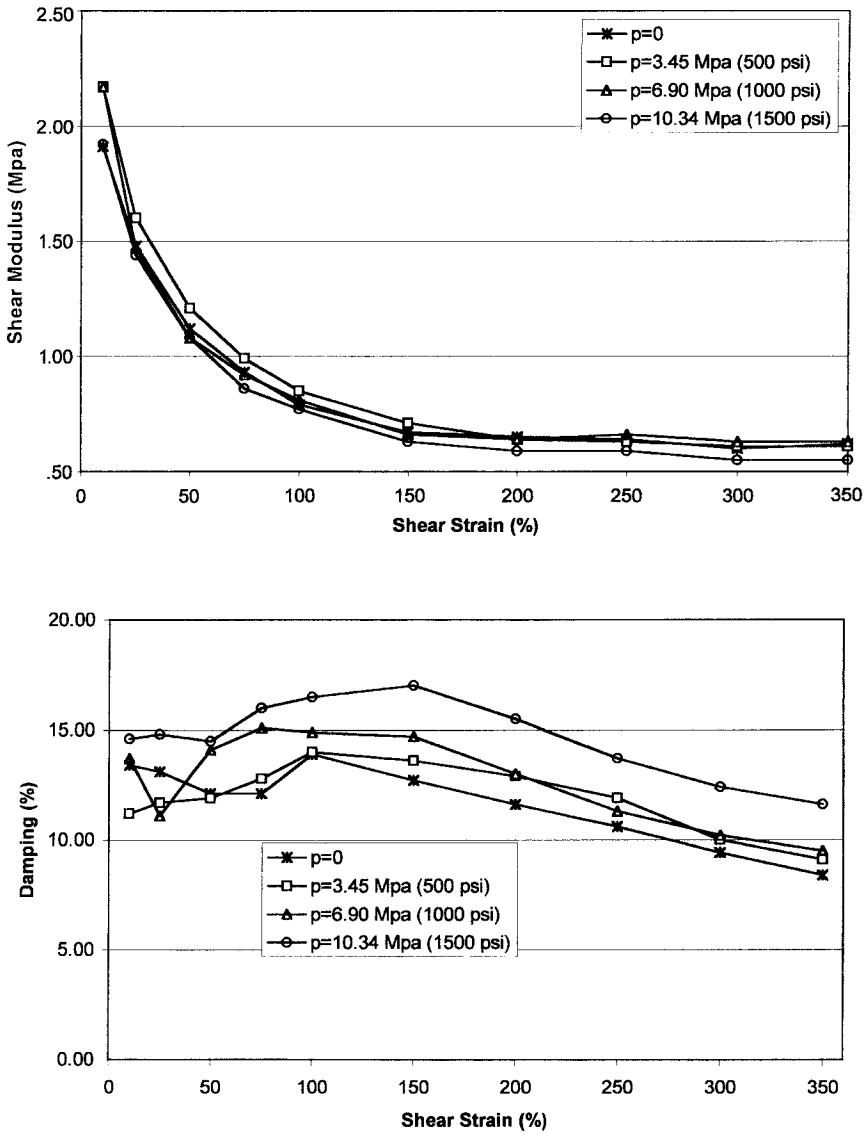

Fig. 3.3 Stress–strain characteristics of high-damping natural rubber isolators.

demonstrate that the energy dissipated per cycle is proportional to the displacement around the value of power 1.5. This characteristic can be exploited so that it is possible to model the bearing response, which combines linear viscous and elastic–plastic elements.

Another serendipitous advantage of the high-damping rubber system is that it provides a degree of ambient vibration reduction. The isolators will act to filter

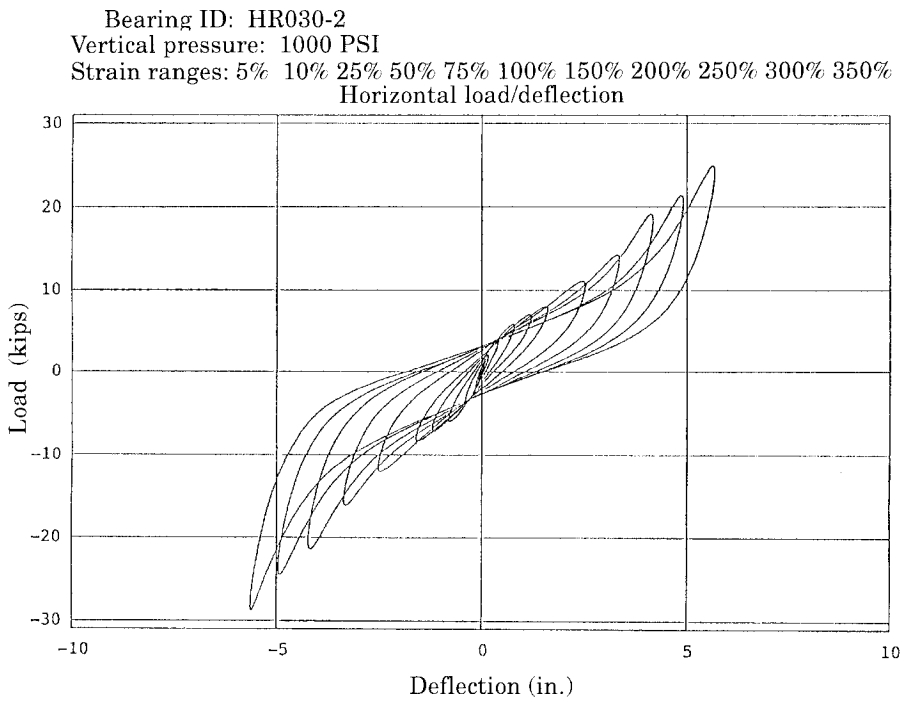

Fig. 3.4 Hysteretic behavior of high-damping natural rubber isolators.

out high-frequency vertical vibrations caused by traffic or adjacent underground railways. This effect was demonstrated in a shake table test program carried out at EERC in 1985 [39a].

3.3 ISOLATION SYSTEMS BASED ON SLIDING

A purely sliding system is the earliest and simplest isolation system to be proposed. A system using pure sliding was proposed in 1909 by Johannes Avetican Calantarients, a medical doctor in England. He suggested separating the structure from the foundation by a layer of talc (shaded portion in Fig. 3.5). As is evident in his diagrams, Calantarients clearly understood that the isolation system reduced accelerations in the isolated building at the expense of large relative displacements between the building and the foundation, for he designed a set of ingenious connections for utilities—in those days restricted to gas lines and sewage pipes—to accommodate these displacements (see Fig. 3.6). In fact, Calantarients's system incorporated all the elements now considered necessary in a base isolation system: a method of decoupling the building and the foundation, a method whereby utility lines can withstand large relative displacements, and a wind restraint system.

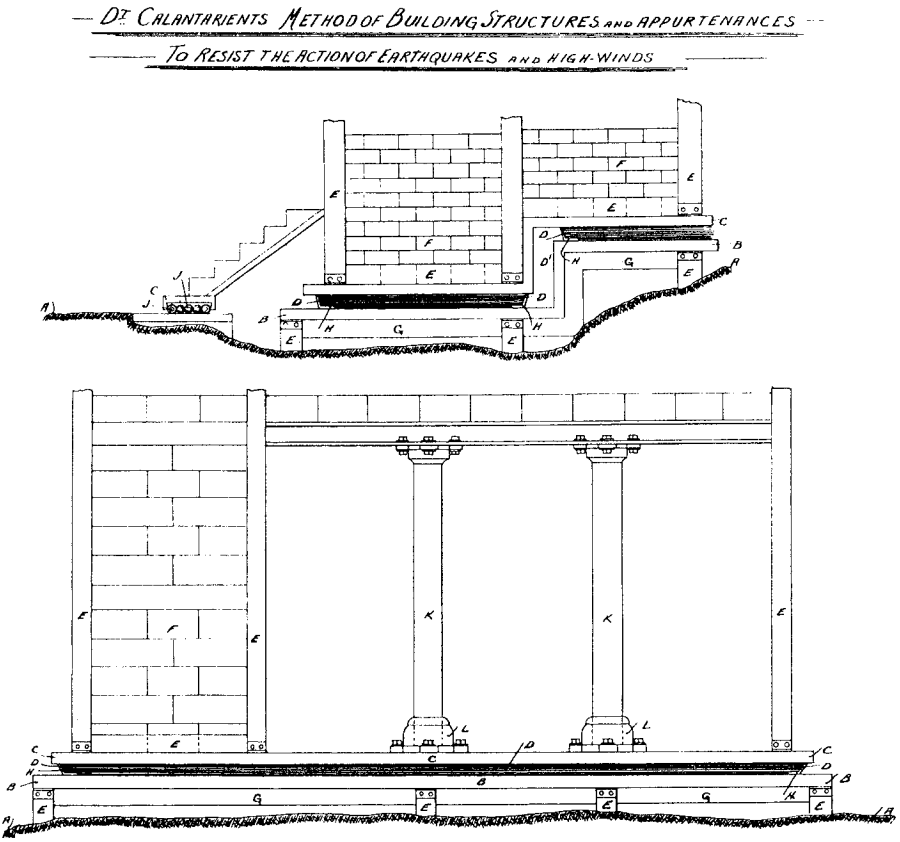

Fig. 3.5 Calantariens's base isolation system using a layer of talc as the isolating medium.

Isolation was first considered as a seismic-resistant design strategy by the Italian government after the great Messimo-Reggio earthquake of 1908, which killed 160,000 people in unreinforced masonry buildings—the typical building type for the area. Almost all buildings of this type collapsed [19]. After the earthquake a commission was appointed to make recommendations for rebuilding the area with earthquake-resistant structures that were both economical and safe. The commission considered two approaches to earthquake-resistant design: The first approach isolated the building from the ground by either interposing a sand layer in its foundation or using rollers under columns to allow the building to move horizontally; the second approach involved a fixed-base design with height limitations and a lateral force design requirement. The latter approach was recommended and sliding isolation systems were not used [2].

The idea is an appealing one, however, and has been proposed time and again. In the severe Indian earthquakes of Dhubai (1930) and Bihar (1934) it was observed that small masonry buildings that slid on their foundations sur-

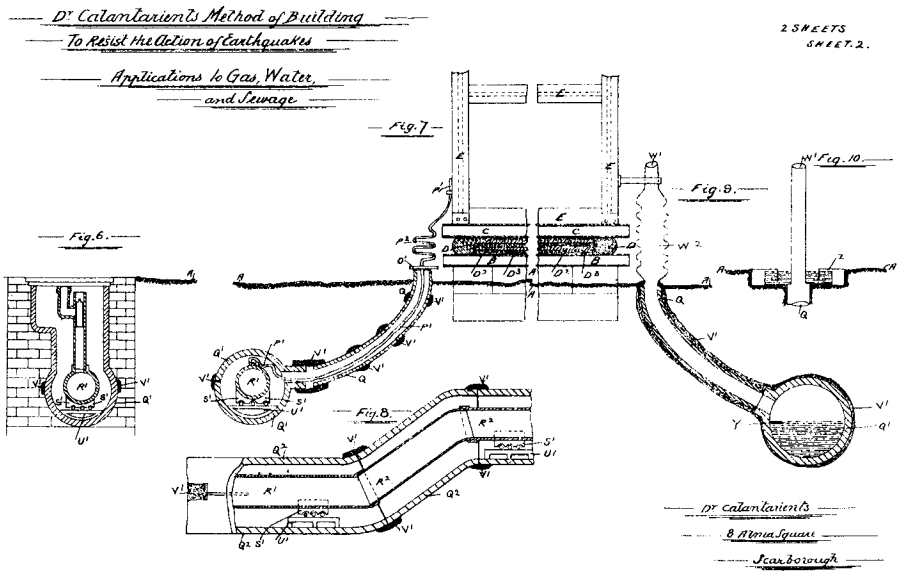

Fig. 3.6 Utility connection proposed for the Calantarients scheme.

vived the earthquake, while similar buildings fixed at the base were destroyed. Based on these observations and because small masonry buildings cannot be isolated cost-effectively using elastomeric isolators, a sliding system was proposed by Arya [15]. Considerable analysis was done on this approach, and an experimental program using a shock-type shake table (the shock produced by rolling a loaded wagon down an incline) [16, 17] was carried out and demonstrated the effectiveness of the approach.

Chinese earthquake engineers observed the same phenomena following the devastating 1976 Tangshan earthquake. It was observed that buildings that survived the earthquake had a horizontal crack at the bottom of the walls that allowed a slip of around 6 cm (2.4 in.). This was interpreted as having protected the masonry superstructure from damage. After much theoretical analysis, a $\frac{1}{8}$-scale shake table test and a blast test on a full-size building were carried out [72]. A number of small buildings were built using this approach. The largest is a four-story dormitory building for the Earthquake Strong Motion Observatory in Beijing in which the sliding surface is a layer of specially selected sand between terrazzo plates that are located above the foundation and under the walls at the ground floor level.

A considerable amount of theoretical analysis has been done on the dynamics of structures on sliding systems subjected to harmonic input or to earthquake input. For example, as a representation of a base-isolated building, Westermo and Udwadia [136] studied the periodic response of a linear oscillator on a coulomb friction sliding interface. Contrary to the general perception that friction will always reduce the response, they found that the response may be larger

than that for the same fixed-base model and that the single degree of freedom model had subharmonic resonance frequencies generated by the sliding interface. The response of a similar model to earthquake input was studied by Mostaghel et al. [85, 87].

The assumption of coulomb friction is generally used in these theoretical analyses but is unlikely to be an accurate representation of real behavior. The most commonly used materials for sliding bearings are unfilled or filled polytetrafluoroethylene (PTFE, or Teflon) on stainless steel, and the frictional characteristics of this system are dependent on temperature, velocity of interface motion, degree of wear, and cleanliness of the surface. Much testing work has been done on these aspects of the mechanical behavior of such sliding components [126, 127], and an extensive review was done by Campbell and Kong [28].

3.3.1 Electricité-de-France System

This system was developed in the early 1970s for application to nuclear power plant facilities. The utility developed a standard nuclear power plant with the safety grade equipment qualified for $0.2g$ acceleration. When the standard plant was to be located at sites of higher seismicity, it was isolated to keep the equipment acceleration levels below the qualification value. The system combines laminated neoprene bearings (essentially standard bridge bearings manufactured to higher quality control standards) with lead–bronze alloy in contact with stainless steel, the sliding surface being mounted on top of the elastomeric bearing. The coefficient of friction of the sliding surface is supposed to be 0.2 over the service life of the isolator. The neoprene pad has a very low displacement capacity, probably not more than ±5.0 cm (2 in.). When the displacements exceed this, the sliding element provides the needed movement. The system does not include any restoring device and permanent displacements could occur. The system has been implemented only once in a large nuclear power plant at Koeberg, South Africa [57].

3.3.2 EERC Combined System

A combination elastomeric and sliding system was developed and tested on the shake table at the EERC. In this system the interior columns of the structure were carried on Teflon on stainless steel sliding elements and the exterior columns on the low-damping natural rubber bearings. The elastomeric bearings provided recentering capability and controlled the torsion of the structure while the sliding elements provided damping [29].

A variant of this system was used to retrofit both the Mackay School of Mines at the University of Nevada, Reno, Nevada, and a new hospital for the County of Los Angeles, the M. L. King, Jr.–C. R. Drew Diagnostics Trauma Center in Willowbrook, California. Both of these structures used HDNR elastomeric bearings; teflon–stainless steel sliding elements were used in the university building while lead–bronze alloy plates on stainless steel were used for the hospital.

3.3.3 The TASS System

The TASS system was developed by the TAISEI Corp. in Japan [62]. In this system the entire vertical load is carried on Teflon–stainless steel elements. In addition, laminated neoprene bearings that carry no load are used to provide recentering forces. The Teflon sliding surface has a pressure of around 10 MPa (1450 psi), and the coefficient friction ranges from 0.05 at slow sliding speeds to around 0.15 at higher speeds. The disadvantages of this system are that because the elastomeric bearings carry no vertical load, they experience tension, and the velocity sensitivity of the sliding surface makes modeling of the system quite difficult.

3.3.4 Resilient-Friction Base Isolation System

The resilient-fraction base isolation (R-FBI) bearing attempts to overcome the problem of the high friction coefficient of Teflon on stainless steel at high velocities by using many sliding interfaces in a single bearing. Thus the velocity between the top and bottom of the bearing is divided by the number of layers so that the velocity at each face is small, maintaining a low friction coefficient (Fig. 3.7). In addition to the sliding elements, there is a central core of rubber that carries no vertical load but provides a restoring force. Tests of this system found

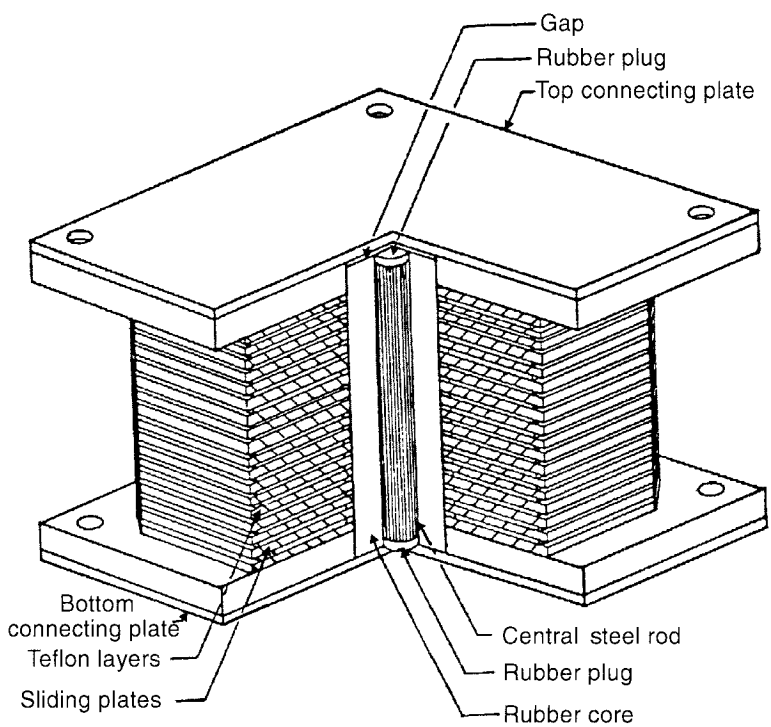

Fig. 3.7 Resilient-friction base isolation system.

that the rubber core did not prevent the displacement from being concentrated at a single interface; therefore, a central steel rod was inserted in the rubber core that improved the distribution of displacement among the sliding layers [84, 86, 88]. A shake table experimental test program using R-FBI bearings and a five-story, 40-ton steel frame model was carried out at the EERC in 1988 [89].

3.3.5 Friction Pendulum System

The friction pendulum system (FPS) is a frictional isolation system that combines a sliding action and a restoring force by geometry. The FPS isolator, shown schematically in Fig. 3.8, has an articulated slider that moves on a stainless steel spherical surface [5]. The side of the articulated slider in contact with the spherical surface is coated with a low-friction composite material. The other side of the slider is also spherical, coated with stainless steel, and sits in a spherical cavity, also coated with the low-friction composite material. As the slider moves over the spherical surface, it causes the supported mass to rise

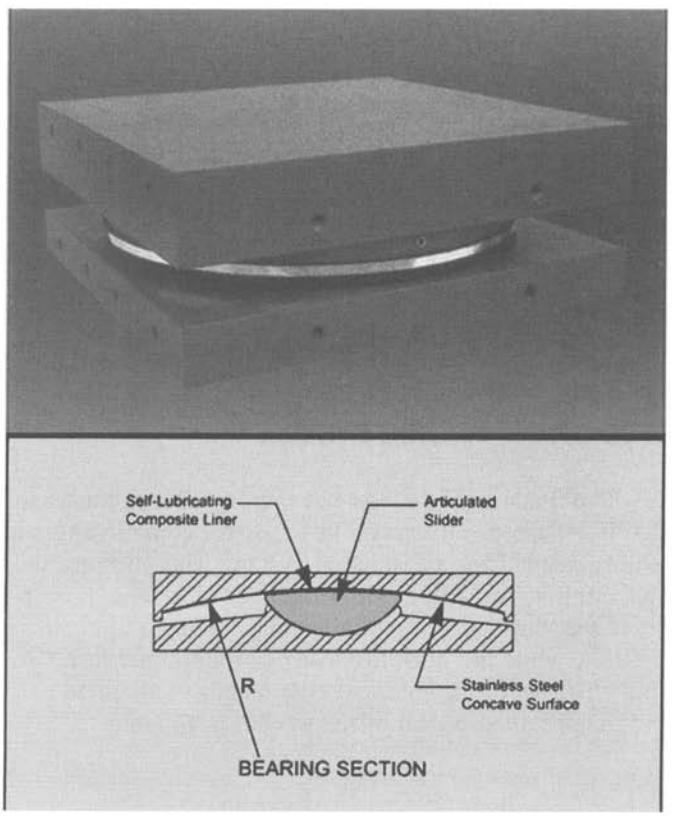

Fig. 3.8 Schematic of friction pendulum system.

and provides the restoring force for the system. Friction between the articulated slider and the spherical surface generates damping in the isolators. The effective stiffness of the isolator and the isolation period of the structure is controlled by the radius of curvature of the concave surface.

3.4 SPRING-TYPE SYSTEMS

Elastomeric and sliding isolation systems are usually configured to provide only horizontal isolation. When full three-dimensional isolation is required, it is possible, but not common, to use elastomeric bearings. Generally, spring-type systems have been used in these cases.

GERB System The GERB system for seismic isolation was developed originally for the vibration isolation of power plant turbine generating equipment. It uses large helical steel springs that are flexible both horizontally and vertically. The vertical frequency is around 3–5 times the horizontal frequency. The steel springs are completely without damping and the system is always used in conjunction with the GERB viscodamper. As in all three-dimensional systems, there is very strong coupling between horizontal motion and rocking motion because the center of gravity of the isolated structure is above the center of stiffness of the isolation system. This type of system becomes practical in situations where the center of gravity and the center of stiffness are at the same level—in a reactor vessel in a nuclear power plant, for example.

The system has been tested on the shake table at Skopje, Macedonia, and has been implemented in two steel frame houses in Santa Monica, California (see Fig. 3.9). These houses were strongly affected by the 1994 Northridge earthquake. Their response was monitored by strong motion instruments and demonstrates that the isolation system was not effective in reducing the accelerations in these buildings due to the rocking motion [76].

3.5 SLEEVED-PILE ISOLATION SYSTEM

In situations where it is necessary to use deep piles—for example, for buildings on very soft soil—it can be advantageous to use these piles to provide the horizontal flexibility needed for an isolation system. The piles are made flexible by enclosing them in tubes with a suitable gap for clearance. It is an interesting consequence of the mechanics of columns that the horizontal stiffness is proportional to EI/l^3, while the buckling load is proportional to EI/l^2, where EI is the bending stiffness of the pile and l its length. If the load carried on the pile is W and the specified period of the system is T, then

$$\frac{\alpha EI}{l^3} = \frac{W}{g}\left(\frac{2\pi}{T}\right)^2$$

Fig. 3.9 GERB system: Lowe residences.

where α is a factor depending on the fixity at each end of the pile. The buckling load of the pile is

$$P_{\text{crit}} = \frac{\beta EI}{l^2}$$

where β depends on the fixity. The safety factor against buckling is given as

$$\text{SF} = \frac{P_{\text{crit}}}{W} = \frac{\alpha}{\beta} \frac{l}{gT^2}$$

thus, for a fixed vertical load and specified horizontal frequency or period, the safety factor against buckling increases as the piles get longer.

This system was implemented in one of the earliest base isolation projects, the Union House in Auckland, New Zealand, which was completed in 1983 [24]. The building, located in an area of poor soil, required extending piles to the bedrock

about 10 m (33 ft) below the surface. These piles are enclosed by steel sleeves with a clearance of 150 mm (6 in.). The building is 12 stories tall of reinforced-concrete construction with exterior bracing. The superstructure is very stiff, and the period of the building on the sleeved-pile system is around 4 sec. Damping is provided by the elastic–plastic deformation of a set of tapered steel plates arranged around the perimeter of the building at ground level. The dampers are located to the top of the sleeved piles and react against an independently supported basement structure. The steel dampers provide elastic stiffness in addition to damping, reduce the period to around 2 sec, and provide an effective damping of about 12%.

A similar approach was used to isolate the Wellington Central Police Station [31]. Completed in 1991, this 10-story reinforced-concrete braced frame structure is supported on 15 m (49.2 ft) long sleeve piles with a clearance of 375 mm (15 in.). The building structural system uses external diagonal bracing. The site is very close to an active fault and the seismic requirements are quite severe. Damping is provided by 24 lead extrusion dampers [109], with a yield level of 250 kN (56.2 kips) and a stroke of ±400 mm (15.7 in.) with lead extrusion dampers as the supplementary system.

A variant of this system is being used for the Randolf Langenbach house in Oakland, California. Referred to as the *damped-sway foundation system*, it uses sleeved piles and hydraulic viscous dampers (Fig. 3.10). A rubber bumper sys-

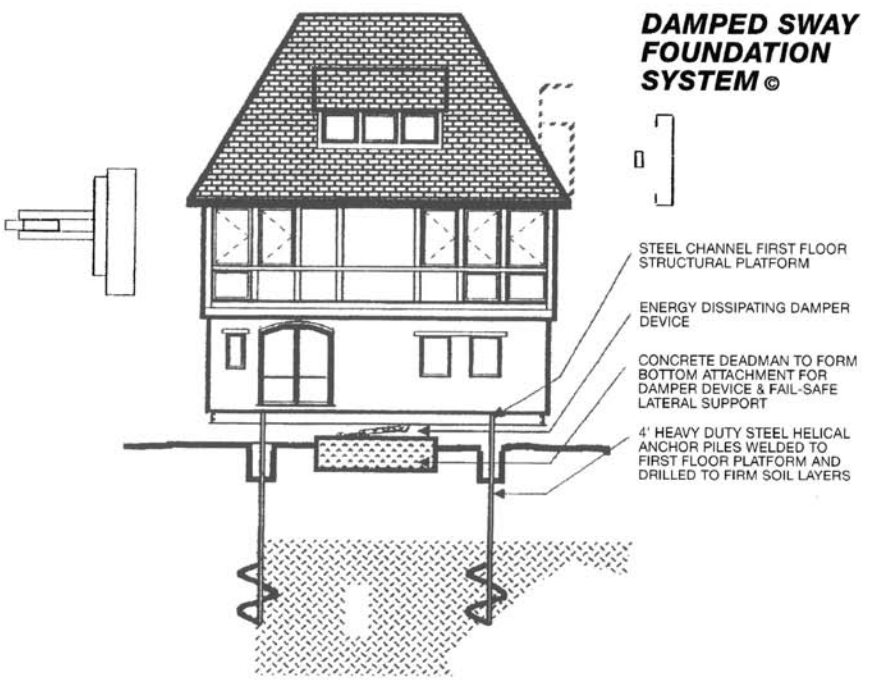

Fig. 3.10 Damped-sway foundation system. (Reproduced with permission of Randolf Langenbach.)

tem is also provided. The developer of the system [71], who is also the owner of the house, estimates that the system has increased the construction cost of the house by $10,000, which represents around 3% of the total cost of the house.

3.6 ROCKING SYSTEMS

Tall slender structures of top-heavy construction will inevitably develop overturning moments that will produce tension at the foundation level. It is extremely expensive to provide tension capacity in building foundations using anchors in deep caissons. As an alternative, it is possible to allow the columns—or piers in the case of bridges—to step off the foundation. This form of partial isolation reduces the seismic loads throughout the structure, particularly the tension forces generated in columns or piers. The dynamics of the stepping structure are quite different from conventional structures but have been extensively studied both theoretically [137] and experimentally in shake table tests at the EERC [33, 67].

This concept has been implemented in a railway bridge in New Zealand [36]. The South Rangitikei River Bridge (Fig. 3.11) has 69-m (226-ft-) long piers that are designed to lift off of the foundation under seismic loading. Inside each pier

Fig. 3.11 South Rangitikei River Bridge.

are two large energy-dissipating devices that are based on the elastic–plastic torsion of mild-steel bars. These provide controlling forces to the piers, both when the pier is moving up and when it is moving down. These devices were designed and tested at the Department of Scientific and Industrial Research Physics and Engineering Laboratory in New Zealand in 1971–1972 [66] and are the first use of energy-dissipating devices in seismic-restraint design. The method has not been used again for bridges but could be a very promising retrofit strategy for large bridges such as the Golden Gate Bridge, the Oakland Bay Bridge, and the Williamsburg Bridge. This approach was used later to isolate a tall chimney structure in Christchurch, New Zealand; in this case tapered-plate steel dampers were included [113].

CHAPTER 4

CODE PROVISIONS FOR SEISMIC ISOLATION

4.1 INTRODUCTION

The design of new seismically isolated buildings in United States is currently governed by either of two codes: the 1997 edition of the Uniform Building Code (UBC-97) published by the International Conference of Building Officials [55], or Title 24, Part 2 of the California Code of Regulations, Division III [115] (referred to as OSHPD-96). Title 24 is very similar to the 1994 UBC but includes more rigorous design requirements for base-isolated hospitals and other state buildings in California. By the time this book reaches the market, it is anticipated that OSHPD-96 will be revised to be compatible with the UBC-97 requirements.

Intended to regulate the design of new buildings, the UBC and OSHPD-96 do not cover the retrofit of existing buildings using isolation, although most retrofit projects do follow the UBC regulations closely. In addition, the UBC does not address the issue of vertical isolation, nor does it cover the isolation of equipment or artifacts such as art objects in museums. The regulations are written in such a way as to be nonspecific with respect to isolation systems. No particular isolation systems are identified as being acceptable, but the regulations require that any isolation system should be stable for the required displacement, provide increasing resistance with increasing displacement, and have properties that do not degrade under repeated cyclic loading.

The underlying philosophy of these codes is that an isolated building designed using these regulations will be expected to outperform fixed-base construction in moderate and large earthquakes. The intent of the code is not to reduce the cost of the structure but to control damage to the structure and its contents by taking advantage of the fact that seismic isolation permits an elastic response in the structure and low floor accelerations for large earthquake input.

Design of Seismic Isolated Structures: From Theory to Practice. F. Naeim and J. M. Kelly

Increasingly, the seismic upgrade design of existing structures is influenced by the National Earthquake Hazards Reduction Program (NEHRP) Guidelines for the Seismic Rehabilitation of Buildings (FEMA-273) and its commentary (FEMA-274), which are published by the Federal Emergency Management Agency [41, 42]. The FEMA-273 provisions are very similar to those of the UBC-97 with one exception: FEMA-273 permits a new analysis approach called *static nonlinear analysis* or the "*pushover*" method.

These codes and guidelines have evolved from design provisions that were developed in the 1980s by a subcommittee of the Structural Engineers Association of Northern California (SEAONC). In 1986 SEAONC published a document [121]—known as the Yellow Book—entitled "Tentative Seismic Isolation Design Requirements." These provisions have served as the basis for various procedures recommended by the Structural Engineers Association of California (SEAOC) and implemented in the various editions of the UBC, the most widely used code for the design of earthquake-resistant buildings in the United States. In the Yellow Book, emphasis was placed on equivalent lateral-force procedures and the level of seismic demand was that required for the design of fixed-base structures—a level of ground motion that has a 10% chance of being exceeded in a 50-year period. Dynamic methods of analysis were permitted (and for some types of structures required), but the simple, statically equivalent formulas provided a minimum level for the design.

In this chapter we introduce and critically evaluate the required procedures of the 1997 UBC. Where appropriate, we will compare and contrast UBC-97 requirements with those of OSHPD-96, FEMA-273, and other important documents.

4.2 SEISMIC HAZARD LEVEL

The seismic criteria adopted by current model codes involve a two-level approach to seismic hazard, which are as follows:

- **Design Basis Earthquake (DBE).** That level of ground shaking that has a 10% probability of being exceeded in 50 years (475-year return period earthquake).
- **Maximum Capable Earthquake (MCE).** The maximum level of ground shaking that may ever be expected at the building site. This may be taken as that level of ground motion that has a 10% probability of being exceeded in 100 years (1000-year return period earthquake)

The NEHRP-97 [100] and FEMA-273 documents refer to the DBE as BSE-1 (Basic Safety Earthquake 1) and the MCE as BSE-2 (Basic Safety Earthquake 2). The SEAOC Vision-2000 document [120] describes a DBE as *rare* and a MCE as *very rare* events, respectively.

4.3 DESIGN METHODS

Earlier versions of the UBC code emphasized a simple, statically equivalent method of design that took advantage of the fact that for an isolated structure the displacements are concentrated at the isolation level and, therefore, the superstructure moves almost as a rigid body. The design was based on a single mode of vibration, and the design forces for the superstructure were computed from the forces in the isolators at the design displacement. This resulted in a very simple design process. As the code has evolved, however, the situations where dynamic analysis must be used have increased, and incentives have been inserted in the code to encourage the use of dynamic analysis in cases where it may not be required.

For all seismic isolation designs it is necessary to perform a static analysis. This establishes a minimum level for design displacements and forces. The static analysis is also useful both for preliminary design of the isolation system and the structure when dynamic analysis is required and for design review; under certain circumstances it may be the only design method used.

Dynamic analysis is required in many cases (in all cases by OSHPD-96) and may be carried out in the form of a response spectrum analysis or a time history analysis. Site-specific ground motions are required in the following cases:

- The isolated structure is located on a soft soil, soil type S_3 or S_4.
- The isolated structure is within 10 km (6.2 miles) of a known active fault [15 km (9.3 miles) in OSHPD-96].
- The isolated structural period (MCE) is greater than 3 sec.

A response spectrum analysis is required in the following cases:

- Site-specific spectra are required.
- The superstructure is irregular, either horizontally or vertically.
- The building is more than four stories or 19.8 m (65 ft) in height.
- The isolation period of the structure (DBE) is less than three times the elastic fixed-base period (i.e., $\epsilon > \frac{1}{9}$).

Time history analysis may be used in lieu of response spectrum analysis, but if either the isolation system or the superstructure is highly nonlinear, a time history analysis is required.

4.4 STATIC ANALYSIS

The static analysis formulas provide displacements and forces and are based on constant-velocity spectra over the period range 1.0–3.0 sec. In UBC-94 [54] and OSHPD-96, the value of the constant-velocity spectrum is derived from

the Applied Technology Council provision ATC-3-06 [13] and for $Z = 0.40$, a soil factor $S = 1$, and 5% damping is 0.60 m/s (23.6 in./sec), leading to a displacement spectrum S_D given by

$$S_D = \frac{S_V}{\omega} = \frac{T}{2\pi}\frac{Z}{4}(0.60) \approx 0.25ZT \text{ m } (10ZT \text{ in.})$$

The spectrum is then modified by a soil factor and a damping factor and adjusted for other seismic zones, leading to the required design displacement D. The three levels of displacement to be calculated are as follows:

- D, the design displacement, being the displacement at the center of rigidity of the isolation system at the DBE;
- D_T, the total design displacement, being the displacement of a bearing at a corner of the building and including the component of the torsional displacement in the direction of D; and
- D_{TM}, the total maximum displacement, being the total design displacement evaluated at the MCE.

The design displacement D in UBC-94 and OSHPD-96 is the starting point for the entire design process and must always be calculated whether or not dynamic analysis is used. It is based on the assumption that the superstructure deformations are negligible and is given by

$$D = \frac{0.25ZNS_IT_I}{B} \text{ m} \qquad \left(\frac{10ZNS_IT_I}{B} \text{ in.}\right) \tag{4.1}$$

where Z = seismic zone coefficient (e.g., 0.4 in zone 4)
N = near-field coefficient
S_I = soil coefficient
T_I = effective period in seconds
B = damping coefficient

While the concept is still the same, the UBC-97 formulation is more complex. A large number of new terms have been added to the code. For example, there are now six different displacements that have to be computed. The number of soil profile types has been increased to six, of which three are hard rock, rock, and soft rock. There are four seismic coefficients to be calculated, but in zone 4, where most isolated buildings in the United States are located, it is necessary to calculate the following factors: N_a and N_v, which depend on seismic source type and seismic source distance; M_M, which depends on ZN_v; and C_{AM} and C_{VM}, which depend on M_M, N_a, and N_v. The result is that the simple static analysis computation of the earlier versions of the code has been replaced by a sequence of table definitions and formulas.

Although all isolated projects are currently designed using dynamic analysis (based on time histories, as there are many computer programs now available for this purpose), static analysis is still required to ensure that the design quantities do not fall below certain minimal levels determined from the static analysis.

According to UBC-97, the two basic displacements to be calculated are D_D and D_M, or DBE and MCE displacement at the center of rigidity of the isolation system. They are calculated using the formulas

$$D_D = \frac{(g/4\pi^2)C_{VD}T_D}{B_D} \quad \text{mm or in.} \tag{4.2}$$

$$D_M = \frac{(g/4\pi^2)C_{VM}T_M}{B_M} \quad \text{mm or in.} \tag{4.3}$$

where g is the gravitational acceleration, C_{VD} and C_{VM} are seismic coefficients, T_D and T_M are isolated periods, and B_D and B_M are damping coefficients corresponding to the DBE and MCE level responses, respectively. The terms C_{VD} and C_{VM} are functions of the seismic zone factor Z, the site soil profile type, and one of the two near-source factors, N_V. Definitions of these and other factors needed for calculating D_D and D_M are presented in the following sections.

4.4.1 Seismic Zone Factor *Z*

Seismic zone factors vary from 0.075 for zone 1 to 0.40 for zone 4 as shown in Fig. 4.1 (UBC-97, Table 16-I). Seismic zone factors are the same as in previous editions of the UBC.

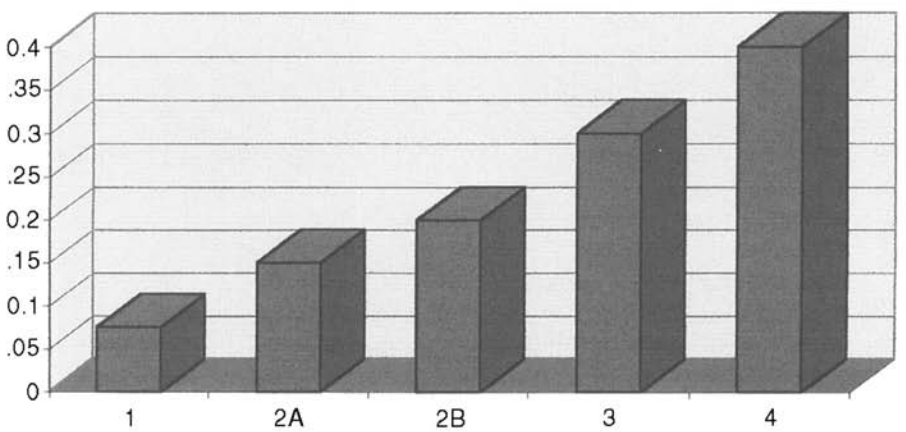

Fig. 4.1 UBC-97 seismic zone factors.

4.4.2 Site Soil Profile Type

Site soil profiles of S_A to S_E are based on the average shear wave velocity in the top 30.5 m (100 ft) of soil (see Fig. 4.2 or UBC-97, Table 16-J). This velocity varies from under 180 m/s (590 ft/sec) for the soft soils (S_E) to over 1500 m/s (4921 ft/sec) for the hard rock profile (S_A). It should be noted that S_A rock in continental United States is found only in eastern United States. Hard rock found in California is classified as S_B, for example. Another class of soil profile type (S_F) requires site-specific evaluation and is not classified based on average shear wave velocity and constitutes very poor site soil conditions prone to liquefaction problems.

4.4.3 Seismic Source Types: A, B, and C

Seismic faults are grouped into three categories based on the seriousness of the hazard they represent. Faults capable of producing large-magnitude earthquakes ($M \geq 7.0$) and have a high rate of seismic activity [annual average seismic slip rate, SR, of 5 mm (0.2 in.) or more] are classified as type A sources. Faults capable of producing moderate-magnitude earthquakes ($M < 6.5$) with a relatively low rate of seismic activity [SR $\leq$ 2 mm (0.08 in.)] are classified as type C sources. All faults other than types A and C are classified as type B sources.

4.4.4 Near-Source Factors: N_a and N_v

Two factors are used to model the ground motion amplification due to near-source effects. The first, N_a, is intended for the short-period range corresponding to a constant-acceleration segment of response spectra. The second factor, N_v, which corresponds to the midperiod range or constant-velocity segment of the response spectra, is the primary near-source factor used in seismic isolation applications. Near-source factors are functions of closest distance to the seismic source and the seismic source type (see Figs. 4.3 and 4.4). UBC-97

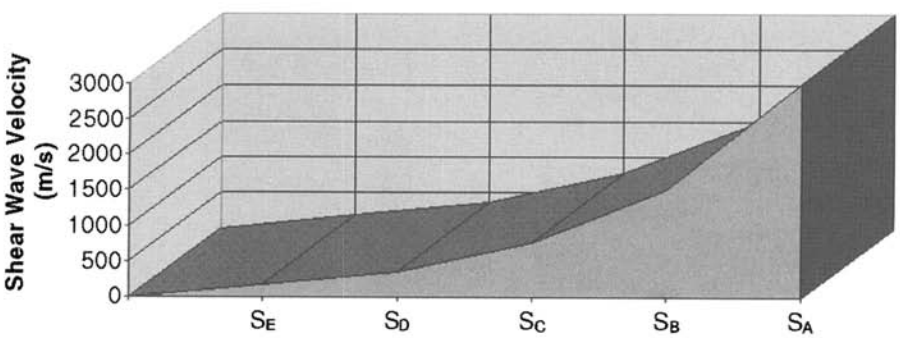

Fig. 4.2 UBC-97 soil-type categories (shear wave velocity range is shown to the right of site profile type).

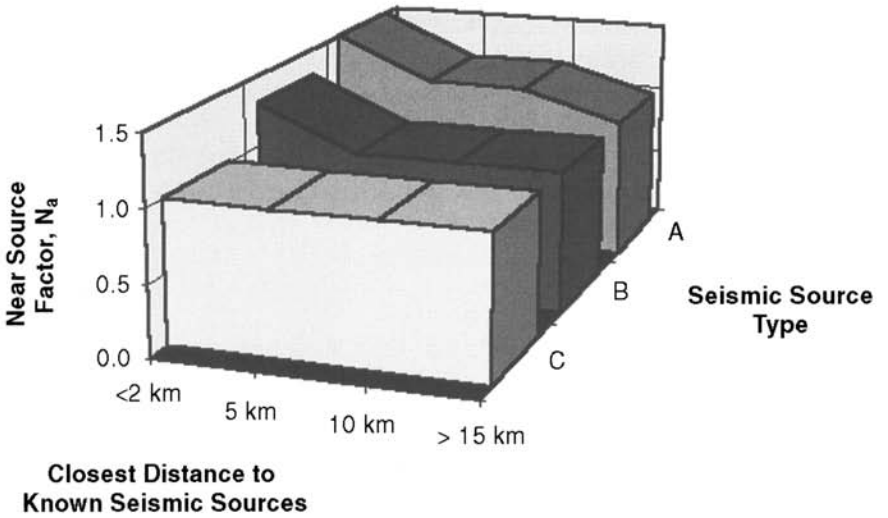

Fig. 4.3 Near-source factor N_a as a function of source type and distance.

defines the site–source distance as the closest distance between the site and the vertical projection of the fault on the surface (see r_{jb} in Fig. 7.7). The surface projection need not include portions of the source at depths 10 km (6.2 miles) or greater; therefore, a site sitting directly on the top of a fault deeper than 10 km (6.2 miles) is not considered a near-source site.

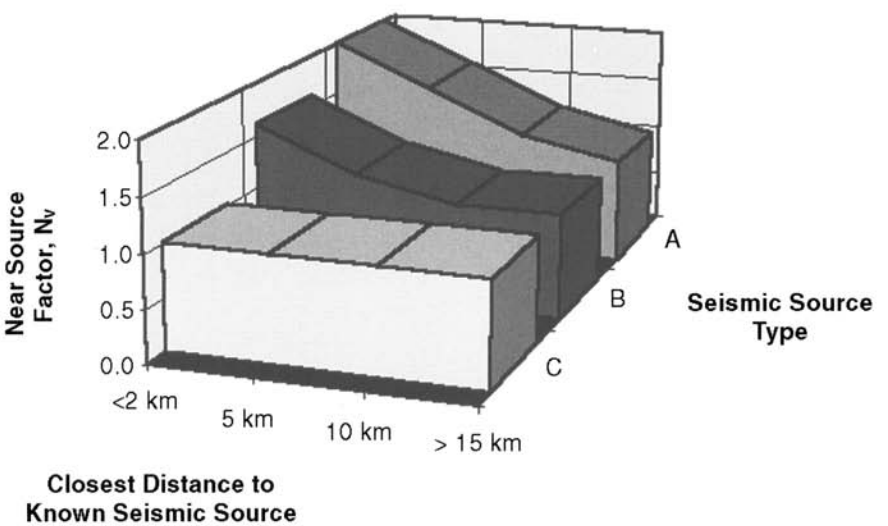

Fig. 4.4 Near-source factor N_v as a function of source type and distance.

4.4.5 MCE Response Coefficient M_M

The MCE response coefficient M_M is intended to estimate the MCE response based on the DBE shaking characteristics. As such, M_M is defined as a function of ZN_v and varies from 2.67 for $ZN_v = 0.075$ to 1.20 for $ZN_v \geq 0.50$ (see Fig. 4.5). The logic for assigning larger M_M values to smaller DBE events stems from the fact that in regions with low seismicity the gap between the DBE and MCE events is generally much larger than that in the zones of high seismicity. Values of M_M are listed in UBC-97, Table A-16-D.

4.4.6 Spectral Seismic Coefficients: C_{VD}, C_{VM} and C_{AD}, C_{AM}

These coefficients are intended to define the minimum spectral ordinates to be used in design. The terms C_{VD} and C_{AD} correspond to constant-velocity and constant-acceleration regions of the DBE spectrum, respectively; C_{VM} and C_{AM} perform the same function for the MCE spectrum. For seismic isolated structures, C_{VD} and C_{AD} are the same as C_V and C_A defined for conventional structures by UBC-97, Tables 16-Q and 16-R. The values of C_{VM} and C_{AM}, however, are given in the Seismic Isolation Appendix of UBC-97 (Tables A-16-G and A-16-F).

As shown in Figs. 4.6 and 4.7, C_{VD} and C_{AD} are functions of seismic zone factor and site soil profile type. Also notice that for zone 4 the values shown in these figures must be multiplied by the appropriate near-source factor N_v or N_a.

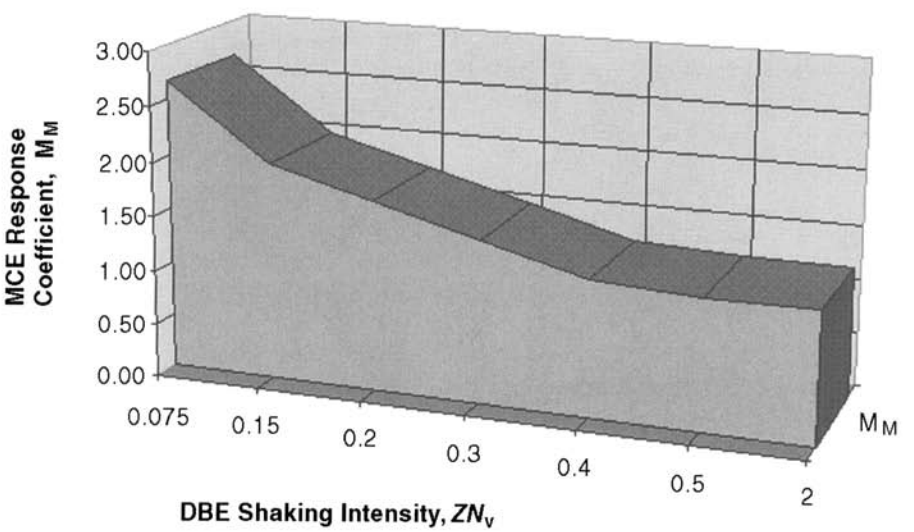

Fig. 4.5 MCE response coefficient M_M.

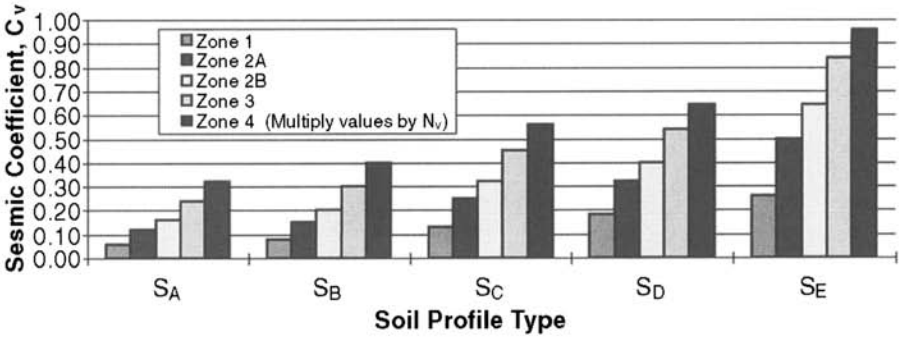

Fig. 4.6 Seismic coefficient C_{VD}.

Similar information for C_{VM} and C_{AM} is shown in Figs. 4.8 and 4.9. Here, the MCE response coefficient comes into play. The values shown in these figures for $M_M Z N_v$ or $M_M Z N_a$ values larger than 0.40 should be multiplied by the factor indicated in the figure.

4.4.7 Damping Coefficients: B_D and B_M

The effective damping in the system, β, at the DBE and MCE response levels (referred to as β_D and β_M) are computed from

$$\beta_D = \frac{1}{2\pi}\left(\frac{\text{total area of hysteresis loop}}{K_{D,\max} D_D^2}\right) \tag{4.4}$$

$$\beta_M = \frac{1}{2\pi}\left(\frac{\text{total area of hysteresis loop}}{K_{M,\max} D_M^2}\right) \tag{4.5}$$

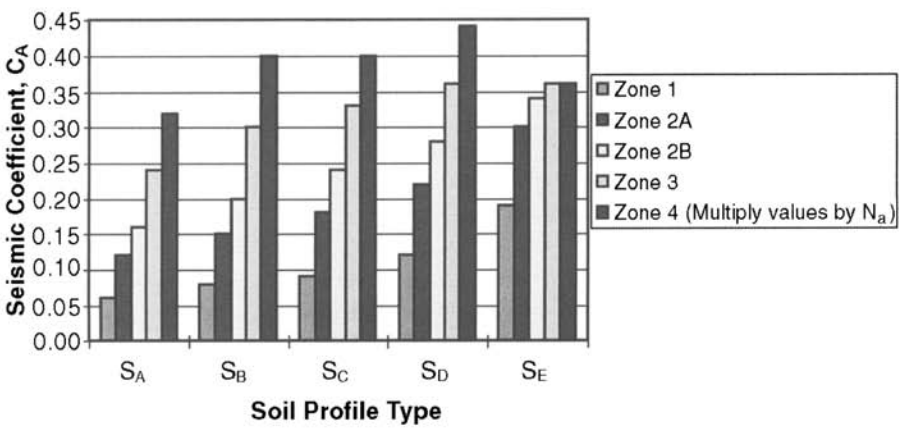

Fig. 4.7 Seismic coefficient C_{AD}.

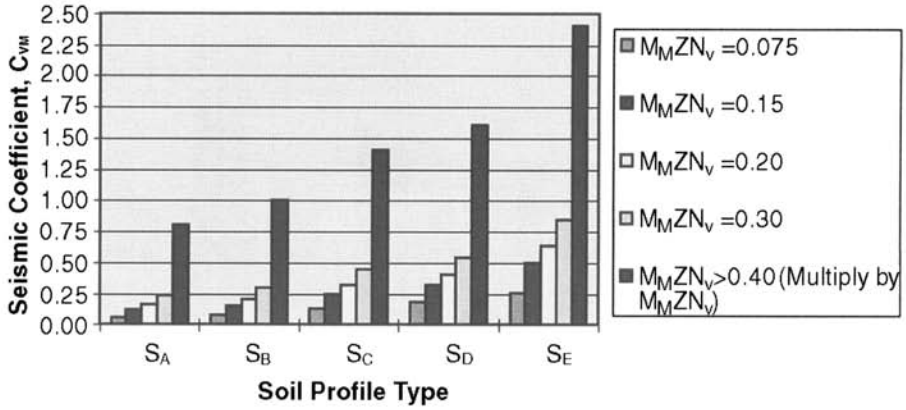

Fig. 4.8 Seismic coefficient C_{VM}.

where $K_{D,\max}$ and $K_{M,\max}$ are effective stiffness terms defined in Section 4.4.8. The damping reduction factor B (B_D for the DBE and B_M for the MCE) is given in terms of β in tabular form (UBC-97, Table A-16-C), with linear interpolation to be used for intermediate values. A very close approximation to the table values is given by

$$\frac{1}{B} = 0.25(1 - \ln\ \beta) \tag{4.6}$$

where β is given as the fraction of critical damping (not as a percentage). Values of B from the code and the formula are shown in Fig. 4.10.

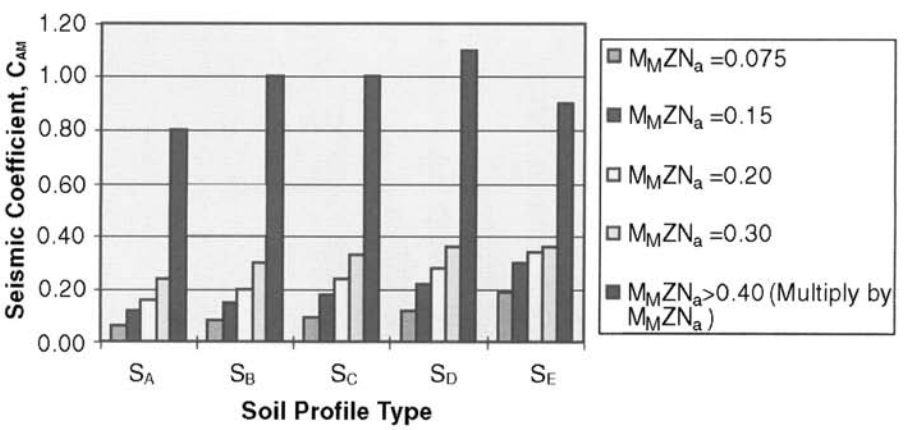

Fig. 4.9 Seismic coefficient C_{AM}.

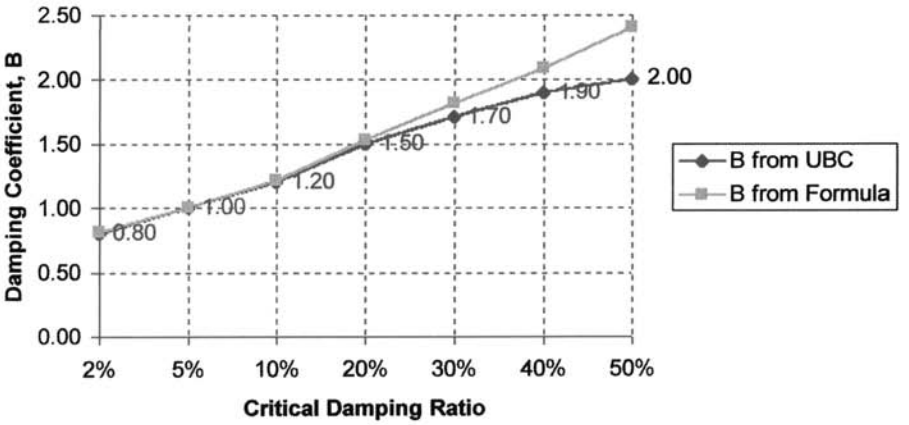

Fig. 4.10 Damping coefficient B from UBC and formula.

4.4.8 Effective System Vibration Periods: T_D and T_M

The periods T_D and T_M that correspond to the DBE and MCE response are computed from

$$T_D = 2\pi \sqrt{\frac{W}{K_{D,\min} g}} \tag{4.7}$$

$$T_D = 2\pi \sqrt{\frac{W}{K_{M,\min} g}} \tag{4.8}$$

where W = weight of building

g = gravity

$K_{D,\text{eff}} = (F_D^+ - F_D^-)/(D_D^+ - D_D^-)$

$K_{M,\text{eff}} = (F_M^+ - F_M^-/(D_M^+ - D_M^-)$

$K_{D,\min}$ = minimum value of $K_{D,\text{eff}}$ at D_D as determined by testing

$K_{D,\max}$ = maximum value of $K_{D,\text{eff}}$ at D_D as determined by testing

$K_{M,\min}$ = minimum value of $K_{M,\text{eff}}$ at D_M as determined by testing

$K_{M,\max}$ = maximum value of $K_{M,\text{eff}}$ at D_M as determined by testing

The values of $K_{D,\min}$, $K_{D,\max}$, $K_{M,\min}$, and $K_{M,\max}$ are not known to the designer during the preliminary design phase. The design procedure will begin with an assumed value of K_{eff}, which is obtained from previous tests on similar components or by using the material characteristics and a schematic of the proposed isolator. After the preliminary design is satisfactorily completed, pro-

totype isolators will be ordered and tested, and the values of $K_{D,\min}$, $K_{D,\max}$, $K_{M,\min}$, and $K_{M,\max}$ will be obtained from the results of the prescribed program of tests on the prototypes. The terms F_D^+, F_D^-, F_M^+, F_M^- and D_D^+, D_D^-, D_M^+, D_M are the maximum and minimum forces and displacements on the prototype bearings, corresponding to DBE and MCE response levels, used to determine the mechanical characteristics of the system. The results of the prototype tests are then used to refine the preliminary design, and when dynamic analysis is used, they establish bounds on the various design quantities. Because the effective stiffness and the effective damping are usually dependent on the displacement, the process of computing the effective system periods and damping is an iterative one.

4.4.9 Total Design Displacements: D_{TD} and D_{TM}

The total design displacements D_{TD} and D_{TM} (which include torsion) are given as

$$D_{TD} = D_D\left(1 + y\,\frac{12e}{b^2 + d^2}\right) \tag{4.9}$$

$$D_{TM} = D_M\left(1 + y\,\frac{12e}{b^2 + d^2}\right) \tag{4.10}$$

where e is the actual eccentricity plus 5% accidental eccentricity and y is the distance to a corner perpendicular to the direction of seismic loading. This formula assumes that the seismic load $K_{\text{eff}}D$ is applied through the center of mass, which is located at a distance e from the center of stiffness (as shown in Fig. 4.11). Assuming a rectangular plan, with dimensions $b \times d$ and a uniform distribution of isolators, the torsional stiffness of the isolation system is $K_{\text{eff}}(b^2 + d^2)/12$, and the rotation θ is thus

$$\theta = \frac{K_{\text{eff}}De}{K_{\text{eff}}[(b^2 + d^2)/12]} = \frac{12De}{b^2 + d^2}$$

The additional displacement due to rotation is

$$\frac{12De}{b^2 + d^2}\,y$$

leading to Eqs. (4.9) and (4.10) above. If the actual torsional stiffness of the system is computed and the additional displacement due to $K_{\text{eff}}D$ through e turns out to be less than the value given by Eqs. (4.9) or (4.10), then this value can be used, but it must be at least 1.1 times D_D and 1.1 times D_M, respectively.

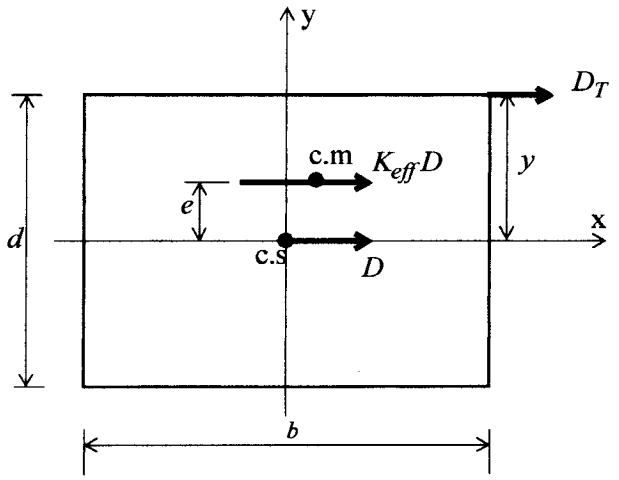

Fig. 4.11 Plan dimensions for calculation of D_{TD} and D_{TM}.

The total maximum displacement D_{TM} is required for verification of the stability of the isolation system.

4.4.10 Design Forces

The strength design forces that the superstructure and the elements below the isolation interface are to be designed for are based on the design displacement D. Elements below the isolation system (working stress design) are calculated using the formula

$$V_b = K_{D,\max} D_D \tag{4.11}$$

The strength level for design of elements above the isolation system in terms of the minimum lateral seismic shear force is given by the formula

$$V_s = \frac{K_{D,\max} D_D}{R_I} \tag{4.12}$$

where R_I is a design force reduction factor (ductility factor) ranging from 1.4 to 2.0. Table 4.1 shows a few examples of fixed-base structural systems with corresponding reduction factor R.

In all cases the value of V_s should not be less than

- the seismic force required by the UBC provisions for a fixed-base structure,
- the base shear corresponding to design wind load, and
- one and a half times the lateral force required to fully activate the isolation

TABLE 4.1 Reduction Factors for Fixed-Base and Isolated Construction

Construction	R_I	R
Special moment-resisting frame	2.0	8.5
Shear wall	2.0	5.5
Ordinary braced frame	1.6	5.6
Eccentric braced frame	2.0	7.0

system, that is, the yield load of a lead-plug rubber bearing or slip threshold of a sliding bearing system.

The reduction factors for fixed-base design are very much higher than those for isolated design for a number of reasons; one major element is period shift. As the structure yields, the period lengthens and the force demand is reduced. Simultaneously, the damping in the structure is increased because of hysteretic action due to yielding in the structural system. In addition, overstrength and redundancy tend to spread the yielding to other elements. In the case of an isolated structure, only overstrength and redundancy are applicable.

For example, if a moment-resisting steel frame is used for the superstructure, the reduction factor allowed by the code is 2.0 to allow for overstrength and redundancy, implying that (a) the structural system will yield at a force level that is twice the nominal yield level and (b) the system will be just on the verge of actual yield at the forces specified by the code formula. Period shift in the structure counters the effectiveness of the isolation system because it decreases the separation between the fixed-base period and the isolation period and could bring larger forces to the structure and more participation from the higher modes. In addition, the damping in the isolated structure will not be as great as in the fixed-base structure. For all these reasons, the R_I factors are substantially smaller than the R factors for the same structural system. Note, larger ductility demands can mean damage to the structural and nonstructural components; thus, the requirement for lower R_I values is equivalent to damage control for isolated structures.

4.4.11 Vertical Distribution of Force

In earlier versions of the code, the vertical distribution of the inertial forces on the structural system was based on the assumption that the participation of the higher modes was negligible and that the accelerations were roughly the same at all levels of the structure. There was some concern, however, that this might not be sufficiently conservative, and the vertical distribution was changed in subsequent editions of the UBC code to one where the lateral force at level x, denoted by F_x, is computed from the base shear V_s by

$$F_x = V_s \frac{h_x w_x}{\sum_{i=1}^{N} w_i h_i} \tag{4.13}$$

where w_x and w_i are the weights at level i or x and h_x and h_i are the respective heights of structure above isolation level.

This formula leads to a triangular distribution of force. While the basic theory would indicate that the distribution should be close to a uniform one, a triangular distribution is specified to account for higher mode contributions generated by nonlinearities in the isolation system, for example, because of lead plugs in elastomeric bearings or the effects of friction in sliding bearings.

What are the implications of this code requirement in terms of a seismic base shear coefficient C_S. If Eq. (4.7) is substituted into Eq. (4.1) and divided by the structure weight W to give C_S, we find

$$C_S = \frac{V_s}{W} = \frac{NZS}{B} \frac{1}{T} \frac{1}{R_I}$$

For example, if $N = 1$, $Z = 0.40$, and $S = 1.40$ (UBC-94 S_2 soil type, which is roughly equivalent to UBC-97 S_E soil profile type) and the system has 10% equivalent viscous damping, then

$$C_S = (0.47)\left(\frac{1}{T} \frac{1}{R_I}\right)$$

so that for a frame structure with $R_I = 2$ and a period of 2.0 sec the code prescribed C_S is 0.1175. The comparable C_S for a fixed-base structure in the same zone and soil type is given by

$$C_S = \frac{0.60}{T^{2/3}} \frac{1}{R}$$

and because $R = 8.5$ when $R_I = 2$, the design shear coefficient is equal to 0.0706 for a 1.0-sec period fixed-base building. Clearly, the reductions in the seismic force that are expected from isolation (around $\epsilon^{1/2}$) are not available to the designer.

4.4.12 Drift Limits

The maximum interstory drift limits for isolated buildings are also more severe than the limits for fixed-based buildings and should not exceed $0.01/R_I$ (i.e., the elastic deformation due to $K_{D,\max} D_D$ applied in a triangular pattern to the structure

should not exceed 1%). This limit is less than half of 2.5% permitted for fixed-based buildings with fundamental periods of less than 0.70 sec and half of the 2% limit permitted for fixed-based buildings with longer fundamental periods.

4.5 DYNAMIC ANALYSIS

Design spectra: Site-specific spectra are required if

- $T_M \geq 3.0$ sec or
- the soil type is S_E, S_F or
- the structure is located within 10 km (6.2 miles) of an active fault.

Dynamic analysis is also required if the effective period of the isolated structure, T_D, is greater than three times the elastic fixed-base period of the structure above the isolation system. If a site-specific spectrum is used, it may be higher, but if smaller, it cannot be less than 80% of the codified response spectrum.

4.5.1 Time History Analysis

Pairs of horizontal components from at least three recorded events are necessary for a time history analysis. The events must be representative of the site, soil, and source characteristics and have durations consistent with the DBE and MCE. Time histories developed for a site within 15 km (9.3 miles) of a major active fault are required to incorporate near-fault phenomena, although near-fault phenomena are not defined. More detailed information on time history analysis requirements are given in Chapter 7.

4.5.2 Scaling

For each ground motion pair, the SRSSs of the 5% damped spectra are computed. The motions are then scaled (multiplied by a factor) so that the average of the SRSS spectra does not fall below 1.3 times the target spectrum for the DBE or MCE by more than 10% over $0.5T_D$ seconds to $1.25T_M$ seconds. When dynamic analysis is used, the design values are calculated in the following way:

- If three time histories are used, the design must be based on maximum response quantities.
- If seven times histories are used, the design can be based on average response quantities.

When dynamic analysis is done, it is possible to have design displacements and design forces that are less than those given by the equivalent static formulas.

Code-specified limits, which limit to what extent the design values can fall below the static values, are summarized in Table 4.2.

The total design displacement D_{TD} for the isolation system can be reduced to not less than 90% of that given by the static formula, and the total maximum displacement D_{TM} can be reduced to not less than 80% of the static formula result. The D_{TD} and D_{TM} are computed from D_D and D_M by the use of multipliers, and the code permits a further reduction by replacing D_D and D_M in the static formulas by D'_D, and D'_M, where

$$D'_D = \frac{D_D}{\sqrt{1 + (T/T_D)^2}} \tag{4.14}$$

$$D'_M = \frac{D_M}{\sqrt{1 + (T/T_M)^2}} \tag{4.15}$$

with T being the elastic fixed-base period of the superstructure computed by the empirical formula of the code.

This further reduction is to allow for the flexibility of the superstructure. The static formulas [Eqs. (4.2) and (4.3)] assume that the superstructure is rigid and that if some deformation takes place in the superstructure, the displacement in the isolation system is reduced. But by using the two-degree-of-freedom (2-DOF) model developed earlier and ignoring the approximations for small ϵ, it is possible to show that this formula is not quite correct. This straightforward analysis and the result, which depends on mass ratio γ and frequency ratio ω_b/ω_s and is shown in Fig. 4.12, demonstrate that the formula corresponds to the result for $\gamma = 1$, corresponding to $m_b = 0$ (i.e., a single-degree-of-freedom system). For all values of $\gamma < 1$ and for $\omega_b/\omega_s \leq 1$, the analysis shows that the correction [Eqs. (4.14) and (4.15)] overestimate the reduction in D_D and D_M due to flexibility in the superstructure.

TABLE 4.2 Code Minimum Values When Dynamic Analysis Is Used

Parameter	Static	Response Spectra	Time History
D_{TD}	$D_{TD} \geq 1.10D_D$	$0.90D_{TD}$	$0.90D_{TD}$
D_{TM}	$D_{TM} \geq 1.10D_M$	$0.80D_{TM}$	$0.80D_{TM}$
V_b	$V_b = k_{D,\max}D_D$	$\geq 0.90V_b$	$\geq 0.90V_b$
V_s regular	$V_s = k_{D,\max}D_D/R_I$	$\geq 0.80V_s$	$\geq 0.60V_s$
V_s irregular	$V_s = k_{D,\max}D_D/R_I$	$\geq 1.0V_s$	$\geq 0.8V_S$
Drift	$0.010/R_I$	$0.015/R_I$	$0.020/R_I$

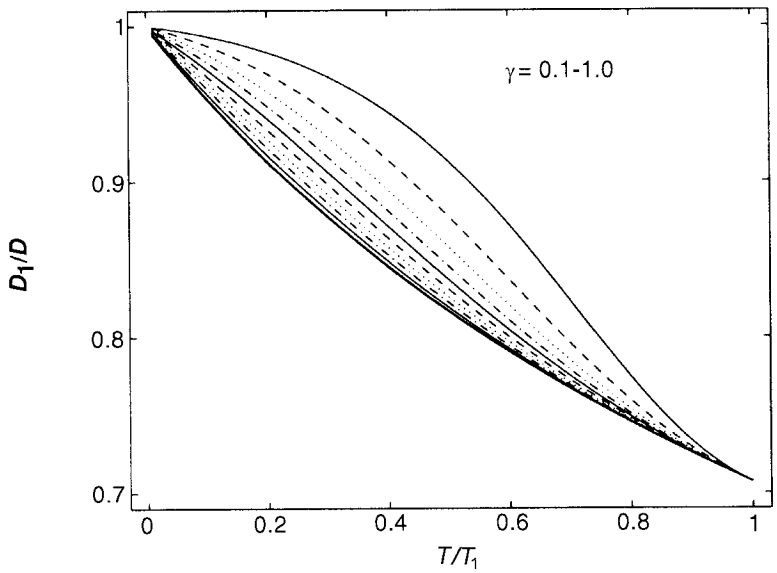

Fig. 4.12 Reduction of design displacement due to flexibility in the superstructure.

4.6 OTHER REQUIREMENTS FOR NONSTRUCTURAL COMPONENTS

For strength design of nonstructural components, either fixed-base requirements may be used or the peak response seismic force computed. Components that cross the interface should be designed for D_{TM}, while fixed-base design procedures are used below the isolation system. In addition, there are other detailed system requirements that must be considered; these include environmental conditions, wind forces, fire resistance, and lateral restoring force.

4.7 PEER REVIEW

The code mandates that there be a peer review of the design of the isolation system. The review team should include persons licensed in the appropriate disciplines and experienced in the theory and application of isolation. The review should evaluate the seismic criteria, the preliminary design, and the final design. In addition the panel should review the prototype test program and the proposed quality control test program. The peer review panel normally includes three people: a structural engineer, an expert in ground motions, and an expert in seismic isolation.

4.8 DESIGN AND TESTING REQUIREMENTS FOR ISOLATORS

There are a number of design requirements for the isolator units that are derived from loads produced on the isolators due to overturning of the building as a result of horizontal accelerations. The building has to be checked for global overturning at the MCE with the full dead load being used in the calculation. Uplift of individual isolators is permitted when this check is made. When some isolators uplift, others will experience increased downward load, and the isolators are required by the code to be designed and tested for this increased downward load as well as net upward load, if any. The precise design requirement states that an isolator should be stable when displaced to the total maximum displacement D_{TM} under $1.2DL + 1.0LL + E_{\max}$ and $0.8DL - E_{\min}$ at the MCE, where $E_{\max}$ is the maximum downward and $E_{\min}$ is the minimum downward (or maximum upward) vertical load on an isolator caused by overturning of the superstructure. The increased or decreased dead load is intended to provide an allowance for vertical accelerations in the ground motion.

This requirement appears again in the testing requirements for the isolators. In many isolation projects the information needed for the preliminary design of the isolation system and the superstructure is obtained by qualification or preprototype tests that are not covered by the regulations. After the preliminary design is completed, isolators are manufactured, and a very extensive program of prototype tests are performed. The code requires that at least two full-sized specimens of each type of isolator be tested. The tests required are a specified sequence of horizontal cycles under $DL + 0.5LL$ for small horizontal displacements up to the total maximum displacement, with these primarily establishing the mechanical characteristics of the bearings for use in verifying the design. A sequence of extreme load tests are required where horizontal displacement cycles are combined with maximum and minimum downward loads. The maximum vertical load for these tests is defined as $1.5DL + 0.5LL + E_{\max}$ and the minimum is $0.8DL - E_{\min}$. In some cases it is possible that the minimum load may actually be a tension load.

Although rubber bearings can take a certain amount of tension, it is very difficult to carry out such a test because most test machines are unable to generate tension forces and apply shear displacements simultaneously. Upward forces on isolators tend to occur in designs where the horizontal forces in the superstructure are carried by a few lines of lateral resistance. This leads to high overturning forces on a few isolators because the dead load on these isolators is not enough to overcome the uplift forces. If numerous columns participate efficiently in resisting the horizontal load in the superstructure, the dead load in each column will eliminate the possibility of uplift on all bearings, avoiding the problem of designing the isolators for tension forces, thereby simplifying the testing requirements. Note, if tension is produced in the bearings, not only will be bearings need to be tested in tension, but the connections of the bearings to the foundation and to the building will also need to be tested.

There are other prototype test requirements in the code that are not generally strictly adhered to because of the lack of suitable testing facilities. The code requires that isolators with a behavior that is dependent on loading rate be tested at real loading rates. Rate dependence is defined as follows: The hysteresis loop at the design displacement at the frequency of the isolated structure does not differ by plus or minus 10% if the test is carried out at any frequency in the range from one-tenth to twice the design frequency. Although natural rubber is relatively insensitive to rate of loading and is well within this range, other polymeric materials and elastomers may not. The power requirements for a test of this kind are quite surprising. If two isolators carry, say, 500 tons (1111 kips) [for a system with a 2.0-sec period and 30 cm (11.8 in.) displacement] one on top of the other, as is the usual test method, and are loaded to their design displacement at 2.0-sec period in a sinusoidal manner, the peak power requirement is about 1800 hp or 1.4 MW.

Similar unattainable test requirements are specified for units dependent on bilateral loads where it is stated that these units must be tested in two directions simultaneously. The criterion for bilateral dependency is similar to that for rate dependency, and the requirement is never carried out because of the lack of suitable test equipment.

Although there are no specific requirements for quality control tests for production isolators, the code demands that such a program be established and reviewed by the peer review panel. The design engineer usually specifies a quality control program that includes a series of standard tests on the material, compression tests, and combined compression and shear tests on all production isolators. In addition, a small percentage of isolators may be selected at random and tested to the MCE displacement. Extra isolators are often kept under load at the site for periodic checks of the long-term stability of the material properties. Although this is not required by the code, the code does specify that access for inspection and removal of all isolators be part of the design.

4.9 OSHPD-96 REQUIREMENTS

The design of hospitals in California is governed by the State Code Title 24, Part 2, which is administered by OSHPD [15]. The current regulations published in May 1996 for base-isolated hospitals are very similar to the 1994 UBC requirements, except that both site-specific ground motions and dynamic analysis are always required. The site-specific ground motions are evaluated for OSHPD by the California Department of Mines and Geology (DMG), and their approval of the design spectra for the DBE and MCE is necessary.

The civil code and the UBC differ in the following respect: Static analysis cannot be used for the design, only for minimum requirements; therefore, even though dynamic analysis is mandatory, a static analysis still must be carried out. The dynamic analysis must include a time history analysis, except under

very restrictive circumstances when a response spectrum analysis is acceptable. Site-specific design spectra have to be prepared for DBE and MCE events. From these site-specific design spectra, time history pairs of recorded events are determined by using the same scaling procedure outlined in the UBC. The duration of the selected and scale time histories has to be consistent with the magnitude and source characteristics of the site-specific DBE and MCE events, and if the site is near field, then near-field effects should be incorporated.

The requirement for design review has become considerably more restrictive. The enforcement agency (e.g., OSHPD) retains the right to require the owner of the facility to retain a review panel and have the review panel serve in an advisory capacity to the agency. The testing requirements for the prototypes are unchanged.

The civil code has additional requirements for hospital buildings that are not mandatory in the UBC code. The isolation system must be monitored for the life of the building and access for monitoring and replacement of the system must be provided. The building is to be instrumented with accelerometers that must be approved by the enforcement agency prior to installation. After every significant earthquake, the structure, the isolators, and the strong motion recorders must be inspected by a structural engineer retained by the owner, and an inspection report must be provided to the enforcement agency. In addition, a proportion of the isolators must be removed every 10 years to be tested and compared with the tests done prior to installation.

Another problem facing the designer is the difficulty of obtaining the approval from the DMG for the design ground motions. In the recent past the DMG has taken a very aggressive role in the selection of design spectra and earthquakes for time history analysis, often resulting in considerable delays in the approval process. As a result, the designer may adopt a very conservative ground motion in the hope that a rapid approval results, thereby significantly impacting the cost and performance of the isolation system.

As the codes for seismic isolation design have evolved in the United States, the trend has been from the simple, straightforward, and rational version of the Yellow Book to the more complicated and less rational versions in the more recent codes. The Yellow Book was put together by a small group of activists who took the position that base isolation was a simplifying approach to seismic design and formulated a design process that was informed by the elementary theory. The requirements were consistent with the theoretical basis of isolation and included incentives for designers to use designs that were consistent with the simple theory. As the codes have evolved, however, they have been influenced by professional engineers who are not comfortable with the technology and see it as too complicated—even dangerous. Their influence on the codes has made the codes correspondingly inconsistent with the theory and has further complicated the process by insisting on excessive testing requirements at every level of the procurement process.

4.10 OTHER CONSIDERATIONS

One feature that has persisted through all versions of the UBC isolation regulations is the scaling of the time histories. In essence, the code requires an increase of 30% in the target spectra to account for bilateral ground motion. Isolation systems are always isotropic, however, and the maximum isolator displacement can be in any direction. Since the basic static formula for maximum displacement is intended to be applied in any direction, it is not clear why the dynamic analysis should include bilateral displacements. Furthermore, this requirement is in direct conflict with the detailed systems design requirements for conventional structures, which states that the "*requirements of orthogonal effects may be satisfied by designing such elements for 100% of the prescribed design seismic forces in one direction plus 30% of the prescribed design seismic forces in the perpendicular direction*" (UBC-97, Sec. 1633.1) [55]. Obviously, the resulting vector summations are very different (see Fig. 4.13).

The extensive testing requirements for prototype isolators remain from the earlier code versions. New requirements for inspection and replacement have been added, including requirements for periodic monitoring, requirements on repair or retrofit of the isolation system, and a requirement for a horizontal displacement monitoring device.

In total, the 1997 version of the UBC regulations for seismic-isolated structures has completed the process of turning the simple straightforward and rational code developed in the 1986 Yellow Book into a complicated and conservative set of requirements that will seriously undermine the use of isolation technology by the general engineering community. The whole impetus for de-

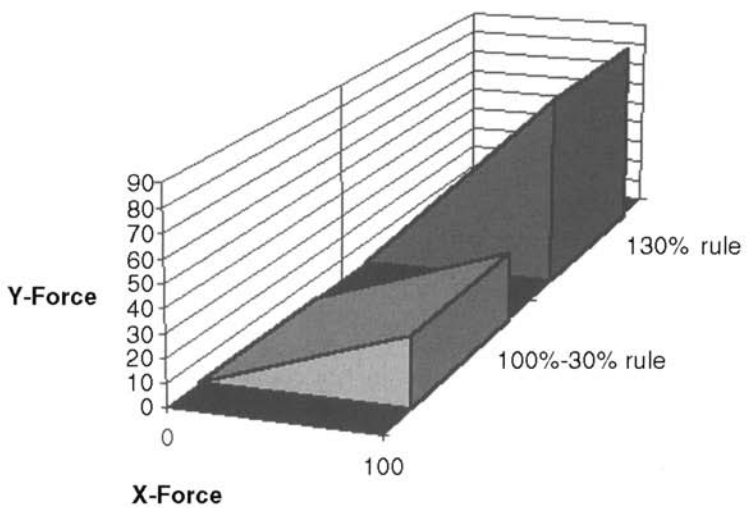

Fig. 4.13 Inconsistency between code requirements on orthogonal effects.

veloping isolation systems by creating cost-effective, simple, strategies to create earthquake-resistant structures has been lost.

4.11 STEP-BY-STEP PROCEDURE FOR UBC-97 COMPLIANT DESIGN

4.11.1 Preliminary Design Steps

Step 1: Establish Seismic Zone Factor Z. Determine the seismic zone factor by establishing the seismic zone of the project's site from UBC-97, Fig. 16-2, and the corresponding seismic zone factor Z from Fig. 4.1 (UBC-97, Table 16-I).

Step 2: Establish Site Soil Profile Category. Determine the site soil profile type from Fig. 4.2 (UBC-97, Table 16-J).

Step 3: Establish Seismic Source Types. For each controlling seismic hazard source (i.e., seismic faults), determine the corresponding seismic source type from Section 4.4.3 or UBC-97, Table 16-U.

Step 4: Establish Near-Source Factors N_a and N_v. For each seismic source type established above, determine corresponding near-source factors N_a and N_v from Figs. 4.3 and 4.4. (UBC-97, Tables 16-S and 16-T).

Step 5: Calculate Maximum Capable Earthquake Response Coefficient M_M. Multiply Z and N_v as calculated above to obtain ZN_v. Use Fig. 4.5 (UBC-97, Table A-16-D) to read the corresponding value of M_M.

Step 6: Determine Seismic Coefficients C_{VD} and C_{AD}. With seismic zone factor and site soil profile as established in the above steps, obtain appropriate seismic coefficients C_V and C_A from Figs. 4.6 and 4.7 (UBC-97, Tables 16-R and 16-Q). Call them C_{VD} and C_{AD}, respectively.

Step 7: Determine Seismic Coefficients C_{VM} and C_{AM}. Using soil profile type determined in step 2, multiply M_M, Z, and N_v to obtain $M_M Z N_v$. Use Fig. 4.8 (UBC-97, Table A-16-G) to obtain C_{VM}. Similarly, calculate $M_M Z N_a$ and use Fig. 4.9 (UBC-97, Table A-16-F) to obtain the value of coefficient C_{AM}.

Step 8: Determine Structural System Reduction Factor R_I. Obtain the reduction factor R_I corresponding to the structural system used above the isolation interface from Table 4.1 or UBC-97, Table A-16-E. The value of R_I for virtually all cases is either 2.0 or 1.6.

Step 9: Select the Type of Isolation Bearings and the Damping Coefficients B_D and B_M. Select the bearing type (or combinations) to be used. Using the information presented in Chapter 5, select an appropriate conservative estimate of the damping level provided. For example, for high-damping rubber systems, use a damping level of 10–12%. With this information use Fig. 4.10 (UBC-97, Table A-16-C) and read the corresponding value of the damping

coefficient. Assign the same value to B_D and B_M at this time. Use linear interpolation if necessary.

Step 10: Select a Desired Isolated Period of Vibration T_D. Decide on an initial estimate for the isolated system fundamental period of vibration at the design basis displacement level. Generally speaking, an isolated period between 2.0 and 3.0 sec is desirable.

Step 11: Estimate the Effective Stiffness of the Isolation System. Use a simple equation [such as Eq. (4.7)] to estimate the stiffness of the isolation system for the isolated period established in step 9. Assign this value to both $K_{D,\min}$ and $K_{D,\max}$ for the moment.

Step 12: Estimate the Minimum Design Lateral Displacement D_D. Use Eq. (4.2) with the values calculated in the previous steps and calculate the initial estimate of the minimum design displacement D_D. *If this value is larger than what is acceptable for your project, you need a stiffer system. Go back to step 10 and start with a smaller estimate of the vibration period. Otherwise, proceed to the next step.*

Step 13: Establish the Minimum Design Lateral Forces V_b and V_s. Use Eqs. (4.11) and (4.12) to estimate the minimum design lateral forces for the isolation systems and structural system at or below the isolation interface (V_b) and structural elements above the isolation interface (V_s), respectively. Also notice the limitations on V_s as described in Section 4.5 of this chapter (see UBC-97, Sec. 1658.4.3). *If the values of either V_b or V_s are larger than what is acceptable for your project, you need a softer system. Go back to step 10 and start with a larger estimate of the vibration period. Otherwise, proceed to the next step.*

Step 14: Perform a Preliminary Design of the Superstructure Elements. With V_s estimated in step 13, calculate static lateral forces at each level of the building using Eq. (4.13). Use these lateral forces for preliminary stress sizing of superstructure elements. For drift design use the maximum interstory drift ratio above the isolation system of $0.010/R_I$ for the static force procedure (UBC-97, Sec. 1658.6). For response spectrum analysis and time history analysis the maximum interstory drift indices are $0.015/R_I$ and $0.020/R_I$, respectively (UBC-97, Sec. 1659.8). *If the period of the fixed-base superstructure as designed is significantly different from that assumed in calculating the limitations on V_s in step 13, go to step 13 and verify the adequacy of V_s as assumed. Otherwise, proceed to the next step.*

Step 15: Perform a Preliminary Design of Isolator Units and their Distribution. Using the preliminary displacement, stiffness, force, and damping properties established in the previous steps and design procedures presented in Chapter 3, design the isolator units to resist the gravity load, lateral load, and displacement requirements. Also establish a preliminary force–displacement hysteretic diagram for each type of isolator unit used. These diagrams may be based on the test results obtained from tests conducted on bearings of similar type and size or on properties provided by isolator manufacturers.

The hysteretic properties assumed at this stage are subject to verification and possible revision during the final design stage when the results of the prototype and production tests become available.

4.11.2 Final Design Steps

Step 16: Construct Mathematical Model(s) of the Isolated Structure. Construct mathematical (i.e., computer) model(s) of the fixed-base and isolated structure subject to requirements of UBC-97, Sec. 1659.5. *Incorporate the force–displacement characteristics of the isolation bearings obtained from step 15 in your models.* There are basically two methods for construction of such models:

a. A model of base isolation system with stick model representation of superstructure. This approach is useful when multiple execution of models subjected to various time histories or minimum eccentricities are required. Typically this may be achieved by constructing a 3D-BASIS model of the base isolation system incorporating the mass properties, eigenvalues, and eigenvectors of the fixed-base superstructure. The limitation of this method is the inherent assumption of rigid diaphragm floors that must be validated and lack of net-uplift modeling capabilities.

b. An integrated model of the isolation system and superstructure constructed with ETABS, SAP-2000, or similar computer codes capable of modeling nonlinear characteristics of the isolators, if necessary. The disadvantage of this approach is the sheer volume of data to be processed for numerous computer runs that are associated with any realistic seismic isolation project.

The recommended approach is to use the first method during the design iterations and the second approach during the final stages to confirm the accuracy of the results obtained and to design for elements inadequately represented by the approximations inherent in the first method.

Step 17: Select an Appropriate Lateral Response Procedure. Use the information presented in Sections 4.4 and 4.5 or UBC-97 criteria selection provisions (UBC-97, Sec. 1657) to select an appropriate design procedure (i.e., static lateral response procedure, response spectrum analysis, or time history analysis). *Regardless of the procedure required by the Code, we recommend that the static lateral and response spectrum procedures be performed before any time history analysis is attempted.* Identify seismic demand definitions to be utilized (i.e., lateral forces, design spectra, time history pairs).

Step 18: Finalize the Target Values of Design Displacements and Isolated Periods. Use the computer model(s) constructed in step 16 and seismic demands established in step 17 in a series of analysis and design iterations to arrive at a design of the isolation system and a superstructure that satisfies the basic project displacement and force response objectives. Finalize the values of

design displacement D_D and maximum displacement D_M for the project. Notice that these values are not the same as the minimum value calculated in step 12 of preliminary design. As selected here, D_M should be larger than D_D, and the D_D assigned here should be larger than the value calculated in step 12 of the preliminary design. Establish the isolated period at design displacement and maximum displacement levels (T_D and T_M). If possible, take advantage of reduced displacements and base shears permitted by the code for dynamic lateral response procedures introduced in Eqs. (4.14) and (4.15) (UBC-97, Sec. 1659.2).

Step 19: Finalize the Target Values of Effective Stiffness. Except for the very unlikely case of an isolation system with markedly different positive and negative response characteristics, use the computer model and results obtained in steps 16–18 to establish the target values of effective stiffness terms as follows:

$$K_{D,\max} = K_{D,\min} = \frac{\text{DBE base shear}}{D_D}$$

$$K_{M,\max} = K_{M,\min} = \frac{\text{MCE base shear}}{D_M}$$

Step 20: Verify the Effective Period Suggested by the Mathematical Model. Verify the effective periods T_D and T_M as determined by the mathematical model against those calculated by minimum values represented by Eqs. (4.2) and (4.3).

Step 21: Verify the Damping Level Suggested by the Mathematical Model. Use Eqs. (4.4) and (4.5) to verify the damping level assumed in or reported by the mathematical model and, if necessary, recalculate the damping coefficients B_D and B_M (Fig. 4.10 or UBC-97, Table A-16-C).

Step 22: Verify Design Displacements and Forces against Code Minimum Values. Compare the design displacements reported by the mathematical model against the corresponding UBC-97 code minimum values as represented by Eqs. (4.2), (4.3), (4.9), and (4.10). If possible, take advantage of reductions permitted by Eqs. (4.14) and (4.15). *If calculated design displacement values are less than code minimums, then adjust all response parameters (including member forces and deformations) proportionally to code suggested values.* Also verify reported base shears against code minimum values represented by Eqs. (4.11) and (4.12).

Step 23: Verification of Performance as Suggested by the Prototype Bearing Test Results. Upon the availability of prototype bearing test results, revise the mathematical model constructed in step 16 to reflect the lower bound and upper bound bearing properties suggested by the prototype test results. Recalculate effective stiffness values $K_{D,\max}$, $K_{D,\min}$, $K_{M,\max}$ and $K_{M,\min}$ using

Eqs. (4.16)–(4.19) (UBC-97, Sec. 1665.5.1). Repeat steps 20–22 using the revised mathematical model(s).

Step 24: Verification of Performance as Suggested by the Production Bearing Test Results. Upon the availability of production bearing test results, revise the mathematical model constructed in step 16 to reflect the lower bound and upper bound bearing properties suggested by the production test results and actual distribution of individual isolators. Recalculate effective stiffness values $K_{D,\max}$, $K_{D,\min}$, $K_{M,\max}$, and $K_{M,\min}$ using Eqs. (4.16)–(4.19) (UBC-97, Sec. 1665.5.1). Repeat steps 20–22 using the revised mathematical model(s):

$$K_{D,\max} = \frac{\sum F^{+}_{D,\max} - F_{D,\max}}{D^{+}_{D} - D_{D}} \tag{4.16}$$

$$K_{D,\min} = \frac{\sum F^{+}_{D,\min} - F_{D,\min}}{D^{+}_{D} - D^{-}_{D}} \tag{4.17}$$

$$K_{M,\max} = \frac{\sum F^{+}_{M,\max} - F^{-}_{M,\max}}{D^{+}_{M} - D^{-}_{M}} \tag{4.18}$$

$$K_{M,\min} = \frac{\sum F^{+}_{M,\min} - F_{M,\min}}{D^{+}_{M} - D^{-}_{M}} \tag{4.19}$$

Step 25: Verification of Performance as Suggested by the Production Bearing Test Results. Upon the availability of production bearing test results, revise the mathematical model constructed in step 16 to reflect the lower bound and upper bound bearing properties suggested by the production test results and actual distribution of individual isolators. Recalculate effective stiffness values $K_{D,\max}$, $K_{D,\min}$, $K_{M,\max}$, and $K_{M,\min}$ using Eqs. (4.16)–(4.19) (UBC-97, Sec. 1665.5.1). Repeat steps 20–22 using the revised mathematical model(s).

4.11.3 Design Example

Consider a small building with a plan dimension of 40 × 20 m (131 × 65.5 ft). The total weight of the structure is estimated at 1600 tons (3550 kips). The lateral-load resisting system consists of reinforced-concrete shear walls, and the building is regular in both the plan and the elevation. The actual distance between the center of mass and the center of rigidity of each floor is 1.0 m (39.4 in.).

The project site is located as seismic zone 4 with an S_E soil profile and it is located about 1.5 km (0.93 miles) away from an active fault capable of producing 7.9 magnitude events with an average seismic slip rate, SR, larger than 5 mm (0.2 in.). The fixed-base period of the building is 0.70 sec. The isolation system should provide effective isolated periods of $T_D = 2.4$ and $T_M = 2.7$ sec, respectively, and a damping of 15% critical. A margin of ±10% variation in stiffness from the mean stiffness values of the isolators is considered acceptable.

Use the step-by-step procedure detailed in Section (4.11.1) to determine the minimum design displacements, minimum lateral forces, and maximum permitted interstory drift ratios according to the UBC-97 requirements.

SOLUTION

Step 1. From Fig. 4.1 (UBC-97, Table 16-I), $Z = 0.40$.

Step 2. Site soil profile category is given as S_E.

Step 3. From Section 4.4.3 (UBC-97, Table 16-U) for $M \geq 7.0$ and SR ≥ 5 mm (0.2 in.), the seismic source type is A.

Step 4. Step 4: From Fig. 4.3 (UBC-97, Tables 16-S) for seismic source type A and closest distance of less than 2 km (1.25 miles), $N_a = 1.5$. Similarly, from Fig. 4.4 (UBC-97, Table 16-T), $N_v = 2.0$.

Step 5. $ZN_v = (0.4)(2.0) = 0.80$. From Fig. 4.5 (UBC-97, Table A-16-D) for $ZN_v \geq 0.50$, $M_M = 1.20$.

Step 6. For $Z = 0.4$ and soil type S_E from Fig. 4.6 (UBC-97, Table 16-R), $C_V = C_{VD} = 0.96N_v = 0.96(2.0) = 1.92$. Similarly, from Fig. 4.7 (UBC-97, Table 16-Q), and 16-Q), $C_A = C_{AD} = 0.36N_a = 0.36(1.5) = 0.54$.

Step 7. $M_M ZN_v = (1.20)(0.40)(2.0) = 0.96 > 0.40$ and $M_M ZN_a = (1.20)(0.40)(1.5) = 0.72 > 0.40$. From Fig. 4.8 (UBC-97, Table A-16-G), $C_{VM} = 2.4M_M ZN_v = 2.4(0.96) = 2.30$. Similarly, from Fig. 4.9 (UBC-97, Table A-16-F), $C_{AM} = 0.9M_M ZN_a = 0.9(0.72) = 0.65$.

Step 8. For reinforced-concrete shear wall system from Table 4.1 (UBC-97, Table A-16-E), $R_I = 2.0$.

Step 9. For preliminary design purposes, 15% damping is assumed. Therefore, from Fig. 4.10 (UBC-97, Table A-16-C), $B_D = B_M = 1.35$.

Step 10. T_D and T_M are given as 2.4 and 2.7 sec, respectively.

Step 11. From Eqs. (4.7) and (4.8)

$$T_D = 2\pi \sqrt{\frac{W}{K_{D,\min} g}}$$

$$2.40 = 2\pi \sqrt{\frac{1600(1000)}{K_{D,\min}(9.81)}} \Rightarrow K_{D,\min} = 1117 \text{ tons/m (63 kips/in.)}$$

$$2.70 = 2\pi \sqrt{\frac{1600(1000)}{K_{M,\min}(9.81)}} \Rightarrow K_{M,\min} = 882 \text{ tons/m (50 kips/in.)}$$

Since we assumed a +10% variation about the mean stiffness values,

$$K_{D,\max} = (1.10)\frac{(1117)}{0.90} = 1365 \text{ tons/m (77 kips/in.)}$$

$$K_{M,\max} = (1.10)\frac{(882)}{0.90} = 1078 \text{ tons/m (61 kips/in.)}$$

Step 12. From Eqs. (4.2) and (4.3)

$$D_D = \frac{(g/4\pi^2)C_{VD}T_D}{B_D} = \frac{(9.81/4\pi^2)(1.92)(2.4)}{1.35} = 0.85 \text{ m (33.5 in.)}$$

$$D_M = \frac{(g/4\pi^2)C_{VM}T_M}{B_M} = \frac{(9.81/4\pi^2)(2.30)(2.7)}{1.35} = 1.14 \text{ m (45.0 in.)}$$

Now, let us calculate total displacements including torsion. The additional accidental eccentricity required by the code is 5% of the plan dimension perpendicular to loading. Therefore,

$$e = (0.05)(40.0) + 1.0 = 3.0 \text{ m (118 in.)}$$

In Eqs. (4.9) and (4.10), the value of the multiplier in both formulas is

$$1 + y\frac{12e}{b^2 + d^2} = 1 + (1.0)\frac{12(3.0)}{40^2 + 20^2} = 1.018$$

Hence

$$D_{TD} = 1.018(0.85) = 0.87 \text{ m (34 in.)} \qquad D_{TM} = 1.018(1.14) = 1.16 \text{ m (46 in.)}$$

Now let us examine the minimum design displacements permitted for dynamic analysis [Eqs. (4.14) and (4.15)]:

$$D'_D = \frac{D_D}{\sqrt{1 + (T/T_D)^2}} = \frac{0.85}{\sqrt{1 + (0.70/2.40)^2}} = 0.82 \text{ m (32.1 in.)}$$

$$D'_M = \frac{D_M}{\sqrt{1 + (T/T_M)^2}} = \frac{1.14}{\sqrt{1 + (0.70/2.70)^2}} = 1.10 \text{ m (43.5 in.)}$$

Step 13. The minimum base shear strength at or below the isolation interface from Eq. (4.11) is

$$V_b = K_{D,\max} V_b = 1365(0.85) = 1160 \text{ tons (2580 kips)} = 73\% \text{ of total weight}$$

and for design of the system and elements above the isolation interface from Eq. (4.12),

$$V_S = \frac{K_{D,\max} D_D}{R_I} = \frac{1365(0.85)}{2.0} = 580 \text{ tons (1290 kips)} = 36\% \text{ of total weight}$$

COMMENTS

The large minimum displacements imposed by the UBC-97 requirements make the designing and implementation of a seismic isolation for this building extremely difficult. Fortunately, UBC-97 near-field factors, which are the primary reasons for these conservative estimates of displacements, are expected to be phased out in the upcoming edition of the code. The year 2000 code, which is to be called the *International Building Code* (*IBC-2000*), is based primarily on the NEHRP-97 guidelines. These guidelines use hazard maps developed by U.S. Geological Survey (USGS) for the continental United States. These maps do not impose a near-fault factor on the top of the hazard estimate for the site as the near-field effect is already considered in establishment of seismic hazard. IBC-2000 is expected to lead to much more reasonable, lower bound values for design displacements.

This design example highlights the UBC-97 inherent bias in the performance requirements for fixed-based versus isolated structures. While fixed-base buildings are routinely designed to a life safety objective, isolated buildings are expected to perform with uninterrupted operation during and immediate occupancy after the design earthquake. The code does not allow seismically isolated structures the same limited life safety objectives accorded to fixed-base buildings. Given the fact that seismic-isolated structures, even when they fail, provide a much more enhanced protection of life and limb for their occupants compared to their fixed-base counterparts, restriction of isolated designs to immediate occupancy objectives is not reasonable and must be changed.

CHAPTER 5

MECHANICAL CHARACTERISTICS AND MODELING OF ISOLATORS

5.1 INTRODUCTION

The design process for an isolation system will generally begin with a preliminary design using parameters from a previous project or from data from a manufacturer to estimate the possible maximum displacement of the system and maximum values of various controlling quantities (such as shear strain) and also for estimating the structural base shear, stability of the isolators, and possibility of uplift. After this preliminary design process is completed, examples of the final design of the isolators will be ordered and subjected to the code-mandated prototype test program. Depending on the results of the prototype tests, the preliminary design may or may not need to be modified. In order to minimize the number of iterations in the design, it is essential to have accurate data and good design procedures in the preliminary design phase. This chapter will provide the isolation designer with the information needed for making the preliminary design.

5.2 MECHANICAL CHARACTERISTICS OF ELASTOMERIC BEARINGS

The mechanical characteristics of multilayered elastomeric bearings have been studied for many decades, and while exact analyses using nonlinear techniques are still quite difficult, simple predictions based on elastic theory have been developed by many researchers and verified by laboratory testing and more recently by finite element analysis. The most important mechanical property of

Design of Seismic Isolated Structures: From Theory to Practice. F. Naeim and J. M. Kelly

the isolation bearing is, of course, its horizontal stiffness; this is given by

$$K_H = \frac{GA}{t_r}$$

where G is the shear modulus of the elastomer, A is the full cross-sectional area (which may differ from the area of the reinforcing shims), and t_r is the total thickness of the rubber. The maximum horizontal displacement D is related to the maximum shear strain γ by

$$\gamma = \frac{D}{t_r}$$

The vertical stiffness K_V and the bending stiffness—expressed as EI by analogy with beam theory—are also given by a simple linear elastic theory and are needed for designing a bearing.

The vertical frequency of an isolated structure, often an important design criterion, is controlled by the vertical stiffness of the bearings that comprise the system. In order to predict this vertical frequency, the designer need only compute the vertical stiffness of the bearings under a specified dead load, and for this a linear analysis is adequate. The initial response of a bearing under vertical load is very nonlinear and depends on several factors. Normally, bearings have a substantial run-in before the full vertical stiffness is developed. This run-in, which is strongly influenced by the alignment of the reinforcing shims and other aspects of the workmanship in the molding process, cannot be predicted by analysis but is generally of little importance in predicting the vertical response of a bearing.

Another important bearing property that must be analyzed for design is the buckling behavior of the isolator. In order to conduct this analysis, the response of the compressed bearing to bending moment is necessary. Referred to as the "bending stiffness," this can be ascertained by an extension of the same analysis that is done to determine the vertical stiffness.

The vertical stiffness of a rubber bearing is given by the formula

$$K_V = \frac{E_c A}{t_r}$$

where A is the cross-sectional area of the bearing (in this case it usually is taken as the area of the shim plates), t_r is the total thickness of rubber in the bearing, and E_c is the instantaneous compression modulus of the rubber–steel composite under the specified level of vertical load. The value of E_c for a single rubber layer is controlled by the shape factor S, defined as

$$S = \frac{\text{loaded area}}{\text{force-free area}}$$

which is a dimensionless measure of the aspect ratio of the single layer of the elastomer. For example, in an infinite strip of width $2b$ and with a single-layer thickness t,

$$S = \frac{b}{t} \tag{5.1}$$

for a circular pad of diameter Φ or radius R and thickness t,

$$S = \frac{\Phi}{4t} \qquad \text{or} \qquad S = \frac{R}{2t} \tag{5.2}$$

and for a square pad of side dimension a and thickness t,

$$S = \frac{a}{4t} \tag{5.3}$$

For a single pad in the form of a complete circle, the compression modulus E_c is given by

$$E_c = 6GS^2$$

and for a square pad, the result is

$$E_c = 6.73GS^2$$

In some cases bearings are designed with unfilled central holes. The result for a bearing with an inside radius a and outside radius b is

$$E_c = 6\lambda GS^2$$

where

$$\lambda = \frac{b^2 + a^2 - [(b^2 - a^2)/(\ln\ b/a)]}{(b - a)^2}$$

If $a/b \to 0$, then $\lambda \to 1$; hence, $E_c = 6GS^2$, which is the result for the full circular pad. If $a/b \to 1$, by writing $a/b = 1 - \epsilon$ and letting $\epsilon \to 0$, we find that $\lambda \to \frac{2}{3}$ and $E_c \to 4GS^2$, which is the result for the infinite strip. It is interesting to evaluate how rapidly the result for λ approaches $\frac{2}{3}$. To illustrate this point, the solution for λ is plotted versus the ratio a/b and from $0 \le a/b \le 1$ in Fig. 5.1. Clearly for the case when $a/b > 0.10$, the value of λ is almost two-

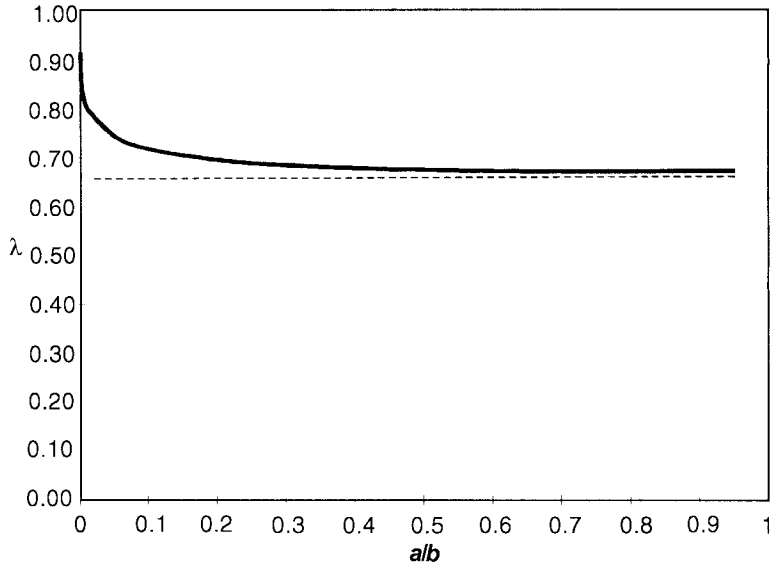

Fig. 5.1 Reduction of compression modulus E_c for an annular pad.

thirds, indicating that the presence of even a small hole has a large effect on E_c; therefore, in most cases for bearings with central holes, the value of E_c should be taken as $4GS^2$ rather than $6GS^2$.

Under direct compression the constraint provided by the bonded steel shims produces a shear strain in the rubber, which is denoted by γ_c. If the nominal compression strain ϵ_c is given by

$$\epsilon_c = \frac{\Delta}{t_r}$$

where Δ is the vertical displacement, then

$$\gamma_c = 6S\epsilon_c$$

This is the maximum shear strain developed at the edges of the pad and often used in design.

The maximum shear strain due to compression is not the only shear strain quantity of interest to the designer. It is also useful to estimate the average strain in the following manner: Because rubber is somewhat strain sensitive, G is often modified according to the strain level, particularly in highly filled rubbers. In compression the shear strain varies widely over the volume of the pad; therefore, the appropriate value of the modulus used to estimate the average strain is based on a calculation of the elastic stored energy in the pad.

From this calculation the average shear strain γ_{ave} is given by

$$\gamma_{\text{ave}} = \sqrt{6} S \epsilon_c$$

Although a certain degree of trial and error is needed, computations of this kind allow the designer to estimate the appropriate value of G, which can then be used to estimate the vertical stiffness. First we must assume a value of G in order to calculate ϵ_c and from that calculate γ_{ave}; we then modify G and iterate as necessary. Because the modulus is not very sensitive to strain above about 20%, few iterations are needed.

The bending stiffness of a pad is computed using a similar approach with the same type of displacement assumptions. The pad is assumed loaded by a pure moment M, and the deformation is assumed to be a rotation of the top and bottom bonded plates, as shown in Fig. 5.2. The relative angle between the top and bottom plates is denoted by α, and the radius of curvature ρ generated by the deformation is related to α by

$$\frac{1}{\rho} = \frac{\alpha}{r}$$

By analogy with beam theory, where

$$M = \frac{EI}{\rho}$$

we write

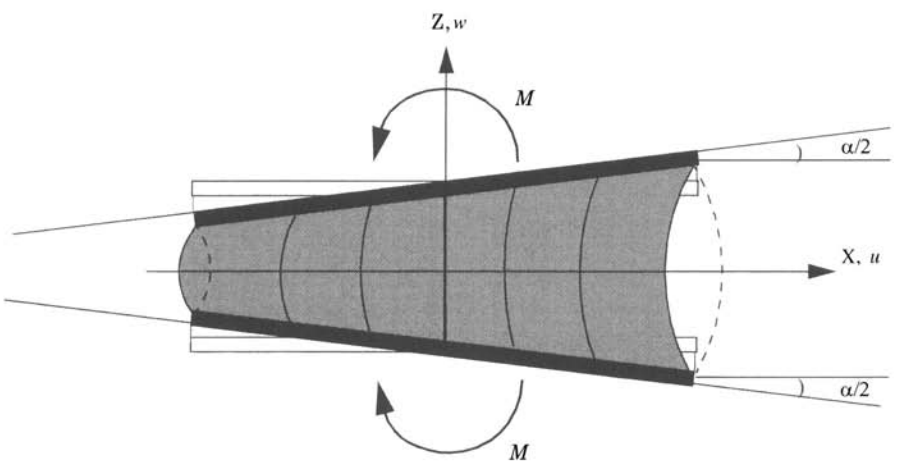

Fig. 5.2 Rubber pad between rigid constraint layers in pure bending [30].

$$M = (EI)_{\text{eff}} \frac{\alpha}{t}$$

For a circular pad of radius R, the result is

$$M = \frac{3\alpha G}{2t^3} \frac{\pi R^6}{12}$$

and for a beam of circular section

$$I = \frac{\pi R^4}{4}$$

But in this case, taking the E in EI as $E_c = 6GS^2$, we have the result $\pi R^4/12$ for I, which is one-third the beam moment of inertia. The difference is caused by the fact that the pressure distribution varies as a cubic parabola across the pad, whereas in a beam, the bending stress distribution is linear. In the case of a square pad, the effective EI is very close to one-third the beam EI, being

$$(EI)_{\text{eff}} = E_c(0.329I)$$

For the circular pad with a central hole, we have

$$(EI)_{\text{eff}} = 2GS^2I \frac{(b+a)^2}{b^2 - a^2}$$

The shear stresses induced by the bending are given by

$$\gamma_b = 6S\epsilon_b$$

where $\epsilon_b = R(\alpha/t)$ is the edge compression strain produced by bending. The average shear strain (in the sense of overall shear strain energy) is given by

$$\begin{aligned} \gamma_b^{\text{ave}} &= \sqrt{2}S^2\alpha \\ &= \sqrt{2}S \frac{R}{4} \frac{\alpha}{t} \\ &= \frac{\sqrt{2}}{4} S\epsilon_b \end{aligned}$$

When the shape factor of the pad becomes large, the effect of compressibility of the rubber begins to be important. Compressibility can be approximately

incorporated in the previous formulas through the ad hoc modification [73]

$$\frac{1}{E_c} = \frac{1}{E_c'} + \frac{1}{K}$$

where $1/E_c'$ is the compression modulus assuming incompressibility behavior and K is the bulk modulus of the material. More exact formulas have been developed for this effect, but the bulk modulus is such a difficult quantity to measure that use of the simple ad hoc formula is good enough for design purposes. The value of K varies quite widely in reference material, ranging from a low of 1000 MPa (145,000 psi) [74] to 2500 MPa (363,000 psi) [78]. The value most commonly used, and which appears to fit laboratory test results on bearings, is 2000 MPa (290,000 psi).

When rewritten for E_c, the ad hoc equation becomes

$$E_c = \frac{E_c' K}{E_c' + K}$$

and for the circular pad, we have $E_c' = 6GS^2$; thus

$$E_c = \frac{6GS^2 K}{6GS^2 + K}$$

$$= 6GS^2 \left[\frac{1}{1 + 6GS^2/K} \right]$$

When S is small, we have

$$E_c = 6GS^2 \left(1 - \frac{6GS^2}{K} \right)$$

so that for, say, better than 10% accuracy, S is such that

$$6S^2 < \frac{K}{60G}$$

with $K = 2000$ MPa (290,000 psi) and $G = 0.7$ MPa (101.5 psi), $S < 7$.

When S is large and $6GS^2/K$ is much greater than unity,

$$E_c = K \left[1 - \frac{K}{6GS^2} \right]$$

showing that K is an upper bound to E_c and will approximate E_c to less than 10% accuracy if

$$\frac{K}{6GS^2} < \frac{1}{10}$$

or

$$S > \left(\frac{K}{0.6G}\right)^{1/2} \approx 70$$

Shape factors of this magnitude are unlikely, but the formulas show that an allowance for compressibility is needed for shape factors above about 10.

5.3 MECHANICAL CHARACTERISTICS OF LEAD-PLUG BEARINGS

Lead-plug bearings are always modeled as bilinear elements, with their characteristics based on three parameters: K_1, K_2, and Q (as shown later in Fig. 5.4). The elastic stiffness K_1 is difficult to measure and is usually taken to be an empirical multiple of K_2, the post-yield stiffness, which can be accurately estimated from the shear modulus of the rubber and the bearing design. The characteristic strength Q is the intercept of the hysteresis loop and the force axis and is accurately estimated from the yield stress of the lead [10.3 MPa (1500 psi)] and the lead-plug area.

The effective stiffness of a lead-plug bearing, defined on the basis of peak-to-peak loads, steadily reduces with displacement. In terms of the basic parameters K_1, K_2, and Q, it is given by

$$K_{\text{eff}} = K_2 + \frac{Q}{D} \qquad D \geq D_y \tag{5.4}$$

where D_y is the yield displacement. The natural frequency ω is given by

$$\omega = \sqrt{\frac{K_{\text{eff}} g}{W}}$$

$$= \sqrt{\omega_0^2 + \mu \frac{g}{D}}$$

where $\mu = Q/W$, $\omega_0^2 = \sqrt{K_2 g/W}$, and the effective period T is given by

$$T = \frac{2\pi}{\omega}$$

$$= \frac{2\pi}{\sqrt{\omega_0^2 + \mu \frac{g}{D}}}$$

The effective damping β_{eff} for $D \geq D_y$ is defined to be

$$\beta_{\text{eff}} = \frac{\text{area of hysteresis loop}}{2\pi K_{\text{eff}} D^2} \tag{5.5}$$

The area of the hysteresis loop is given by $4Q(D - D_y)$; to put β_{eff} in terms of these basic parameters, we note that

$$D_y = \frac{F_y}{K_1} \qquad F_y = Q + K_2 D_y$$

so that

$$D_y = \frac{Q}{K_1 - K_2} \tag{5.6}$$

Using the definition of β_{eff} and the result [Eq. (5.4)] for K_{eff}, we have

$$\beta_{\text{eff}} = \frac{4Q(D - D_y)}{2\pi(K_2 D + Q)D}$$

As a general rule of thumb, elastic stiffness K_1 is taken as $10K_2$, so that $D_y = Q/(9K_2)$, giving

$$\beta_{\text{eff}} = \frac{4Q(D - Q/9K_2)}{2\pi(K_2 D + Q)D}$$

5.4 MECHANICAL CHARACTERISTICS OF FRICTION PENDULUM SYSTEM

If the load on an FPS isolator is W, the horizontal displacement is D, and the friction coefficient is μ, then the resisting force F is given by

$$F = \frac{W}{\mathbf{R}} D + \mu W(\text{sgn } \dot{D})$$

where **R** is the radius of curvature of the dish. The first term is the restoring force due to rise of the mass, providing a horizontal stiffness

$$K_H = \frac{W}{\mathbf{R}}$$

which produces an isolated structure period T given by

$$T = 2\pi\sqrt{\mathbf{R}/g}$$

which is independent of the carried mass. The second term is the friction force between the slider and the concave surface. The coefficient of friction μ depends on pressure p and sliding velocity $\dot{D}$. The coefficient decreases with increasing pressure and becomes independent of velocity for speeds above 51 mm/s (2 in./sec) at pressures greater than about 14 MPa (20 ksi). A typical hysteresis loop for a FPS system for a shake table experimental program is shown in Fig. 5.3 [5]. The very linear nature of the restoring force, the high stiffness before sliding occurs, and the energy dissipation due to the sliding friction are clear from this figure. The equivalent (peak-to-peak) stiffness is given by

$$K_{\text{eff}} = \frac{W}{\mathbf{R}} + \frac{\mu W}{D}$$

The damping produced by friction at the sliding surfaces can be estimated

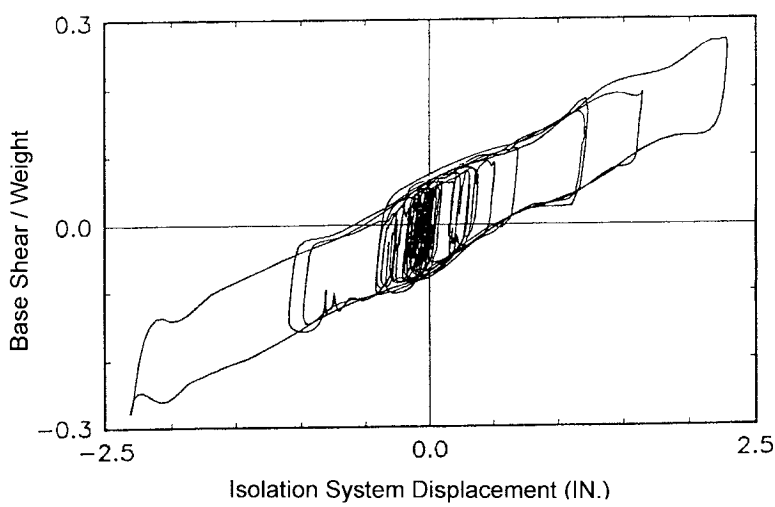

Fig. 5.3 Hysteresis loop from shake table tests for FPS.

by the code formula

$$\beta_{\text{eff}} = \frac{\text{area of hysteresis loop}}{4\pi K_{\text{eff}} D^2}$$

The area of the hysteresis loop is $4\mu WD$; thus

$$\beta = \frac{4\mu W d}{2\pi[(W/\mathbf{R})D + \mu W]d} = \frac{2}{\pi} \frac{\mu}{D/\mathbf{R} + \mu}$$

which ranges from $2/\pi$ for small D to $2\mu/(\pi\mathbf{R}/D)$ as D increases. For example, if D = 254 mm (10 in.) and $\mathbf{R}$ = 1 m (39.4 in.) with μ = 0.06, we have β = 12%.

To understand the geometry of the FPS, it is useful to invert the equation above relating T to $\mathbf{R}$. For fixed period T, we have

$$\mathbf{R} = \frac{gT^2}{(2\pi)^2} \approx 10T^2$$

so that we need a radius of around 1 m (39.4 in.) for a 2-sec period. If the horizontal displacement D of the system is 254 mm (10 in.), then the upward displacement δ_V given by

$$\delta_V = \mathbf{R}\left[1 - \cos\left(\arcsin\frac{D}{\mathbf{R}}\right)\right]$$

will be around 32 mm (1.26 in.). Thus, a horizontal motion of ±254 mm (±10 in.) at around 2-sec period also generates a vertical motion with a range of 32 mm (1.26 in.) at a period of 1 sec. The approximate form for the vertical displacement

$$\delta_V = \frac{1}{2}\frac{D^2}{\mathbf{R}}$$

indicates that the vertical displacement is roughly quadratic in the horizontal displacement.

Another aspect of the FPS is that if the displacement is less than a certain factor of the radius, the restoring force can be less than the frictional force and the system will not be recentering. This factor is obtained by equating the two terms in the force equation. Thus, the system will not recenter if $D/\mathbf{R} \leq \mu$. This can be a problem in long-period systems; for example, if T = 5 sec, $\mathbf{R}$ = 6.35 m (20.8 ft), with μ = 0.06, the system will not recenter if $D \leq$ 381 mm (15 in.).

The extremely simple modeling of the FPS makes it very attractive; however, its very simplicity is the main disadvantage of the system. It is essentially a one-parameter system, and that parameter is controlled by the radius of the concave surface. In order for the various articulated surfaces to slide together, all surfaces have to be spherical. Thus, the response is linear over the entire range of displacement.

5.5 MODELING OF ISOLATION BEARINGS BY BILINEAR MODELING

In practice all isolation bearings are modeled by a bilinear model based on the three parameters K_1, K_2, and Q, as shown in Fig. 5.4. The elastic stiffness K_1 is either estimated from available hysteresis loops from elastomeric bearing tests or as a multiple of K_2 for lead-plug bearings and friction pendulum bearings. The characteristic strength Q is estimated from the hysteresis loops for the elastomeric bearings. For lead-plug bearings Q is given by the yield stress in the lead and the area of the lead, while in the friction pendulum bearings it is given by the friction coefficient of the sliding surface and the load carried by the bearing. The postyield stiffness can be accurately estimated or predicted for all three types of bearings.

The effective stiffness, defined as the secant slope of the peak-to-peak values in a hysteresis loop, is given by

$$K_{\text{eff}} = K_2 + \frac{Q}{D} \qquad D \geq D_y$$

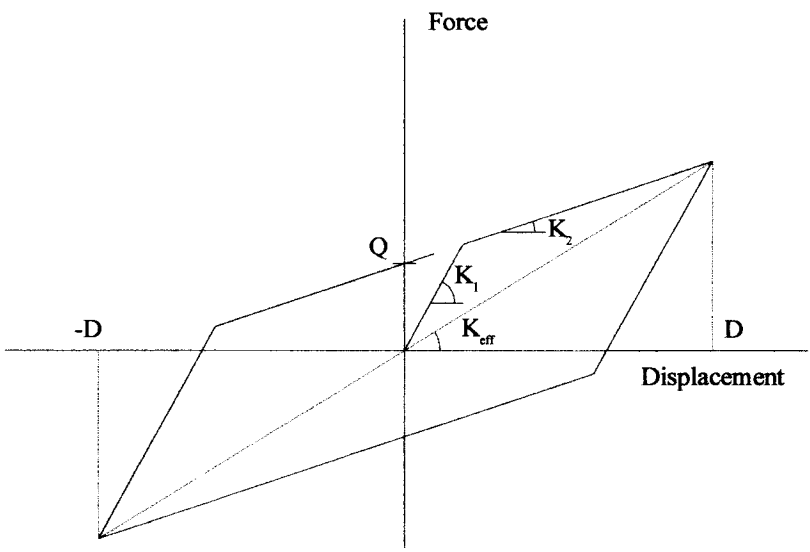

Fig. 5.4 Parameters of basic hysteresis loop for example problem.

where D_y is the yield displacement. In terms of the primary parameters,

$$D_y = \frac{Q}{K_1 - K_2}$$

and the area of the hysteresis loop (the energy dissipated per cycle), W_D, is given as

$$W_D = 4Q(D - D_y)$$

The effective damping β_{eff} is defined by

$$\beta_{\text{eff}} = \frac{4Q(D - D_y)}{2\pi K_{\text{eff}} D^2}$$

This can be expressed in nondimensional quantities by defining a nondimensional displacement

$$y = \frac{D}{D_y}$$

and a nondimensional characteristic strength

$$a = \frac{Q}{K_2 D_y}$$

whereby the effective damping becomes

$$\beta_{\text{eff}} = \frac{2a}{\pi} \frac{y - 1}{(y + a)y} \qquad y \geq 1 \tag{5.7}$$

For fixed a, $\beta = 0$ at $y = 1$ and tends to zero as $y \to \infty$. The maximum value of β given by $d\beta/dy = 0$ occurs at

$$y = 1 + (1 + a)^{1/2}$$

with

$$\beta_{\max} = \frac{2a}{\pi} \frac{1}{2(1 + a)^{1/2} + (2 + a)} \tag{5.8}$$

Now $a = Q/K_2 D_y$; thus from Eq. (5.6), we have

$$a = \frac{K_1 - K_2}{K_2} \tag{5.9}$$

This leads to the curious result that the maximum value of the effective damping depends only on the ratio of K_1 to K_2. The second slope, K_2, is easy to determine for any type of isolation system, but the first slope, K_1, is usually done by eye and can vary over a wide range. Since the characteristic strength Q can also be accurately determined, the value of K_1 has no influence on the effective stiffness but obviously has a strong influence on the damping and, in particular, on the maximum value, which can be an important promotional value for a proprietary system.

To illustrate the effect of the selection of K_1 on the damping, consider a system with the same Q and K_2 values (thus the same effective period at all values of D and the same hysteresis loop) but modeled by different values of K_1 (Fig. 5.4).

We take Q = 44.5 kN (10 kips) and K_2 = 350 kN/m (2 kips/in.):

$K_1^1 = 51K_2$ Corresponding to a friction pendulum system

$K_1^2 = 21K_2$ Corresponding to a lead-plug bearing

$K_1^3 = 6K_2$ Corresponding to a high-damping rubber bearing

$K_1^4 = 3K_2$ Another example of high-damping rubber bearing

The values of D_y, a for these are

$$D_y^1 = \frac{44.5}{50 \cdot 2} = 2.5 \text{ mm (0.10 in.)} \qquad a^1 = 50.0$$

$$D_y^2 = \frac{44.5}{20 \cdot 2} = 6.35 \text{ mm (0.25 in.)} \qquad a^2 = 20.0$$

$$D_y^3 = \frac{44.5}{5 \cdot 2} = 25.4 \text{ mm (1.00 in.)} \qquad a^3 = 5.0$$

$$D_y^4 = \frac{44.5}{2 \cdot 2} = 63.5 \text{ mm (2.50 in.)} \qquad a^4 = 2.0$$

The peak values of β and the displacement at which it occurs are as follows:

$\beta_{\max}^1 = 0.480$ at D = 20.8 mm (0.82 in.)

$\beta_{\max}^2 = 0.410$ at D = 35.6 mm (1.40 in.)

$\beta_{\max}^3 = 0.268$ at D = 87.6 mm (3.45 in.)

$\beta_{\max}^4 = 0.170$ at D = 173.5 mm (6.83 in.)

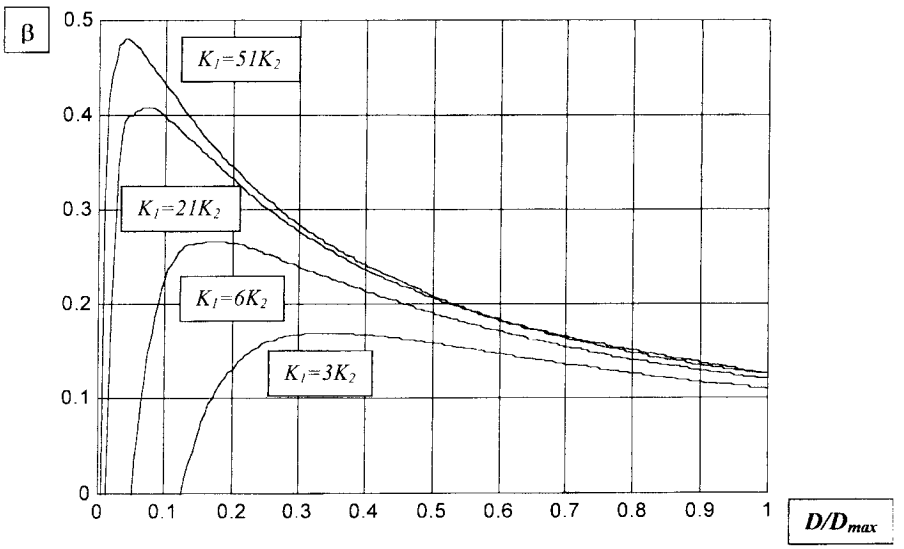

Fig. 5.5 Effective damping as a function for displacement for different choices of K_1.

The variation of β with D for the three cases is shown in Fig. 5.5, illustrating how the damping at small displacements can be very high if K_1 is selected to be large. It also shows that as D becomes large, all β-versus-D curves tend to become the same. The point is that the same hysteresis curve when modeled by a bilinear model can have a very different pattern of damping values, depending only on how the initial stiffness is selected.

To put the values used in Fig. 5.5 in perspective, suppose that the second slope, K_2 = 350 kN/m (2 kips/in.), corresponds to an isolator in a system with a period of 3 sec. The carried weight on an isolator is then

$$W = \frac{K_2}{\omega^2} g = \frac{2 \times 9}{(2\pi)^2} \times 386 = 786 \text{ kN (176 kips)}$$

The characteristic strength Q = 44.5 kN (10 kips) then means

$$\mu = \frac{Q}{W} = 5.6\%$$

which represents the friction factor for a friction pendulum system or the strength ratio for a lead-plug bearing.

5.6 IMPLICATIONS OF BILINEAR MODELING

The problem facing the isolation designer is that having obtained the value of C_{VM} for the site and assumed possible values for period and damping, there

is still the constraint of maximum acceptable value for the MCE displacement D_M. Suppose then that T, β, and D are specified and it is necessary to calculate the parameters of the model, namely, K_2 and Q, to provide these values.

With the period specified, the effective stiffness K_{eff} is given by

$$K_{\text{eff}} = \frac{W}{g}\left(\frac{2\pi}{T}\right)^2$$

then

$$W_D = 2\pi K_{\text{eff}} D^2 \beta$$

can be calculated, leading to

$$4Q(D - D_y) = 2\pi\left(\frac{W}{g}\right)\left(\frac{2\pi}{T}\right)^2 D^2\beta$$

At this point we neglect D_y and estimate Q from

$$Q = \frac{W_D}{4D} = \frac{\pi}{2} K_{\text{eff}} D\beta$$

leading to an initial value of Q/W. It is then possible to estimate $K_2 = K_{\text{eff}} - Q/D$ and D_y, assuming, for example, for a lead-plug bearing that $K_1 = 10K_2$ or for a friction pendulum system that $K_1 = 100K_2$. With the approximate value of D_y, the estimate of Q and K_2 can be improved, and with these values the design of the system can proceed.

For example, suppose the code formula for D_M leads to a displacement of 76 cm (30 in.) for a period of 2.5 sec and 5% damping. To reduce this to a feasible level of displacement, say, 50 cm (20 in.), requires that $B = 1.5$ and $\beta = 0.30$. The value of K_{eff} for $T = 2.5$ sec is

$$K_{\text{eff}} = 0.644W \text{ kN/m} \qquad (K_{\text{eff}} = 0.01636W \text{ kips/in.})$$

and the value of W_D is given as

$$W_D = (0.3)2\pi(0.644)(0.25)W = 0.308W \text{ kN/m}$$
$$[W_D = (0.3)2\pi(0.01636)(400)W = 12.3W \text{ kips/in.}]$$

from which we get (neglecting D_y from the first estimate)

$$\frac{Q}{W} = \frac{W_D}{4D} = \frac{0.303}{4(0.5)} = 0.154 \qquad \left(\frac{Q}{W} = \frac{12.3}{4(20)} = 0.154 \right)$$

The first estimate for K_2 is

$$K_2 = \left(0.644 - \frac{0.154}{0.5} \right) W \qquad \left(K_2 = 0.01636W - \frac{0.154}{20} W \right)$$
$$= 0.366W \qquad \left(= 0.00865W \right)$$

and

$$D_y = \frac{0.154}{9(0.336)} = 0.51 \text{ m} \qquad \left(D_y = \frac{0.154}{9(0.00865)} = 1.98 \text{ in.} \right)$$

A recalculation of Q, including this estimate of D_y, is $Q/W = 0.171$, with a second estimate of K_2 as

$$K_2 = 0.306W \text{ kN/m} \qquad (K_2 = 0.00768W \text{ kips/in.})$$

Thus we need a lead core that produces a characteristic force of 17% of W to get this level of damping. Suppose now we postulate a service level earthquake (SLE), for example, that earthquake that might have a 50% chance of being exceeded in 50 years, and assume that for this level of input the seismic coefficient C_V is half that at the DBE, that is, $C_{VS} = \frac{1}{2} C_V D$, then $C_{VS} = (1/2.4)C_{VM}$. Therefore, we can anticipate a displacement D_S that is not more than $(1/2.4)D_M$. Assuming that in this case D is approximately 125 mm (5 in.), at this level of displacement we have

$$K_{\text{eff}} = 0.306W + \frac{0.171}{0.125} W \qquad \left(K_{\text{eff}} = 0.00781W + \frac{0.171}{5} W \right)$$
$$= 1674 \text{ kN/m} \qquad \left(= 0.0420W \text{ kips/in.} \right)$$

and

$$W_D = 4Q(D - D_y) \qquad \left(W_D = 4Q(D - D_y) \right.$$
$$= 4(0.171)(0.125 - 0.51) \qquad \left. = 4(0.171)(5 - 1.98)W \right)$$
$$= 0.0506 \text{ kN/m} \qquad \left(= 2.066W \text{ kips/in.} \right)$$

giving

$$\beta = 0.31$$

and

$$B = 1.5 + 0.20 \times \tfrac{1}{10} = 1.52$$

The period $T = 1.56$ sec. Assuming that $C_{VS} = (1/2.4)C_{VM}$ and that C_{VM} leads to 76 cm (30 in.) at $T = 2.5$ sec and $\beta = 5\%$, we have

$$D_S = \frac{30}{2.4}\,\frac{1.56}{2.5}\,\frac{1}{1.52} = 130 \text{ mm } (5.13 \text{ in.})$$

The unreduced base shear at this displacement is

$$K_{\text{eff}}D_S = 1.674W \times 13 = 0.22W \text{ kN} \qquad \left(K_{\text{eff}}D_S = 0.0420W \times 5.13 = 0.22W \text{ kips} \right)$$

which is only just above the characteristic strength $Q = 0.171W$; therefore, with this design, very little isolation effect is possible.

For a friction pendulum device the results are similar. Since D_y for the friction pendulum system is generally negligible, the required Q is only $0.154W$, corresponding to a friction factor of 15.4%. The required K_2 in this case is

$$K_2 = 0.644 - \frac{0.154}{0.508} = 0.34W \text{ kN/m} \qquad \left(K_2 = 0.01636 - \frac{0.154}{20} = 0.00965W \text{ kips/in.} \right)$$

If we assume that for a SLE we have a displacement D_S of around 125 mm (5 in.), we find

$$K_2 = 0.341W + \frac{0.154W}{0.125} = 1.573W \text{ kN/m} \qquad \left(K_{\text{eff}} = 0.00865W + \frac{0.154}{5}W = 0.0395W \text{ kips/in.} \right)$$

and

$$W_D = 4(0.154W)0.125 = 0.077W \text{ kN/m} \qquad \left(W_D = 4(0.154W)5 = 3.08W \text{ kips/in.} \right)$$

giving

$$\beta = 0.496 \qquad T = 1.61 \text{ sec} \qquad B = 2.0$$

leading to

$$D_S = \frac{1}{2.4}\,\frac{1.61}{2.50}\,\frac{30}{2} = 100 \text{ mm (4 in.)}$$

and the unreduced base shear is $4 \times K_{\text{eff}} = 0.189W$, which exceeds the slip force, $0.154W$; therefore, for this level of input, the system will not move.

These results mean that the code formulas and the modeling procedure lead to isolation systems that will not work at what might be considered occasional rather than rare levels of earthquake input. In case the impression is that a displacement of 76 cm (30 in.) at 2.5-sec period and 5% damping represents the extreme case of the code formula, it should be noted that buildings in downtown Berkeley and all of the University of California at Berkeley are within 2 km (1.24 miles) of an active fault that could produce a moment magnitude greater than or equal to 7.0 and has a slip rate exceeding 5 mm (0.2 in.) per year, thus qualifying for seismic source type A. With these site parameters and S_D soil type, the MCE displacement at 2.5 sec and 5% damping can exceed 1 m (40 in.).

5.6.1 Energy Dissipation in High-Damping Natural Rubber Bearings

The mechanical characteristics determined from cyclic testing of seismic isolation devices at a constant frequency are typically expressed as a function of displacement D using two parameters: the effective stiffness K_{eff} and the equivalent viscous damping β_{eq}. (Note that in the following discussion, global bearing properties such as displacement, force, and viscous damping coefficient are used. Alternatively, the model can be formulated in terms of rubber material properties such as strain, stress, and material damping coefficient, thereby allowing analyses to be performed based on only material properties and not requiring test results from actual bearings.)

High-damping natural rubber isolators are characterized by stiff behavior (high K_{eff}) at shear strains up to about 25%, a substantial decrease in K_{eff} up to a strain of 150–200%, and then an increase in K_{eff} above this strain due to strain crystallization in the material. (The strains at which these stiffness changes are observed depend on the elastomer compound.) Examples of the variation of K_{eff} and β_{eq} as a function of displacement are shown in Fig. 5.6 for the bearings evaluated in this study.

For high-damping natural rubber bearings, β_{eq} typically decreases with increasing strain but W_D does not. Several recent tests of elastomeric isolators [64, 68] have shown that over a wide range of strains W_D is proportional to the shear strain γ raised to an exponent of approximately 1.5. (In practice, the actual value varies from about 1.45 to 1.75, depending on the compound

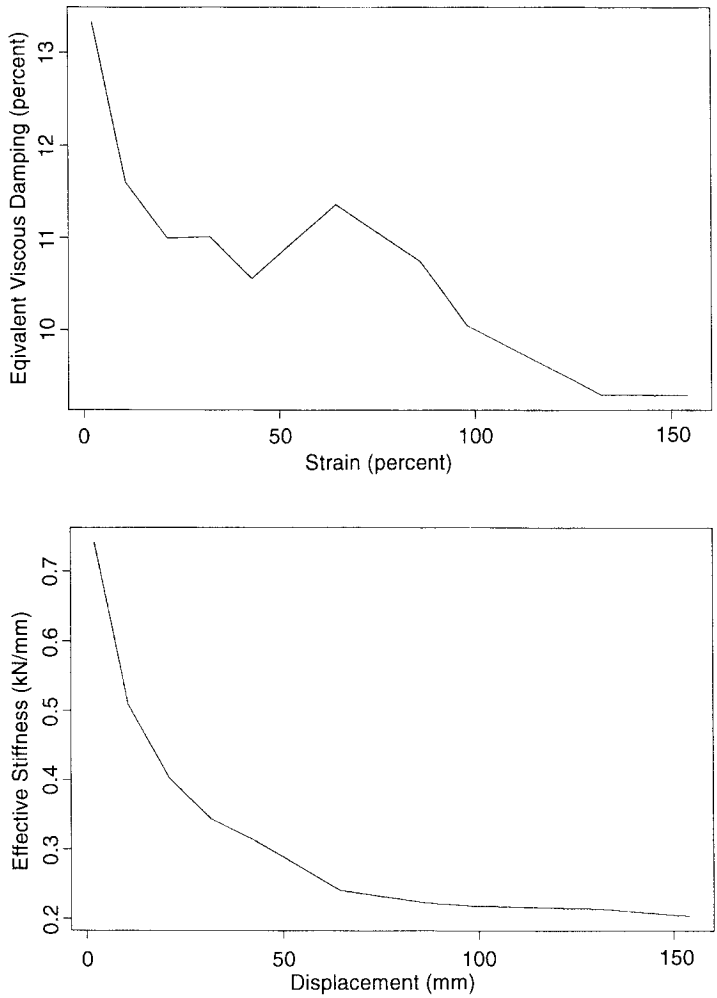

Fig. 5.6 Stiffness and damping of high-damping natural rubber isolators.

under consideration.) Similar results, expressed in terms of displacement, can be seen for the bearings in this study in a log-log plot of displacement versus W_D (Fig. 5.7). In this case the exponent is about 1.61. Considered on a molecular level, the nature of the high-damping natural rubber material suggests that the internal energy dissipation mechanisms may be a combination of frictional and viscous components; however, no fundamental physical process that leads to a constant near 1.5 has been identified.

Definition of Energy-Based Model The empirical observations outlined above can be used to model an elastomeric isolation system as a combination of a linear elastic spring element, a pure hysteretic element (W_D proportional

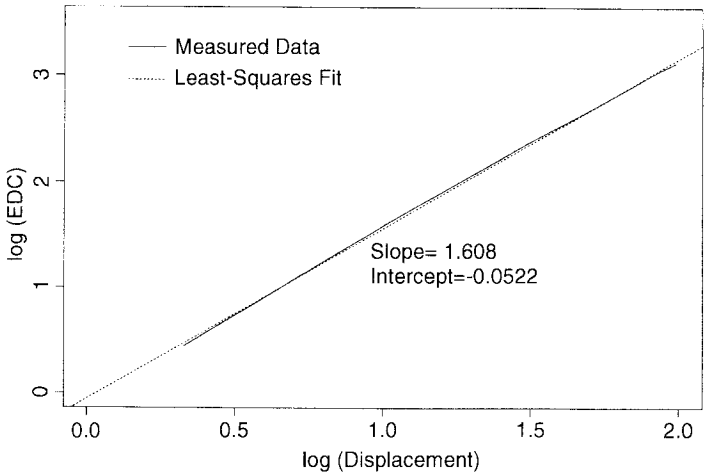

Fig. 5.7 Energy dissipation characteristics of high-damping rubber isolators.

to $D^{1.0}$), and a pure viscous element (W_D proportional to $D^{2.0}$). The goal is to determine the properties of each of these elements such that the W_D of the combined system is proportional to approximately $D^{1.5}$ over a given strain range. The four parameters necessary for the basic form of the model are K_1 (the elastic stiffness of the linear spring element), K_2 [the elastic stiffness of the hysteretic (elastic–plastic) element], F_y (the yield force of the hysteretic element, alternately D_y, the yield displacement of the hysteretic element), and C (the viscous coefficient of the linear damping element). Once these parameters are determined, the model can be implemented directly in any nonlinear structural analysis program that includes this basic set of elements (for example, 3D-BASIS [96], DRAIN-2DX [6], or LPM [59]).

To derive the equations for the nonlinear element properties, the energy dissipated by the model in one cycle is first expressed as

$$W_{D_m} = 4F_y(D - D_y) + \pi C\omega D^2 \tag{5.10}$$

which, neglecting the terms in D_y for large bearing displacements under a design level earthquake, becomes

$$W_{D_m} = 4F_yD + \pi C\omega D^2 = aD + bD^2 \tag{5.11}$$

where a and b are unknown constants.

Based on the observations in the previous section, the energy dissipated in a bearing during a cyclic test at a constant frequency can be approximated by the relationship

$$W_{D_b} = cD^{\alpha} \tag{5.12}$$

where $\alpha \cong 1.5$ for filled elastomers and c is an experimentally determined constant. The coefficients a and b, which define the energy-based model, are then determined by minimizing the difference between the energy dissipated in the model [Eq. (5.11)] and the energy dissipated in the bearing [Eq. (5.12)] over some displacement limits D_1 and D_2 as follows:

$$\epsilon = \int_{D_1}^{D_2} (W_{D_m} - W_{D_b})^2 \, dD \tag{5.13}$$

$$\frac{d\epsilon}{dD} = 0 \tag{5.14}$$

The best choices of a and b can be shown to be

$$a = c \frac{\left(\frac{D_2^{2+\alpha} - D_1^{2+\alpha}}{2+\alpha}\right)\left(\frac{D_2^5 - D_1^5}{5}\right) - \left(\frac{D_2^{3+\alpha} - D_1^{3+\alpha}}{3+\alpha}\right)\left(\frac{D_2^4 - D_1^4}{4}\right)}{\left(\frac{D_2^3 - D_1^3}{3}\right)\left(\frac{D_2^5 - D_1^5}{5}\right) - \left(\frac{D_2^4 - D_1^4}{4}\right)^2} \tag{5.15}$$

$$b = c \frac{\left(\frac{D_2^{3+\alpha} - D_1^{3+\alpha}}{3+\alpha}\right)\left(\frac{D_2^3 - D_1^3}{3}\right) - \left(\frac{D_2^{2+\alpha} - D_1^{2+\alpha}}{2+\alpha}\right)\left(\frac{D_2^4 - D_1^4}{4}\right)}{\left(\frac{D_2^3 - D_1^3}{3}\right)\left(\frac{D_2^5 - D_1^5}{5}\right) - \left(\frac{D_2^4 - D_1^4}{4}\right)^2} \tag{5.16}$$

If the model parameters F_y and C are given by

$$F_y = a/4 \quad \text{and} \quad C = b/(\pi\omega) \tag{5.17}$$

over which displacement range should the energy difference be minimized? If D_1 and D_2 are selected as zero and the maximum anticipated displacement, respectively, it is unlikely that good agreement will be obtained over the entire displacement range. Therefore, D_1 and D_2 should be chosen to bracket the expected maximum displacement by perhaps ±20–30%, ensuring that the energy dissipated during the peak displacement cycles will be accurately represented by the model. Repeated analyses with some iteration may be required to converge on the appropriate displacement range, depending on the intensity of the input.

The selection of the final model parameters, K_1 and K_2, is best made using the shape of the measured hysteresis loop at the target displacement. This is shown schematically in Fig. 5.8. The logical choice for K_2 is the tangent stiffness at zero displacement; in the figure, K_2 was determined by performing a least-squares fit on the data to ±70% of the maximum displacement (solid lines). The choice of K_1 is best done by eye to match approximately the initial unloading stiffness after the peak excursion of the loop. Note that while K_2 may remain approximately constant over a wide displacement range, the best choice for K_1 (the unloading slope) will likely vary.

5.6.2 Adjustments to the Model to Account for High-Strain Stiffening

An additional refinement to the basic model is required if the bearing is expected to displace into the stiffening portion of its force–displacement curve, and this is best achieved by incorporating a gap element that is activated above a certain displacement. The most straightforward approach is to use a linear elastic gap element that does not dissipate energy; this type of element is available in several widely used analysis programs, including DRAIN-2DX and SAP2000. From actual bearing tests, however, it is apparent that the stiffness does not change suddenly but increases rather smoothly as a function of strain until near failure. The stiffening model incorporated in the program 3D-BASIS-ME [125] captures this behavior relatively well by combining a hysteretic element with an elastic element having a stiffness that can be defined to increase linearly over a defined displacement range. This approach exhibits hysteretic behavior that is closer to that recorded in real bearings, but it still does not guarantee that the energy dissipation characteristics will be captured accurately. In particular,

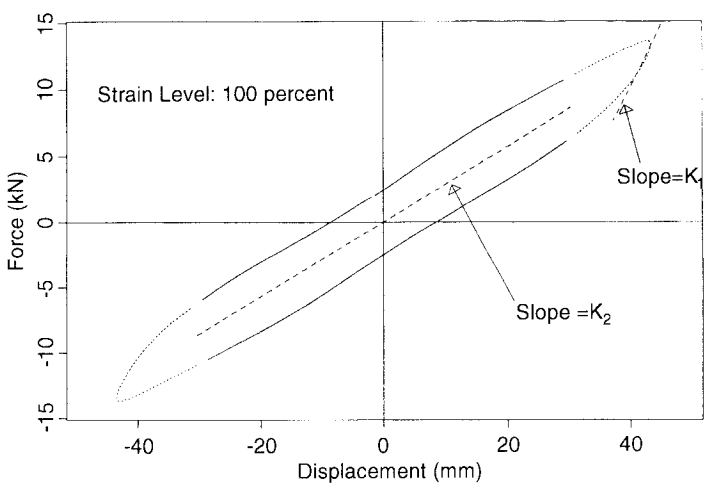

Fig. 5.8 Selection of model parameters—K_1 and K_2.

because the stiffening element is elastic, it may not reproduce the substantial dissipation that high-damping natural rubber bearings exhibit upon unloading from the stiffening portion of the force–displacement curve.

The gap/stiffening element proposed here alleviates this shortcoming by defining separate loading and unloading curves that enhance the energy dissipation in the stiffening portion of the loop. The element force in both curves is a power function of the displacement in the element, and the exponent in the unloading branch is greater than that in the loading branch to provide dissipation. The general expressions for the element force in terms of the displacement are

$$F_S = \begin{cases} K_U \operatorname{sgn}(D)(|D| - D_{\text{gap}})^n & \text{for loading} \quad (5.18) \\ K_L \operatorname{sgn}(D)(|D| - D_{\text{gap}})^m & \text{for unloading} \quad (5.19) \end{cases}$$

where F_S is the force in the element, D_{gap} is the displacement where stiffening initiates, n and m are the hardening exponents, and K_L and K_U are the stiffness coefficients (loading and unloading). Because K_L and K_U must be defined such that the loading and unloading branches intersect at the top of the loop, K_U is, therefore, dependent on the previously calculated maximum force and displacement. The exponents n and m are best determined by eye to achieve a close approximation to the measured loading and unloading curves.

Finally, to ensure that the composite model (the combination of linear, viscous, hysteretic, and stiffening elements) dissipates the desired quantity of energy at the target displacement, we need to define the parameters for the viscous and hysteretic elements at the displacement at which the gap element is activated, then determine the required W_D at the target displacement using the logarithmic relationship, and finally calculate the energy dissipated by the composite element at the target displacement.

The energy dissipated by the gap element in a fully reversed hysteresis cycle can be shown to be

$$W_{D_{\text{gap}}} = 2\left[K_L \frac{(D_{\max} - D_{\text{gap}})^{n+1}}{n+1} + K_U \frac{(D_{\max} - D_{\text{gap}})^{m+1}}{m+1}\right] \quad (5.20)$$

Note that this calculation assumes that the frequency of loading at the target displacement is the same as at the displacement where the gap element is activated. If this is true, the energy dissipated by the viscous element will have been increased inadvertently. To correct this shortcoming, the coefficient of the viscous element is reduced so that the energy dissipated by the model equals that dissipated in the bearing (based on the observed logarithmic relationship).

5.6.3 Comparisons with Experimental Data

The validity of the model and its sensitivity to frequency variations are evaluated by comparing its performance to recorded bearing hysteresis loops. While the goal of the formulation is to dissipate equal energies in the model and the bearing, the fit with the observed force–displacement (neglecting stiffening) depends in large part on the selection of parameters K_1 and K_2. As mentioned above, the selection of K_2 is straightforward; in the examples shown here it is taken as the least-squares fit on the data to ±70% of the maximum displacement (before stiffening). The choice of K_1 is not as easy, however, because it defines the stiffness under two separate modes of behavior—the initial stiffness when the bearing is first loaded and the unloading stiffness after a displacement peak has been reached. To achieve the close fit in the fully reversed loop shown in Fig. 5.9, K_1 has been chosen to be much lower than the initial tangent stiffness to the unloading curve. If K_1 is too soft, however, the assumption that D_y is negligible compared to D_{max} that was made in the derivation of the model may not be correct, and the energy dissipation of the hysteretic element will be less than required. In most cases the majority of the energy is dissipated by the viscous element, so this should not be a significant problem. But if reproducing the behavior of the bearing at small displacements is essential, a large initial stiffness will be required for the hysteretic element, with the trade-off that the unloading behavior near the peak displacements will not be matched closely.

An additional consideration in the basic model relates to the frequency of loading, since the coefficient of the viscous element is defined to be inversely related to the loading frequency [Eq. (5.17)]. In the examples provided here, the bearings were tested at a rate of 1.0 Hz; however, a typical design fre-

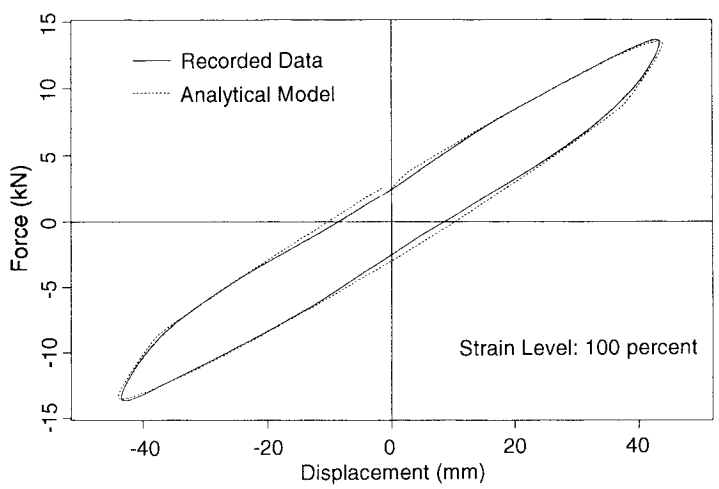

Fig. 5.9 Comparison of analytical model with recorded data.

quency might be 0.5 Hz. If the model derived from 1.0 Hz testing is subjected to cyclic loading at 0.5 Hz, the viscous element will dissipate substantially less energy than anticipated. Most high-damping natural rubber compounds do not exhibit significant rate dependence within the range of frequencies anticipated in seismic applications, so there will be relatively little change in the energy dissipated by the real bearing, as illustrated in Fig. 5.10. It is important to note that the oversensitivity to frequency in the model will lead to conservative results in terms of displacement because the energy dissipated reduces as the loading frequency reduced. For the low-frequency ground motions that are most critical to the behavior of isolated structures, the energy dissipated will be underpredicted, leading to conservative displacement estimates. This problem can be solved by modifying the frequency used to define the coefficient of the viscous element over a series of analyses until the computed response frequency in the cycle or cycles at the maximum displacement equals that assumed in the analysis. This assures the proper energy balance between the model and the bearing.

When the model is extended to larger displacements, three parameters must be defined: the displacement at which the gap/stiffening element is activated, the exponent on loading, and the exponent on unloading. (Both exponents may vary somewhat with displacement, depending on the shape of the loop and the accuracy with which the force–displacement relationship must be matched.) Figure 5.11 compares observed hysteresis data to 350% shear strain, with the response of the model defined using the procedure outlined above. In this case stiffening begins at a displacement of 4 in. (225% shear strain), and the parameters of the viscous and hysteretic elements are also defined at this displacement. The stiffening element has an exponent upon loading of 1.5 and an exponent upon unloading of 1.7. The parameters K_L and K_U are defined based on the maxi-

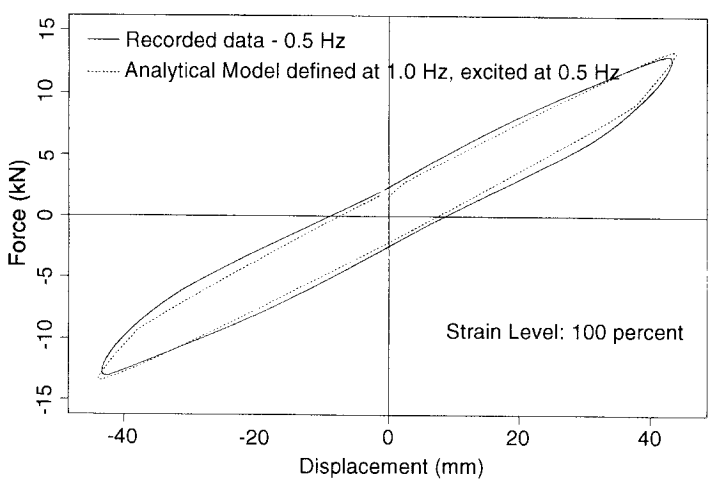

Fig. 5.10 Sensitivity of model to loading frequency.

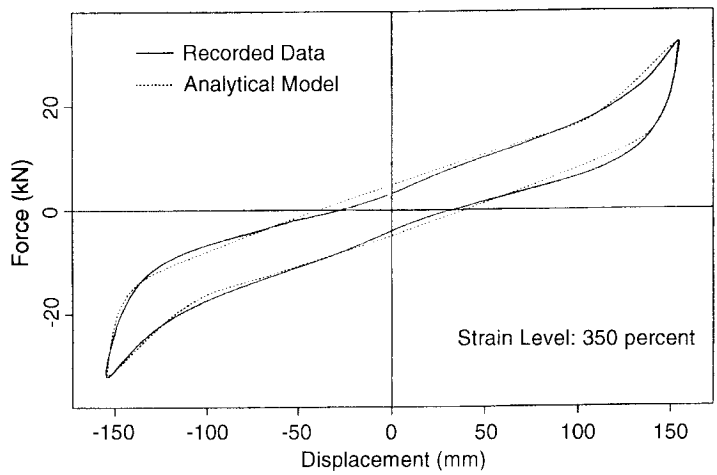

Fig. 5.11 Large displacement behavior of the model.

mum recorded force in the bearing and their respective exponents. To ensure appropriate energy dissipation in the analytical loop (including the contribution from the stiffening element), the coefficient of the viscous element is reduced by 34%, and the final analytical loop area is only 1.4% different than the measured area. The analytical relationship does not precisely track the measured force–displacement (particularly near-zero displacement where the measured loop is slightly pinched) but should be satisfactory for dynamic analyses.

CHAPTER 6

BUCKLING AND STABILITY OF ELASTOMERIC ISOLATORS

6.1 INTRODUCTION

A multilayered elastomeric bearing can be susceptible to a buckling type of instability similar to that of an ordinary column but dominated by the low-shear stiffness of a bearing. The previous analysis of the overall deformation of a single pad can be used in a buckling analysis that treats the bearing as a continuous composite system. This analysis considers the bearing to be a beam, and the deformation is assumed to be such that plane sections normal to the undeformed central axis remain plane but not necessarily normal to the deformed axis.

The theory for the buckling of isolation bearings is an outgrowth of work by Haringx in 1947 on the mechanical characteristics of helical steel springs and rubber rods used for vibration mountings. This work was published in a series of reports, the third of which [49] covers the stability of solid rubber rods. The Haringx theory was later applied by Gent [44] to the problem of the stability of multilayered rubber compression springs, and it is this application that forms the basis for the theory given here.

The method parallels the linear elastic analysis of the Euler buckling of a column. To model the rubber isolator as a continuous beam, it is necessary to introduce certain modifications to the quantities defined in the previous section. Consider the bearing to be a column of length h with a cross-sectional area A and define the shear stiffness per unit length as $P_S = GA_S$, where A_S is an effective shear area given by

$$A_S = A \frac{h}{t_r}$$

Design of Seismic Isolated Structures: From Theory to Practice. F. Naeim and J. M. Kelly

where h is the total height of the bearing (rubber plus steel) and t_r is, as defined earlier, the total height of rubber. The increase in A is needed to account for the fact that steel does not deform in the composite system. The bending stiffness is similarly modified, so that $(EI)_{\text{eff}}$ for a single pad of thickness t becomes EI_S, where

$$EI_S = E_C(\tfrac{1}{3})I \frac{h}{t_r}$$

In terms of these quantities, the overall horizontal stiffness K_H (which was GA/t_r) becomes

$$K_H = \frac{GA_S}{h}$$

and the Euler buckling load for a column with no shear deformation is

$$P_E = \pi \frac{EI_S}{h^2}$$

The usual situation for a bearing in an isolation system is shown in Fig. 6.1. The bearing is constrained against rotation at both ends and is free to move sideways at the top. The result for the critical buckling load P_{crit} is the solution of the equation

$$P^2 + PP_S - P_S P_E = 0 \tag{6.1}$$

from which the critical load P_{crit} is given by

$$P_{\text{crit}} = \frac{-P_S + \sqrt{P_S^2 + 4P_S P_E}}{2} \tag{6.2}$$

If we now assume that $P_S \approx GA$ and

$$P_E \approx \frac{1}{3} \frac{6GS^2 I\pi^2}{h^2} \approx GA\left(\frac{2\pi^2 S^2 I}{A}\right)$$

then, for most types of bearings where $S \geq 5$, $P_E \gg P_S$, the critical load can be approximated by

$$P_{\text{crit}} = (P_S P_E)^{1/2} \tag{6.3}$$

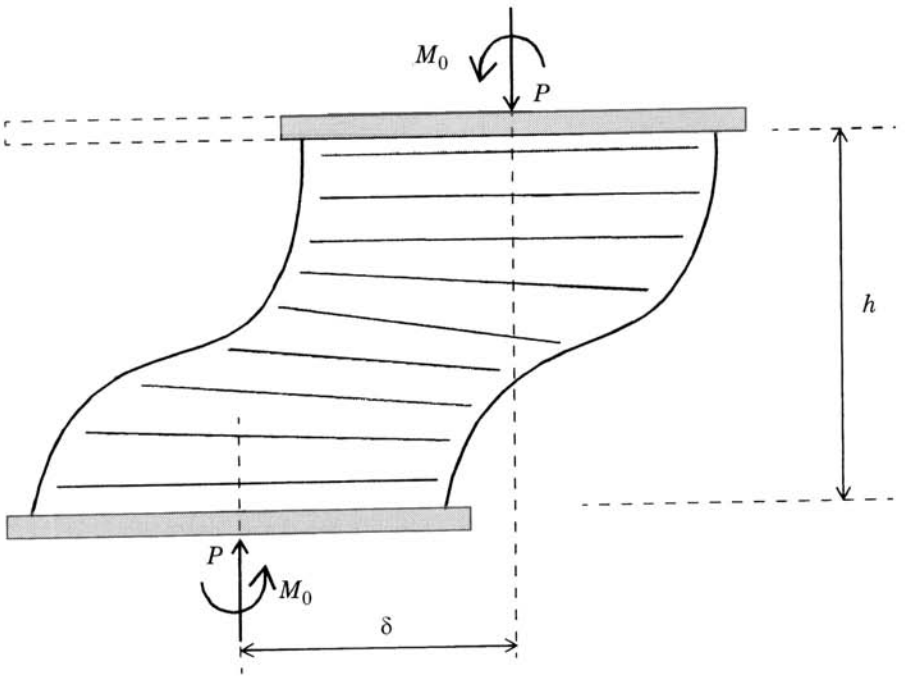

Fig. 6.1 Boundary conditions for an isolation bearing under a vertical load P (the bearing buckles with no lateral-force constraint but is prevented from rotating at each end).

Using this expression and recalling that

$$P_S = GA\,\frac{h}{t_r} \qquad P_E = \frac{\pi^2}{h^2}\,\frac{1}{3}\,E_c I\,\frac{h}{t_r} \tag{6.4}$$

we have

$$P_{\text{crit}} = \begin{cases} \left(GA\,\dfrac{h}{t_r}\right)^{1/2}\left(\dfrac{\pi^2}{h^2}\,\dfrac{1}{3}\,6GS^2\,Ar^2\,\dfrac{h}{t_r}\right)^{1/2} \\ \dfrac{\sqrt{2}\pi GASr}{t_r} \end{cases}$$

where the radius of gyration is denoted by $r = \sqrt{I/A} = a/2\sqrt{3}$ for a square bearing with side dimension a and $\Phi/4$ for a circular bearing with diameter Φ.

The critical pressure $p_{\text{crit}} = P_{\text{crit}}/A$ can be expressed in terms of S and the

quantity S_2, referred to as the aspect ratio or the second shape factor, defined by

$$S_2 = \frac{\Phi}{t_r} \quad \text{or} \quad \text{or} \quad \frac{a}{t_r}$$

Thus

$$\frac{p_{\text{crit}}}{G} = \begin{cases} \dfrac{\pi}{2\sqrt{2}} SS_2 & \text{for a circular bearing} \\ \dfrac{\pi}{\sqrt{6}} SS_2 & \text{for a square bearing} \end{cases} \tag{6.5}$$

In actual design the load carried by a bearing (say, W) will be less than the critical load, and neglecting the effect of the vertical load on the horizontal stiffness K_H of the bearing, that is given by $K_H = GA/t_r$, which in turn is related to the horizontal frequency ω_H through

$$\omega_H^2 = \frac{K_H}{W} g$$

Thus, the safety factor SF against buckling, which is defined by $\text{SF} = P_{\text{crit}}/W$, becomes

$$SF = \frac{\sqrt{2}\pi S \omega_H^2 r}{g} \tag{6.6}$$

All other things being equal, the safety factor increases with shape factor S, frequency ω_H, or bearing size (either a or Φ).

The bearing size will, of course, depend on the carried load. If the pressure $p = W/A$ is specified, then

$$r = \begin{cases} 2\sqrt{\pi} \left(\dfrac{W}{p}\right)^{1/2} & \text{for a circular bearing} \quad (6.7) \\ \dfrac{1}{2\sqrt{3}} \left(\dfrac{W}{p}\right)^{1/2} & \text{for a square bearing} \quad (6.8) \end{cases}$$

If the pressure is fixed, the safety factor will diminish as $W^{1/2}$, leading to the unexpected result that buckling can become a problem for bearings that are lightly loaded.

To get a feeling for the magnitude of the quantities involved, suppose that the safety factor must be at least 3, the shape factor S is 10, and the frequency is π radians per second (2.0-sec period), all of which are typical values. In this case, r must be at least

$$r = \frac{3 \times 9810}{\sqrt{2}\pi \times 10 \times \pi^2} = 67.0 \text{ mm } (2.64 \text{ in.})$$

If the bearing is circular, then $\Phi = 268$ mm (10.6 in.). This minimum dimension is independent of the carried load or the pressure, but if the pressure is specified, say, for example, at 6.90 MPa (1000 psi), it translates to a minimum load of 390 kN (88 kips). For most buildings the bearings will be much larger than this minimum size and the carried loads will be in the hundreds of tons, so that buckling is not likely to be a problem for the design.

There have been cases, however, when it has been necessary to design isolators for lighter loads, for example, circuit breakers in electric power plant switch yards. These components weigh as little as a few tons and the bearing design should be stable under loads that range from 10 to perhaps 50 kN (2–10 kips). Bearings developed for such applications are referred to as "enhanced stability bearings." In these bearings the tilting stiffness is increased either by making the bearing an assembly of small bearings connected by steel plates [69] or by individual rubber discs connected by steel plates [128]. The first application of a bearing of this kind was carried out for circuit breakers at the Edmunson Power Plant near Bakersfield, California [69]. The stability analysis given here for the single bearing is applicable to these enhanced stability bearings.

Influence of Vertical Load on Horizontal Stiffness When the load carried by the bearing is comparable to the buckling load, the horizontal stiffness K_H is reduced. The reduction is obtained by using the same linear elastic analysis and is given by

$$K_H = \frac{GA_S}{h}\left[1 - \left(\frac{P}{P_{\text{crit}}}\right)^2\right] \tag{6.9}$$

If the load is less than 0.32 times the buckling load, the accuracy of the usual formula for K_H is better than 10%, and in most designs that requirement will ensure that this is the case.

The downward displacement δ_V of the top of a bearing carrying a vertical load P and displaced through a sideways movement at the top of D is also given by the buckling analysis in the form

$$\delta_V = \frac{P_S + P}{P_E} \frac{D^2}{h} \tag{6.10}$$

In most cases, $P \gg P_S$; thus

$$\delta_V = \frac{P}{P_{\text{crit}}} \frac{P_{\text{crit}}}{P_E} \frac{D^2}{h}$$

$$= \left(\frac{P}{P_{\text{crit}}} \right) \sqrt{\frac{P_S}{P_E}} \frac{D^2}{h} \tag{6.11}$$

Now

$$\frac{P_S}{P_E} = \frac{GA_S h^2}{\pi^2 E I_S} = \frac{Ah^2}{2\pi^2 I S^2} \tag{6.12}$$

In terms of $r = (I/A)^{1/2}$, we have

$$\frac{\delta_V}{h} = \frac{P}{P_{\text{crit}}} \frac{h}{\sqrt{2}\pi r S} \frac{D^2}{h^2} \tag{6.13}$$

This downward displacement is in addition to that produced by pure compression of the isolator and is caused by the rotation of the reinforcing steel shims in the center of the bearing. This rotation produces a shear stress caused by the component of the vertical load along the rotated layers, and the resulting shear strain causes the downward movement of the top of the bearing.

6.2 STABILITY UNDER LARGE LATERAL DISPLACEMENT

The buckling analysis for an elastomeric isolator is based on the linear theory that is analogous to the buckling analysis of a column and, as is the case in the usual theory, provides the buckling load or buckling stress in the undisplaced position but no information on the stability of a bearing in the displaced position, the instability will manifest itself by the loss of positive incremental horizontal stiffness. This type of instability is of crucial importance in bearing design since the peak downward load on an isolator will occur at the same time as the peak horizontal displacement and in combination will be one of the limit states for which the isolator will need to be proportioned.

In principle, a complex nonlinear analysis will be needed to predict the bearing behavior under the combination of peak vertical load and maximum horizontal displacement. There are two simple hypotheses for an approximation

to the limit state when an isolator is loaded in shear and with vertical load. The first is that the critical displacement, defined as the displacement under which that bearing exhibits zero incremental horizontal stiffness, is the lateral displacement at which the reduced area compression stress calculated from the axial load divided by A_r (the area of overlap between top and bottom) reaches the critical stress p_{crit} given by Eq. (6.5).

The second hypothesis is that the area A in the expression for the critical load in the undeformed configuration [Eq. (6.4)] is replaced by the reduced area A_r. This is perhaps the most plausible for the two possibilities as the concentration of the vertical stress due to displacement will not affect the bending resistance but could reduce the resistance due to shear.

For a square bearing of side dimension B, the reduced area A_r is given by

$$A_r = B(B - D) \tag{6.14}$$

so that if the first hypothesis is correct, the critical displacement D_{crit} under a specified load P is given by

$$\begin{aligned} P &= p_{\text{crit}} A_r \\ &= \frac{\pi}{\sqrt{6}} GSS_2 B(B - D_{\text{crit}}) \end{aligned} \tag{6.15}$$

that is,

$$\begin{aligned} D_{\text{crit}} &= B - \frac{P}{(\pi/\sqrt{6})GSS_2 B} \\ \frac{D_{\text{crit}}}{B} &= 1 - \frac{P}{(\pi/\sqrt{6})GSS_2} \\ &= 1 - \frac{P}{P_{\text{crit}}} \end{aligned} \tag{6.16}$$

On the other hand, if the second hypothesis is correct, the critical displacement is given by

$$\begin{aligned} P &= \sqrt{GA_r \frac{\pi^2 (EI)_{\text{eff}}}{t_r^2}} \\ &= \left(\frac{A_r}{A}\right)^{1/2} P_{\text{crit}} \end{aligned} \tag{6.17}$$

$$\frac{A_r}{A} = \left(\frac{P}{P_{\text{crit}}}\right)^2$$

$$\frac{B(B - D_{\text{crit}})}{B^2} = \left(\frac{P}{P_{\text{crit}}}\right)^2$$

$$1 - \frac{B}{D_{\text{crit}}} = \left(\frac{P}{P_{\text{crit}}}\right)^2 \quad \text{or} \quad \frac{D_{\text{crit}}}{B} = 1 - \left(\frac{P}{P_{\text{crit}}}\right)^2 \tag{6.18}$$

Both results are the same for P close to P_{crit} but differ for the range of practical application where $P < P_{\text{crit}}$.

The best empirical evidence for the use of the second hypothesis is a series of tests on small rubber bearings conducted at the EERC by I. G. Buckle in 1995. The experimental results were reported by Nagarajiah [98]. The bearings used in this test series were 127 × 127 mm (5 × 5 in.) and had 5.1 mm (2 in.) of elastomer. The elastomer was a low-damping natural rubber with a shear modulus of 0.74 MPa (108 psi) over the range of shear strain from 50 to 200%. The low damping and constant modulus meant that the effects of the hysteresis of the material on the stability were minimized. The bearings were loaded under constant vertical load and displaced under displacement control in the test machine. The critical displacement at which the horizontal force generated by the test machine no longer increases with increasing displacement was recorded. The results demonstrated that the first hypothesis is much too conservative, and the second, while conservative, is fairly accurate for the range of loads and displacements that would arise in practical designs. The results for very high axial loads and small lateral critical displacements are not well predicted by the formula, but the fact is that in these tests the bearings are loaded to axial load levels that exceed the predicted buckling load of the undisplaced bearing. This can happen since the bearing in the test machine is under displacement control and the end conditions are not those of the theory described in Section 6.1.

The overlap area for a square bearing is easy to calculate but is harder for a circular bearing of radius R. With the notation shown in Fig. 6.2, where θ is the half-angle subtended at the center of the intersection of the top and bottom circles and $\phi = \frac{1}{2}\pi - \theta$, the displacement D and the reduced area A_r are given by

$$D = 2R\cos\ \theta = 2R\sin\ \theta \tag{6.19}$$

and

$$\begin{aligned} A_r &= 2R^2(\theta - \sin\ \theta\ \cos\ \theta) \\ &= 2R^2\left(\frac{\pi}{2} - \phi - \sin\ \phi\ \cos\ \phi\right) \end{aligned} \tag{6.20}$$

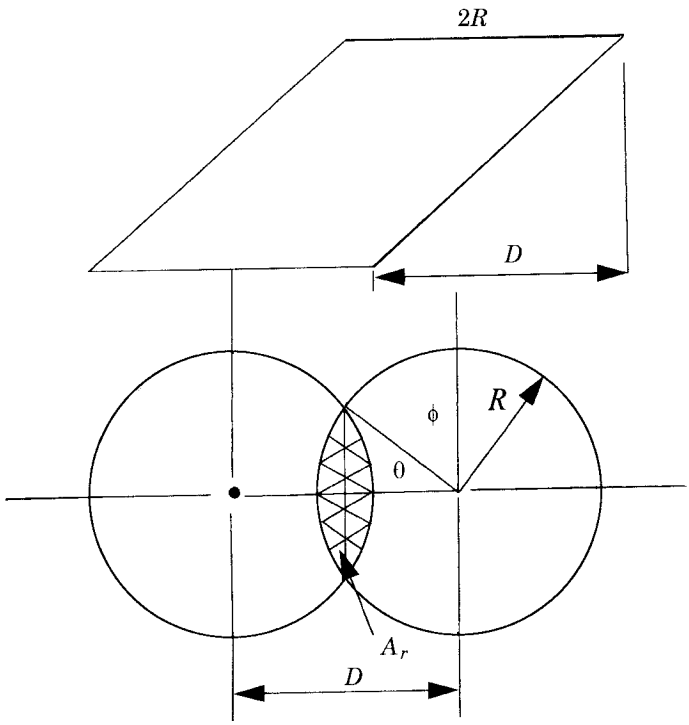

Fig. 6.2 Notation for reduced area.

It is convenient to nondimensionalize these by defining

$$d = \frac{D}{2R} \quad \text{and} \quad a = \frac{A_r}{\pi R^2}$$

leading to

$$\begin{aligned} d &= \cos\theta = \sin\phi \\ a &= \frac{2}{\pi}(\theta - \sin\theta\cos\theta) \\ &= 1 - \frac{2}{\pi}\phi - \frac{2}{\pi}\sin\phi\cos\phi \end{aligned} \tag{6.21}$$

The single curve that results from the simultaneous solution of these two equations is given in Table 6.1 and shown in Fig. 6.3. For rapid calculation of the results in the absence of a table or a figure, it is useful to expand the two equations for small values of ϕ corresponding to small d and small displacements

TABLE 6.1 Normalized Reduced Area

d	θ rads	a	a_a^{1a}	a_a^{2a}	p
0.10	1.471	0.873	0.873		0.934
0.20	1.369	0.747	0.747		0.864
0.30	1.266	0.624	0.624		0.790
0.40	1.159	0.505	0.505		0.710
0.50	1.047	0.391	0.391		0.625
0.60	0.927	0.285	0.284		0.534
0.70	0.795	0.188	0.0187		0.434
0.80	0.644	0.1044	0.1005	0.1074	0.323
0.85	0.555	0.0683		0.0697	0.261
0.90	0.451	0.0374		0.0380	0.193
0.95	0.318	0.0136		0.0134	0.117

[a]Note: $a_a^1 = 1 - (4d/\pi) + (2/3\pi)\, d^3 + (d^5/10\pi)$ and $a_a^2 = (8\sqrt{2}/3\pi)\,(1 - d)^{3/2}$.

or for small values of θ corresponding to small values of a and very large displacements.

When ϕ is small, the first equation can be written as

$$\phi = \sin^{-1} d$$

$$= d + \frac{d^3}{6} + \frac{3d^5}{40} + \cdots$$

and

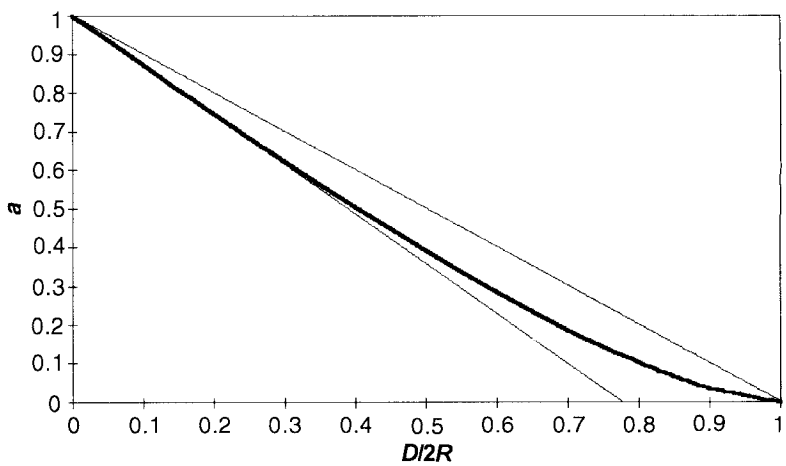

Fig. 6.3 Normalized reduced area $a = A_r/\pi R^2$ as a function of $D/2R$.

$$\sin\phi\cos\phi = \frac{1}{2}\sin 2\phi$$
$$= \frac{1}{2}\left(2\phi - \frac{8\phi^3}{6} + \frac{32\phi^5}{120} + \cdots\right)$$

Thus

$$\phi + \sin\phi\cos\phi = 2\phi - \tfrac{2}{3}\phi^3 + \tfrac{2}{15}\phi^5$$
$$= 2(d + \tfrac{1}{6}d^3 + \tfrac{3}{40}d^5) - \tfrac{2}{3}d^3(1 + \tfrac{1}{6}d^6)^3 + \tfrac{2}{15}d^5$$
$$= 2d - \tfrac{1}{3}d^3 - \tfrac{1}{20}d^5$$

leading to the approximation a_a^1 for a in the form

$$a_a^1 = 1 - \frac{4d}{\pi} + \frac{2}{3\pi}d^3 + \frac{d^5}{10\pi} \tag{6.22}$$

This expansion is accurate to 4% up to $d = 0.80$ and better for values of less than this, as shown in Table 6.1. Beyond this it is possible to use an expansion for small values of θ, with

$$d = 1 - \frac{\theta^2}{2} \qquad \theta = \sqrt{2(1-d)} \tag{6.23}$$

We find a second approximate a_a^2 given by

$$a_a^2 = \frac{2}{\pi}\left[\theta - \frac{1}{2}\left(2\theta - \frac{8}{6}\theta^3\right)\right]$$
$$= \frac{2}{\pi}\frac{2}{3}\theta^3$$
$$= \frac{4}{3\pi}[2(1-d)]^{3/2}$$
$$= \frac{8\sqrt{2}}{3\pi}(1-d)^{3/2} \tag{6.24}$$

This is accurate to 3% at $d = 0.80$ and better for values of d larger than that.

For a circular bearing the critical displacement, D_{crit} is given by $2Rd_{\text{crit}}$,

where d_{crit} is that value of d that leads to

$$a = \left(\frac{P}{P_{crit}}\right)^2 \tag{6.25}$$

For small values of the vertical load relative to the undisplaced critical load, the approximation of a by a_a^2 is valid and leads to

$$\frac{\delta\sqrt{2}}{3\pi}(1-d)^{3/2} = \left(\frac{P}{P_{crit}}\right)^2 \tag{6.26}$$

giving

$$\begin{aligned} d &= 1 - \left(\frac{3\pi}{\delta\sqrt{2}}\right)^{2/3}\left(\frac{P}{P_{crit}}\right)^{2/3} \\ &= 1 - \left(\frac{3\pi}{\delta\sqrt{2}}\right)^{2/3}\left(\frac{P}{P_{crit}}\right)^{4/3} \\ &= 1 - \frac{1}{2}\left(\frac{3\pi}{4}\right)^{2/3}\left(\frac{P}{P_{crit}}\right)^{4/3} \end{aligned} \tag{6.27}$$

This should be reasonably accurate for those values of d for which a_a^2 was accurate (i.e., $0.8 \le d \le 1.0$ and $0.1 \ge a \ge 0$). Since $a = (P/P_{crit})^2$, this means that it covers the range

$$0 \le \left(\frac{P}{P_{crit}}\right) \le 0.3$$

At the other extreme, the approximation

$$a = 1 - \frac{4d}{\pi} \tag{6.28}$$

was very good for $d \le 0.5$ and fairly good (10% accurate) for $d \le 0.8$. This

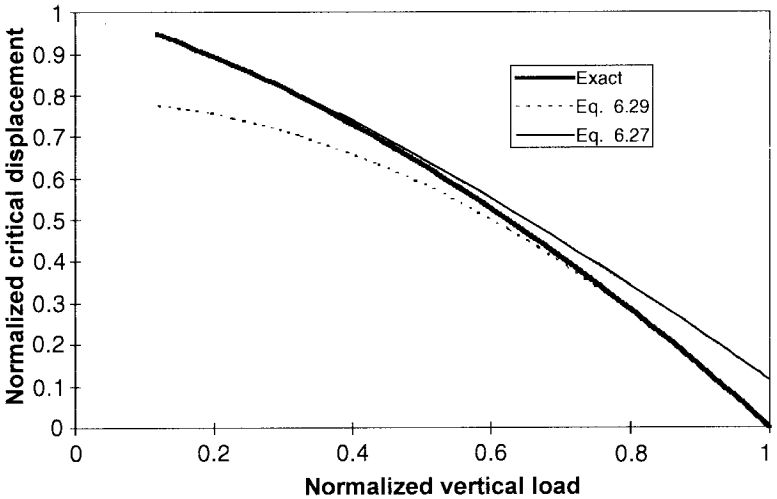

Fig. 6.4 Normalized critical displacement versus normalized vertical load.

leads to

$$d = \frac{\pi}{4}(1 - a)$$

$$= \frac{\pi}{4}\left[1 - \left(\frac{P}{P_{\text{crit}}}\right)^2\right] \tag{6.29}$$

Since $d = 0.5$ means $a = 0.4$, this should be accurate for $0.6 \leq p \leq 1$.

The exact answer for the value of P/P_{crit} that makes a specific value of d critical is obtained in Table 6.1, and the curve produced by this inverse solution can be compared to the two approximations. When plotted together in Fig. 6.4, it is clear that the approximation for small P/P_{crit} lies above the exact curve and is accurate up to $P/P_{\text{crit}} = 0.5$ and that for P/P_{crit} closer to 1 lies below and is accurate for $P/P_{\text{crit}} \geq 0.6$.

6.3 ROLLOUT STABILITY

An isolation bearing, even if inherently stable under its design load, can experience another form of instability if it is connected to the foundation below and the superstructure above through shear keys that cannot sustain tensile loads. Initially designers felt that rubber should not be subjected to tension; therefore, early designs of rubber bearings used dowelled shear connections rather than bolted connections. Dowelled bearings, however, can experience an unstable mode of behavior—called "rollout"—that is associated with lateral displace-

ment and puts a limit on the maximum displacement that the bearing can sustain. The bearing is unstable in the sense that beyond this displacement the force–displacement curve has a decreasing slope. Because the bearing cannot sustain tension, the movement at the top and bottom of the bearing is produced by a change in the line of action of the resultant of the vertical load, as shown in Fig. 6.5*a*. The limit of this migration of the resultant is reached when the resultant is at the edge of the bearing, and equilibrium of the moment generated by the lateral force F_H with that generated by the vertical load P gives

$$P(b - \delta_{\max}) = hF_H$$

where b is the bearing width (either a if square of Φ if circular). The relationship between the lateral force F_H and the displacement δ is shown in Fig. 6.5*b*.

Taking $F_H = K_H\delta$ gives

$$\frac{\delta_{\max}}{b} = \frac{P}{P + K_H h}$$

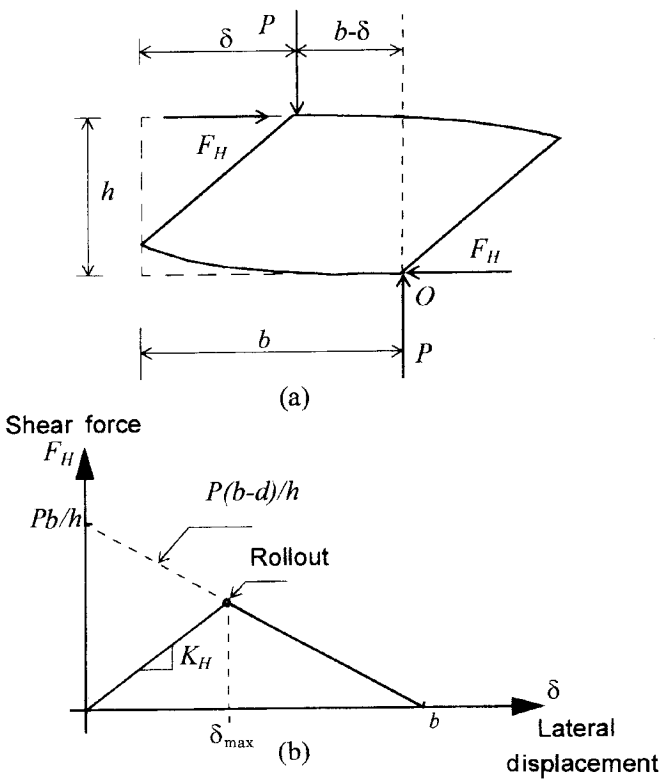

Fig. 6.5 Mechanics of rollout for dowelled bearings.

If we take K_H as GA/t_t and the pressure $p = P/A$, this becomes

$$\frac{\delta_{max}}{b} = \frac{1}{1 + (G/p)(h/t_r)}$$

In typical bearings where $G \approx 0.828$ MPa (120 psi), $p \approx 6.90$ MPa (1000 psi), and $h = 1.2t_r$, for example,

$$\frac{\delta_{max}}{b} = 0.88$$

Thus, if the lateral displacement is less than about 88% of the least plan dimension of a dowelled bearing, it can be expected to be stable against rollout. Conversely, if a bearing is bolted into place, no significant tension will develop in the bearing until the displacement exceeds this value. Recent tests done at the EERC and in Japan demonstrate that rubber is capable of sustaining quite high tensile stresses, and it has now become more common to use bolted rather than dowelled connections for isolation bearings. Additional research, however, needs to be done as the failure process in tension is not yet well understood; in bearings it can involve cavitation in the rubber [45] or loss of bond. Although some tests [64] have shown that there have been cases where the displacement has exceeded the bearing diameter, it is certainly good design practice to limit the displacement to the rollout value, even when bolted connections are used.

CHAPTER 7

DESIGN EARTHQUAKE GROUND MOTIONS

7.1 INTRODUCTION

Every structural system is designed to have a *seismic capacity* that exceeds the anticipated *seismic demand.* Capacity is a complex function of strength, stiffness, and deformability conjectured by the system configuration and material properties of the seismic isolation system and the superstructure. Seismic demand, on the other hand, for a given structure is controlled by what is commonly termed the *design ground motion criteria.* This criteria may be defined in one or more of the following three distinct forms:

- static base shear and lateral-force distribution formulas,
- a set of *design spectra,* and
- a suite of earthquake *time histories.*

The design ground motion may be defined in its most simple form by application of codified design base shear equations and static lateral-force distribution formulas such as those represented by Eq. (4.13) of Chapter 4. These formulas are in essence simplified interpretations of a design spectrum of certain shape and amplitude at the vibration period corresponding to a conservative estimate of the isolated fundamental period of the structure.

For more complex analyses the design ground motion criteria may be defined by a series of either code-specified or site-specific design spectra and rules on how to apply these spectra and how to interpret the results. If seismic design of a project requires application of dynamic time history analysis, then an appropriate set of earthquake records have to be selected and rules have to be established

Design of Seismic Isolated Structures: From Theory to Practice. F. Naeim and J. M. Kelly

on how these records are to be applied in analysis and design. The earthquake records, in this case, are needed in addition to a site-specific design spectra, and rules have to be set on how application of these records produce a demand that is consistent with the site-specific seismic hazard, which is usually summarized in the form of design spectra.

While a properly established design ground motion criterion is expected to provide a consistent expression of demand regardless of its form, overzealous emphasis on one form over the others, without proper understanding of the strength and limitations of each form, can result in very unrealistic and sometimes ridiculous design ground motion requirements. Such unreasonable requirements may prove self-defeating when applied blindly to the design of seismic-isolated structures.

The objective of this chapter is to familiarize the reader with the basic assumptions and procedures involved in development of design ground motions for seismic-isolated projects and common pitfalls associated with such efforts. To this end, since all forms of design ground motions are based on observed earthquake ground motions, a brief review of the characteristics and limitations of existing data on observed earthquake ground motions is presented. Contemporary design of seismic-isolated structures seems to be inseparable from the application of response spectrum analysis in one form or another. Since a good understanding of the concepts of earthquake response spectra and design spectra is essential for a meaningful design of an isolated structure, the basic principles are introduced and contrasted.

Evaluation of the seismic hazard at a given site requires an estimate of likely earthquake ground motions at the site. This is because (a) sites for which a recorded earthquake ground motion is readily available are extremely rare and (b) even for the sites where such recordings are available, there is no guarantee that future ground motions will have the same characteristics of previously observed motions. Possible ground motions for a site are estimated by use of various regression analysis techniques on a selected subset of available earthquake recordings deemed proper for such estimation. The resulting mathematical formulas that provide estimates of maximum response parameters such as peak ground acceleration or response spectral ordinates for a site are called *predictive relations* or *attenuation relations*. The term attenuation is used because these empirical relations in fact represent formulas for attenuation of seismic waves originating from a given source at a given distance through a given medium (i.e., site soil conditions). Dozens of attenuation relations have been developed. We will introduce a small number of the most widely used of these relations.

Response spectrum analysis, while relatively simple and straightforward, has certain limitations when applied to seismic-isolated structures. We will examine these limitations by exploring the energy content of earthquake ground motions, particularly in the near-source regions, and by evaluating the influence of high-damping values on the accuracy of common assumptions that routinely accompany response spectrum analyses.

Once the seismic hazard sources in the vicinity of the site (e.g., active and semiactive faults within a radius of 100 km of the site) and soil site conditions are established, the postulated seismic hazard at the site may be established by deterministic and/or probabilistic seismic hazard analysis techniques. Principles of these seismic hazard analysis techniques and the nature of uncertainties involved are described with the design consequences of ground motion uncertainties.

At least in California, the design of seismic-isolated structures requires the performance of a nonlinear time history analysis. Such analysis requires careful selection of a suite of appropriate time histories and selection of procedures for scaling time histories in either the time domain or frequency domain to approximate the site-specific seismic hazard commonly represented in the form of design spectra. The issue of scaling time histories has been, and continues to be, the most troubling aspect of development and application of design ground motion criteria for seismic-isolated structures. In some instances, the governing code requirements have mandated irrational designs by strictly adhering to irrational scaling procedures. We will present a series of time histories that we consider suitable for design of base-isolated structures. In addition, we will examine the procedures currently used for scaling time histories to match a given design spectra and will highlight the inconsistencies and poor designs that can result from blindly following some of these procedures. We will also evaluate some of the current code requirements for design by time history analysis techniques and highlight the most troubling aspects of these requirements while suggesting more rational alternatives.

7.2 CHARACTERISTICS OF EARTHQUAKE GROUND MOTIONS

The number of earthquake records available has grown rapidly during the past decade. While obtaining earthquake accelerograms was not simple up to about the mid-1980s, hundreds of earthquake records may now be screened, viewed, and downloaded from the Internet or obtained at a nominal cost from various public agencies. Figure 7.1 shows the interval and cumulative distributions of available earthquake records of significance for design applications [$M > 5.5$; [peak ground acceleration (PGA) $> 0.05g$] for North and Central America during the period 1933–1994. The number of records, less than 100 before the 1971 San Fernando event, now surpasses 2000.

Staff at the National Center for Earthquake Engineering Research (NCEER) at the State University of New York at Buffalo, the Earthquake Engineering Research Center (EERC) at the University of California, Berkeley, and the U.S. Geological Survey (USGS) routinely track and document sources of earthquake records. The Earthquake Engineering Research Institute World Wide Web (WWW) site also provides links to many of these resources. An up-to-date listing of and links to pages containing such information may be obtained from these agencies. With the information revolution currently underway, it is

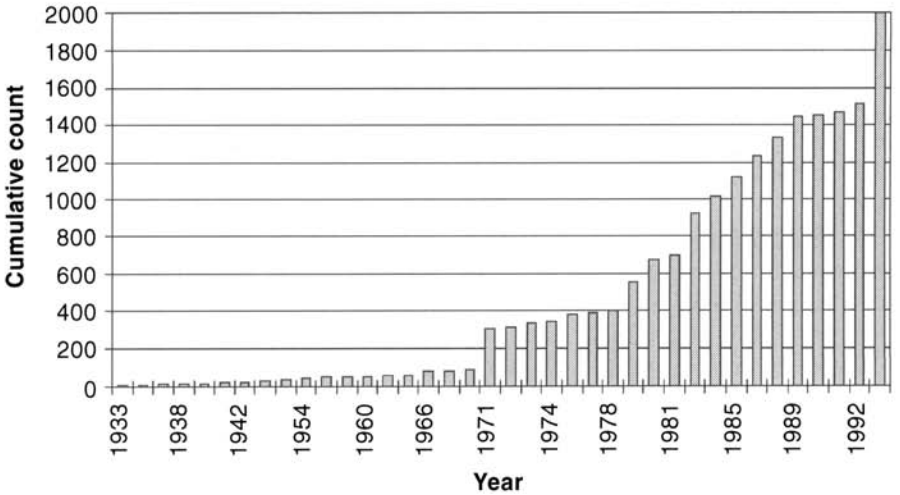

Fig. 7.1 Earthquake records of North and Central America ($M > 5.5$; PGA $> 0.05g$) during the period 1933–1994 [93].

expected that the ease of access to global databases of earthquake records will improve exponentially during the next few years.

The parameters that can be used to characterize the severity and damage potential of earthquake ground motions can be grouped into three main categories: (a) time-domain values obtained either directly or with some simple calculations from the digitized and corrected version of the instrument record, (b) spectral values obtained from the parametric integration of the equation of motion of elastic and inelastic single-degree-of-freedom (SDOF) systems, and (c) spectral values obtained by considering the energy balance equation for elastic and inelastic systems.

Time-domain parameters include peak ground acceleration (PA), peak ground velocity (PV), and peak ground displacement (PD). Of these, the one most often associated with the severity of a recorded ground motion is the peak ground acceleration. However, it has generally come to be recognized that this is a poor parameter for evaluating damage potential. This is particularly true for seismic-isolated structures. Peak ground acceleration is often associated with high vibration frequencies (low periods), which are far from the effective vibration periods of typical isolated structures. Studies by Naeim and Anderson [91, 92] have shown that peak ground velocity is a much better overall indicator of damage potential than peak acceleration.

Anderson and Bertero [9] have suggested the use of maximum incremental velocity (IV) and maximum incremental displacement (ID) to characterize the damage potential of earthquake motions in the near-fault region. Incremental velocity represents the area under an acceleration pulse. Hence, the larger the

change in velocity, the larger is the acceleration pulse. In a similar manner, the area under a velocity pulse is equal to the incremental displacement.

Another important time-domain parameter is the duration of strong ground motion. There are several methods for assigning a strong motion duration to an accelerogram [82]. McCann and Shah [77] use the average energy arrival rate. Bolt [25] and Page et al. [105] use a bracketed duration that is defined as the time interval between the first and last acceleration peaks greater than a specified value, usually chosen as a value (such as $0.05g$) below which no damage is expected to occur. This definition implies a coupling between ground motion level (specifically, acceleration level) and duration. As a consequence, scaling a record will change its bracketed duration.

Husid et al. [50] define the duration of strong motion as the time interval in which a significant contribution of the square of the time series, referred to as time series intensity, takes place (see Fig. 7.2). If the starting time history is a broadband velocity time history, the quantity being measured by the squared

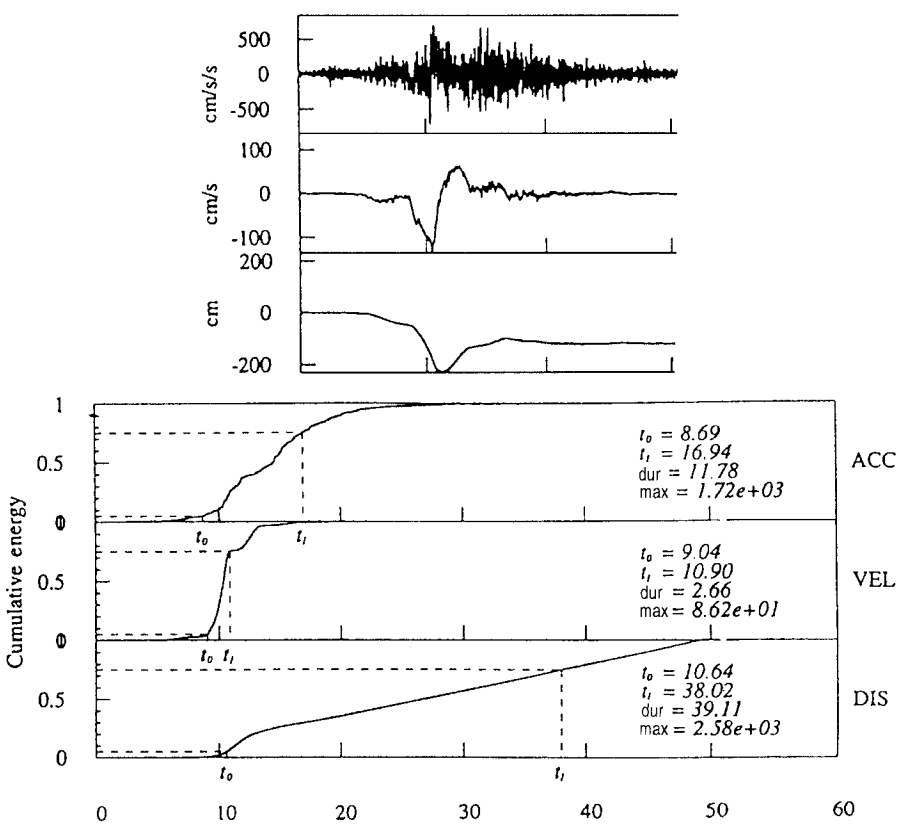

Fig. 7.2 Calculation of the Husid et al. duration for an earthquake record [93].

velocity is actual energy. The Husid et al. definition of duration is independent of the level of the ground motion and can be used in conjunction with measures of ground motion level such as peak acceleration, peak velocity, and response spectral ordinates at specified frequencies to provide a more complete characterization of the ground motion. Scaling a time history does not change the duration measured by this method.

Both the Bolt and Husid et al. definitions give increasing duration with increasing magnitude as a result of the increasing rupture dimensions of the earthquake. However, in other respects the two definitions of duration behave in ways that are quite different and in some ways opposite to each other. For example, the bracketed duration decreases away from the earthquake source because of its dependence on ground motion level, while the Husid et al. duration increases away from the source because the energy tends to become increasingly scattered as the distance increases.

Ground motion parameters based on response spectra include effective peak acceleration (EPA) and effective peak velocity (EPV). These parameters, which were initially defined in the Applied Technology Council publication ATC-3-06 [13], are based on average response spectral ordinates in selected period bands (0.1–0.5 sec for EPA and about 1.0 sec for EPV) and are widely used in contemporary seismic design codes.

Fourier spectrum and elastic and inelastic response spectra calculated at a set of distinct periods are the most common representations of earthquake records in the frequency domain. Response spectrum analysis is the most common technique used for dynamic analysis of structures. Even if more elaborate analysis is needed, it should always be preceded by a detailed analysis of spectral response. Due to the importance of the response spectrum and its design counterpart, the design spectrum, these topics are discussed in more detail in Section 7.3.

Inelastic spectrum is an attempt to extend response spectrum analysis into the nonlinear range of structural response. One of the more significant shortcomings of current design spectra, both elastic and inelastic, is the fact that they do not adequately account for the duration of input ground motion. This is a significant characteristic that can be addressed by the use of energy spectra that reflect the possibility of high-energy dissipation demand with long duration.

Impulse-type ground motions result in a sudden burst of energy into the structure that must be dissipated immediately. This is usually characterized by one large yield excursion with few reversals. On the other hand, a sinusoidal ground motion of longer duration requires a more steady dissipation of energy over a longer period of time with numerous yield reversals. Time-domain characteristics of this kind are not adequately represented by current earthquake response spectrum methods.

Energy attributes of strong ground motion such as rate of input and hysteretic energies as well as input and hysteretic energy spectra provide a more reliable indication of damage potential. However, the technology for direct application of energy concepts in design of complex structures has not yet fully developed.

7.3 FROM RESPONSE SPECTRA TO DESIGN SPECTRA

The response of a SDOF system to general excitation may be obtained through the application of Duhamel's integral. For a typical SDOF system subjected to base excitation (see Fig. 7.3), we can designate $v(t)$ to be the time-dependent displacement of the mass (m) relative to the ground, $u(t)$, to be the absolute displacement of the mass (m) with respect to a Newtonian "fixed" coordinate system and $u_g(t)$ to be the absolute displacement of the ground with respect to the same fixed reference. The equation of motion for the mass is

$$\ddot{v} + 2\omega\beta\dot{v} + \omega^2 v = -\ddot{u}_g \tag{7.1}$$

where $\omega = \sqrt{k/m}$ is the undamped natural frequency of the system and $\beta = c/2m\omega$ is the fraction of critical damping. From Duhamel's integral, if the system starts from rest [$\dot{v}(0) = v(0) = 0$] and recalling that the damped natural frequency is $\overline{\omega} = \omega\sqrt{1-\beta^2}$, the displacement is

$$v(t) = -\frac{1}{\overline{\omega}} \int_0^t \ddot{u}_g(\tau) e^{-\beta\omega(t-\tau)} \sin \overline{\omega}(t-\tau)\, d\tau \tag{7.2}$$

Similar expressions for velocity and acceleration may be obtained as

$$\dot{v}(t) = -\int_0^t \ddot{u}_g(\tau) e^{-\beta\omega(t-\tau)} \cos \overline{\omega}(t-\tau)\, d\tau + \beta \int_0^t \frac{\ddot{u}_g(\tau)}{\sqrt{1-\beta^2}} e^{-\beta\omega(t-\tau)} \sin \overline{\omega}(t-\tau)\, d\tau \tag{7.3}$$

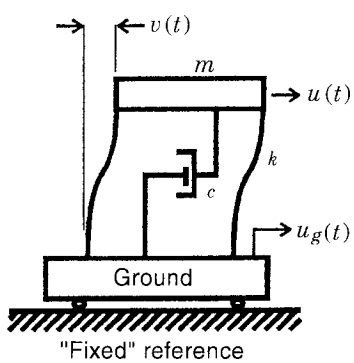

Fig. 7.3 Idealization of a structure as an SDOF system.

$$\ddot{u}(t) = 2\beta\bar{\omega} \int_0^t \ddot{u}_g(\tau) e^{-\beta\omega(t-\tau)} \cos \bar{\omega}(t-\tau)\, d\tau + \int_0^t \frac{\ddot{u}_g(\tau)\omega(1-2\beta^2)}{\sqrt{1-\beta^2}} e^{-\beta\omega(t-\tau)} \sin \bar{\omega}(t-\tau)\, d\tau \tag{7.4}$$

Notice that we are interested in *absolute* acceleration and *relative* displacement and *relative* velocity. The reason is rather obvious. According to Newton's second law, the inertial forces are proportional to absolute acceleration. From Hooke's law, however, member forces are proportional to relative displacements, and the viscous damping is directly proportional to the relative velocity.

Spectral values are defined as the absolute values of the maximum response, or

$$\begin{aligned} \text{SD} &= |v(t)|_{\max} = \text{relative displacement spectral value} \\ \text{SV} &= |\dot{v}(t)|_{\max} = \text{relative velocity spectral value} \\ \text{SD} &= |\ddot{u}(t)|_{\max} = \text{absolute acceleration value} \end{aligned} \tag{7.5}$$

A closer look at Eqs. (7.2)–(7.4) reveals very interesting and important relationships among the above spectral entities. If β is small ($\beta \ll 1$), then β^2 is very small; in that case $1 - \beta^2 \cong 1 - 2\beta^2 \cong 1$ and $\bar{\omega} \cong \omega$. The second term in Eq. (7.3) and the first term in Eq. (7.4) that are directly proportional to β are small and may be ignored. Hence, with small damping as the simplifying assumption, Eqs. (7.4) and (7.5) may be rewritten as

$$\dot{v}(t) \cong -\int_0^t \ddot{u}_g(\tau) e^{-\beta\omega(t-\tau)} \cos \bar{\omega}(t-\tau)\, d\tau \tag{7.6}$$

$$\ddot{u}(t) \cong \int_0^t \ddot{u}_g(\tau)\omega e^{-\beta\omega(t-\tau)} \sin \bar{\omega}(t-\tau)\, d\tau \tag{7.7}$$

The value $|\omega^2 v(t)|$, which is a good approximation of the absolute acceleration *only when damping is small* is called *pseudoacceleration* (PSA).

If in Eq. (7.6) there was a $\sin \bar{\omega}(t-\tau)$ term instead of $\cos \bar{\omega}(t-\tau)$, a similar deduction could be made about spectral velocity. While this is not the case, for the sake of convenience, the relative *pseudovelocity* is defined to be equal to

$|\omega v(t)|$. Hence

$$\text{PSV} = \omega \text{ SD} = 2\frac{\pi}{T} \text{ SD} = \text{spectral pseudovelocity} \tag{7.8}$$

$$\text{PSA} = \omega \text{ SV} = \left(2\frac{\pi}{T}\right)^2 \text{ SD} = \text{spectral pseudoacceleration} \tag{7.9}$$

where T is the period of the SDOF system.

In conventional structures, damping rarely exceeds 5–10% critical and can always be assumed to be small; hence, PSA provides a good approximation of SA. Many seismic isolation systems and devices, however, rely on increased damping to reduce the amount of energy input to the superstructure. In such cases, PSA approximation of SA should be evaluated carefully since it might lack accuracy. Also obvious from the above discussion is that PSA approximation of SA is always much better than PSV approximation of SV. It can be shown, however, that PSV provides a reasonable estimate of SV for small damping values and relatively short natural periods. Hence, substitution of PSV for SV, which is an inherent part of the tripartite logarithmic representation of response spectra, should be examined with extreme caution for seismic-isolated structures, where neither natural period nor damping may be small enough to justify these simplifying assumptions. In Fig. 7.4, SV and PSV values obtained

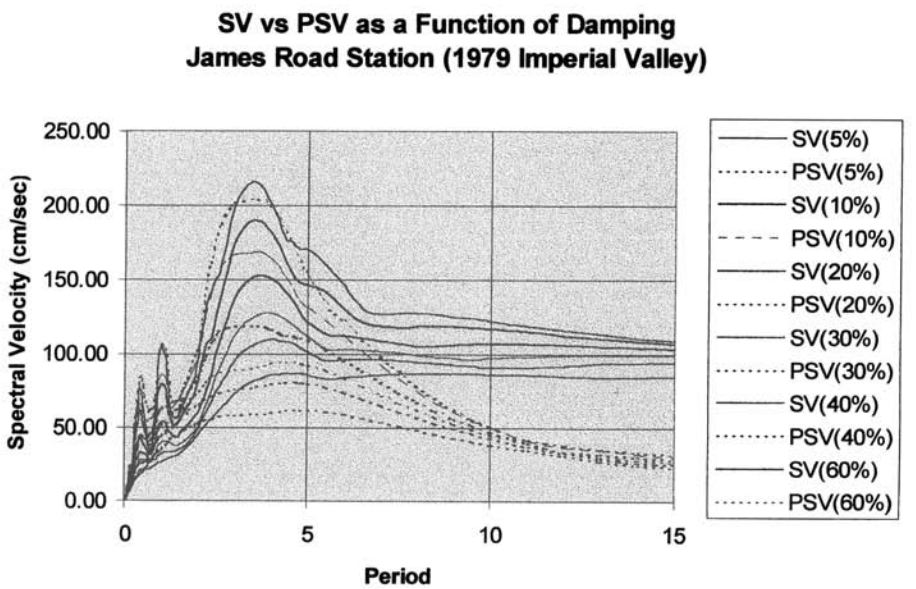

Fig. 7.4 PSV and SV are significantly different at long periods ($T > 6$ sec). The difference is amplified for high-damping values (shown in parentheses) and extended to midperiods ($3 < T < 6$ sec).

for a typical earthquake record are compared. Notice the PSV's large margin of error at the low-frequency (long-period) range of the plot and large damping ratios.

Now let us examine the limiting values of spectral entities at the extreme case where $T \rightarrow \infty$ ($\omega \rightarrow 0$). In this case, we have a very flexible system that does not seem to move at all relative to the ground. Therefore, SD (the maximum relative displacement) equals the maximum absolute good displacement, $|u_g(t)|_{\max}$. Similarly, SV (the maximum relative velocity) reaches the maximum absolute ground velocity, $|\dot{u}(t)_g|_{\max}$. Notice, however, that PSV, being proportional to ω, reaches zero but SV does not. On the other hand, SA, which is the absolute acceleration of an almost stationary system, reaches zero and so does PSA because of its proportionality to ω^2. From a purely theoretical standpoint, this system represents a perfectly isolated structure because no vibrations are transmitted to the mass that represents the structure.

So far we have defined a set of maximum response values for a SDOF system as functions of only three parameters: (1) the natural frequency of the system, ω; (2) the amount of damping, β; and (3) a ground motion acceleration time history, $\ddot{u}_g(t)$. By varying the natural frequency of the system, one can obtain charts depicting maximum response values for all SDOF systems within the frequency or period range of interest. Each one of these charts is called an *elastic response spectrum*, and a collection of them (i.e., for various damping levels) are termed *elastic response spectra.*

For each earthquake record, response spectra can be constructed. Earthquakes share many common characteristics but have their own unique attributes as well. Response spectra of earthquake records usually contain many peaks and valleys as a function of period (see Fig. 7.5 for an example). There is no reason to believe that the spectra for future earthquakes will exhibit exactly the same peaks and valleys as previous recordings. Furthermore, the natural periods and mode shapes of building structures cannot be exactly predicted. Many uncertainties are present that include but are not limited to (a) unavoidable variations in the mass and stiffness properties of the building from those used in design, (b) difficulties involved in establishing exact properties of site soil conditions, and (c) inelastic response that tends to lengthen the natural period of the structure. For these reasons, it is more rational to use average curves obtained from a number of earthquake records for design purposes. These average curves, which do not reflect the sharp peaks and valleys of individual records, are also known as *smoothed response spectra*, or more commonly as *design spectra.* While a response spectrum is an attribute of a particular ground motion, a design spectrum is not. A design spectrum is merely a definition of a criterion for structural analysis and design.

A relatively new trend in the generation of design spectra is the extension of ground motion attenuation relationships to predict spectral ordinates. One advantage of this approach is the fact that the substantial influences of earthquake magnitude and distance may be modeled. Because of the ever-increasing volume of information obtained from the worldwide network of strong motion

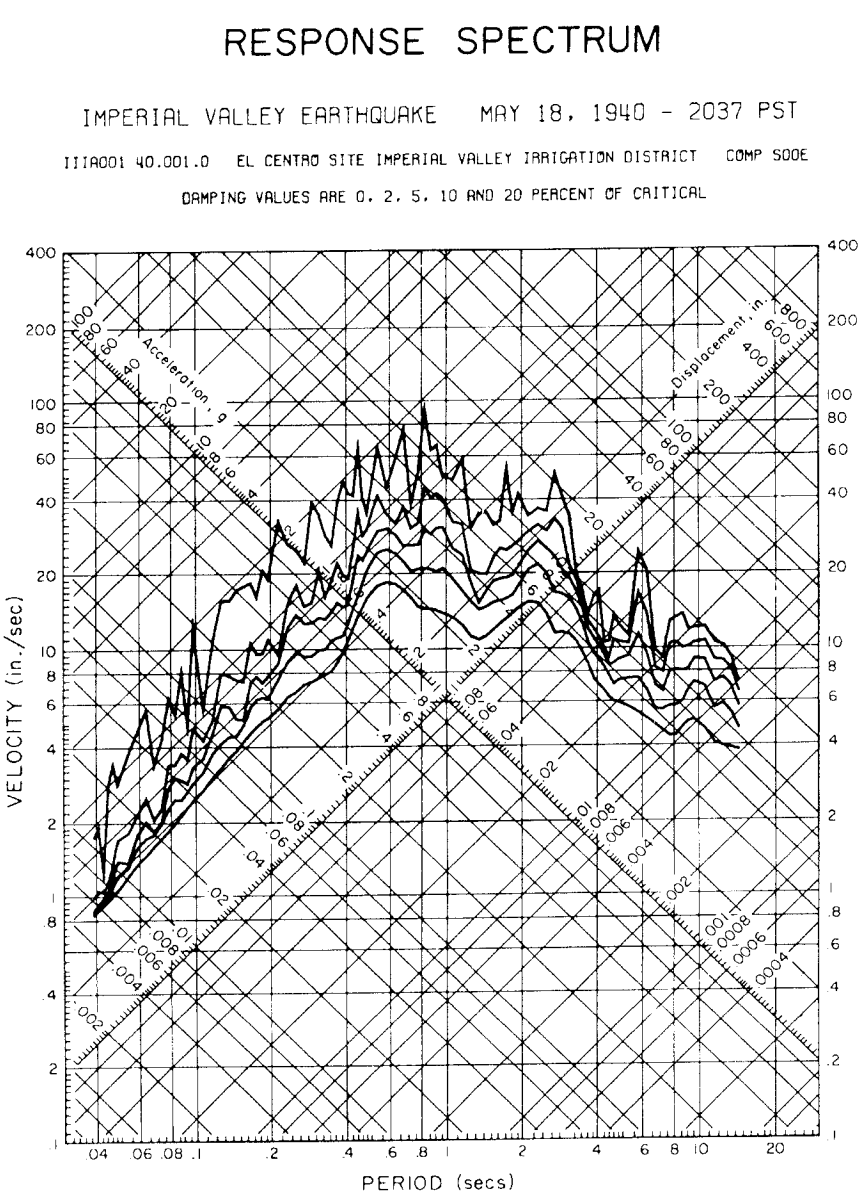

Fig. 7.5 Typical earthquake response spectra exhibiting a number of sharp peaks and valleys.

accelerometers, this approach has the potential for accounting for many important factors absent from most other formulations. Faulting type (reverse vs. strike slip), source directivity (rupture toward the site or not), and more detailed explanations of site conditions (free field, basements of low-rise buildings, basements of high-rise buildings) are a few examples of such factors.

The *inelastic response spectrum* method is an attempt to extend the application of response spectrum analysis beyond the linear elastic range. Generally, the elastic–perfectly plastic (EPP) idealization is used (Fig. 7.6). Construction of inelastic response spectra is more complicated than that of elastic spectra. Inelastic deformation is usually defined in terms of the displacement ductility of a SDOF oscillator, which has an EPP resistance. For this system, the displacement ductility is expressed as

$$\mu_d = \frac{\delta_{\max}}{\delta_y} = 1 + \frac{\delta_p}{\delta_y} \tag{7.10}$$

where $\delta_{\max}$ = maximum displacement
δ_y = yield displacement, and
δ_p = plastic displacement

It should be noted that EPP models are not appropriate for seismic-isolated structures. Linear models are closer to actual behavior of most isolated systems than EPP models.

Inelastic spectra are usually developed by a numerical integration of the equation of motion for an inelastic SDOF oscillator having an EPP resistance (R). This equation, which is similar to Eq. (7.1), has the form

$$\ddot{v} + 2\omega\beta\dot{v} + R = -\ddot{u}_g \tag{7.11}$$

where $R \leq R_y = C_y W$ and C_y is the yield resistance seismic coefficient of the structure.

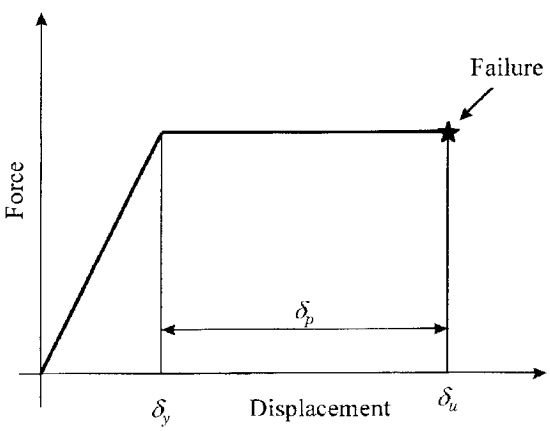

Fig. 7.6 The EPP material model.

If constant viscous damping is assumed, there remain three variables for each ground acceleration: period, displacement ductility, and yield resistance seismic coefficient. The solutions of the equation of motion for the inelastic response can be presented in two ways: (a) in terms of a constant yield resistance seismic coefficient (constant strength spectra) in which the ductility is a variable or (b) in terms of a constant displacement ductility (constant ductility response spectra) in which the yield resistance seismic coefficient is a variable.

Several procedures have been suggested for construction of inelastic design spectra [12, 14, 41, 82]. The theoretical basis for most such modifications is Newmark's observation [101] that three equivalencies can be made between elastic and inelastic response: (1) at low frequencies displacements are equal; (2) at intermediate frequencies, absorbed energies are the same; and (3) at high frequencies, forces are equal.

The authors believe that, in general, care should be taken in application of inelastic spectra in structural design of complex structures. Many studies [9, 10, 91] have consistently shown that there are many parameters not considered in construction of such spectra that can dominate nonlinear response of multi-degree-of-freedom (MDOF) systems. It should be noted that a general consensus on proper methods for application of inelastic design spectra in analysis of MDOF systems has not yet been achieved.

One of the more significant shortcomings of current design spectra, both elastic and inelastic, is the fact that they do not account for the duration of input ground motion. Impulse-type ground motions result in a sudden burst of energy into the structure that must be dissipated immediately. This is usually characterized by one large yield excursion with few reversals. On the other hand, a sinusoidal-type ground motion of longer duration requires a more steady dissipation of energy over a longer period of time with numerous yield reversals. This type of information, which more often than not controls the design of near-fault structures, cannot be easily obtained from earthquake response spectra and hence cannot be properly represented by current design spectra.

7.4 EARTHQUAKE ENERGY CONTENT AND ENERGY SPECTRA

The Concept During the past 10 years there has been a renewed interest in the application of energy concepts to earthquake-resistant design. Energy formulations are particularly beneficial for seismic-isolated structures, since most isolation systems behave in a nonlinear fashion. In addition, the nonlinear response to ground motions at the isolation plane of the structure will depend on the intensity, frequency content, and duration of the ground motion and on the dynamic characteristics of the isolation system and the superstructure. Consideration of these factors had led many investigators to conclude that one of the most reliable parameters for defining the damage potential of an earthquake ground motion is the input energy.

The hysteretic energy that is dissipated by inelastic deformation is also thought to be a reliable parameter for evaluating the damage potential of earthquake ground motions. This component is calculated as the area enclosed by the hysteresis loops developed by the dynamic response of the system. However, consideration of hysteretic energy introduces the additional variables of the yield resistance seismic design coefficient and postelastic stiffness into the evaluation process.

Noting that $u(t) = v(t) + u_g(t)$, Eq. (7.1) may be written as

$$m\ddot{u} = -c\dot{v} - kv \tag{7.12}$$

Multiplication of each term by $\dot{u}$ gives

$$m\ddot{u}\dot{u} = -c\dot{v}\dot{v} - kv\dot{v} - (-c\dot{v} - kv)\dot{u}_g \tag{7.13}$$

which can be written as

$$\frac{d}{dt}\left(\frac{1}{2}m\dot{u}^2\right) + \frac{d}{dt}\left(\frac{1}{2}kv^2\right) = -c\dot{v}^2 - (-c\dot{v} - kv)\dot{u}_g \tag{7.14}$$

or

$$\frac{d}{dt}[\text{KE} + \text{PE}] = -\dot{D} + \dot{W} \tag{7.15}$$

This means that the rate of change of the sum of the potential (PE) and kinetic (KE) energies is equal to the rate of work done by the ground motion minus the rate of loss of energy by dissipation. When we use the nonlinear equation of motion [Eq. (7.11)], the work of the nonlinear restoring force $R(v)\dot{v}$ is partitioned between the potential energy and hysteretic energy dissipation.

Numerical procedures for calculating the various energy components are described by Mahin and Lin, [75].

7.5 VARIOUS GROUND MOTION PREDICTIVE FORMULATIONS

7.5.1 Source Characterizations

Several empirical relationships have been developed to relate earthquake magnitude, fault rupture length, rupture width, rupture area, and surface displacement. Wells and Coppersmith [134] compiled and studied a worldwide database of 421 historical earthquakes to study the relationship between the *moment mag-*

nitude (**M**) and various other source parameters. The moment magnitude scale [48] is the most widely used magnitude scale in academic and professional circles. Regression relations between various earthquake source parameters as suggested by Wells and Coppersmith may be summarized in the form

$$\mathbf{M} = a + b \log \mathbf{X} \tag{7.16}$$

where **X** can be any source parameter such as rupture length or fault displacement and a and b are regression coefficients that are functions of the type of faulting and the source parameter of interest. Typical values of a and b and the degree of prediction uncertainties in terms of standard errors and deviations are presented in Tables 7.1 and 7.2.

Empirical relations have been also developed that relate the fault slip rates, which can now be monitored by Global Positioning System (GPS) satellites. One such example is the relation [51]

$$\mathbf{M} = 7.223 + 1.263 \log \mathbf{S} \tag{7.17}$$

where S is the fault slip rate in millimeters per year.

The main function of equations such as (7.16) and (7.17) is to estimate the likely size (**M**) of future events based on available geological and tectonic information, although they could be used to estimate the likely range of source parameters associated with an earthquake of a given size. The following example helps illustrate such exercises.

Example 7.1. Estimate the likely earthquake magnitude associated with each of the following source parameters:

(a) a surface rupture length (SRL) of 100 km on a reverse fault

(b) a maximum displacement of 5 m on a strike-slip fault

(c) a slip rate of 2 mm/year on a strike-slip fault

Evaluate uncertainty of predicted values by assuming a dispersion of one standard deviation to be reasonable.

SOLUTION. (a) From Table 7.1

$$M = 5.00 + 1.22 \log(100) \pm 0.28 = 7.44 \pm 0.28$$
$$= 7.4(\text{expected value}), 7.2(\text{lower bound}), 7.7(\text{upper bound})$$

TABLE 7.1 Regressions of Rupture Length, Rupture Width, Rupture Area, and Moment Magnitude

Equation[a]	Slip Type[b]	Number of Events	Coefficients and Standard Errors[c]		Standard Deviation	Correlation Coefficient	Magnitude Range	Length/Width Range (km)
			a	b	s	r		
$\mathbf{M} = a + b \log(\text{SRL})$	SS	43	5.16 (0.13)	1.12 (0.08)	0.28	0.91	5.6 to 8.1	1.3 to 432
	R	19	5.00 (0.22)	1.22 (0.16)	0.28	0.88	5.4 to 7.4	3.3 to 85
	N	15	4.86 (0.34)	1.32 (0.26)	0.34	0.81	5.2 to 7.3	2.5 to 41
	All	77	5.08 (0.10)	1.16 (0.07)	0.28	0.89	5.2 to 8.1	1.3 to 432
$\log(\text{SRL}) = a + b\mathbf{M}$	SS	43	−3.55 (0.37)	0.74 (0.05)	0.23	0.91	5.6 to 8.1	1.3 to 432
	R	19	−2.86 (0.55)	0.63 (0.08)	0.20	0.88	5.4 to 7.4	3.3 to 85
	N	15	−2.01 (0.65)	0.50 (0.10)	0.21	0.81	5.2 to 7.3	2.5 to 41
	All	77	−3.22 (0.27)	0.69 (0.04)	0.22	0.89	5.2 to 8.1	1.3 to 432
$\mathbf{M} = a + b \log(\text{RLD})$	SS	93	4.33 (0.06)	1.49 (0.05)	0.24	0.96	4.8 to 8.1	1.5 to 350
	R	50	4.49 (0.11)	1.49 (0.09)	0.26	0.93	4.8 to 7.6	1.1 to 80
	N	24	4.34 (0.23)	1.54 (0.18)	0.31	0.88	5.2 to 7.3	3.8 to 63
	All	167	4.38 (0.06)	1.49 (0.04)	0.26	0.94	4.8 to 8.1	1.1 to 350
$\log(\text{RLD}) = a + b\mathbf{M}$	SS	93	−2.57 (0.12)	0.62 (0.02)	0.15	0.96	4.8 to 8.1	1.5 to 350
	R	50	−2.42 (0.21)	0.58 (0.03)	0.16	0.93	4.8 to 7.6	1.1 to 80
	N	24	−1.88 (0.37)	0.50 (0.06)	0.17	0.88	5.2 to 7.3	3.8 to 63
	All	167	−2.44 (0.11)	0.59 (0.02)	0.16	0.94	4.8 to 8.1	1.1 to 350

$\mathbf{M} = a + b \log(\mathrm{RW})$	SS	87	3.80 (0.17)	2.59 (0.18)	0.45	0.84	4.8 to 8.1	1.5 to 350
	R	43	4.37 (0.16)	1.95 (0.15)	0.32	0.90	4.8 to 7.6	1.1 to 80
	N	23	4.04 (0.29)	2.11 (0.28)	0.31	0.86	5.2 to 7.3	3.8 to 63
	All	153	4.06 (0.11)	2.25 (0.12)	0.41	0.84	4.8 to 8.1	1.1 to 350
$\log(\mathrm{RW}) = a + b\mathbf{M}$	SS	87	−0.76 (0.12)	0.27 (0.02)	0.14	0.84	4.8 to 8.1	1.5 to 350
	R	43	−1.61 (0.20)	0.41 (0.03)	0.15	0.90	4.8 to 7.6	1.1 to 80
	N	23	−1.14 (0.28)	0.35 (0.05)	0.12	0.86	5.2 to 7.3	3.8 to 63
	All	153	−1.01 (0.10)	0.32 (0.02)	0.15	0.84	4.8 to 8.1	1.1 to 350
$\mathbf{M} = a + b \log(\mathrm{RA})$	SS	83	3.98 (0.07)	1.02 (0.03)	0.23	0.96	4.8 to 7.9	3 to 5,184
	R	43	4.33 (0.12)	0.90 (0.05)	0.25	0.94	4.8 to 7.6	2.2 to 2,400
	N	22	3.93 (0.23)	1.02 (0.10)	0.25	0.92	5.2 to 7.3	19 to 900
	All	148	4.07 (0.06)	0.98 (0.03)	0.24	0.95	4.8 to 7.9	2.2 to 5,184
$\log(\mathrm{RA}) = a + b\mathbf{M}$	SS	83	3.42 (0.18)	0.90 (0.03)	0.22	0.96	4.8 to 7.9	3 to 5,184
	R	43	3.99 (0.36)	0.98 (0.06)	0.26	0.94	4.8 to 7.6	2.2 to 2,400
	N	22	−2.87 (0.50)	0.82 (0.08)	0.22	0.92	5.2 to 7.3	19 to 900
	All	148	−3.49 (0.16)	0.91 (0.03)	0.24	0.95	4.8 to 7.9	2.2 to 5.184

[a]SRL, surface rupture length (km); RLD, subsurface rupture length (km); RW, downdip rupture width (km). RA, rupture area (km^2).
[b]SS—strike slip; R—reverse; N—normal.
[c]Numbers in parentheses are standard errors.

Source: From D. L. Wells and K. S. Coppersmith, *Bulletin of Seismological Society of America*, Vol. 84, No. 4, 1994. Reproduced with permission of the Seismological Society of America.

TABLE 7.2 Regression of Displacement and Moment Magnitude (M)

Equation[a]	Slip Type[b]	Number of Events	Coefficients and Standard Errors[a]		Standard Deviation	Correlation Coefficient	Magnitude Range	Displacement Range (km)
			a	*b*	*s*	*r*		
$\mathbf{M} = a + b \log(\mathrm{MD})$	SS	43	6.81 (0.05)	0.78 (0.06)	0.29	0.90	5.6 to 8.1	0.01 to 14.6
	R[d]	*21*	*6.52 (0.11)*	*0.44 (0.26)*	*0.52*	*0.36*	*5.4 to 7.4*	*0.11 to 6.5*
	N	16	6.61 (0.09)	0.71 (0.15)	0.34	0.80	5.2 to 7.3	0.06 to 6.1
	All	80	6.69 (0.04)	0.74 (0.07)	0.40	0.78	5.2 to 8.1	0.01 to 14.6
$\log(\mathrm{MD}) - a + b\mathbf{M}$	SS	43	−7.03 (0.55)	1.03 (0.08)	0.34	0.90	5.6 to 8.1	0.01 to 14.6
	R[d]	*21*	*−1.84 (1.14)*	*0.29 (0.17)*	*0.42*	*0.36*	*5.4 to 7.4*	*0.11 to 6.5*
	N	16	−5.90 (1.18)	0.89 (0.18)	0.38	0.80	5.2 to 7.3	0.06 to 6.1
	All	80	−5.46 (0.51)	0.82 (0.08)	0.42	0.78	5.2 to 8.1	0.01 to 14.6
$\mathbf{M} = a + b \log(\mathrm{AD})$	SS	29	7.04 (0.05)	0.89 (0.09)	0.28	0.89	5.6 to 8.1	0.05 to 8.0
	R[d]	*15*	*6.64 (0.16)*	*0.13 (0.36)*	*0.50*	*0.10*	*5.8 to 7.4*	*0.06 to 1.5*
	N	12	6.78 (.012)	0.65 (0.25)	0.33	0.64	6.0 to 7.3	0.08 to 2.1
	All	56	6.93 (0.05)	0.82 (0.10)	0.39	0.75	5.6 to 8.1	0.05 to 8.0
$\log(\mathrm{AD}) = a + b\mathbf{M}$	SS	29	−6.32 (0.61)	0.90 (0.09)	0.28	0.89	5.6 to 8.1	0.05 to 8.0
	R[d]	*15*	*−0.74 (1.40)*	*0.08 (0.21)*	*0.38*	*0.10*	*5.8 to 7.4*	*0.06 to 1.5*
	N	12	−4.45 (1.59)	0.63 (0.24)	0.33	0.64	6.0 to 7.3	0.08 to 2.1
	All	56	−4.80 (0.57)	0.69 (0.08)	0.36	0.75	5.6 to 8.1	0.05 to 8.0

[a]MD—maximum displacement (m); AD—average displacement (m).

[b]SS—strike slip; R—reverse; N—normal.

[c]Numbers in parentheses are standard errors.

[d]Regressions for reverse-slip relationships shown in italics are not significant at a 95% probability level.

Source: From D. L. Wells and K. J. Coppersmith, *Bulletin of Seismological Society of America*, Vol. 84, No. 4, 1994. Reproduced with permission of the Seismological Society of America.

(b) from Table 7.2

$$M = 6.81 + 0.78 \log(5) \pm 0.29 = 7.48 \pm 0.29$$
$$= 7.5(\text{expected value}), 7.2(\text{lower bound}), 7.8(\text{upper bound})$$

(c) from Eq. (7.17)

$$M = 7.223 + 1.263 \log\ 2.0 = 7.6$$

Example 7.2. Estimate the SRL, subsurface rupture length (RLD), downdip rupture width (RW), and maximum displacement (MD) for a magnitude 7.4 event with a strike-slip (SS) faulting. Also evaluate uncertainty of predicted values by assuming a dispersion of one standard deviation.

SOLUTION. From Table 7.1

$$\log(\text{SRL}) = -3.55 + 0.74(7.4) \pm 0.23 = 1.926 \pm 0.23$$
$$\text{SRL} = 84 \text{ km (expected value), } 50 \text{ km (lower bound), } 143 \text{ km (upper bound)}$$
$$\log(\text{RLD}) = -2.57 + 0.62(7.4) \pm 0.15 = 2.018 \pm 0.15$$
$$\text{RLD} = 128 \text{ km (expected value), } 74 \text{ km (lower bound), } 147 \text{ km (upper bound)}$$
$$\log(\text{RW}) = -0.76 + 0.27(7.4) \pm 0.14 = 1.238 \pm 0.14$$
$$\text{RW} = 17.3 \text{ km (expected value), } 12.5 \text{ km (lower bound), } 23.9 \text{ km (upper bound)}$$

From Table 7.2

$$\log(\text{MD}) = -7.03 + 1.03(7.4) \pm 0.34 = 0.592 \pm 0.34$$
$$\text{MD} = 3.9 \text{ m (expected value), } 1.8 \text{ m (lower bound), } 8.6 \text{ m (upper bound)}$$

From the above examples it is clear that the range of possible values relating the size of an event to the relevant source parameters is rather large. As we will see later in this chapter, sizable uncertainties are associated with practically every aspect of seismic hazard evaluation.

7.5.2 Attenuation Relations

Analogues to empirical relations that relate estimates of source parameters to the size of an event, empirical relations are developed to relate the extent of shaking at a site given the magnitude of the event characteristics of the source. The design ground motion at a site is arrived at by (a) establishing seismic sources and their characteristics, (b) determination of the travel path influences

on the seismic waves generated by various sources, and (c) evaluation of site soil role in amplification or deamplification of the arriving seismic waves.

There exist legitimate and unsettled differences of opinion regarding mapping of the fault sources. Different geotechnical engineers, for example, map the extent of the Elysian Park structure in the Southern California very differently. The differences of opinion on perceived rate of seismicity, maximum magnitude size, and other source characteristics, although significantly decreased during the past several years, are still large enough to make a critical difference in design.

The travel path influence is modeled by various attenuation or predictive relations. Until the mid-1980s most predictive relations provide an estimate for the peak horizontal ground acceleration (PHGA). The geotechnical engineers then used PHGA in association with established spectral shapes such as those developed by Newmark and Hall [102] to construct earthquake design spectra. Since late 1980s many predictive relations have been developed to provide direct estimates for response spectral ordinates at predetermined vibration periods.

Many factors influence the design ground motion estimates that are obtained from various predictive relations. These include but are not limited to the following:

- The choice of earthquake records that form the database for the regression analysis.
- The selected mathematical form for the regression equations.
- The degree by which site soil classification of the recording sites is documented as a part of the earthquake record database and used in regression analyses. For example, while some predictive relations make a binary distinction between soil and rock sites, others use shear wave velocity as a part of regression analyses.
- The model used for incorporation of ground motion dispersion.
- The choice of horizontal components used. For example, some predictive relations only use the larger horizontal component while others use both components in the database.
- The definition of distance from the source to the site as modeled in the relation.
- The regional bias built into the earthquake record database.

Added to the above factors is the scarcity of the records obtained from large events ($M > 7.0$) in relatively close distances (<10 km), causing most attenuation relations to simply extrapolate the existing data to these cases. Therefore, it is not surprising to see large differences in estimates provided for large nearby events, since we are in fact comparing various curve-fitting techniques rather than actual earthquake characteristics.

Abrahamson and Shedlock [1] reviewed several of the most commonly used

predictive relations and their range of applicability. Since different predictive relations use different measures for gauging site-to-source distance, an understanding of various distance measures utilized is essential for proper application of these relations. The most common source-to-site distance measures are (see Fig. 7.7) r_{jb}, the closest distance to the vertical projection of the rupture; r_{rup}, the closest distance to the rupture surface; r_{seis}, the closest distance to the seismological rupture surface; and r_{hypo}, the hypocentral distance. Predictive relations yield best results if they are used for hazard assessment in regions with tectonic settings similar to the selection of earthquake records represented in the database used in their development.

One of the most commonly used attenuation relations proposed by Boore,

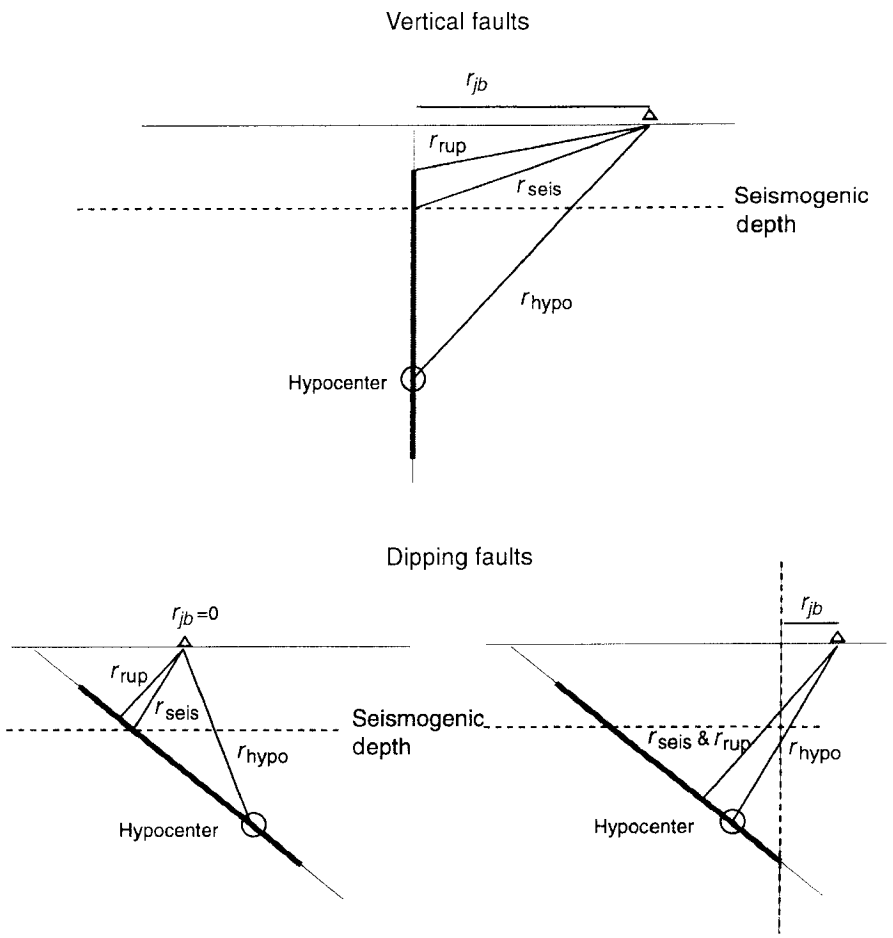

Fig. 7.7 Common source-to-site distance measures. (From N. A. Abrahamson and K. M. Shedlock, *Seismological Research Letters*, Vol. 68, No. 1, 1997. Reproduced with permission of the Seismological Society of America.)

Joyner, and Fumal in 1997 [26] estimates the ground motion estimation at the site in the form

$$\ln Y = b_1 + b_2(M - 6) + b_3(M - 6)^2 + b_5 \ln r + b_V \ln \frac{V_s}{V_A} \tag{7.18}$$

where

$$r = \sqrt{r_{jb}^2 + h^2}$$

In this equation Y is a ground motion parameter, namely peak horizontal acceleration or pseudoacceleration response in g. The predictor variables are moment magnitude (M), distance (r_{jb}, in km), and average shear wave velocity in the upper 30 m of soil (V_s, in m/s). Coefficients to be determined are b_1 (a function of the faulting type), b_2, b_3, b_5, h (a fictitious depth determined by regression), b_V, and V_A, provided in a tabular form for various situations.

Commonly used predictive relations use very different assumptions on the functional form of attenuation. For example, the Boore et al. relation [see Eq. (7.18)] assumes that distance dependence is independent of magnitude, while some others assume otherwise. While this difference in shape does not yield significant difference where data are abundant, it can make a huge difference where data are sparse (large-magnitude, close-by events). A comparison of median predicted 5% damped spectral accelerations for a rock site in western United States on a vertical strike-slip fault for a magnitude 7.0 event at rupture distance of 10 km is shown in Fig. 7.8. Notice the large difference in predicted values provided by various formulas.

7.6 DETERMINISTIC AND PROBABILISTIC APPROACHES

Until a decade ago, most seismic hazard evaluations were performed using deterministic principles. Increasingly, however, more modern probabilistic techniques have defined the standards of practice. Even building codes currently relate their definition of seismic demand in probabilistic terms (i.e., 50% probability of exceedance in 50 years). Code requirements on design ground motions in many respects, however, continue to be eclectic collections of deterministic and probabilistic ideas presented through a probabilistic vocabulary. We will review some of the difficulties inherent in such a mixed approach, particularly as embodied in the 1997 edition of the Uniform Building Code.

7.6.1 Deterministic Seismic Hazard Evaluation

In deterministic procedures a causative active fault and appropriate earthquake magnitude are selected. The closest distance from the fault to the site is measured, and a ground motion attenuation relationship is used to determine the

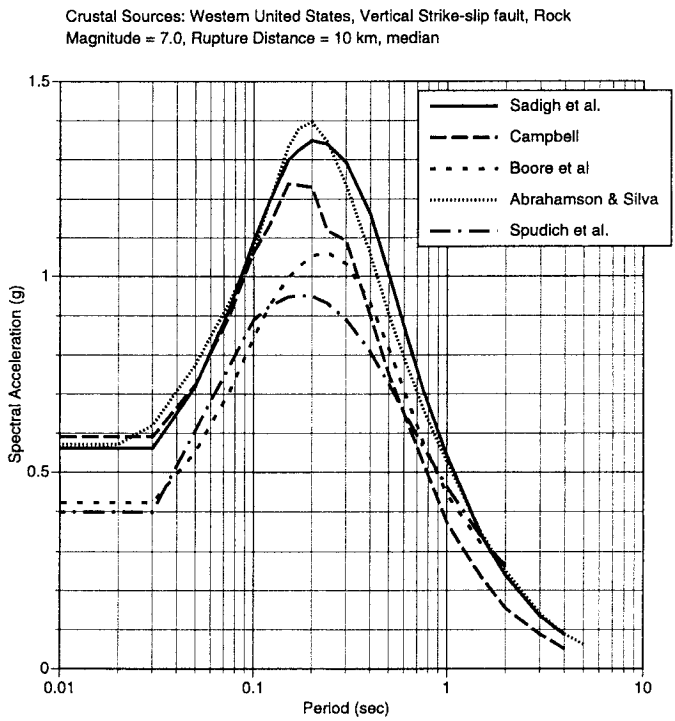

Fig. 7.8 Comparison of the median estimates of SA for a strike-slip earthquake of magnitude 7.0 at a distance of 10 km. (From N. A. Abrahamson and K. M. Shedlock, *Seismological Research Letters*, Vol. 68, No. 1, 1997. Reproduced with permission of the Seismological Society of America.)

likely ground motion at the site given the selected magnitude, distance, and site soil condition. Since more than one fault source may contribute to the critical hazard at a site, the procedure is repeated for all likely fault candidates. In southern California, for example, two design spectra are usually developed: one for a local fault with smaller magnitude and closer distance, and one for the San Andreas or another large fault representing the motion produced by a large event at a further distance. Traditionally, median values provided by the attenuation relation are used in deterministic procedures.

There are several problems associated with deterministic seismic hazard procedures. First, there is no reason to believe that a fault will break at its closest distance to the site (a very conservative assumption). Second, the method gives no assessment of the relative seismic risk posed by various sources.

7.6.2 Probabilistic Seismic Hazard Evaluation

A probabilistic seismic hazard analysis usually begins by developing mathematical models that are used to estimate the recurrence intervals of future earth-

quakes of a certain size. These models are then used with an attenuation relationship and a complex procedure to estimate the ground motions for which the probability of being exceeded is less than a specified threshold (such as 10% in 50 years).

The most common recurrence model is the Guenberg–Richter relationship, also known as the Richter law of magnitudes [26]. This relationship states that there exists an approximate linear relationship between the logarithm of the average number of earthquakes per unit time and earthquake magnitude in the form

$$\log N = a - bM \tag{7.19}$$

where N is the average number of earthquakes per year of magnitude M and larger and a and b are coefficients derived from analysis of data associated with a region, a fault, or a fault system. It is generally accepted that the regional catalogs of seismicity are well described by the Gutenberg–Richter model [135].

According to Wesnousky [135], this model, when applied to seismic hazard analysis, generally implies a stationary process whereby seismic events of all sizes occur continually on a fault during the interval between the occurrences of the maximum ($M_{\max}$) expected events. At the other extreme, one could argue that the time between $M_{\max}$ events along a fault or a fault segment is rather quiet, marked primarily by foreshocks and aftershocks. The latter model is commonly referred to as the *characteristic earthquake model* [112]. The differences between the two models are graphically shown in Fig. 7.9. The figure

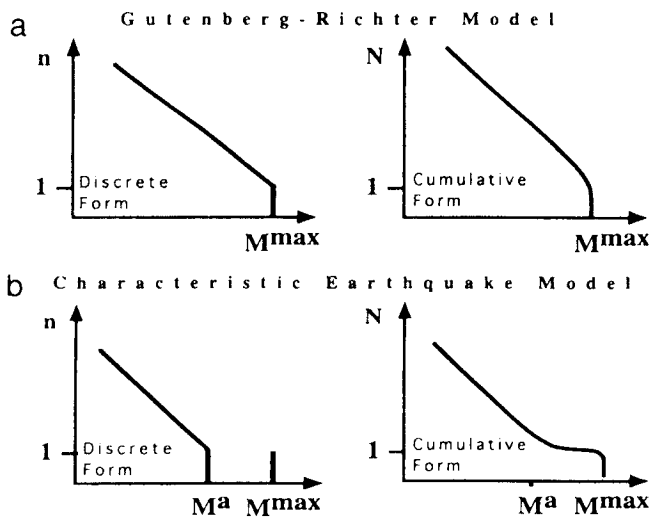

Fig. 7.9 Gutenberg–Richter and characteristic models of earthquake recurrence. (From S. G. Wesnousky, Bulletin of Seismological Society of America, Vol. 84, No. 6, 1994. Reproduced with permission of the Seismological Society of America.)

gives the distribution of the number of events versus the magnitude implied by the assumption of either (a) the Gutenberg–Richter or (b) the characteristic earthquake model of fault behavior during the repeat time of one maximum-magnitude ($M_{\max}$) event along a fault. Both the discrete and cumulative forms of the expected-magnitude distribution, where n equals the number of events equal to a given magnitude and N equals the number of events greater than or equal to a given magnitude, are provided in (a) and (b). For the characteristic earthquake model, the largest earthquake during the repeat time of a maximum-size event is defined to equal the size of the largest aftershock (M^a), and the size distribution of aftershocks is assumed to satisfy the Gutenberg–Richter relationship. It appears, at this time, that the Gutenberg-Richter model is best suited for assessing regional seismicity and the characteristic model represents a better fit with observed seismicity of faults and fault segments.

Principles of probabilistic seismic hazard analyses were established by Cornell in 1968 [37]. This procedure (as summarized by Blake [22]) is as follows:

- Seismic sources (point, line, or areal) that may be capable of generating future earthquakes are delineated (Fig. 7.10*a*).
- A recurrence model is selected, $f_M(m)$, and its parameters are established for each source (Fig. 7.10*b*).
- A rupture length or area versus magnitude relation is selected to assess the extent of faulting associated with an event of certain size. A logarithmic standard deviation on rupture size, $\sigma_{\log(Ar)}$, is used to model the uncertainty in rupture size (Fig. 7.10*c*).
- For a given magnitude and rupture size, a zone of possible energy center locations of the rupture along the source is defined. In that zone a grid of energy centers is developed to model the uncertainty in earthquake locations (Fig. 7.10*d*).
- For each energy center location and rupture size, a rupture propagation is modeled and its boundaries along the source are defined. Then the distance measures of interest to the site are evaluated.
- By evaluating distances for all energy center locations, a probability distribution of distance for a given magnitude is established.
- An attenuation relationship predicting mean (or median) site response values and the corresponding standard deviation is selected (Fig. 7.10*e*).
- The probabilistic response parameters are computed by application of the *total probability theorem*. If the probability that a ground motion amplitude x is exceeded is noted by $\lambda[X \geq x]$ and the respective activity rates by v_i, the theorem states that

$$\lambda[X \geq x] = \sum_{\text{sources}(i)} v_i \sum_{\text{magnitudes}(j)} \sum_{\text{distances}(R)} P[X \geq x | m, r] P[M = m] P[R = r] \tag{7.20}$$

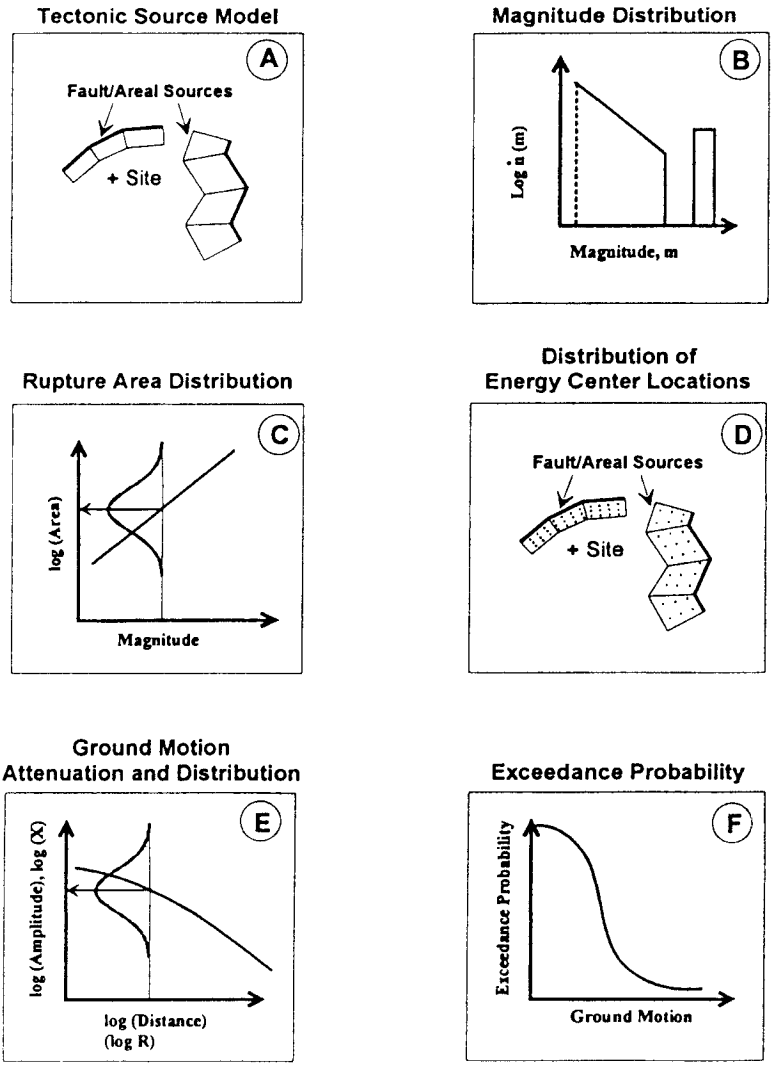

Fig. 7.10 General procedure for performing probabilistic seismic hazard analyses. (From T. F. Blake *FRISKSP User's Manual*, Newbury Park, CA, [22]. Reproduced with permission.)

- Finally, the mean return period T_a in years is obtained from

$$T_x = \frac{1}{\lambda_a} \tag{7.21}$$

where λ_a is the average annual probability that the selected response parameter exceeds a certain limit a. Assuming a Poisson distribution, the

probability of a selected parameter exceeding a during the life of structure T_{Life} can be estimated by

$$P = 1 - e^{-\lambda_a T_{\text{Life}}} \tag{7.22}$$

Example 7.3. This example illustrates a typical application of deterministic and probabilistic procedures for a preliminary seismic hazard analysis of a site located at Thousand Oaks, California. The local soil condition is assumed to be shallow alluvium underlain by rock. In part A the implications of historical data obtained from earthquake catalogs are examined. Part B presents a deterministic hazard analysis for establishing the expected peak ground accelerations at the site for two distinct classes of earthquakes. Finally, in part C, probabilistic procedures are used to postulate site-specific design spectra corresponding to various exceedance probabilities. Analysis of historical data is performed using the EQSEARCH computer program [20]. Deterministic analysis is performed using the EQFAULT program [21], and probabilistic analysis is performed using the FRISKSP computer code [22].

A. Historical Data: Estimation of Peak Horizontal Acceleration from California Earthquake Catalogs

Site coordinates: Latitude: 34.1817 N, Longitude: 118.7879 W
Type of search: Radius, Search radius: 62.4 miles
Search magnitudes: 4.0–9.0
Search dates: 1800–1996
Attenuation relation: 6) Joyner & Boore, Horiz.—Random
Uncertainty (M = mean, S = mean + 1-sigma): M
Soil condition assumed: Rock, shallow alluvium
Fault type assumed (DS = reverse, SS = strike-slip): DS
Time period of exposure for statistical comparison: 25 years
Source of depth values (A = attenuation file, E = earthquake catalog): A

Search Results Summary (*see related data in tables on pages 164–165.*)
614 Historical records found
Maximum mean site acceleration during time period 1800–1996: **0.14g**
Maximum mean site intensity (MM) during time period 1800–1996: **VIII**
Maximum magnitude encountered in search: **7.70**
Nearest historical earthquake was about **6 miles** away from site.
Number of years represented by search: **197 years**

Verification for Mean Acceleration Probabilities
Probability of exceedance for $0.05g$ in 10 years:

$$\text{Number of times exceeded} = 18$$

$$\text{Average occurrence per year} = 18/(1996 - 1800 + 1) = 0.0914 \quad \text{Ok}$$

$$P = 1 - e^{-N a t L} = 1 - e^{-0.0914(10)} = 0.5991 \quad \text{Ok}$$

Probability of Exceedance for Mean Acceleration Based on Historical Data Alone

Acceleration g	No. of Times Exceeded	Average Occurrences	Recurrence Interval, years	Computed Probability of Exceedance					
				In 0.5 year	In 1 year	In 10 years	In 50 years	In 75 years	In 100 years
0.01	299	1.518	0.659	0.5318	0.7808	1.0000	1.0000	1.0000	1.0000
0.02	135	0.685	1.459	0.2901	0.4961	0.9989	1.0000	1.0000	1.0000
0.03	65	0.330	3.031	0.1521	0.2810	0.9631	1.0000	1.0000	1.0000
0.04	36	0.183	5.472	0.0873	0.1670	0.8392	0.9999	1.0000	1.0000
0.05	18	0.091	10.944	0.0447	0.0873	0.5990	0.9896	0.9989	0.9999
0.06	9	0.046	21.889	0.0226	0.0447	0.3667	0.8982	0.9675	0.9896
0.07	7	0.036	28.143	0.0176	0.0349	0.2991	0.8308	0.9304	0.9714
0.08	4	0.020	49.250	0.0101	0.0201	0.1838	0.6377	0.7819	0.8687
0.09	4	0.020	49.250	0.0101	0.0201	0.1838	0.6377	0.7819	0.8687
0.10	3	0.015	65.667	0.0076	0.0151	0.1413	0.5330	0.6809	0.7819
0.11	2	0.010	98.500	0.0051	0.0101	0.0965	0.3981	0.5330	0.6377
0.12	2	0.010	98.500	0.0051	0.0101	0.0965	0.3981	0.5330	0.6377
0.13	2	0.010	98.500	0.0051	0.0101	0.0965	0.3981	0.5330	0.6377

Probability of Exceedance for Magnitude

Magnitude	No. of Times Exceeded	Average Occurrences per Year	Recurrence Interval years	Computed Probability of Exceedance				
				In 1 year	In 10 years	In 50 years	In 75 years	In 100 years
4.00	614	3.117	0.321	0.9557	1.0000	1.0000	1.0000	1.0000
4.50	237	1.203	0.831	0.6997	1.0000	1.0000	1.0000	1.0000
5.00	86	0.437	2.291	0.3537	0.9873	1.0000	1.0000	1.0000
5.50	29	0.147	6.793	0.1369	0.7706	0.9994	1.0000	1.0000
6.00	13	0.066	15.154	0.0639	0.4831	0.9631	0.9929	0.9986
6.50	5	0.025	39.400	0.0251	0.2242	0.7189	0.8510	0.9210
7.00	4	0.020	49.250	0.0201	0.1838	0.6377	0.7819	0.8687
7.50	1	0.005	197.000	0.0051	0.0495	0.2242	0.3166	0.3981

Verification for Exceedance Probability for Magnitude
Probability of exceedance for magnitude 6.0 in 10 years:

Number of times exceeded = 13
Average occurrence per year = 13/(1996 − 1800 + 1) = 0.0660 Ok
Average recurrence interval = 1/0.0660 = 15.154 years Ok
$P = 1 - e^{-N_a t_L} = 1 - e^{-0.0660(10)} = 0.4831$ Ok

B. Deterministic Seismic Hazard Analysis: Estimation of Peak Horizontal Acceleration from Digitized California Faults

Site Coordinates: Latitude: 34.1817 N, Longitude: 118.7879 W
Faults considered in the radius of: 62.4 miles (100 km)
Attenuation relation: 6) Joyner & Boore, Horiz.—Random
Uncertainty (M = mean, S = mean + 1-sigma): M
Soil condition assumed: Rock, shallow alluvium
Source of depth values (A = attenuation file, E = earthquake catalog): A
Analysis Results Summary: (see related data in tables on pages 167–169.)
39 Faults found within the specified search radius.
The **Simi–Santa Rosa Fault** is closest to the site. It is about **6.4 miles** away.
Largest mean maximum credible site acceleration: **0.324g**
Largest mean maximum probable site acceleration: **0.172g**

C. Probabilistic Seismic Hazard Analysis: Estimation of Site Design Spectra from Probabilistic Combination of Fault Hazards

Site coordinates: Latitude: 34.1817 N, Longitude: 118.7879 W
Faults considered in the radius of: 62.4 miles (100 km)
Attenuation relation: Idriss (1993)
Uncertainty (M = mean, S = mean + 1-sigma): **S**
Soil condition assumed: rock, shallow alluvium
Source of depth values (A = attenuation file, E = earthquake catalog): A

Plots of the probabilistic estimates of the response spectra are shown in Fig. 7.11.

7.6.3 Limitations of Deterministic and Probabilistic Seismic Hazard Analysis

Probabilistic procedures provide for consideration of earthquake ground motion uncertainties in design. Considering the fact that uncertainties are large, probabilistic procedures seem to present the most prudent approach to seismic hazard analysis for most structures at the present time. Deterministic procedures are still useful in evaluating scenario earthquakes, dealing with worst-case scenario events, and for design of structures of critical importance such as nuclear power

Summary of Deterministic Analysis

Abbreviated Fault Name	Approximate Distance		Maximum Credible Event			Maximum Probable Event		
	Miles	km	Maximum Credible Magnitude	Peak Site Acceleration *g*	Site Intensity MM	Maximum Probable Magnitude	Peak Site Acceleration	Site Intensity MM
Anacapa	16	26	7.00	0.143	VIII	5.00	0.050	VI
Arroyo Parida–More Ranch	26	43	7.50	0.105	VII	5.25	0.032	V
Big Pine	44	70	7.30	0.049	VI	5.50	0.019	IV
Catalina Escarpment	35	57	7.00	0.055	VI	6.25	0.037	V
Chino	60	96	7.00	0.026	V	5.50	0.012	III
Clearwater	31	50	7.00	0.066	VI	3.00	0.008	III
Cucamonga	55	89	7.00	0.029	V	6.25	0.020	IV
Elysian Park Seismic Zone	28	45	7.00	0.075	VII	5.75	0.038	V
Frazier Mountain	37	60	6.50	0.040	V	3.00	0.006	II
Garlock (West)	45	72	7.80	0.062	VI	6.50	0.031	V
Holser	17	28	6.60	0.106	VII	5.75	0.068	VI
Malibu Coast	10	16	7.50	0.293	IX	6.50	0.172	VIII
Mesa	53	85	6.00	0.019	IV	5.25	0.013	III
Midchannel	29	46	7.50	0.096	VII	5.50	0.033	V
Newport-Inglewood (Offshore)	23	36	7.00	0.097	VII	5.75	0.505	VI
North Channel Slope	57	92	7.50	0.036	V	5.75	0.014	IV
Northridge Hills	13	20	6.50	0.139	VIII	5.00	0.063	VI
Oak Ridge (offshore)	21	34	7.20	0.118	VII	5.50	0.048	VI
Oak Ridge (onshore)	14	22	7.20	0.189	VIII	6.50	0.130	VIII
Ozena	47	76	7.00	0.037	V	4.75	0.011	III

Summary of Deterministic Analysis (Continued)

Abbreviated Fault Name	Approximate Distance		Maximum Credible Event			Maximum Probable Event		
	Miles	km	Maximum Credible Magnitude	Peak Site Acceleration *g*	Site Intensity MM	Maximum Probable Magnitude	Peak Site Acceleration	Site Intensity MM
Palos Verd-Coron.B.-A. Blan	16	25	7.50	0.192	VIII	6.75	0.129	VIII
Pine Mountain	29	47	7.00	0.072	VI	4.25	0.017	IV
Pleito	51	83	7.00	0.033	V	5.75	0.017	IV
Raymond	32	51	7.50	0.083	VII	4.00	0.013	III
Red Mountain	31	50	7.30	0.077	VII	5.25	0.026	V
San Andreas (Mojave)	39	62	8.30	0.098	VII	8.00	0.084	VII
San Cayetano	15	24	7.50	0.200	VIII	6.25	0.103	VII
San Clemente–San Isidro	43	69	8.00	0.072	VII	6.50	0.033	V
San Gabriel	21	34	7.00	0.105	VII	5.75	0.054	VI
Santa Cruz Island	39	63	7.40	0.060	VI	4.75	0.015	IV
Santa Monica–Hollywood	15	24	7.50	0.203	VIII	5.25	0.062	VI
Santa Susana	12	19	7.00	0.198	VIII	6.00	0.116	VII
Santa Ynez (East)	28	45	7.50	0.097	VII	5.25	0.030	V
Sierra Madre–San Fernando	18	30	7.50	0.160	VIII	6.00	0.072	VII
Simi–Santa Rosa	**6**	**10**	**7.00**	**0.324**	**XI**	**5.25**	**0.128**	**VIII**
Ventura–Pitas Point	24	38	7.20	0.102	VII	5.75	0.047	VI
Verdugo	21	34	6.70	0.091	VII	4.50	0.028	V
White Wolf	58	93	7.80	0.042	VI	6.00	0.016	IV
Whittier–North Elsinore	34	54	7.50	0.078	VII	6.00	0.035	V

Summary of Probabilistic Analysis

Period (sec)	Spectral Acceleration (g) for 5% Damped Systems by Average Return Period				
	72 years	100 years	200 years	475 years	1000 years
0.01	0.31	0.34	0.42	0.51	0.60
0.03	0.31	0.34	0.41	0.51	0.60
0.05	0.39	0.43	0.53	0.69	0.83
0.08	0.48	0.54	0.69	0.86	1.00
0.10	0.60	0.68	0.85	1.03	1.22
0.11	0.66	0.74	0.88	1.09	1.29
0.13	0.71	0.79	0.95	0.18	1.38
0.15	0.74	0.82	1.00	1.23	1.45
0.20	0.78	0.87	1.05	1.30	1.54
0.25	0.77	0.85	1.05	1.31	1.55
0.30	0.73	0.81	1.00	1.24	1.47
0.35	0.68	0.75	0.93	1.16	1.38
0.40	0.62	0.69	0.85	1.06	1.26
0.50	0.51	0.57	0.71	0.89	1.07
0.60	0.42	0.47	0.59	0.74	0.89
0.70	0.35	0.40	0.50	0.64	0.76
0.80	0.29	0.33	0.42	0.53	0.64
0.90	0.25	0.28	0.36	0.45	0.55
1.00	0.22	0.25	0.32	0.41	0.49
1.50	0.12	0.14	0.18	0.23	0.28
2.00	0.08	0.10	0.13	0.17	0.20
3.00	0.05	0.06	0.07	0.10	0.12
4.00	0.03	0.04	0.05	0.07	0.08

plants. Extreme care should be taken not to extend either of the methods beyond the available tectonic, geologic, and historical data that form the logical basis of these procedures.

For example, the historical data on California earthquakes goes back less than 200 years. Available geologic data provides us with useful information on large earthquakes on known major faults such as the San Andreas Fault dating back to a few hundred years. Smaller earthquakes (i.e., $M < 5.0$) are practically absent from available data prior to late 1800s. Add to this the existence of buried thrust faults in southern California, not known before their rupture, which have been responsible for the past three major events in this region (1971, San Fernando; 1987, Whittier; 1994, Northridge). This abundance of unknowns and limitations of our knowledge makes it extremely imprudent for us to forecast long-term probabilities for earthquakes, spanning thousands of years. However, this is exactly what is being done in some applications. For example, according

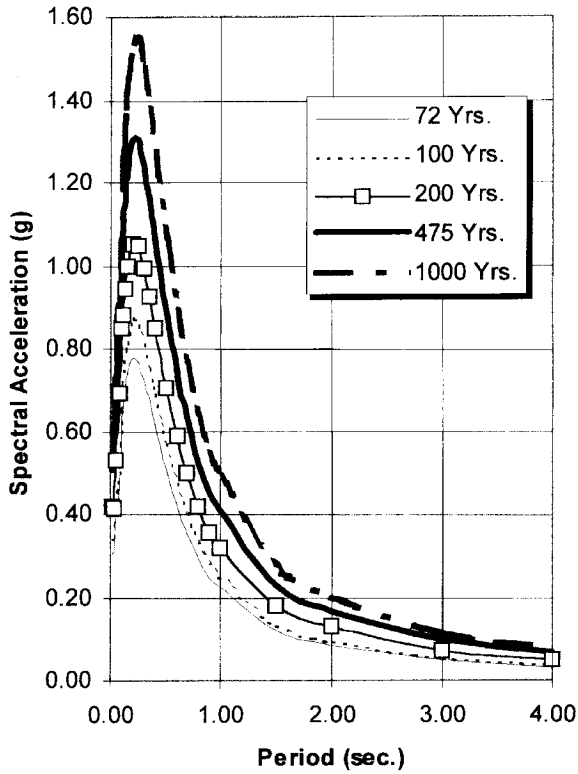

Fig. 7.11 Probabilistic estimates of site response spectra for Example 5.3.

to Krinitzsky [70], the Department of Energy requires mean annual probabilities of exceedance of 1×10^{-4} and 1×10^{-5} for its performance categories 3 and 4. These requirements translate into mean return periods on the order of 10,000 and 100,000 years, respectively. It is obvious that we do not have sufficient data to probabilistically forecast earthquakes into such distant futures. A more prudent approach for such low-risk tolerances would be to use deterministic worst-case scenario events, which are most likely to produce smaller motions than the probabilistic methods extrapolated beyond their rational range of applicability. As Krinitzsky [70] stated: "*Earthquake motions derived by probabilistic seismic hazard analysis and assigned for tens of thousands of years represent innumeracy, the numbers equivalent of illiteracy.*" [emphasis added]

7.6.4 Seismic Hazard Maps

It has been long a tradition of the Uniform Building Code to carry a seismic zone map of the United States. Recent advances in computing, geographic

information systems (GISs), networking, and seismic hazard analysis techniques have made it possible for the USGS and California Division of Mines and Geology (CDMG) to develop detailed seismic hazard maps of California and the rest of continental United States. The CDMG maps, as a matter of fact, are made an integral part of the 1997 UBC for California practice as the official source of evaluating the near-fault factors necessary for design. At the time of preparing this manuscript, these maps are undergoing the final stages of their development. However, these maps for many regions and soil conditions are available from the USGS and CDMG WWW sites on the Internet. Figures 7.12 and 7.13 show examples of maps available via the Internet. This national mapping effort has great promise for providing a de facto standard for seismic hazard analysis, thereby reducing the large variations observed in seismic hazard assessments for a given site provided by different geotechnical engineers.

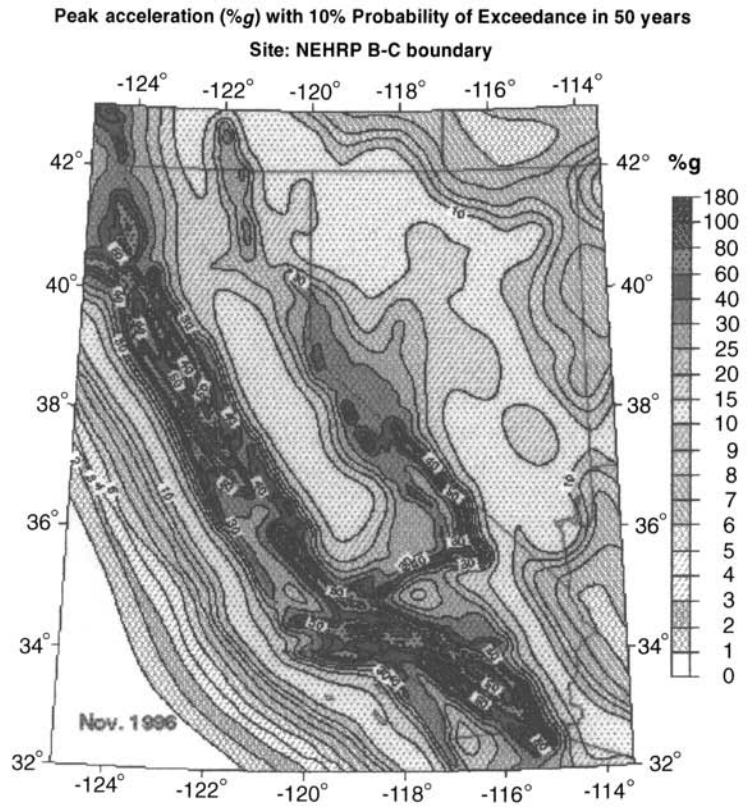

Fig. 7.12 Representative sample of seismic hazard maps available on the Internet from the USGS WWW site.

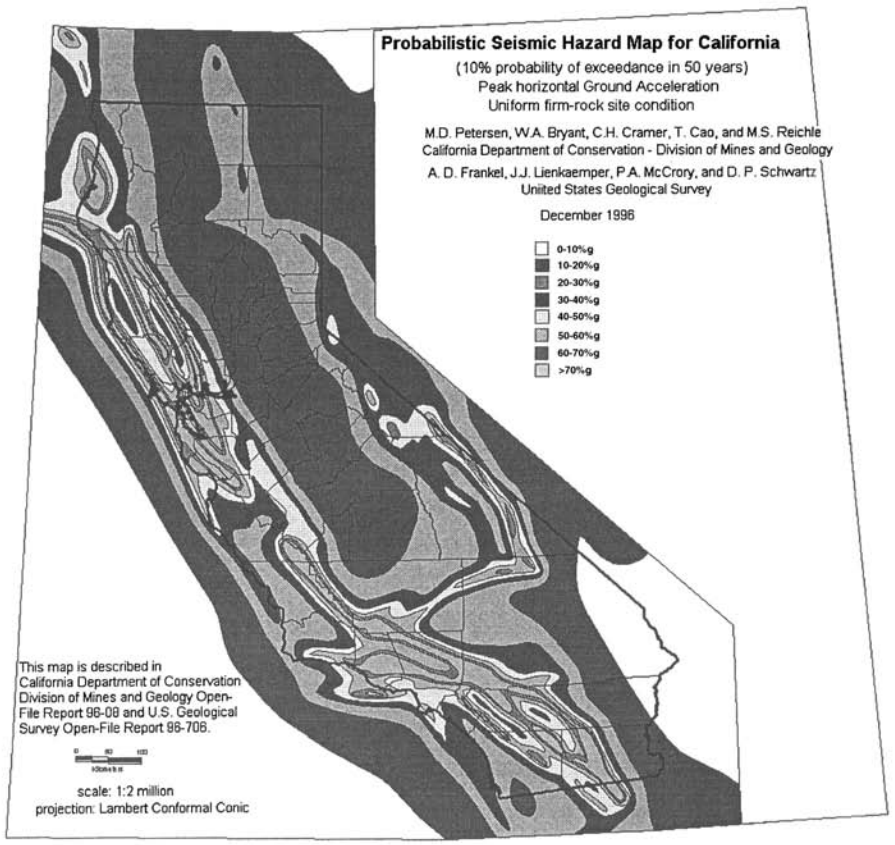

Fig. 7.13 Representative sample of seismic hazard maps available on the Internet.

7.7 CODE INTERPRETATIONS OF DESIGN GROUND MOTIONS

All contemporary seismic design codes have adopted a probabilistic framework for defining design ground motions. While there is no shortage of confusing terminology, the basic specification of seismic hazard is very similar in most codes and guidelines.

The basic design level hazard is 10% probability of exceedance in 50 years (a mean return period of 475) years. Prior to the 1994 edition, the UBC referred to this as the *maximum probable earthquake* (MPE). Now the UBC refers to it as the *design basis earthquake* (DBE). The FEMA-273 guidelines for seismic rehabilitation of buildings refers to this as *Basic Safety Earthquake 1* (BSE-1). The Structural Engineers Association of California in their Vision-2000 document refer to this as a *rare event.*

The upper bound hazard generally used for ensuring structural stability dur-

ing ground motions that exceed the basic design level event is 10% probability of exceedance in 100 years. UBC-91 referred to this as the maximum credible earthquake (MCE), UBC-94 changed the name to the maximum capable earthquake, and UBC-97 changed it again to the maximum considered earthquake. FEMA-273 guidelines call it *Basic Safety Earthquake 2* (BSE-2). In the Vision-2000 document it is considered a *very rare event.* One reason for successive name changes is that initially MCE represented the deterministic concept of the most severe ground shaking possible at the site given the geologic and regional tectonic framework, realizing that designing building structures that have a useful life of 50–100 years for such large motions is unreasonable, an equivalent probabilistic definition was adopted. This definition, which in some documents such as the 1991 edition of the California Building Code was 10% in 250 years, has been generally reduced to the current level of 10% in 100 years. Obviously, the original deterministic definition (maximum credible) has been replaced by the maximum shaking that is now being considered in design (maximum considered).

Neither of the codes or guidelines mention the specifics of hazard calculations. For example, how the inherent uncertainties in the data are to be dealt with, is one standard deviation enough or is it too much, can mean values be used and dispersion of data about mean values ignored, and what choices of source and attenuation parameters are acceptable for use in a given region and which ones are not. Legitimate variations in procedures deemed appropriate for a region can result in spectral ordinates that can differ by as much as 100%. Proper procedures and guidelines are needed to help reduce the differences in hazard analysis results projected for a given site.

Large variations in estimated design ground motions may very well impact the choice of the structural system, the isolation system, and the whole decision of going ahead with a project or not. At least one new seismic-isolated design project in southern California was shelved, and design of several others were adversely affected due to strict adherence to very conservative design ground motion estimates. For existing structures, the situation can be ironic: The design requirements may become so excessive that an upgrade is deemed unfeasible and the occupants will stay in a building in its existing condition, which may be far less safe than if upgraded under a more modest design criterion.

Contrary to conventional buildings, design of seismic-isolated structures for superconservative ground motions may have self-defeating results. By basing the performance of the isolation system to a very rare event, one can risk making the system so stiff that it will not behave properly during more frequent events that can occur several times during the life of the structure.

Extreme care must be taken in design of isolated structures to balance the legitimate desire for reasonably conservative design ground motions and the need for isolated buildings to minimize floor accelerations, secondary-mode effects, and nonstructural damage during smaller events.

7.8 APPLICATION OF EARTHQUAKE TIME HISTORIES

Recorded earthquake time histories or records constitute the most fundamental information needed for earthquake-resistant design. Our understanding of earthquake ground motion and its important characteristics improves significantly after each earthquake. All seismic design provisions, in one way or another, are ultimately justified or rejected on the basis of the general characteristics observed in or interpreted from earthquake records.

Contemporary seismic design procedures rely heavily on response spectrum presentation of design ground motions. When design procedures are based entirely on the response spectrum, the response spectrum constitutes all of the ground motion information required for the design. However, if the design procedure involves time history analysis in conjunction with a design response spectrum, then some method is required to select time histories that are representative of the response spectrum. The process by which earthquake records are manipulated to produce some level of design spectrum compatibility is called *scaling*. Scaling may be performed in the time domain or the frequency domain. The pristine records before application of the scaling procedure are commonly referred to as the *seeds*. The desired scaled result may also be obtained by development of synthetic earthquake records. The extent of the required scaling is generally defined by the governing seismic design code provisions. These provisions have been changing quite frequently during the recent years.

One common pitfall in scaling earthquake time histories is scaling a single component or pair of components in the frequency domain to match the target design spectrum very closely over a wide range of vibration periods. As we will see in this section, such practices may totally distort the energy characteristics of the seeds and produce very unrealistic seismic demands.

7.8.1 UBC-94 Provisions

According to UBC-94 provisions for design of seismic-isolated structures, time history analysis may be used for design of all seismic-isolated structures and *shall be used* for design of all seismic-isolated structures not meeting the criteria for either static analysis or response spectrum analysis. Hence, quite properly, the code considers time history analysis as the most accurate of the three methods of seismic analysis (namely static, response spectrum, and time history).

UBC-94 requires the following for the selection and application of time histories in the analysis and design of seismic-isolated structures:

- At least three pairs of recorded horizontal ground motion time history components should be selected and used.
- These time histories should exhibit strong motion durations consistent with the magnitude and source characteristics of the design ground motions (DBE and/or MCE).

- The time histories developed for sites within 15 km of major active faults should incorporate near-fault phenomena.
- For each pair of horizontal ground motion components, the SRSS of the 5% damped spectrum of the scaled horizontal components is to be constructed.
- The time histories are to be scaled such that the *average value* of the SRSS spectra does not fall below 1.3 times the 5% damped design spectrum (DBE or MCE) by more than 10% over a range of $T_I - 1$ to $T_I + 2$, where T_I is the period of seismic-isolated structure in the direction under consideration. The explicit reference to the "average value" for the SRSS spectra is new and was adopted recently in the 1993 supplement to the 1991 edition of the code. Prior to that, the common interpretation was that each ground motion pair, a pair at a time, was to be scaled to match the SRSS spectra.
- Each pair of time histories is to be applied simultaneously to the model considering the most disadvantageous location of mass eccentricity. The maximum displacement of the isolation system is to be calculated from the vectorial sum of the two orthogonal components at each time step.
- The parameters of interest are calculated for each time history analysis. If three time history analyses are performed, then the maximum response of the parameter of interest is to be used for design. If seven or more time histories are used, then the average value of the response parameter of interest may be used. The reference to seven pairs of time histories and authorization to use the average value of the response parameters in this case is new and was adopted as a part of the 1993 supplement to the 1991 code provisions. Prior to that, use of maximum response parameters obtained from a three-pair time history analysis was viewed as a mandatory requirement.

This formulation contains implicit recognition of the crucially important fact that design spectra are definitions of a criterion for structural analysis and design and are not meant to represent characteristics of a single event.

7.8.2 UBC-97 Provisions

UBC-97 provisions for application of time histories is essentially the same as UBC-94 with the following exceptions:

- UBC-97 distinguishes between *recorded* time histories and *simulated* ones. It requires a minimum of three recorded time histories. However, it permits substitution of recorded time histories by simulated ones if appropriate recorded time histories are not available.
- The period range of scaling has been changed from $T_I - 1$ to $T_I + 2$ to $0.5T_D$ to $1.25T_M$, where T_D and T_M are effective isolated periods at design displacement and maximum displacement, respectively.

7.8.3 OSHPD-91 Provisions

The provisions of this document were among the most controversial time history analysis requirements. Fortunately, due to many criticisms [94, 95], they are no longer in effect. According to these provisions: "*If time history analysis is used, the input time histories should be selected from different recorded events and based on similarity to source magnitude and distance, foundation material and tectonic conditions. They should be scaled in the frequency domain such that their 5%-damped response spectrum essentially envelopes the site-specific spectrum and does not fall below the site-specific spectrum by more than 10% at any period. Time histories developed for sites within 15 km of an active fault must incorporate near-fault phenomena. Duration of time histories should be consistent with the magnitude and source characteristics of an event*" (underlining by the authors).

As demonstrated by Naeim and Lew [94, 95], the above interpretation of design requirements, which mandates a scaling of a single time history to match a design spectrum (particularly in frequency domain), is inconsistent with the definition, purpose, and application concept of design spectra and may lead to unrealistic and physically incorrect (or impossible) ground motion time histories with serious practical implications.

7.8.4 OSHPD-96 Provisions

The new OSHPD provisions for time history analysis are essentially the same as UBC-94 with the following exceptions:

- Pairs of horizontal ground motion time history components shall be selected from not less than three *recorded* events.
- The period range for matching is specified as $T_I - 1.0$ sec to $T_I + 1.0$ sec.
- The duration of the time histories shall be consistent with the magnitude and source characteristics of the design basis earthquakes (or maximum capable earthquake).
- Time histories developed for sites with a near-field factor N greater than 1.0 shall incorporate near-field phenomena.
- The SRSS of the scaled time history components is to be equal to or greater than the 5% damped spectra at the period T_I.

7.8.5 Time-Domain Scaling of Time Histories

The aforementioned code provisions, with the exception of OSHPD-91, are not clear on the method by which scaling has to be applied. The most straightforward interpretation is that they (again with the clear exception of OSHPD-91) imply a time-domain scaling procedure, that is, applying a series of scalar multipliers to peak ground acceleration of each time history. Lack of clarity, however,

makes is possible to interpret these provisions as permitting frequency-domain procedures as needed to obtain the desired spectrum-matching objectives.

Example 7.4. The 5% damped design spectrum for a site located at close proximity to an active fault is given in Fig. 7.14. To illustrate scaling differences implied by various code provisions, three pairs of earthquake time histories from the 1994 Northridge earthquake are selected: (a) the record obtained from the Newhall fire station; (b) the free-field record obtained from the Sylmar County Hospital parking lot; and (c) the record obtained from Santa Monica City Hall grounds. These time histories are included in the companion CD-ROM disc. The 5% damped response spectra for the design spectrum as well as these records in the period range of interest for scaling are presented in Table 7.3. Assuming a building with $T_I = T_D = T_M = 3.0$ sec, determine the scaling factors for each time history pair according to the provisions of (a) UBC-94, (b) OSHPD-96, and (c) UBC-97.

SOLUTION

(a) for a T_I of 3.0 sec the vibration period band to match is 2.0–5.0 sec. Calculation of time-domain scaling factors for UBC-94 results in scale factors of 1.82, 1.47, and 4.63 for the Newhall, Sylmar, and Santa Monica records, respectively. As a result of this scaling, at the isolated period of 3.0 sec, the scaled time histories exceed the design spectrum by a factor of 1.89. Given the fact that the Newhall and Sylmar ground motions are among the most potent earthquake ground motions ever recorded in California, the superconservatism of this scaling procedure becomes more apparent. Furthermore, notice that scal-

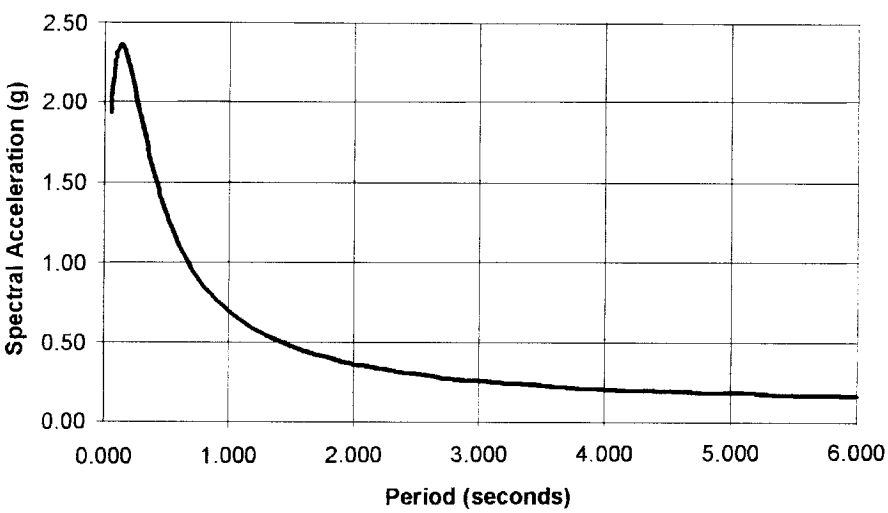

Fig. 7.14 Target 5% damped design spectrum for Example 5.4.

TABLE 7.3 Spectral Ordinates for the Target and Ground Motion Pairs

Period (sec)	Design SA (in/s/s)	Newhall		Sylmar		Santa Monica	
		Component 1	Component 2	Component 1	Component 2	Component 1	Component 2
1.50	0.46	0.52	0.77	0.45	0.85	0.34	0.25
1.60	0.43	0.42	0.63	0.38	0.82	0.33	0.22
1.70	0.41	0.35	0.55	0.39	0.77	0.28	0.21
1.80	0.39	0.30	0.52	0.41	0.71	0.24	0.19
1.90	0.37	0.27	0.48	0.44	0.66	0.24	0.17
2.00	0.35	0.26	0.44	0.45	0.62	0.26	0.16
2.20	0.32	0.24	0.35	0.46	0.53	0.30	0.19
2.40	0.30	0.22	0.26	0.41	0.51	0.26	0.19
2.60	0.28	0.19	0.23	0.36	0.46	0.20	0.17
2.80	0.26	0.17	0.20	0.30	0.40	0.16	0.11
3.00	0.24	0.16	0.19	0.27	0.35	0.13	0.08
3.20	0.23	0.14	0.18	0.23	0.27	0.11	0.06
3.40	0.22	0.12	0.16	0.19	0.22	0.09	0.06
3.60	0.20	0.12	0.17	0.15	0.19	0.08	0.06
3.80	0.19	0.11	0.17	0.12	0.16	0.07	0.04
4.00	0.19	0.10	0.15	0.09	0.13	0.06	0.03
4.20	0.18	0.09	0.13	0.08	0.12	0.05	0.03
4.40	0.17	0.08	0.12	0.07	0.11	0.05	0.03
4.60	0.16	0.07	0.11	0.06	0.10	0.05	0.02
4.80	0.16	0.06	0.09	0.05	0.09	0.04	0.02
5.00	0.15	0.05	0.09	0.04	0.09	0.04	0.02

ing the Santa Monica pair by a factor of 4.63 creates a record with maximum spectral acceleration of $12.59g$ (Fig. 7.15). Needless to say, such a large acceleration has never been observed in practice.

(b) Scaling for OSHPD-96 is similar and results in scaling factors of 1.37, 1.10, and 3.46 for the Newhall, Sylmar, and Santa Monica records, respectively. These scaling factors may be used, however, only if the SRSS of spectral acceleration for each pair at the period of 3.0 sec is above the target spectra. Here, indeed, this is the case:

1.37 (SRSS of Newhall at 3.0 sec) = $0.329 > 0.24g$,

1.10 (SRSS of Sylmar at 3.0 sec) = $0.484 > 0.24g$, and

3.46 (SRSS of Santa Monica at 3.0 sec) = $0.519 > 0.24g$.

(c) for UBC-97, the vibration period matching band is from 1.50 to 3.75 sec and the scaling factors corresponding to the Newhall, Sylmar, and Santa Monica pairs are 1.21, 0.97, and 3.07, respectively. These values are less than those obtained for UBC-94 and OSHPD-96 but still are very conservative.

The problem of trying to match a design spectrum by simple scaling procedures may be better understood by looking at Figs. 7.15 and 7.16. A glance at Fig. 7.16 shows that between the periods of 0.5 and 3.25 sec the Sylmar record is above the design spectrum. Hence, rationally speaking, there is no need for scaling the Sylmar components. The Newhall record is above the target spectrum between 0.50 and 2.20 sec where it goes slightly below the

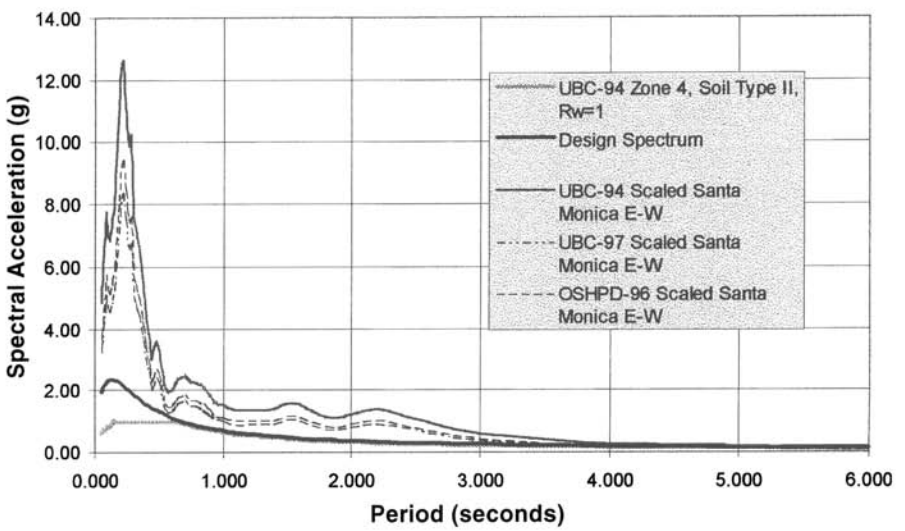

Fig. 7.15 The 1994 Northridge at Santa Monica Record as scaled by various code procedures.

design spectrum. In our opinion, there is no need for scaling this pair either. The Santa Monica record, although very rich in low-period content, does not have a high long-period content. Trying to overcome this "problem" by applying large-scale factors, as the above procedures do, creates components with no physical meaning (Fig. 7.15), which will highly exaggerate higher mode participation in response. A more prudent approach would be to use this record unscaled to gauge the performance of the system to far-field effects and replace it with another record for scaling purposes.

7.8.6 Frequency-Domain Scaling of Time Histories

To a designer of a nonlinear structure, there is nothing more attractive than a real or simulated ground motion time history whose response spectrum matches the target design spectrum. At first glance the frequency-domain scaled and/or simulated design spectrum-compatible time histories (hereafter referred to as DSCTH) furnish the designer with a consistency and compatibility bridge between two very different worlds: the familiar realm of linear elastic behavior in which the principle of superposition holds and the less familiar world of nonlinear response in which 2 + 2 may equal 3 or even 8! It is only recently that the problems associated with application of DSCTH have been realized and reported by Naeim and Lew [94, 95]. *Notice that our discussion of limitations of DSCTH relates only to cases where a single component or a single pair is manipulated to match a given design spectrum. We do not see anything wrong with realistic collections of DSCTH developed to match a design spectrum, on average, as a group.*

As mentioned before, OSHPD-91 provisions mandate a frequency-domain scaling of ground motion time histories. Since simultaneous manipulation of a

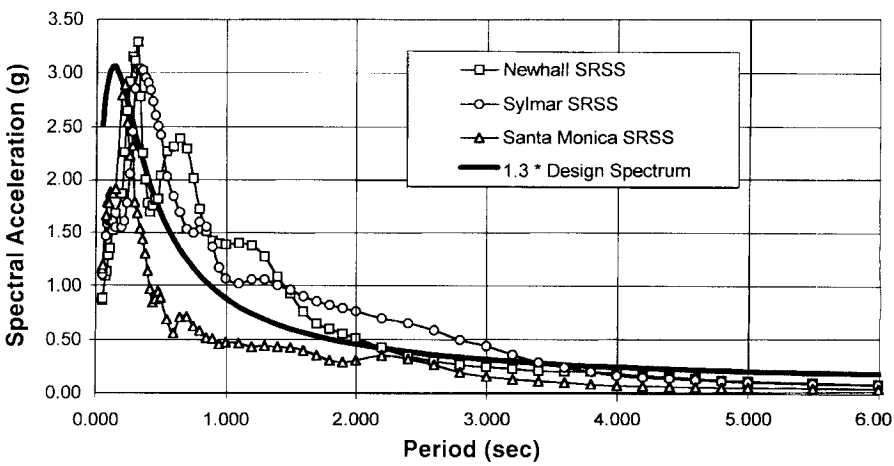

Fig. 7.16 Design spectrum versus the unscaled SRSS of the selected time history pairs.

pair of time histories for their SRSS to match the target spectrum is very difficult, usually each component is scaled in the frequency domain to individually match the design spectrum. OSHPD commonly insists on simultaneous application of both pairs of spectrum-compatible time histories, without allowing for any reduction factor on the component in the transverse direction. This is in contrast with the common practice of applying 100% in one direction and 30% in the orthogonal direction, which is widely used in the design of conventional structures.

The response spectra are generally determined using a probabilistic seismic hazard analysis (PSHA). The PSHA considers all possible earthquake sources in the region surrounding the subject site. If the result of the PSHA is a site-specific response spectrum, the response spectrum represents the cumulative contribution of risk from the seismic sources in the region for that given risk level. Thus the PSHA response spectrum represents an envelope of the ground motion levels based upon the cumulative risk for all seismic sources deemed to be significant. As it is customary to include the dispersion in the ground motion attenuation relationship in the PSHA, it is likely that the predicted ground motion response spectrum values have an inherent built-in conservatism.

Thus a PSHA-generated response spectrum does not and was never intended to represent the response of a SDOF structure to any specific single ground motion event. To the contrary, it is intended to envelope multiple events with a built-in conservatism for a specified risk level. To generate an acceleration–time history to be spectrum compatible for a PSHA-generated spectrum is neither reasonable nor realistic. This would be especially true if the seismic risk at a given site was due to several earthquake sources. Therefore, the resulting response spectrum-compatible acceleration–time history will contain energy over the whole range of structural periods that is not present in actual recorded time histories. The requirement to make both orthogonal components spectrum compatible is also conservative, as response spectra from actual acceleration–time histories rarely contain the same energy content in two orthogonal horizontal directions.

To illustrate this problem. Naeim and Lew [94, 95] developed frequency-domain scaled DSCTHs for six pairs of horizontal ground motion time histories using two entirely independent techniques. In both methods, the original horizontal ground motion records were used as "seeds" to generate DSCTH records. The two methods use different iterative procedures that involve scaling the Fourier amplitudes of the processed signal to match the corresponding amplitudes in the target response spectrum. In both cases, convergence was assumed when the ratio of the response spectra areas (signal/target) was less than 2% and the average error on all frequencies was smaller than 5%. This study concluded the following:

1. The acceleration response spectra of all 24 DSCTH components developed (six pairs, two methods) match the target design acceleration spectra remarkably well.

2. Displacement records obtained via direct double integration from all of the 24 DSCTH components represented very unrealistic and physically impossible results.

3. The input energy spectra of the DSCTH records exhibit high levels of input energy spread over a very wide band of natural periods. Such behavior is not supported by observed data from real earthquake records. As Figs. 7.17 and 7.18 indicate, the energy content represented by DSCTH records is consistently higher than the real records used as the basis for their development. The input energy spectrum for the 230° component of the 1979 Array No. 6 record, which exhibits the largest long-period input energies of any observed California record and is superimposed on the plots of Fig. 7.17, clearly demonstrates the exaggerated nature of energy spectra suggested by DSCTH records. The average input energy spectra for all real and DSCTH records are compared in Fig. 7.18, where it can be noticed that, when considered across the board, DSCTHs represent unrealistic energy contents that exceed the content of their real counterparts by an order of magnitude.

4. In most cases the overall distribution of energy across the various period bands show no resemblance to the real records used as seeds (see Figs. 7.17 and 7.18).

5. The energy contents of DSCTH records obtained by the two different

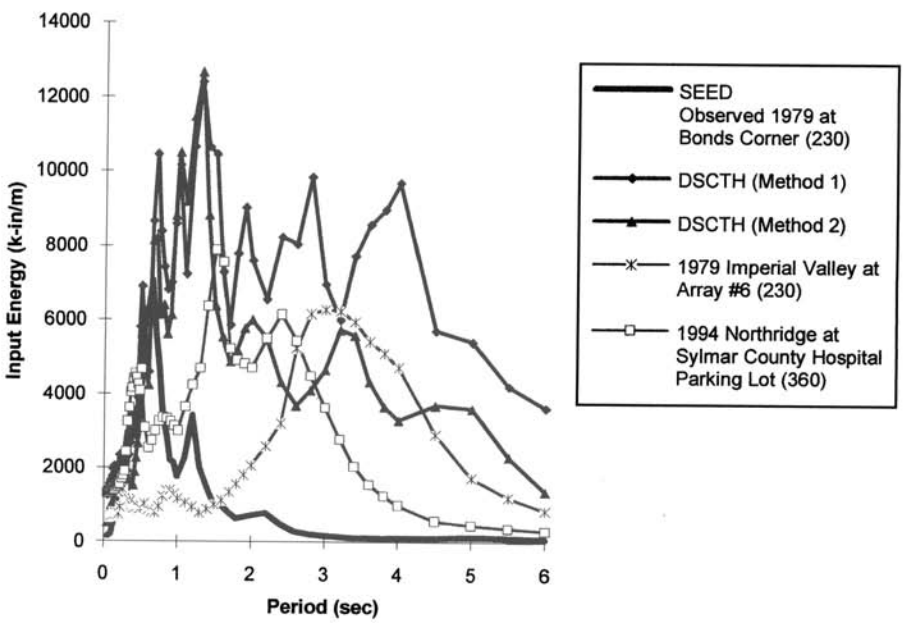

Fig. 7.17 Input energy of real records versus those of DSCTH.

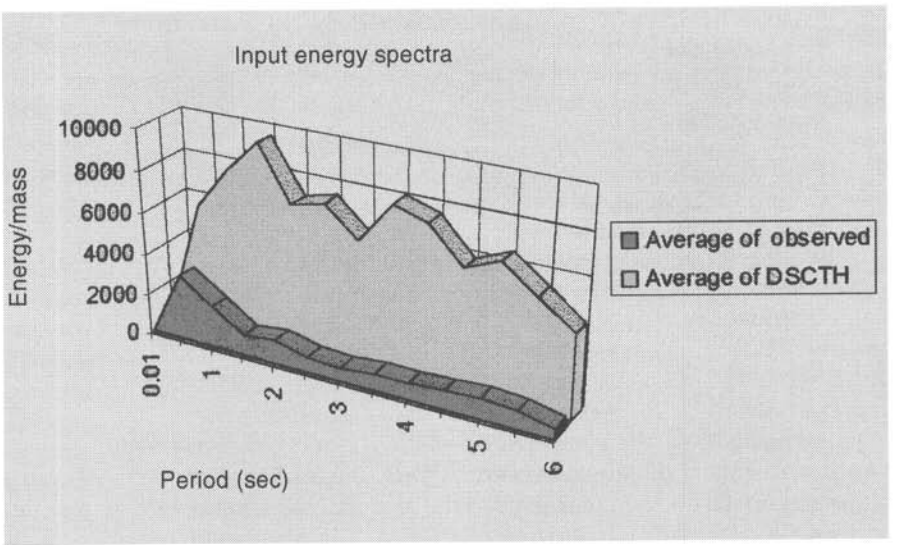

Fig. 7.18 Comparison of energy contents of real records and their DSCTH counterparts.

methods may represent sharply distinct input energy contents in certain frequency bands.

6. As a result of the frequency filtering process, the DSCTH records obtained are very different in all characteristics from the real records, which were used as seeds for their generation. Hence, this process has effectively eliminated the geologic, tectonic, and source characteristics that these records were initially selected to represent.

It is in light of the above considerations that the authors strongly believe that the application of single-component or single-pair frequency-domain scaled design spectrum-compatible time histories in design of seismic-isolated structures should not be encouraged and certainly not be mandated.

7.8.7 Analytic Dilemma of Designing by Time History Analysis

Earthquake time histories are useful and often essential elements for designing sound seismic-isolated structures. The most useful application of time histories is in verification of seismic performance of buildings designed using more simple procedures such as response spectrum analysis techniques. Increasingly, however, suites of time histories are used as the primary vehicles for analysis and design. The number of different analyses required for this approach and the volume of information generated by such analyses is so excessive that it can easily obscure the proper application of engineering judgment.

For example, consider a project that is to be designed by application of time history analysis using the average of seven pairs. As shown in Table 7.4, the

TABLE 7.4 Number of Computer Runs Required for Design by Time Histories

Considerations	Number of Computer Runs
Pairs of time histories for averaging	7
Isolator lower and upper bound properties	2
MCE and DBE events	2
Possible directions for application of each pair	2
Center-of-mass locations to model minimum eccentricity	5
Total	280

required number of computer runs will be 280. (See Fig. 7.19 for center-of-mass locations to model minimum eccentricity.) If scragged and unscragged bearing properties are also to be considered in the analysis, the number of required runs will be 540. Obviously, gathering average design information from so many computer runs is a monumental task and should be avoided whenever possible.

The degree of uncertainty in the ground motions, the properties of the isolation system, and the structural system properties make designing by hundreds of time histories meaningless. Time histories, therefore, should be used for verification of designs already achieved by simpler means (i.e., response spectrum method) and not as a direct design strategy.

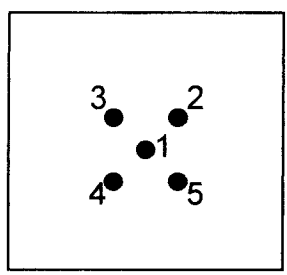

Fig. 7.19 Possible locations of center of mass to model code minimum eccentricity requirements.

CHAPTER 8

DESIGN EXAMPLES

8.1 DESIGN EXAMPLE FOR A HIGH-DAMPING RUBBER BEARING

As a design example consider a small building similar to the EOC building of Los Angeles County and the Caltrans San Diego Center. We take the site to be zone 4 with S_C soil type and assume that the site is not less than 15 km (9.32 miles) from a known active fault. Using the 1997 UBC Appendix Chapter 16 requirements [55], the parameters associated with the location are $Z = 0.4$, $S = S_C$, $N_D = 1$, and $M_m = 1.25$. The structural system can be taken as a reinforced-concrete shear wall building, which allows a R_{WI} of 2.0. The building has a regular plan with three rows of columns 10 m (33 ft) apart and spaced at 10 m (33 ft) each, as shown in Fig. 8.1.

The bearing loads are as follows:

$$\begin{aligned} \text{Four at 50 tons} &= 200 \text{ tons (441 kips)} \\ \text{Eight at 100 tons} &= 800 \text{ tons (1765 kips)} \\ \text{Three at 200 tons} &= \underline{600 \text{ tons (1324 kips)}} \\ &\quad 1600 \text{ tons (3530 kips)} \end{aligned}$$

The selection strategy for the bearings is to use one bearing size (to save the cost of an extra mold) and use two different high-damping compounds, which will be denoted A (soft) and B (hard):

$$G_A = 0.4 \text{ MPa (58 psi)} \quad \text{and} \quad \beta_A = 0.08$$
$$G_B = 1.0 \text{ MPa (145 psi)} \quad \text{and} \quad \beta_B = 0.15$$

Design of Seismic Isolated Structures: From Theory to Practice. F. Naeim and J. M. Kelly

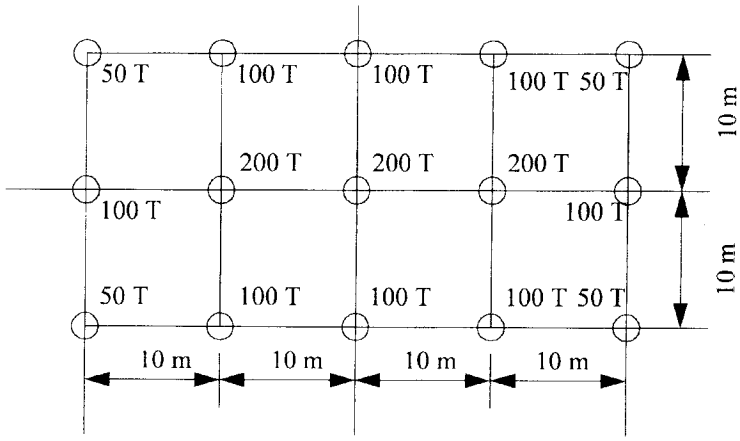

Fig. 8.1 Plan for design example.

We will begin with the assumption of a target period of 2.5 sec and a target maximum shear strain of 1.5. We will try to use 12 type A and 3 type B bearings. It should be noted that it would be possible to use only a single bearing design for this project since the building is small, but the design using two types is given to illustrate the procedure.

8.1.1 Bearing Stiffnesses

Type A. Twelve at 100 tons (221 kips):

$$K_H^A = 100 \times 1000 \text{ kg} \times \left(\frac{2\pi}{2.5}\right)^2$$

$$= 632,000 \text{ N/m}$$

$$= 0.632 \text{ MN/m (3.61 kips/in.)}$$

Type B. Three at 200 tons (442 kips):

$$K_H^B = 200 \times 1000 \text{ kg} \times \left(\frac{2\pi}{2.5}\right)^2$$

$$= 1.265 \text{ MN/m (7.22 kips/in.)}$$

8.1.2 First Estimate of Design Displacement D_D

$$D_D = \frac{g}{4\pi^2} \frac{C_{VD} T_D}{B_D}$$

Assume composite damping of 10%; thus

$$B_D = 1.2 \quad \text{(from Table A-16C)}$$

$$C_{VD} = 0.56 \quad \text{(from Table 16-R)}$$

$$D_D = \frac{(9.81)(0.56)(2.5)}{(4\pi^2)(1.2)} = 0.289 \text{ m (11.4 in.)}$$

With $\gamma = 1.5$, take $t_r = 200$ mm (7.9 in.). Thus

$$K_H^A = \frac{G_A A}{t_r} = 0.632 \text{ MN/m}$$

gives

$$A = \frac{0.632 \text{ MN/m}}{0.4 \text{ MN/m}^2} \times 0.2 \text{ m}$$

$$= 0.316 \text{ m}^2$$

Therefore

$$\Phi = 0.634 \text{ m (25 in.)}$$

Take

$$\Phi = 600 \text{ mm (24 in.)} \qquad A = 0.283 \text{ m}^2$$

Then

$$p^A = 100 \times 10^4 = 3.54 \text{ MPa (513 psi)}$$

$$p^B = 7.08 \text{ MPa (1027 psi)}$$

8.1.3 Actual Bearing Stiffness

$$K_H^A = \frac{0.4 \times 0.283}{0.200} = 0.566 \text{ MN/m (3.23 kips/in.)}$$

$$K_H^B = \frac{1.0 \times 0.283}{0.200} = 1.415 \text{ MN/m (8.08 kips/in.)}$$

8.1.4 Composite Stiffness

$$K_H = 12 \times 0.566 + 3 \times 1.415 = 11.04 \text{ MN/m (63.1 kips/in.)}$$

Therefore

$$(\text{Actual frequency})^2 = (11.04 \times 10^6 \text{ N/m}) \frac{1}{1600 \times 10^3 \text{ kg}}$$

$$= 6.90 \text{ sec}^{-2}$$

$$\omega_H = 2.62 \text{ rad/sec}$$

$$T = 2.39 \text{ sec}$$

8.1.5 Composite Damping

Recall that

$$\beta = \frac{W_D}{2\pi K_H D^2}$$

Therefore

$$\beta = \frac{W_D}{2\pi K_D D^2} = \frac{2\pi K_D^A D^2 \beta_A + 2\pi K_H^B D^2 \beta_B}{2\pi K_D D^2}$$

$$= \frac{K_H^A \beta_A + K_H^B \beta_B}{K_D}$$

$$\beta = \frac{12 \times 0.566 \times 0.08 + 3 \times 1.1415 \times 0.15}{11.04}$$

$$= 0.107$$

$$B_D = 1.2 + \frac{0.7}{10} \times 0.3 = 1.22$$

Using this period and damping factor, the design displacement D_D becomes

$$D_D = \frac{9.81}{4\pi^2} \frac{(0.56)2.39}{1.22}$$

$$= 0.272 \text{ m } (10.7 \text{ in.})$$

8.1.6 Allowance for Torsion

The code formula is

$$D_T = D\left(1 + y \frac{12e}{b^2 + d^2}\right)$$

and e is 0.05 times the long direction, as shown in Fig. 8.2, so that

$$D_T = 0.272\left[1 + \frac{20(12)^2}{400 + 1600}\right] = 0.272(1 + 0.24)$$

$$= 0.338 \text{ m } (13.3 \text{ in.})$$

This seems too large, and it is worthwhile in this case to calculate the real torsional stiffness of the isolation system and calculate the additional displacement. The torsional stiffness is given by

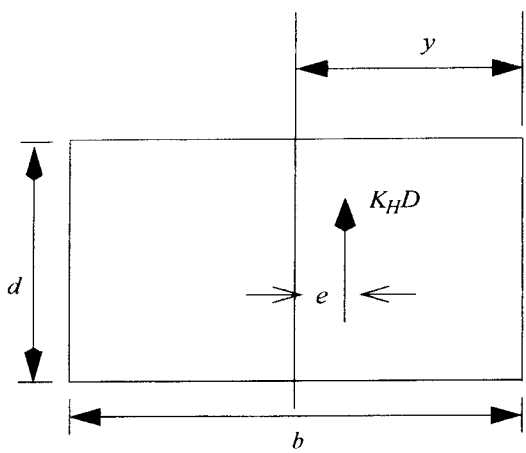

Fig. 8.2 Dimensions for torsion formula.

$$K_\theta = \sum_{i=1}^{N} K_H^i (x_i^2 + y_i^2)$$

$$= 0.566[4 \times (10^2 + 20^2) + 4 \times (10^2 + 10^2) + 2 \times 20^2 + 2 \times 10^2]$$

$$+ 1.415(2 \times 10^2)$$

$$= 0.566(2000 + 800 + 200 + 800) + 1.415 \times 200$$

$$= 2433 \text{ MN m}$$

The applied torque (Fig. 8.2) is given as

$$M = (K_H D)e$$

Therefore

$$\text{Additional displacement} = \theta y$$

$$= \frac{K_H D e}{K_\theta} y$$

$$= \frac{11.04(0.274)(2)(20)}{2433}$$

$$= 0.05 \text{ m (2.0 in.)}$$

$$D_T = 0.272 + 0.05 = 0.322 \text{ m (12.7 in.)}$$

Thus $\gamma_{max} = 1.6$—larger than target but acceptable. (Code mandatory minimum allowance for torsion is $1.1D = 0.300$ m, so take $D_T = 0.322$ m.)

8.1.7 Elastic Base Shear from Code

$$V_S = \frac{K_H D}{R_{WI}}$$

$$= \frac{11.04 \times 0.272}{2}$$

$$= 1.50 \text{ MN}$$

$$C_S = \frac{V_S}{W}$$

$$= \frac{1.50 \text{ MN}}{1.6 \times 10^7 \text{ N}}$$

$$= 9.4\%$$

8.1.8 Bearing Detail

Select vertical frequency $f_V = 10$ Hz; then $6S^2 \approx f_V^2/f_H^2$ means

$$S \approx \frac{1}{\sqrt{6}} \frac{f_V}{f_H} = \frac{1}{\sqrt{6}} \frac{10}{1/2.39} = 10$$

To calculate the vertical frequency and the buckling load for the bearing, it is necessary to have the small strain shear modulus for each rubber, for example, at $\gamma = 20\%$. These compounds will have

$$G_{0.2}^A = 0.7 \text{ MPa} \qquad G_{0.2}^B = 1.4 \text{ MPa}$$

and an assumed $K = 2000$ MPa for both. Thus

$$E_c = \frac{6GS^2K}{6GS^2 + K}$$

becomes

$$E_c^A = \frac{6GS^2K}{6G_AS^2 + K}$$

$$= \frac{6(0.7)(100)2000}{420 + 2000}$$

$$= 347 \text{ MN/m}^2$$

$$E_c^B = \frac{8.4 \times 100 \times 2000}{2840}$$

$$= 592 \text{ MN/m}^2$$

$$\text{Composite } K_H = \frac{(12 \times 347 + 3 \times 592)(0.283)}{0.200}$$

$$= 8405 \text{ MN/m}$$

$$\omega_V^2 = 8405 \times 10^6 \text{ N/m}$$

$$f_V = 11.5 \text{ Hz}$$

Therefore, any S in the range 9–10 is adequate:

$$S = \frac{\Phi}{4t} \qquad t = \frac{\Phi}{4S} = \frac{600}{40} = 15 \text{ mm}$$

$$nt = 200 \text{ mm} \qquad n = 13.33 \text{ layers}$$

Take $n = 12$; then $t = 16.7$ mm, and

$$S = \frac{600}{4(16.7)} = 9 \qquad f_V = \tfrac{9}{10}(11.5) = 10.4 \text{ Hz}$$

This allows us to complete the design of the bearing, as shown in Fig. 8.3. The end plates are 25 mm thick, and the shims are 2 mm each. The total height is

$$h = 50 + 200 + 11 \times 2 = 272 \text{ mm}$$

The shims will have a diameter ϕ_S,

$$\phi_S = 590 \text{ mm}$$

giving 5 mm cover.

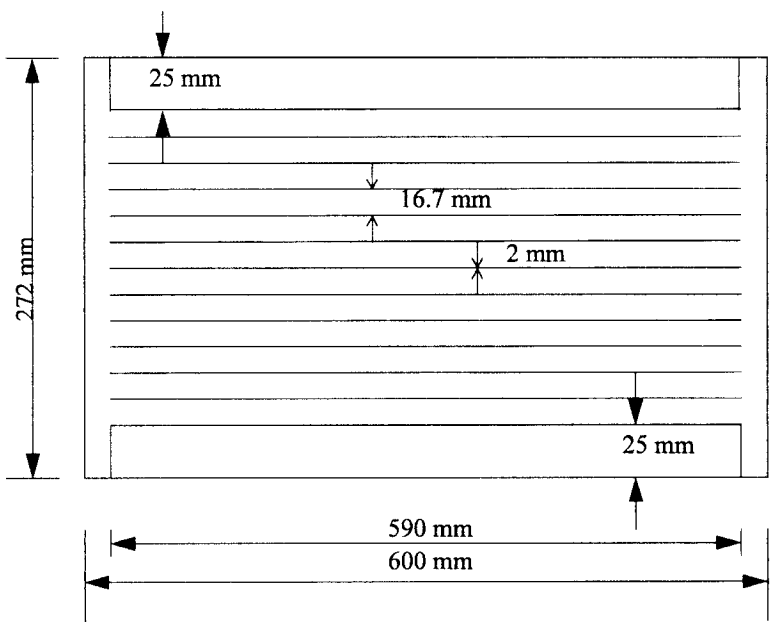

Fig. 8.3 Detail design of isolator (metric).

This design example has been worked out for metric sizes. When the dimensions are converted to U.S. units and rounded off slightly, different details will emerge. Figure 8.4 shows an equivalent isolator in these units. Most dimensions are obvious transformations of the metric sizes; the shim thickness is from standard gage sizes for thin steel sheets. Here, 12 gage has been selected with a thickness of 0.1046 in.

8.1.9 Buckling Loads: Safety Factor

The buckling load is given by

$$P_{\text{crit}} = \sqrt{P_S P_E}$$

where

$$P_S = GA_S \qquad P_E = \frac{\pi^2 (EI)_{\text{eff}}}{t_r^2}$$

and

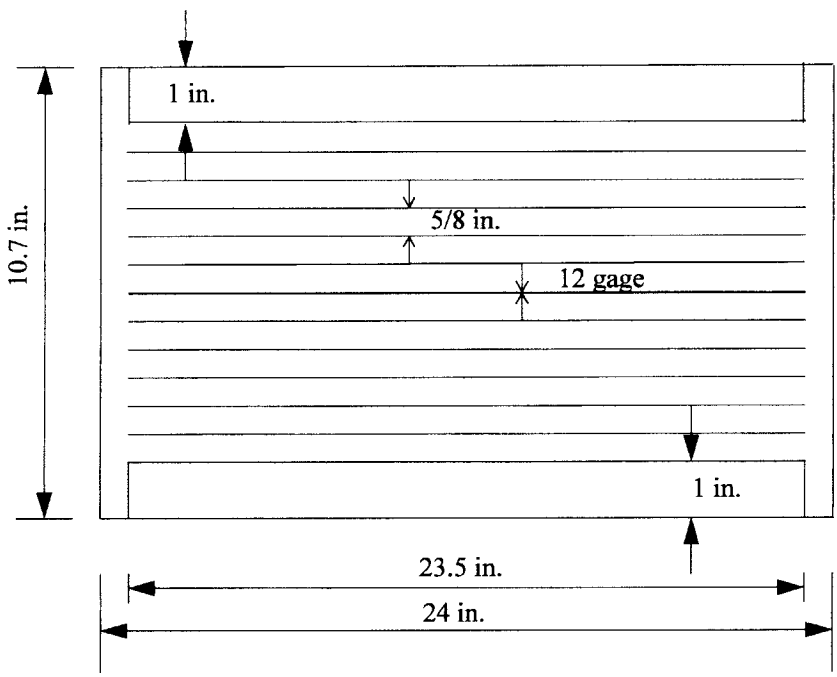

Fig. 8.4 Detail design of isolator (U.S. units).

$$(EI)_{\text{eff}} = E_c(\tfrac{1}{3})I$$

From the earlier sections, we have

$$E_c = 6GS^2$$

where for this calculation we use the value of G at 20% shear strain, that is,

$$G^A_{0.2} = 0.70 \text{ MPa}$$

from which we have

$$E^A_c = \frac{6G^A_{0.2}S^2K}{6G^A_{0.2}S^2 + K}$$

with $K = 2000$ MPa and $S = 9$, giving

$$E^A_c = 290 \text{ MPa}$$

By the same process, using $G^B_{0.2} = 1.14$ MPa, we get

$$E^B_c = 507 \text{ MPa}$$

For a shim diameter of 0.590 m,

$$I = \frac{\pi}{4}\left(\frac{0.590}{R}\right)^4 = 0.00595 \text{ m}^4$$

From these values, we determine the buckling loads for each type of bearing:

$$P_{\text{crit}}^{A} = \frac{\pi}{t_r}\sqrt{\left(E_c^A \frac{I}{3}\right) G^A A_S} \qquad A_S = \frac{\pi}{4}(0.590)^2$$

$$= \left(\frac{\pi}{0.20}\right)\left(290 \times 10^6 \times \frac{0.00595}{3} \times 0.7 \times 10^6 \times 0.273\right)^{1/2}$$

$$= 5.21 \times 10^6 \text{ N}$$

$$= 5210 \text{ kN (1170 kips)}$$

$$P_{\text{crit}}^{B} = \left(\frac{\pi}{0.20}\right)\left(507 \times 10^6 \times \frac{0.00595}{3} \times 1.4 \times 10^6 \times 0.273\right)^{1/2}$$

$$= 9740 \text{ kN (2190 kips)}$$

$$SF^A = 5.2 \qquad \text{SF}^B = 4.87$$

Buckling loads will have negligible effects on horizontal stiffness:

$$K_H \approx K_H^0\left[1 - \left(\frac{P}{P_{\text{crit}}}\right)^2\right] \approx K_H^0\left(1 - \frac{1}{25}\right) \approx \frac{24}{25} K_H^0 = 0.96K_H^0$$

where K_H^0 is the horizontal stiffness with zero vertical load.

8.1.10 Calculation of MCE Displacement D_M

The code also requires recalculating the period and damping at the MCE level. Both compounds show an increase in stiffness at around 200% shear strain. The modulus of the softer compound is around 0.48 MPa, and the stiffer compound is around 1.20 MPa. The damping in the softer compound is still around 8%, but that for the harder compound has dropped to 12.5%. Using these values, the MCE composite stiffness becomes

$$K_H^A = \frac{0.48 \times 0.283}{0.200} = 0.679 \text{ MN/m (3.88 kips/in.)}$$

$$K_H^B = \frac{1.2 \times 0.283}{0.200} = 1.678 \text{ MN/m (9.58 kips/in.)}$$

$$K_H = 13.24 \text{ MN/m (75.6 kips/in.)}$$

and the composite damping is

$$\beta = \frac{12 \times 0.679 \times 0.08 + 3 \times 1.698 \times 0.125}{13.24} = 9.7\%$$

giving a damping reduction factor B of 1.19. The period for this stiffness is T_M = 2.18 sec. The resulting value of D_M is

$$D_M = \frac{9.81}{4\pi^2} \frac{(0.70)}{1.19} (2.18) = 0.318 \text{ m (12.5 in.)}$$

and with the earlier allowance for torsion, the final result for D_{TM} is

$$D_{TM} = \frac{0.322}{0.272} \times 0.318 = 0.377 \text{ m (14.8 in.)}$$

This result is the maximum displacement to which the prototype bearings will need to be tested. It represents less than 200% shear strain and less than 80% of the rollout displacement. There is no reason to expect that the bearings would not pass this test.

The material properties of the soft compound discussed above are based on the isolation system designed for the UNIDO demonstration project building in China [122]. The bearings for this project were 600 mm (24 in.) in diameter, with 120 mm (48 in.) of rubber. Both hard and soft compounds were used in this project, and extra bearings of both types were made and sent to the EERC for testing. In addition to the stiffness and damping characterization tests, the bearings were subjected to rollout tests. These bearings are held in place by a recessed endplate detail that is very simple and cost-effective but allows a bearing to roll out if the vertical load is low. The softer bearing was tested to over 350% shear strain without rollout, as shown in Fig. 8.5 (the test was halted at a shear force of 600 kN (135 kips), which is the force capacity of the test machine). The bearing made up of the hard compound could only be tested to 220% shear strain, at which point the force capacity of the machine was reached.

8.1.11 Rollout Displacement

Use a large strain shear modulus:

$$D^A_{\max} = \frac{\Phi}{1 + K^A_H h/W}$$

$$= \frac{0.600}{1 + (0.566 \times 10^6 \times 0.272)/(100 \times 10^6)}$$

$$= 0.519 \text{ m (20.4 in.)}$$

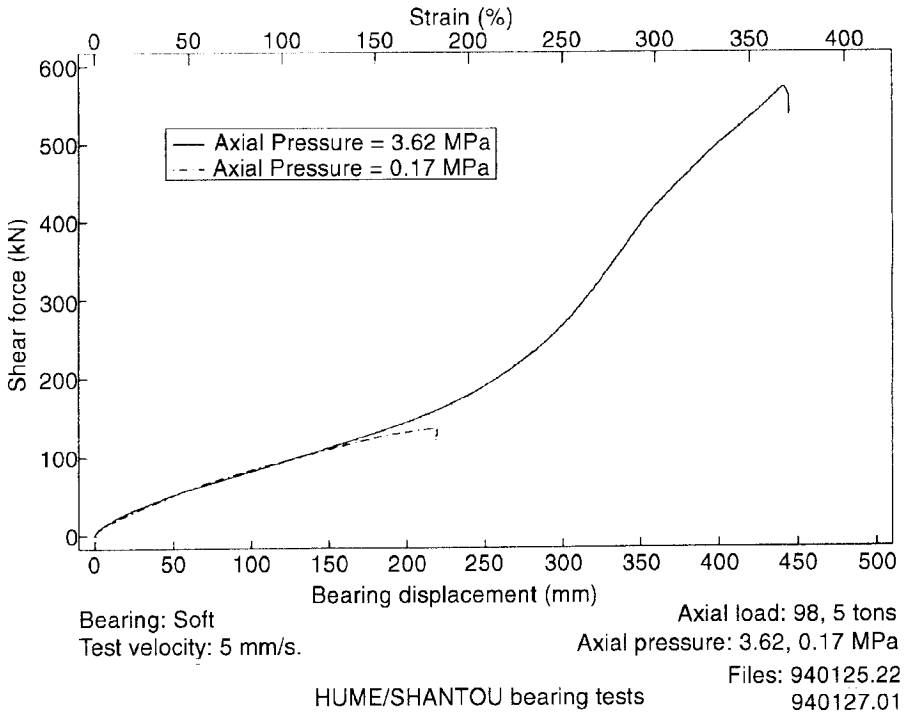

Fig. 8.5 Shear force versus displacement at rollout for soft bearings.

$$D^{B}_{\max} = \frac{0.6}{1 + (1.41 \times 0.272)/2}$$

$$= 0.502 \text{ m (20 in.)}$$

A final check is global overturning: We assume that the unreduced shear force $K_H D$ is applied to the center of mass of the building in the short direction, as shown in Fig. 8.6. Assume the center of mass is 5 m (16 ft) above the isolation system; then the overturning moment is $5K_H D$. This is resisted by two rows of five bearings 10 m (33 ft) from the center so that the addition loads E (plus and minus) are

$$E = \frac{11.04 \times 0.274}{5 \times 20 \text{ m}} \times 5 \text{ MN/m}$$

$$= 0.15 \text{ MN (33.7 kips)}$$

This is well under the smallest downward load on the corner columns, indicating that the bearings will not be subjected to upward (tensile) forces.

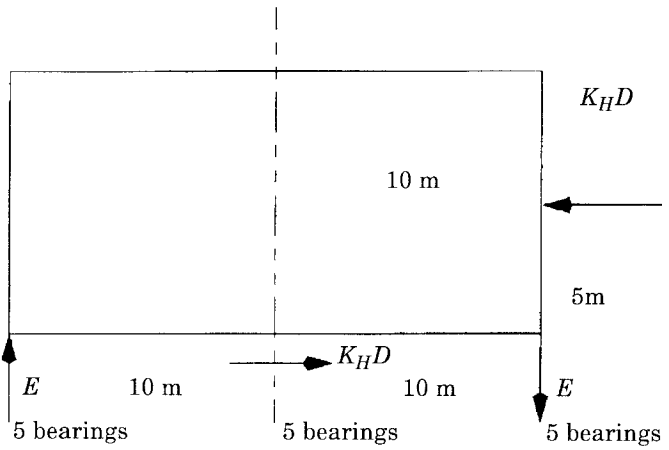

Fig. 8.6 Overturning analysis.

8.2 DESIGN EXAMPLE FOR A LEAD-PLUG BEARING

The design of a lead-plug bearing system that provides the same period and global damping at the design displacement obtained for the high-damping rubber system is a straightforward procedure. When designing for sites with moderate seismicity, it is easy to develop a damping factor of around 15% of critical viscous damping, and if we use this level as a target value, the design displacement at a period of 2.5 sec becomes

$$D_D = \frac{9.81}{4\pi^2}\frac{(0.56)(2.5)}{1.35}$$

$$= 0.258 \text{ m (10 in.)}$$

The required stiffness to provide a period of 2.5 sec is

$$K_H = 1600 \times 1000 \times \left(\frac{2\pi}{2.5}\right)$$

$$= 10.1 \text{ MN/m (57.7 kips/in.)}$$

The global energy dissipated per cycle is

$$W_D = 2\pi K_{\text{eff}} D^2 \times \beta_{\text{eff}}$$

$$= 2\pi(10.1)(0.285)^2(0.15)$$

$$= 0.634 \text{ MN m (5613 kips in.)}$$

The relationship of these quantities to the two lead-plug bearing parameters Q and K_r is

$$K_{\text{eff}} = K_r + \frac{Q}{D}$$

and

$$W_D = 4Q(D - D_y)$$

where

$$D_y = \frac{Q}{K_1 - K_2}$$

and as an approximate rule of thumb, we take $K_1 \approx 10K_2$.

If we neglect D_y, we have a first approximation for Q:

$$\begin{aligned} Q &= \frac{W_D}{4D} \\ &= \frac{0.634 \text{ MN/m}}{4(0.258)} \\ &= 0.611 \text{ MN (137 kips)} \end{aligned}$$

It follows that

$$\begin{aligned} K_2 &= K_{\text{eff}} - \frac{Q}{D} \\ &= 10.1 - \frac{0.614}{0.258} \\ &= 7.72 \text{ MN/m (44.1 kips/in.)} \end{aligned}$$

Correcting the first estimate of Q for D_y gives

$$\begin{aligned} D_y &= \frac{0.614}{9(7.72)} \\ &= 0.009 \text{ m (0.35 in.)} \end{aligned}$$

so a recalculation gives

$$Q = \frac{0.634}{4(0.249)} = 0.637 \text{ MN (143 kips)}$$

The yield level of lead is around 10 MPa (1500 psi), so that the area of lead plug needed is

$$A_{pb} = 0.0637 \text{ m}^2 \text{ (99 in.}^2\text{)}$$

The design philosophy for lead plugs is that they should not be too slender or too squat. For bearings around 0.6 m (24 in.) in diameter, lead plugs with diameters in the range of 100–150 mm (2.5–3.75 in.) are appropriate. The areas of 100- and 125-mm-diameter plugs are 0.0079 and 0.0123 m^2, respectively. Three 125-mm-diameter plugs under the three most heavily loaded columns provide 0.0368 m^2 and four 100-mm plugs under four other columns (to provide symmetry) provide a total of 0.0684 m^2 (106 $in.^2$).

The total rubber stiffness K_r needed is given by

$$K_r = K_H - \frac{Q}{D_D}$$

$$= 10.1 - \frac{0.634}{0.258}$$

$$= 7.64 \text{ MN/m (43.6 kips/in.)}$$

and if all bearings are the same, this means a stiffness of 0.5 MN/m (2.9 kips/in.) for each bearing.

Lead-plug bearings are usually made from a low-damping, high-strength rubber with a modulus at 100% shear strain that might vary from 0.4 to 0.7 MPa (60–100 psi). Selecting the total rubber thickness as 0.258 m (10 in.) and using the lowest modulus value, the required area per bearing is 0.318 m^2 (493 in^2), which is close to a 600-mm- (24-in.-) diameter bearing. The final design would be a bearing with 20 layers of 12 mm (0.5 in.) each, a diameter of 600 mm (24 in.) in a compound with 0.4-MPa (60-psi) modulus. The central three heavily loaded bearings will have 125-mm- (4.9-in.-) diameter lead plugs, the four others will have 100-mm (3.9-in.) plugs, and the remainder will have no lead plugs.

The stiffness of the plain elastomeric bearings is given by

$$K_r = \frac{(0.4)(0.283)}{0.240} = 0.472 \text{ MN/m}$$

and the total Q for the system is 0.684 MN. Therefore, at a displacement of 0.258 m, the stiffness K_{eff} is given as

$$K_{\text{eff}} = 15 \times 0.472 + \frac{0.684}{0.258} = 9.73 \text{ MN/m}$$

and

$$W_D = 4(0.684)(0.258 - 0.009) = 0.681 \text{ MN/m}$$

giving $\beta = 16\%$. With the total stiffness and DBE displacement of 0.258 m (10 in.), the reduced base shear becomes

$$V_s = \frac{9.73 \times 0.258}{2} = 1.26 \text{ MN/m or } 8\%W$$

When we compute the MCE displacements, the code requires recalculating the period and damping at the larger displacements. This is, of course, an iterative process, and we begin by assuming that the MCE displacement is around M_M times the DBE displacement. The M_M is given in UBC-97, Table A-16-D, and for $ZN_v = 0.40$ is 1.25. When computing the MCE displacement (at the center of mass), D_M is given as

$$D_M = \frac{(g/4\pi^2)C_{VM}T_{VM}}{B_M}$$

where C_{VM} is given in UBC-97, Table A-16-9, for S_C soil type as $1.4\,M_M ZN_v$, that is, in this case 0.7.

To compute the period T_M, we return to the formula for the effective stiffness of the lead-plug system, namely,

$$K_{\text{eff}} = K_r + \frac{Q}{D}$$

where $K_r = 7.08$ MN/m (40.4 kips/in.) and $Q = 0.684$ MN (154 kips). With D_M assumed as $1.25\,D_D = 0.323$ m (12.7 in.), we have

$$K_{\text{eff}} = 9.2 \text{ MN/m (52.5 kips/in.)}$$

The total energy dissipated per cycle, W_D, is $4Q(D_M - D_y)$, and

$$D_y \approx \frac{Q}{9K_r} = 0.011$$

giving

$$W_D = 0.854 \text{ MN m (7558 kips in.)}$$

and

$$\beta_{\text{eff}} = \frac{W_D}{2\pi K_{\text{eff}} D_M^2} = 14\%$$

This means that $B = 1.32$ and the new period T_M is given by

$$T_M = \frac{2\pi}{\sqrt{9.2/1.6}} = 2.62 \text{ sec}$$

leading to

$$D_M = \frac{(g/4\pi^2)(0.7)(2.62)}{1.32} = 0.345 \text{ m (13.6 in.)}$$

To correct the first guess, recalculate K_{eff} at 0.345 m (13.6 in.); this is

$$K_{\text{eff}} = 7.08 + \frac{0.684}{0.345} = 9.06 \text{ MN/m (51.7 kips/in.)}$$

giving

$$T = 2.64 \text{ sec} \qquad \beta_{\text{eff}} = 13.5\%$$

These numbers are close enough to the first guess for the displacement to be taken as 0.345 m. To estimate the additional displacement due to torsion in the lead-plug case, it is probably enough to use the code default formula since the displacements are relatively modest. Once done, we have from the earlier calculation

$$D_T = D(1 + 0.24)$$

leading to

$$D_{TD} = 0.320 \text{ m (12.6 in.)}$$
$$D_{TM} = 0.428 \text{ m (16.9 in.)}$$

These will be used to establish the prototype test program.

CHAPTER 9

COMPUTER APPLICATIONS

9.1 INTRODUCTION

In this chapter we will first introduce techniques for preliminary selection of design loads and optimizing the number of different isolator sizes for a project. We will describe application of the computer program ISOSEL, included on the companion CD-ROM disc, which efficiently utilizes these techniques. An overview of available computer programs for analysis of seismic-isolated structures is presented next. Finally, we present examples of using the SAP2000 nonlinear program to model nonlinear isolation systems and demonstrate nonlinear dynamic time history analysis of such systems subjected to a variety of earthquake ground motions. Furthermore, we will explain the use of the nonlinear gap and hook elements to model trilinear hysteretic behavior of isolation systems and to model pounding of the isolated system against a rigid external obstacle such as a retaining wall.

All computer programs and data files discussed in this chapter are included on the companion CD-ROM disc. We will explain how to access and use these programs and data files as a part of our presentation of computer application examples in this chapter. Also available to the reader are several AVI animation files, which demonstrate the response of example systems when subjected to selected time histories.

9.2 PRELIMINARY SELECTION OF DESIGN LOADS AND ISOLATOR SIZES

9.2.1 Overview

The preliminary design of a bearing in an isolation system begins with determining the sustained vertical gravity loads to be carried by that bearing. The

Design of Seismic Isolated Structures: From Theory to Practice. F. Naeim and J. M. Kelly

sustained gravity load consists of the dead load and a realistic estimate of the live load. Realistic estimates of live load are usually much smaller than the live load prescribed by codes for design of structures. A safety factor of about 2.0 is considered in proportioning the isolators for sustained gravity load, which means these isolators can sustain twice this load when they are experiencing the maximum total displacement with a safety factor of 1.

In order to minimize the total cost of the isolation system, we usually need to minimize the number of different isolators. The total cost of the isolation system consists of a fixed cost for each mold and a variable cost for the volume of rubber:

$$C = M \times m + \sum (\text{VOL}) \times c \tag{9.1}$$

where C = total cost of isolation system
M = number of different isolators
m = cost of an isolator mold
c = cost per unit volume of isolator

The typical cost of an isolator mold is about \$100,000 and c is roughly $6¢/\text{cm}^3$ ($\$1.00/\text{in.}^3$). Therefore, unless the isolators are available off the shelf in predetermined sizes with no mold cost, increasing the number of different isolators, from four to six, for example, can significantly increase the total cost of the isolation system.

Traditionally, the engineer plots the sequence of column gravity loads from smallest to largest; then, by looking at the plot, he or she decides how many bearing types may be necessary and tries to select the design loads by minimizing the variation of load on various isolator types. This process is very subjective and can lead to inaccuracies and designs that are not optimized. The computer program ISOSEL accompanying this book can be of great value in taking the guesswork out of this very important decision process.

9.2.2 Selection of Design Loads by Linear Regression and Least-Squares Analysis Techniques

The problem may be stated as follows. Given a sequence of N column loads ordered from smallest to largest $(1, \ldots, N)$, where the column loads CL_i are ordered such that

$$\text{CL}_{i-1} \le \text{CL}_i \le \text{CL}_{i+1} \qquad i = 1, \ldots, N$$

select L bearing design loads and K spaces,

$$M_1, M_2, \ldots, M_j, \ldots, M_L \qquad S_1, S_2, \ldots, S_k$$

respectively, to minimize the difference between the histogram of N ordered column loads and the reduced histogram of L design loads and K partitions (see Fig. 9.1).

For each partition, the least-squares technique may be applied in order to compute the best design load for that partition. If the least-squares approximation is represented by the line $y = ax + b$, then the sum of squares of the deviations represented by Eq. (9.2) is a minimum:

$$I = \int_{S(i-1)}^{S(i)} [f(x) - (ax + b)]^2 \, dx \tag{9.2}$$

Therefore,

$$\frac{dI}{da} = 0 = -\int_{S(i-1)}^{S(i)} \{2[f(x) - (ax + b)]\}(x) \, dx \tag{9.3}$$

$$\frac{dI}{db} = 0 = -\int_{S(i-1)}^{S(i)} \{2[f(x) - (ax + b)]\} \, dx \tag{9.4}$$

In each partition, the design load M is a constant ($M = b$). Hence Eq. (9.4), which is the only equation needed, reduces to

$$[S(i) - S(i-1)]b = \sum_{S(i-1)}^{S(i)} f(x) \tag{9.5}$$

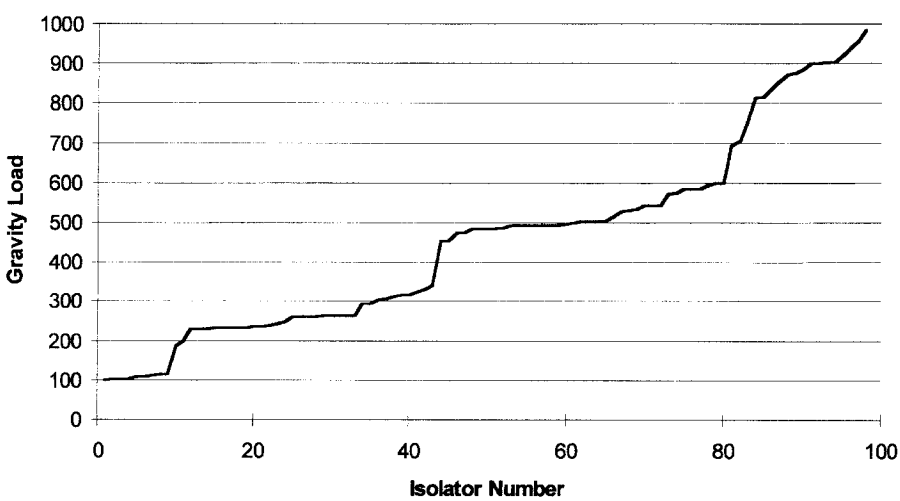

Fig. 9.1 Typical histogram of gravity loads on isolators sorted in ascending order of loads.

and

$$M = \frac{\sum_{S(i-1)}^{S(i)} f(x)}{S(i) - S(i-1)} \tag{9.6}$$

This means that the best value of M is simply the average of the column loads, $f(x)$, for each partition.

Given the number of design loads or the isolator types, a computer program can be written that investigates every possible location of partition lines and selects those locations that result in the least possible cumulative value of deviation I. As demonstrated later, however, such a procedure is very inefficient, resulting in an inordinate number of floating-point operations (FLOPs). The number of FLOPs become so excessive that if the number of isolator types exceeds three or four, the procedure becomes practically unusable.

In contrast, the ISOSEL computer program deploys an approximate strategy that leads to practically the same result but with a fraction of computational effort as compared with the direct scheme described above.

9.2.3 The ISOSEL Solution Strategy

To obtain the optimum design distribution of the isolators for a given number of bearing sizes, ISOSEL employs a linear search technique. Two different methods are implemented in ISOSEL. For both approaches, the column axial load distribution $[f(x)]$ on the isolators is sequentially arranged in ascending order of axial load by the computer program. In the first approach, or method 1, the maximum and minimum loads are divided into n equal segments giving n partitions, where n is the number of different isolator types. The isolator number of the start location for the first partition is always 1, which is the number of the isolator with the lowest axial load. The isolator numbers identifying the start of the subsequent partitions of the distribution are obtained by drawing a vertical line at the point of intersection of the design axial load and the plot of axial load $f(x)$ versus isolator number x. The isolator number that just exceeds this value of x is the program's initial guess of the design distribution. For example, if there are two partitions, the starting isolator number for the second partition is the number at which the axial load on that isolator just exceeds the mean of the maximum and minimum axial loads. In the second approach, or method 2, the isolator numbers identifying the start of each partition are equally spaced between 1 and the maximum number of isolators.

Starting with the initial guess, the isolator number between partitions i and $i + 1$ (or the start isolator number for partition $i + 1$) is decremented one number at a time until the variance of the axial load for partitions i and $i + 1$ is a minimum. This is done while keeping the start numbers of the ith and $i + 2$

TABLE 9.1 Individual Gravity Loads on FCLJC 98 Isolators

198	234	498	754	903
265	242	116	983	239
231	231	115	942	487
231	185	594	495	532
235	495	545	295	533
250	234	100	294	486
325	261	103	305	600
265	260	504	704	495
232	234	515	693	502
232	235	901	495	598
265	261	904	504	452
341	483	584	901	575
265	501	853	875	543
316	815	957	495	584
318	817	109	543	572
309	494	834	873	484
315	485	529	885	495
262	101	109	453	475
331	102	113	475	
265	502	584	918	

partitions constant. The search direction is reversed if the variance increases with decreasing isolator number. This isolator number then serves as the new starting isolator number for partition $i+1$. The iterations are carried out starting with the first and second partitions and ending with the $n-1$ and nth partition, moving over one partition at a time. The total variance of the axial load is then computed for all partitions in the revised configuration of isolator distribution. This process is repeated until the total variance converges to a constant number.

9.2.4 Application of the ISOSEL Computer Program[1]

The utility of the ISOSEL program is demonstrated by applying it to the design of the Foothill Communities Law and Justice Center (FCLJC), the first seismically isolated building in the United States. There are a total of 98 isolators used in this project (Fig. 9.1). The distribution of sustained gravity loads on individual isolators is presented in Table 9.1. A file containing this information in a free-format form, which serves as the ISOSEL input file for this problem

[1]Before you use the ISOSEL program for the first time, you need to install it from the companion CD-ROM disc. Place the disc in your CD-ROM drive. If the SAP2000 demonstarion automatically starts, exit from it by clicking the cross on the top right-hand corner of the SAP2000 window. Use Windows Explorer from the Windows 95 or NT Start menu and double click on the Setup icon contained in the \ISOBOOK\SETUP directory of the CD-ROM disc. The setup program will guide you through the rest of the installation process.

(BEARLOAD.DAT), may be found in the same directory on your hard disk where you installed the ISOSEL program.

Start the ISOSEL program. The window shown in Fig. 9.2 will appear on your screen.

Click on Open under the File menu and open the BEARLOAD.DAT file (Fig. 9.3). Then click on the Calculate button for the ISOSEL to perform its computations. The window shown in Fig. 9.4 will appear on your screen.

Here you see that method 1 is activated using only one isolator type. The mean value of the isolator loads and the corresponding deviation are shown on the grid to the left side of the window. A histogram of isolator loads is shown on the plot to the left, and the deviation as a function of number of isolator types is shown on the plot to the right of the window. You can change to method 2 by clicking on the corresponding radio button next to it and clicking on the Calculate button. The program will recompute the values based on the selected method.

Click on the zoom button displayed on the variation plot to see a clearer picture of how the variation reduces with increasing number of isolator types (Fig. 9.5). From this figure you can see that for this project we enter a zone of diminishing returns for more than four isolator types. Exit from this window and click on the right arrow of the scroll bar shown below the isolator load plot to increase the number of isolator types. You will see that the locations of selected partitions on the load plot changes and the values on the grid are

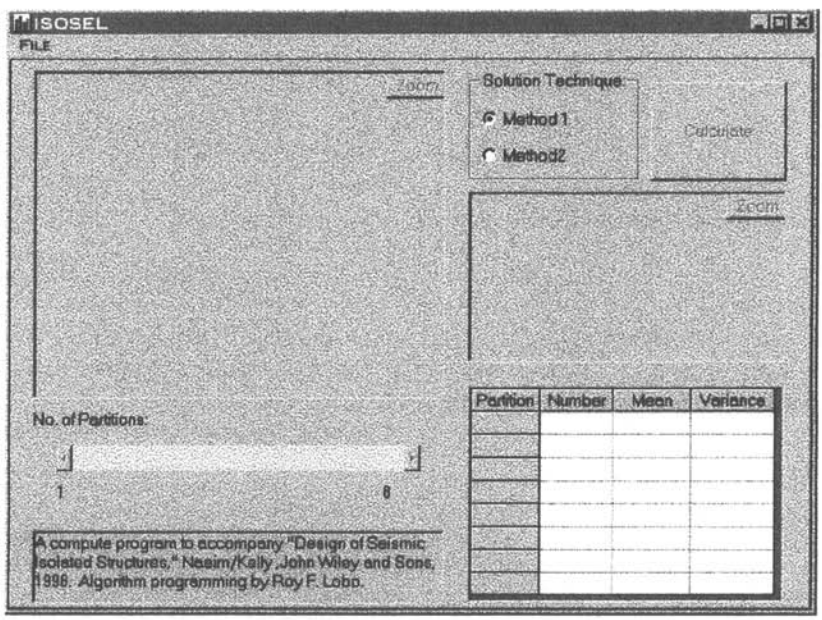

Fig. 9.2 ISOSEL program's initial screen.

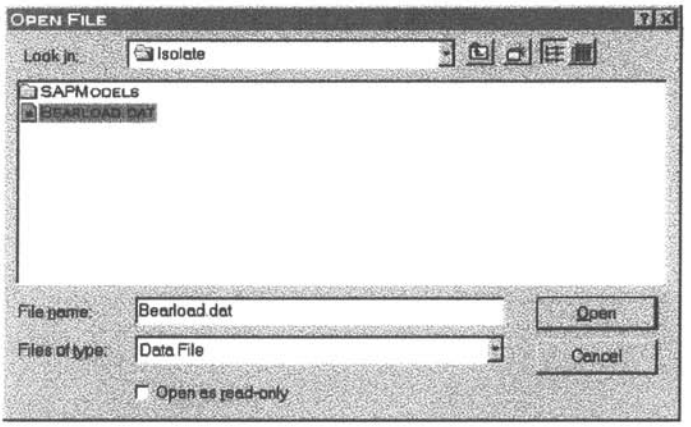

Fig. 9.3 ISOSEL input file selection window.

immediately updated to reflect the design loads and the amount of variation for the number of isolator types you select.

Click on the right arrow of the scroll bar two more times to select four isolator types. Notice that the number of each isolator type needed and the corresponding design sustained load are displayed on the grid. Click the Zoom

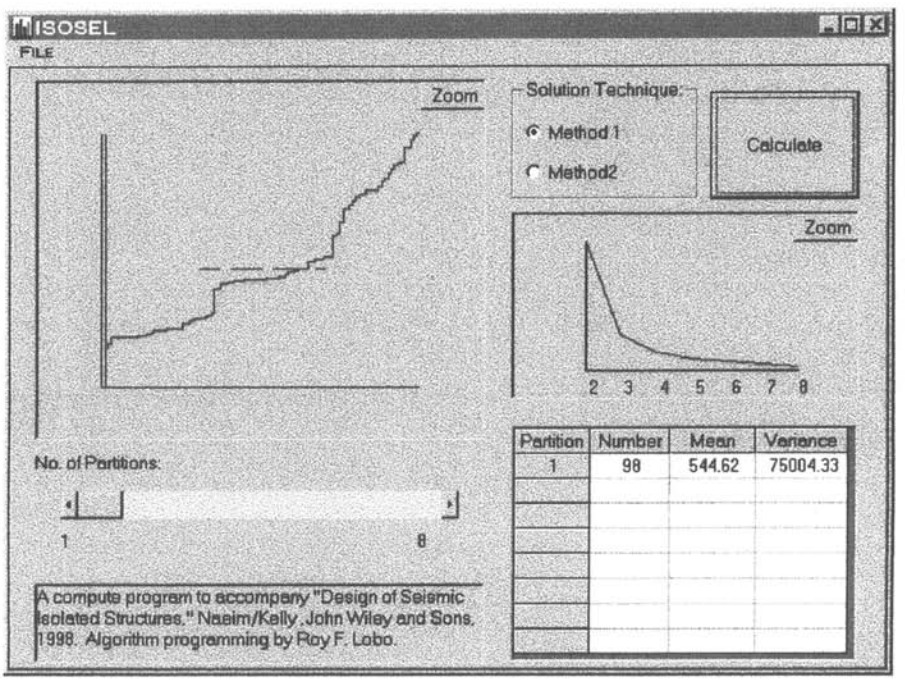

Fig. 9.4 ISOSEL result screen showing the results obtained using one isolator type.

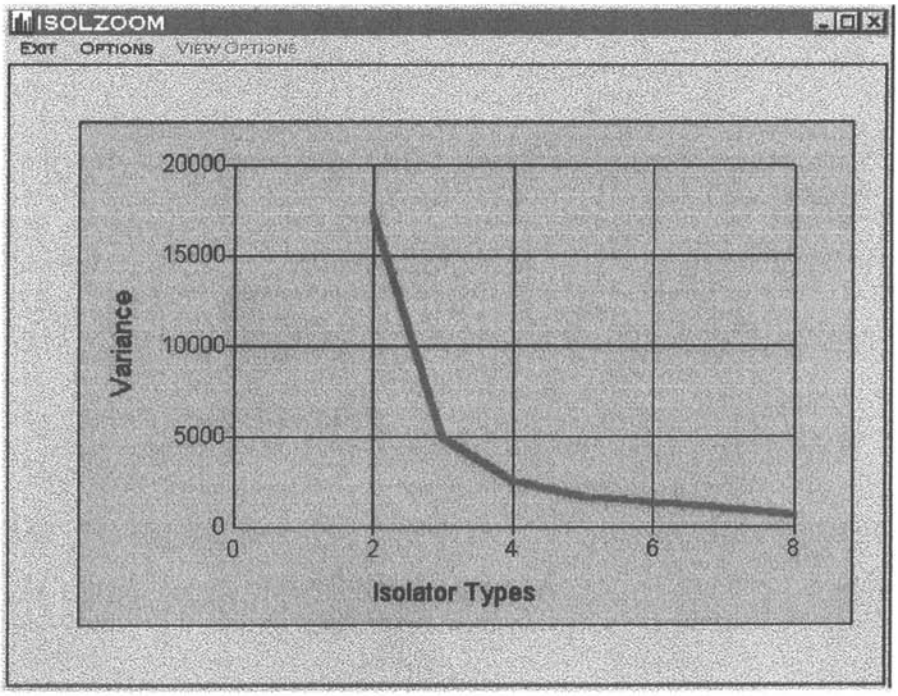

Fig. 9.5 Variance as a function of number of isolatory types used.

button on the isolator load plot. The window shown in Fig. 9.6 will appear on your screen showing a bar chart of the design loads for each isolator type.

Click on Isolator Distribution, Sustained Load, or Variance from the Options menu to see the corresponding bar chart (see Fig. 9.7 for an example).

You may also select other chart types in addition to the bar chart from the View Options menu (see Figs. 9.8 and 9.9).

The results of ISOSEL design using methods 1 and 2 are given in Tables 9.2 and 9.3 for a number of bearing types ranging from 2 to 9. The minimum variance in the axial load and the number of FLOPs for convergence are also shown.

Figure 9.10 shows isolator distribution obtained from the two methods for number of bearing types equal to three. Clearly the results using partitioning based on method 1 are better, since they correspond to a lower variance. ISOSEL results are also consistent with the solution obtained by a direct search program where all possible combinations are investigated to minimize the total variance. Figure 9.11 shows the plot of the variance of the axial load versus number of bearing types, and Fig. 9.12 shows the required number of FLOPs versus number of bearing types using methods 1 and 2. For three isolator types, ISOSEL converged using 6822 FLOPs for method 1 and 3660 flops using method 2. The direct search procedure would require 1,560,527 FLOPs to pro-

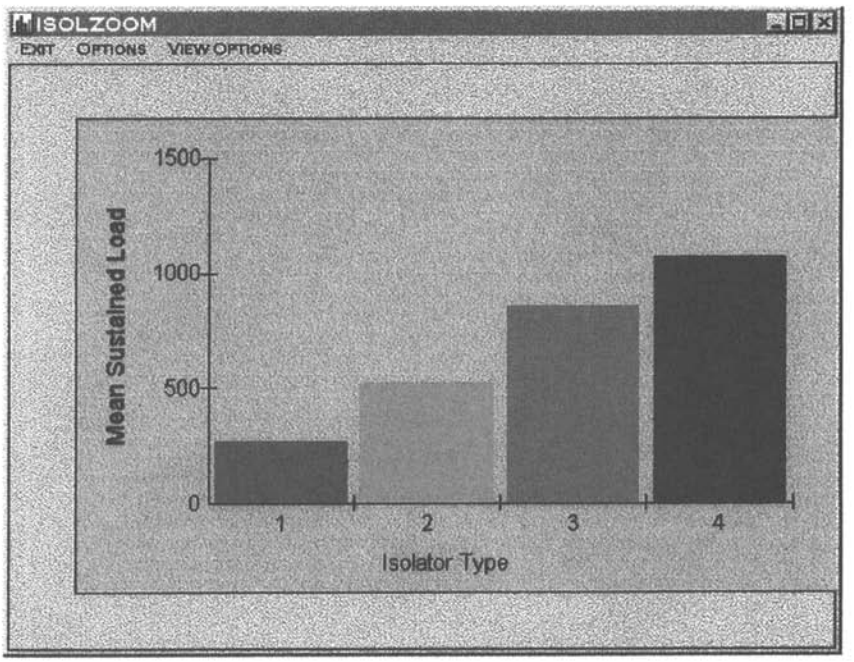

Fig. 9.6 Design sustained loads selected by ISOSEL for four isolator types.

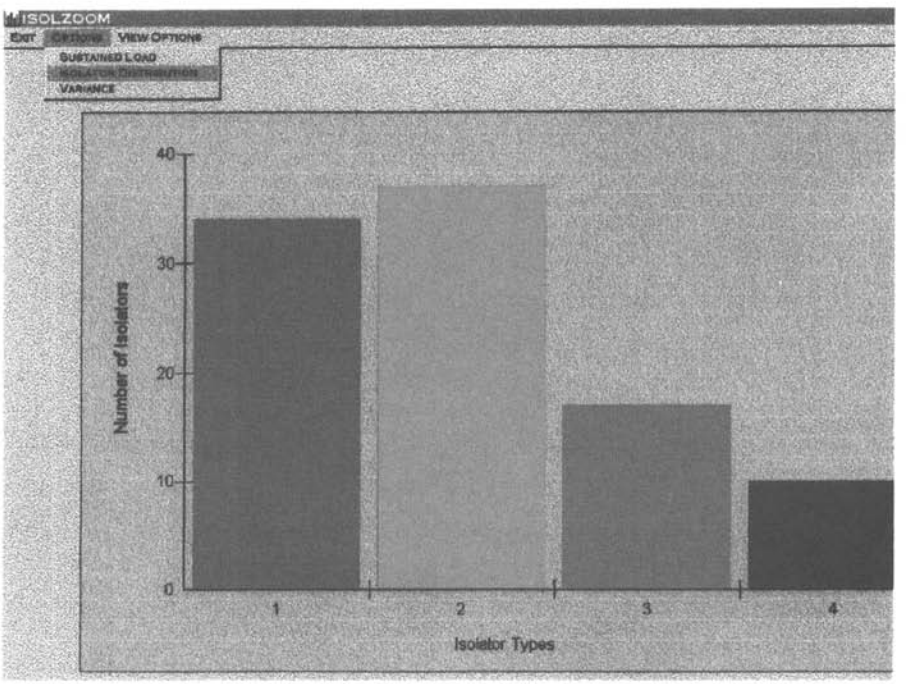

Fig. 9.7 Number of required isolators of each type.

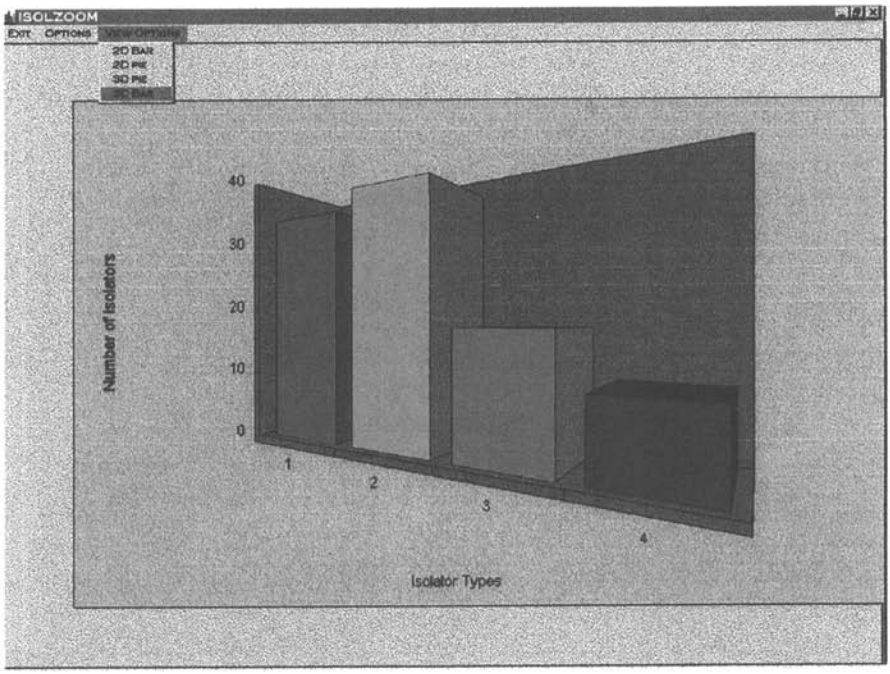

Fig. 9.8 Three-dimensional bar-chart view of information presented in Fig. 9.8.

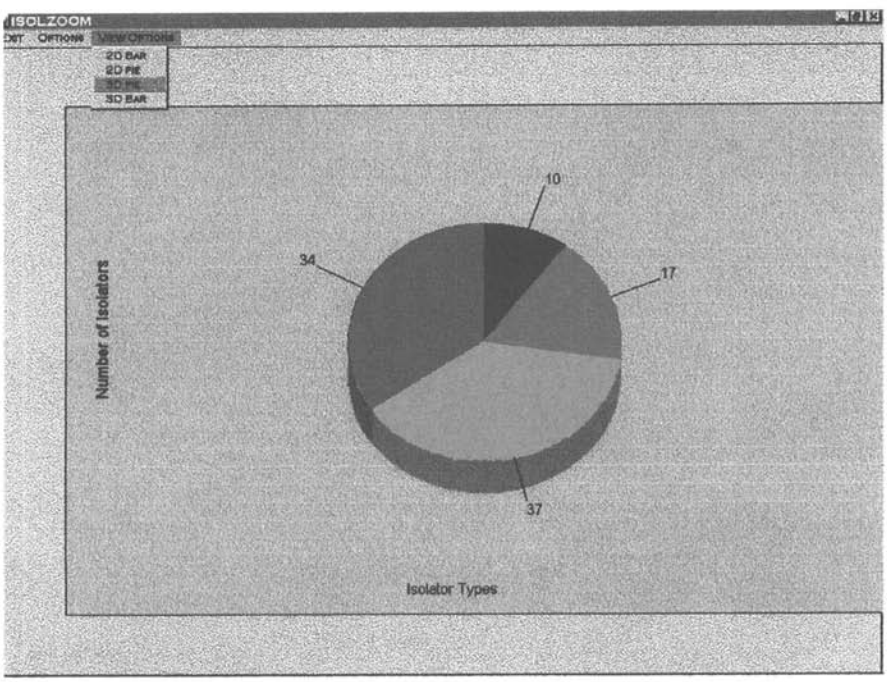

Fig. 9.9 Pie-chart view of information presented in Fig. 9.8.

TABLE 9.2 ISOSEL Results Using Method 1

Bearing Types	Variance	FLOPs		Partition								
				1	2	3	4	5	6	7	8	9
2	17260.17	2051	Start	1	72							
			Mean	396.44	934.3							
3	4906.96	6822	Start	1	35	74						
			Mean	263.56	527.77	953.16						
4	2534.08	3072	Start	1	35	72	89					
			Mean	263.56	518.54	854.65	1069.7					
5	1696.14	4606	Start	1	35	64	74	89				
			Mean	263.56	499.83	608.8	875.47	1069.7				
6	1321.34	3283	Start	1	35	61	72	78	90			
			Mean	263.56	494.77	574.73	769.5	907.92	1079.33			
7	1042.6	4752	Start	1	35	64	73	77	88	94		
			Mean	263.56	499.83	598.22	772.5	889.91	1002	1128.4		
8	659.3	6013	Start	1	25	35	61	72	74	87	94	
			Mean	242.17	314.9	494.77	574.73	698.5	864.08	993.43	1128.4	
9	541.03	5337	Start	1	25	35	61	73	75	79	88	94
			Mean	242.17	314.9	494.77	584.58	729	829.75	900.22	1002	1128.4

TABLE 9.3 ISOSEL Results Using Method 2

Bearing Types	Variance	FLOPs		Partition								
				1	2	3	4	5	6	7	8	9
2	17260.17	6137	Start	1	72							
			Mean	396.44	934.3							
3	4906.96	3660	Start	1	35	74						
			Mean	263.56	527.77	953.16						
4	3779.9	4523	Start	1	35	64	75					
			Mean	263.56	499.83	622	961.46					
5	1696.14	9716	Start	1	35	64	74	89				
			Mean	263.56	499.83	608.8	875.47	1069.7				
6	1315.1	6613	Start	1	25	35	64	74	89			
			Mean	242.17	314.9	499.83	608.8	875.47	1069.7			
7	1236.65	6409	Start	1	25	35	44	64	74	89		
			Mean	242.17	314.9	475.45	510.75	608.8	875.47	1069.7		
8	893.89	7401	Start	1	25	35	39	61	72	78	90	
			Mean	242.17	314.9	463.75	500.41	574.73	769.5	907.92	1079.33	
9	820.33	7400	Start	1	15	25	35	44	61	72	78	90
			Mean	228.07	261.9	314.9	475.56	504.94	574.73	769.5	907.92	1079.33

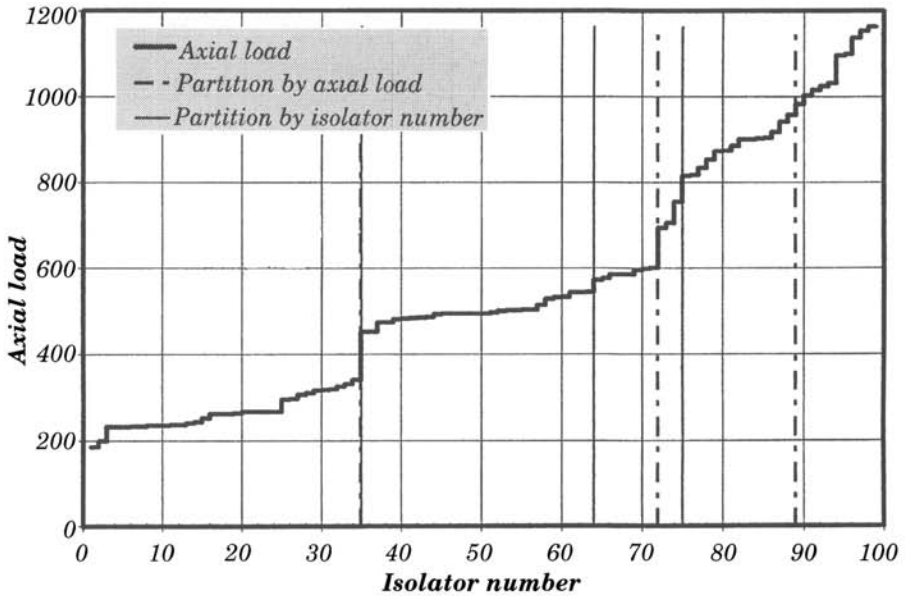

Fig. 9.10 Comparison of ISOSEL solutions by methods 1 and 2.

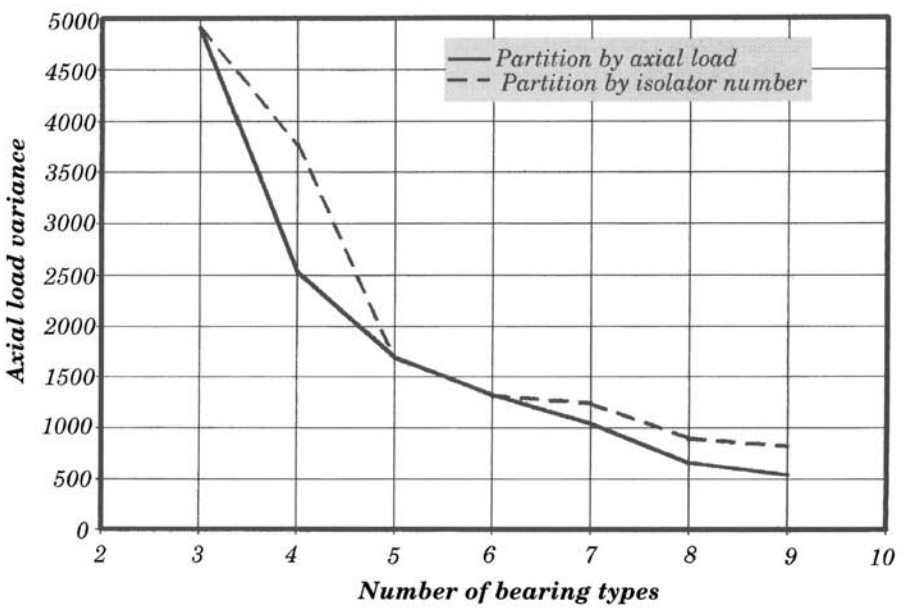

Fig. 9.11 ISOSEL design variances after convergence for methods 1 and 2.

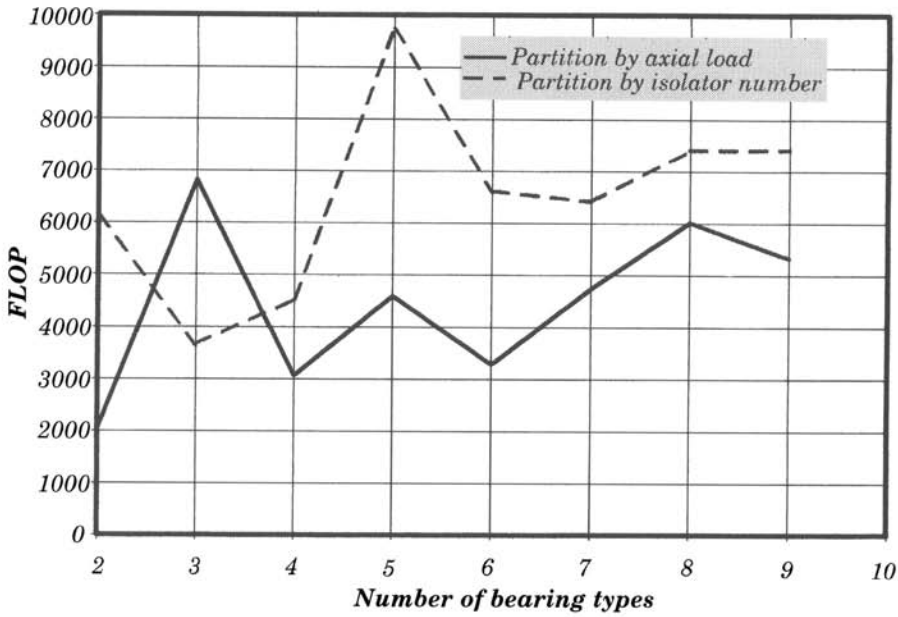

Fig. 9.12 Number of FLOPs required by ISOSEL for convergence by methods 1 and 2.

vide the same answers. For four isolator types, ISOSEL converged with 4600 or 4523 FLOPs depending on the selected method. The direct search procedure would require 35,780,370 FLOPs to reach the same conclusion. While the number of FLOPs using the direct search method increases exponentially with any increase in the number of isolator types considered, the number of FLOPs for the procedures implemented in the ISOSEL program is not a strong function of the number of isolator types. For any case, no matter how many isolators and isolator types are considered, ISOSEL may be used to provide exact or near-exact solutions in a matter of seconds.

9.3 COMPUTER PROGRAMS FOR ANALYSIS OF SEISMICALLY ISOLATED STRUCTURES

Although linear elastic models can be used for the preliminary design of high-damping natural rubber seismic isolation systems, a more accurate representation of the nonlinear force–displacement relationship of the bearings is typically required for final design verification analyses. This necessitates using specialized computer programs to analyze isolator models made of combinations of discrete nonlinear elements with superstructure models that are fully elastic or that permit some localized nonlinear behavior. Several programs running on

platforms from personal computers to mainframes are available for this purpose, and the selection of a particular program depends largely on the requirements of the end user. Described below are some of the more widely used computer programs for the analysis of seismically isolated structures.

9.3.1 N-PAD

The first computer code developed specifically for the analysis of seismically isolated buildings is known as N-PAD [56, 132]. This program explicitly models the nonlinear isolation elements but adopts a simplified model of the superstructure. The rationale behind this approach is that the period shift and energy dissipation inherent in a nonlinear isolation system serve to reduce the force transmitted to the superstructure to the point where it can be assumed to remain elastic. A rigid diaphragm assumption is used in the superstructure representation so that only three degrees of freedom are present at each floor (two translational and one rotational). Equivalent viscous damping can be specified separately for each mode of the superstructure. This type of structural model is commonly referred to as a "stick model."

Two isolation elements are available in N-PAD that can model elastic–plastic or bilinear elastic behavior. Each uses a two-dimensional yield surface in strain space to define the element shear force–displacement relationship. Of course, linear elastic behavior can also be represented in such a model. A global viscous damping coefficient may be defined for the isolation system, and the vertical stiffness of the individual isolators is included.

The substructuring of the upper structure and the isolation elements in N-PAD leads to a computationally efficient solution scheme. Its drawbacks, however, include the inability to fully capture the behavior of a general three-dimensional superstructure and the lack of a model to account for stiffening of elastomeric isolators because of strain crystallization. This second limitation applies to the current version of many of the programs outlined here. N-PAD runs on IBM-compatible personal computers and is proprietary software of Base Isolation Consultants of San Francisco, California.

9.3.2 3D-BASIS

The most widely used code for analyzing isolated structures today is the 3D-BASIS suite of programs, developed at the State University of New York at Buffalo [96]. The basic version of the program was introduced in 1989 and then updated in 1991 [97, 99]. It represents the superstructure with a linear elastic stick model similar to N-PAD, but incorporates several different models for the isolation elements intended to capture bilinear, frictional, and linear viscous behavior. The bilinear element produces a smooth force–displacement relationship via a modified Wen model, but the response is uncoupled in the two horizontal directions. The frictional element does account for bidirectional loading and incorporates a friction coefficient that varies with sliding velocity.

Discrete linear elastic and linear viscous elements may also be used to represent moderately damped elastic bearings. 3D-BASIS does not incorporate any vertical analysis capabilities.

An efficient solution scheme is implemented in 3D-BASIS in which the nonlinear element forces are moved to the right-hand side of the equations of motion and solved iteratively. Like N-PAD, however, there is no capability to model a general three-dimensional superstructure or a stiffening isolation system. 3D-BASIS was originally developed on a workstation but is now available for a wide variety of platforms. Several modified versions have also been developed to model the response of multiple structures supported on a single isolated base mat (3D-BASIS-M), seismically isolated tanks (3D-BASIS-ME), and to interface with the commonly used building analysis software ETABS (3D-BASIS-TABS). 3D-BASIS is distributed through the National Center for Earthquake Engineering Research (NCEER) at SUNY Buffalo and the National Information Service for Earthquake Engineering (NISEE) at the University of California at Berkeley.

9.3.3 ETABS

ETABS (from Computers and Structures of Berkeley, California) is the most popular computer program for dynamic analysis of major building systems in western United States. Recent releases of this program (Versions 6.0 and higher) introduced several nonlinear elements appropriate for modeling seismic isolation components. These include simple bilinear elements with constant hardening and viscous elements with variable-velocity exponents. Combinations of these elements may be used to reproduce the behavior of high-damping rubber, lead–rubber, or sliding isolation bearings. A complete, three-dimensional linear superstructure model is typically decomposed into mode shapes and then combined with the nonlinear elements at the foundation level in a time history analysis. Concentrated nonlinear elements may also be used in the superstructure, for example, to model passive energy dissipators. Using the gap and nonlinear spring elements, the net tension and uplift of the isolators may be modeled. At this time, however, the masses are not activated in the vertical direction, and hence the impact force created by return of the uplifting isolators to the equilibrium position is underestimated. One important and rather unique feature of this program is the relative ease by which complex nonrigid floor diaphragms may be modeled.

9.3.4 SAP-2000 Nonlinear

The development of the SAP series of computer programs was initiated by Edward L. Wilson of the University of California, Berkeley, in the early 1970s. Many generations of this program have been developed over the years. The most famous public domain versions of the program released during the 1970s were SAP-IV, NONSAP, and SOLID-SAP. With the advent of personal comput-

ers, new generations of the SAP programs were developed for efficient execution on personal computers by Computers and Structures of Berkeley, California. SAP-2000 (a replacement for SAP-90) is the latest and most sophisticated member of this new generation. This is the first version of SAP completely integrated within Microsoft Windows. It features a powerful graphical user interface unmatched in terms of ease of use and productivity. Creation and modification of the model, execution of the analysis, and checking and optimization of the design are all done through this single interface. Graphical displays of the results, including real-time display of time history displacements, are easily produced. SAP-2000 significantly simplifies model creation and modification as well as the way analysis and design are managed.

Three different versions of SAP-2000 are available: SAP-2000, SAP-2000 PLUS, and SAP-2000 Nonlinear. All three versions use the same graphical user interface.

All of these programs feature sophisticated capabilities, such as fast equation solvers, force and displacement loading, nonprismatic frame elements, highly accurate shell elements, Eigen and Ritz dynamic analysis, multiple coordinate systems for skewed geometry, many different constraint options, the ability to merge independently defined meshes, a fully coupled 6-×-6 spring stiffness, and the option to combine or envelope multiple dynamic analyses in the same run. The SAP-2000 PLUS version adds unlimited capacity, bridge-analysis capabilities, a complete range of finite elements, and time history analysis options. Ground motion effects with multiple base excitations can be included. The SAP-2000 Nonlinear version extends the PLUS capabilities by adding a dynamic nonlinear link element for gaps, hooks, isolators, dampers, hinges, and more. This nonlinear link element (Nllink) allows users to model the dynamic behavior of everything from tension-only braces in buildings to postyield hinges in three-dimensional frames to elastomeric bearings for bridges and base-isolated buildings.

SAP-2000 also features powerful and completely integrated design modules for steel and concrete, available from within the same interface used to create and analyze the model. The design of steel frame members features initial member sizing and iterative optimization. The design of concrete frame members includes the calculation of the amount of reinforcing steel required. Members can be grouped for design purposes, and a single mouse click on an element brings up the detailed design calculations.

SAP-2000 uses a solution scheme similar to that used in 3D-BASIS in which the forces in the nonlinear elements are moved to the right side of the equations of motion and then solved by iteration until convergence is reached. A rigid diaphragm option is available for simplified analyses of regular building models. SAP-2000 is very suitable for analysis of complex structures with local nonlinearities (such as base isolators or local yielding of the superstructure elements).

The educational version of SAP-2000 Nonlinear and a complete set of user manuals, verification manuals (which includes a three-dimensional dynamic time history analysis of a seismic-isolated structure), and tutorials are contained in the companion CD-ROM. The education version included in the com-

panion CD-ROM has all the features of SAP-2000 Nonlinear, except the number of nodes is limited to 30.

9.3.5 General Nonlinear Three-Dimensional Analysis Programs

Several other general-purpose programs have been developed in both the research and commercial environments that are suitable for analysis of base-isolated structures. The code LPM (Lumped Parameter Model) was originally developed for modeling the nonlinear three-dimensional behavior of masonry structures but has also been used for isolated structures [59]. This program includes a number of one-dimensional nonlinear elements suitable for isolation bearings and can also incorporate nonlinear elements in the superstructure model. LPM can model stiffening of elastomeric bearings and can incorporate vertical degrees of freedom. LPM is proprietary software and runs on IBM-compatible personal computers.

The programs DRAIN-2D, DRAIN-3D, and ANSR were developed at the University of California at Berkeley for the nonlinear analysis of two- and three-dimensional structures [58, 83, 106]. Similarly, IDARC-2D and IDARC-3D computer programs were developed at the State University of New York at Buffalo. These programs have libraries of nonlinear elements that are appropriate for many types of seismic isolators, and the source codes are distributed with the programs so that additional elements can be added by the end user. This group of programs run on a variety of different platforms.

A similar program named INADEL, which runs under the MATLAB environment, is also applicable to isolated structures as well as structures incorporating damping elements or active control devices [52]. INADEL uses a state-space formulation with partitioned integration to enhance the computational efficiency and offers the advantage of the postprocessing capabilities of MATLAB. Adding elements to the existing nonlinear element library is straightforward. While the programs DRAIN, ANSR, and INADEL have the advantage of extensibility by the end user, because they have been developed in the research community, they are not always ideally suited for commercial users.

Five other general-purpose nonlinear three-dimensional analysis programs should be included in this summary: ABAQUS, NASTRAN, ADINA, ANSYS, and COSMOS. Each of these incorporates a variety of sophisticated nonlinear models for dynamic analysis, and some provide the option of incorporating user-defined elements. These may be appropriate for analyzing complex superstructures on isolators but typically require a substantial initial investment in terms of both money and time spent becoming familiar with the programs.

9.4 NONLINEAR DYNAMIC TIME HISTORY ANALYSIS

Recall the simple example presented in Section 8.1. Assume that two types of isolators are selected as given in Table 9.4. For the exterior isolators we use

TABLE 9.4 Properties of Example High-Damping, Rubber Bearings

Isolator Type	Service Level Gravity Load Range (metric tons)[a]	Effective Linear Stiffness (ton/m)	Initial Stiffness (ton/m)	Yield Force (ton)	Post-Yield to Pre-Yield Stiffness Ratio	Vertical Stiffness (ton/cm)	Bearing Diameter (cm)	Bearing Height (cm)
A	60–100	110	794	7.94	0.043	1100	55	18
B	160–220	190	1270	12.70	0.055	2800	80	18

[a]A safety factor of 2 is considered. That is, the ultimate vertical load capacity in the deformed shape is twice the value shown here.

the type A bearings, and for the interior isolators we use the type B bearings. Bilinear force-displacement backbone curves for these isolators are shown in Fig. 9.13. Additionally, we assume that the floor diaphragm immediately above the plane of isolation is rigid in its own plane. In order to work within the 30-node limitation of the educational version of SAP-2000 accompanying this book, the two floors above this diaphragm are not modeled, and the total mass of the building is dumped on the diaphragm directly above the isolators. Obviously, if this was a real project, those floors and the structural system above the isolation plane would have been explicitly modeled. To further simplify this example, we will ignore the minimum-eccentricity requirements and place the center of mass at its calculated position, which is the center of the diaphragm.

We will examine the response of this system when subjected to any of the seven pairs of time histories given in Table 9.5 (which are selected from the CDMG list of ground motions considered appropriate for modeling seismic-isolated buildings subjected to near-fault effects). The damping in the systems is assumed to come entirely from the hysteretic behavior of the isolators. To preserve the numerical stability of the solution scheme and to reduce the required number of subiterations, we have assigned a total of 1% viscous damping to the structural system.

The bilinear properties of isolators are modeled via the SAP-2000 ISOLATOR1 elements. The SAP-2000 input file for this example is named Example1.s2k and may be found in the SAPModels subdirectory of the directory

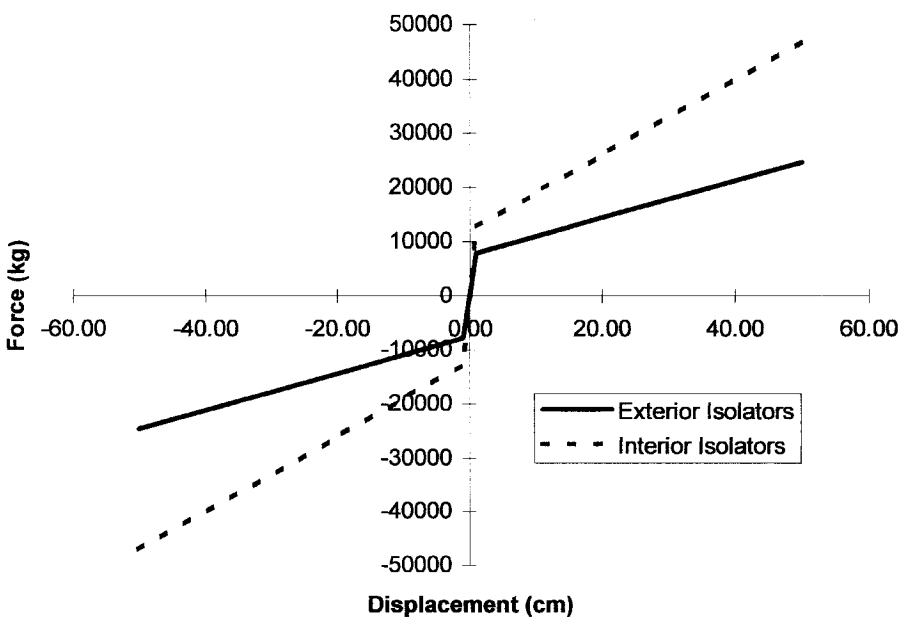

Fig. 9.13 Bilinear isolator models.

TABLE 9.5 Selected Pairs of Time Histories for Nonlinear Analysis Example

Pair No.	Event Name	Station	Year	Component	PGA (g)	Peak Ground Velocity (cm/s)	Peak Ground Displacement (cm)
1	Imperial Valley, CA	Array #6	1979	230°	0.436	100.709	55.165
				140°	0.376	63.130	26.942
2	Loma Prieta, CA	Hollister, South and Pine	1989	0°	0.369	62.778	30.176
				90°	0.178	30.891	20.418
3	Loma Prieta, CA	Lexington Dam	1989	0°	0.442	84.434	14.673
				90°	0.409	34.982	25.814
4	Landers, CA	Lucerne Valley	1992	L	0.703	25.718	8.824
				T	0.665	68.443	28.220
5	Landers, CA	Yermo Fire Station	1992	270°	0.245	50.812	41.275
				360°	0.151	29.032	22.779
6	Petrolia, CA	Petrolia	1992	0°	0.589	48.304	15.235
				90°	0.662	89.454	30.577
7	Northridge, CA	Sylmar, County Hospital Parking Lot	1994	90°	0.604	76.936	15.217
				360°	0.843	128.884	32.550

where you installed the ISOSEL program. Also included in the same subdirectory are the data files corresponding to all of the seven pairs of time histories listed in Table 9.5. To run this problem, execute SAP-2000 by clicking on the SAP-2000 Educational entry from the Windows 95/NT Start/Programs menu. Once SAP-2000 is loaded, select the SAP2000. S2k file type from the Files/Import menu (see Fig. 9.14) and select Example1.s2k in the subsequent window (Fig. 9.15). The model as shown in Fig. 9.16 will appear on your screen. To perform analysis, simply click on the → icon on the SAP-2000 menu bar. The analysis is performed for all seven pairs of time histories.

Once the analysis is completed, you may examine both the general response characteristics and individual isolator response. For example, base shear time histories in the longitudinal and transverse direction corresponding to the Sylmar pair of horizontal components are superimposed in Fig. 9.17 and the energy imparted on the system by the same pair is shown in Fig. 9.18.

Figure 9.19 shows the time history of X-direction forces for the corner isolator located at the origin of the global coordinate system when subjected to the Sylmar pair of ground motions. The force deflection response for the same isolator and the same pair of ground motions is shown in Fig. 9.20. For further information on effective use of the SAP-2000 analytical capabilities and user

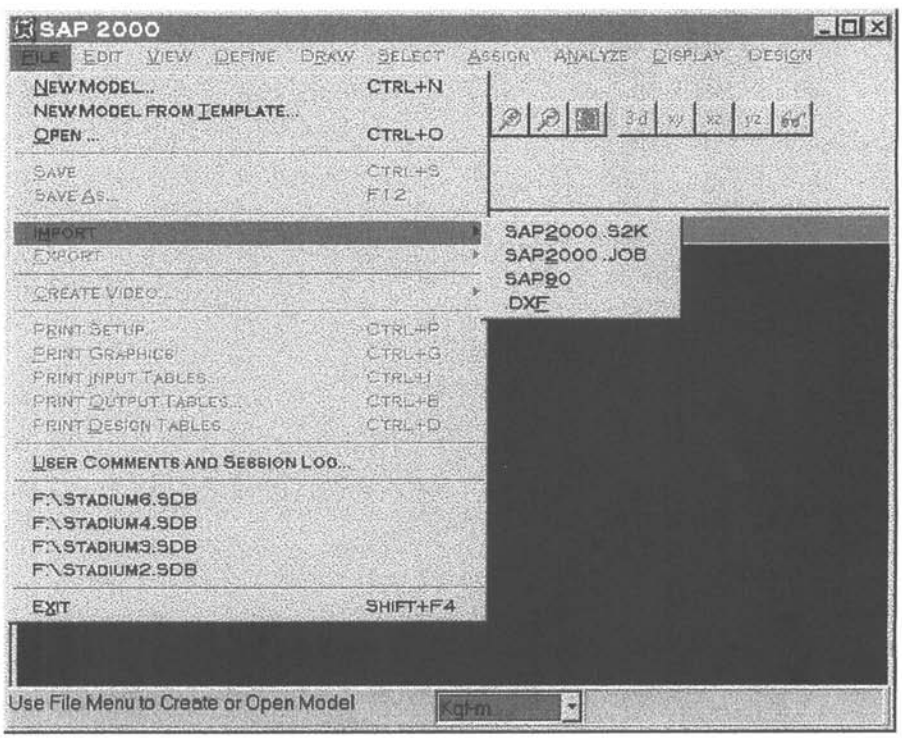

Fig. 9.14 Selection of input file type from the SAP-2000 File menu.

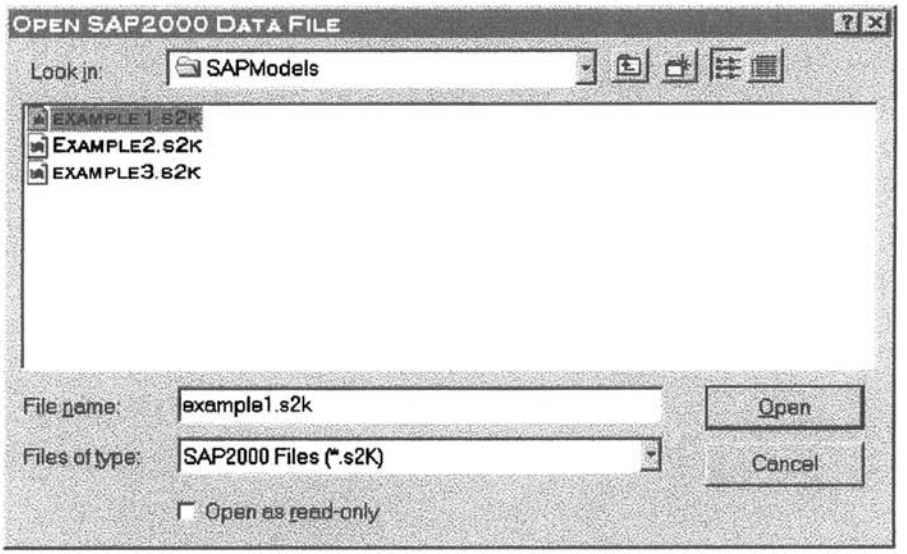

Fig. 9.15 Selection of input file to be used.

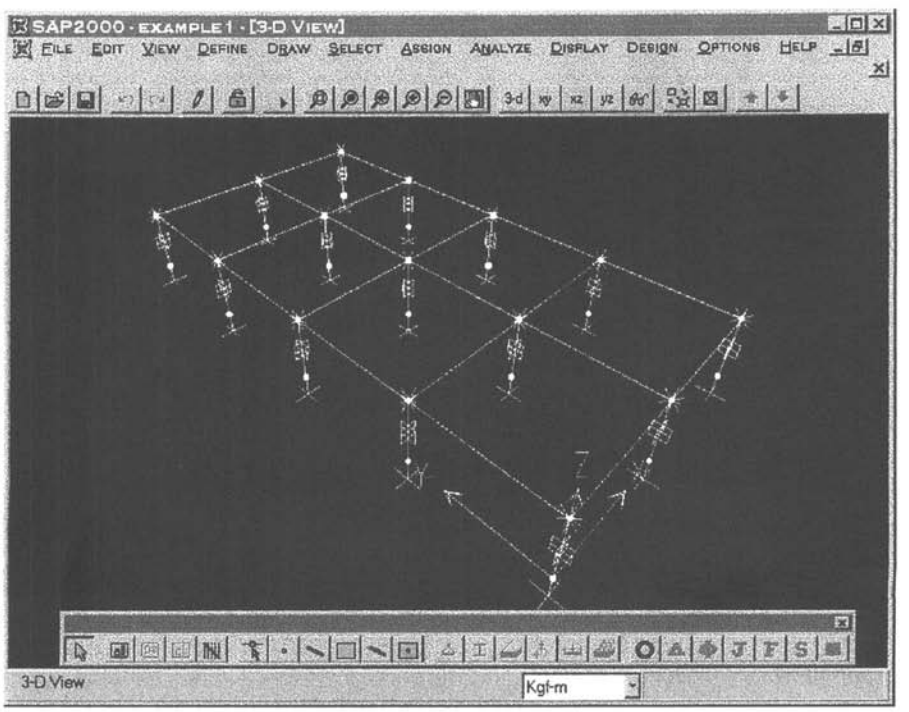

Fig. 9.16 Three-dimensional view of the SAP-2000 nonlinear model.

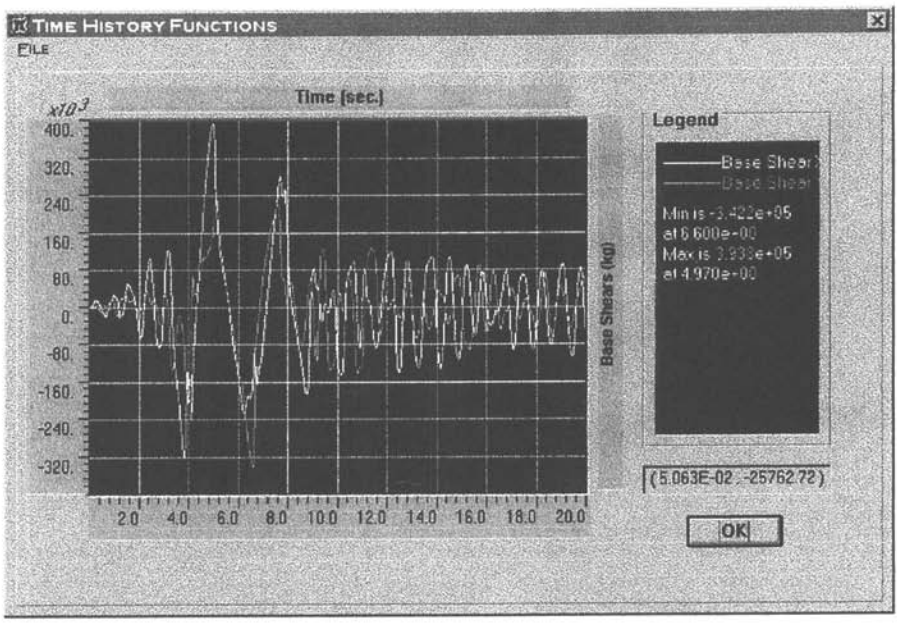

Fig. 9.17 Base shears in principal directions when subjected to the 1994 Northridge at Sylmar time history pair.

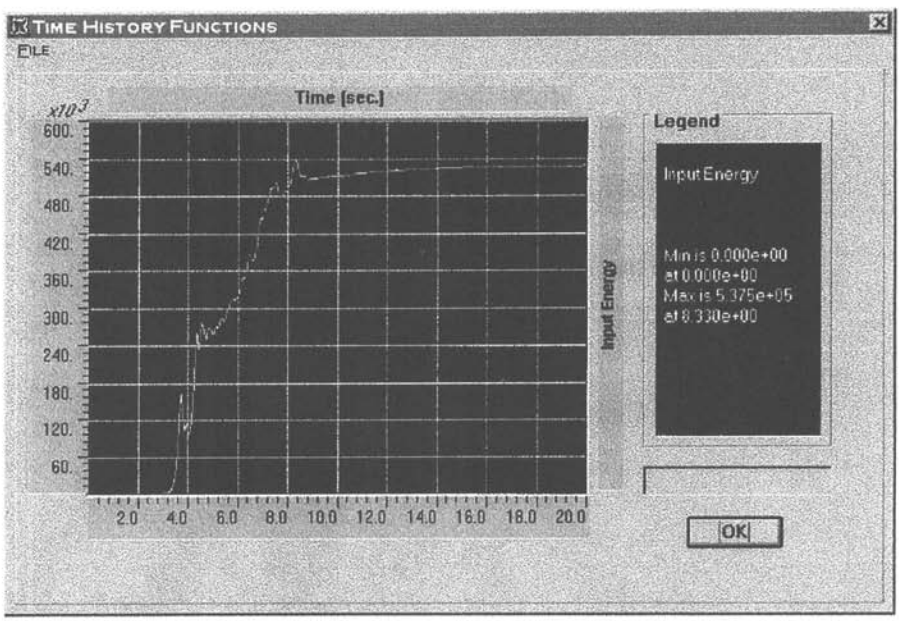

Fig. 9.18 Input energy when subjected to the 1994 Northridge at Sylmar time history pair.

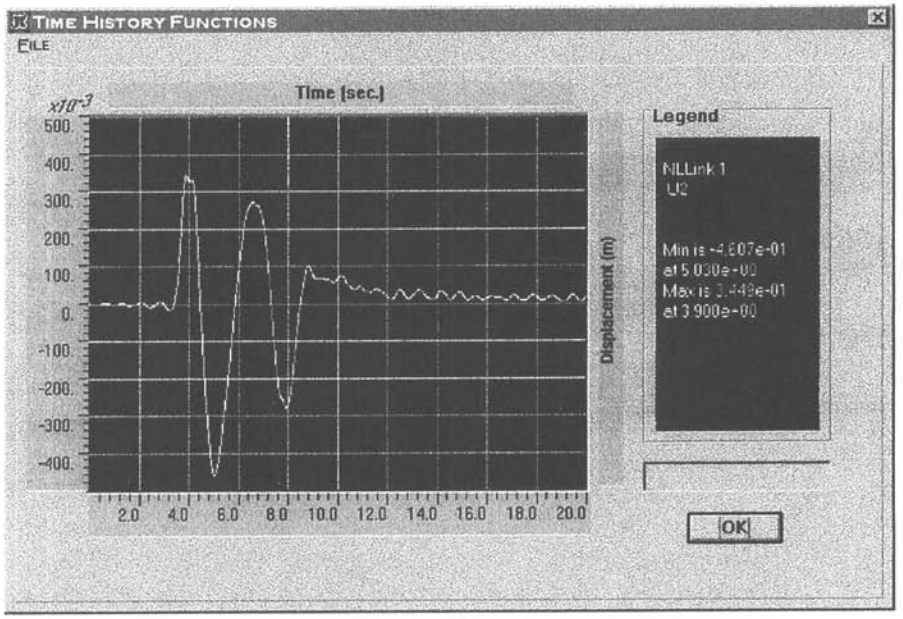

Fig. 9.19 Shear force on a corner isolator (1994 Northridge at Sylmar time history pair).

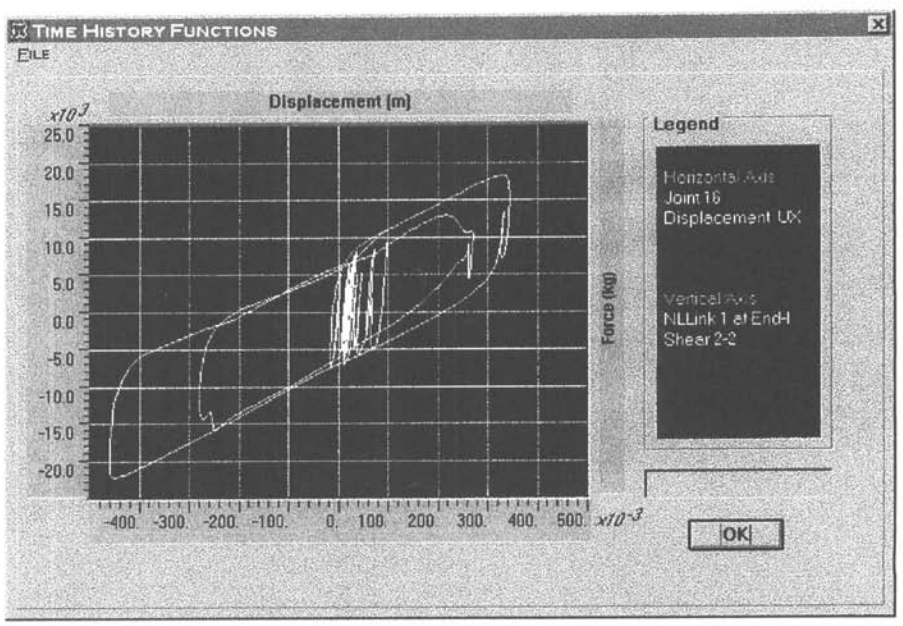

Fig. 9.20 Force–displacement hysteresis loops for a corner isolator (1994 Northridge at Sylmar time history pair).

interface, consult the comprehensive on-line tutorials and documentation that are included in the companion CD-ROM disc.

Summary of the displacement response obtained from this analysis is presented in Table 9.6. Clearly the 1979 Array #6 pair and the 1994 Sylmar pair control the maximum response of this system. Response to the other five pairs is much less significant. Also notice that for all cases the maximum displacement demands in the two orthogonal directions are significantly different. Of course rotating the ground motion pair will rotate the results since the stiffness of the isolation system is the same in both directions. This table clearly demonstrates why the procedure called for by many codes for scaling both components simultaneously to exceed the design spectrum is both irrational and overconservative.

High-damping rubber bearings generally exhibit a significant stiffening at large displacements. To investigate the possible effects of this hardening, a second SAP-2000 input file was generated (Example2.s2k). In this example the force deflection backbone curve of the isolators were modeled to have a trilinear shape with post–elastic stiffness doubling at the arbitrarily selected displacement value of 25 cm (10 in.). Since the SAP-2000 element library accommodates only bilinear behavior for elastomeric isolators, we augmented each ISOLATOR1 element with a pair of nonlinear compression-only (gap) and tension-only (hook) elements (in each direction) with stiffness values corresponding to the net hardening stiffness of the isolators. The force deflection characteristics of these gap and hook elements are shown in Fig. 9.21. Although this technique is approximate because it ignores the cross-coupling of motion in orthogonal directions (SAP-2000 gap and hook elements are uniaxial), it is accurate enough for most practical applications.

TABLE 9.6 Summary of Displacement Results Obtained by Nonlinear Time History Analysis

Pair No.	Time History Pair	Maximum *X*-Direction Displacement		Maximum *Y*-Direction Displacement		Maximum Resultant Displacement		Time of Maxima
		cm	in.	cm	in.	cm	in.	(sec.)
1	Array #6	61.8	24.3	33.5	13.2	70.4	27.7	5.05
2	Hollister, South Pine	8.8	3.5	25.6	10.1	27.0	10.6	8.36
3	Lexington Dam	23.3	9.2	22.3	8.8	31.9	12.6	4.41
4	Lucerne Valley	4.5	1.8	27.0	10.6	27.1	10.7	11.25
5	Yermo Fire Station	4.7	1.9	15.8	6.2	16.1	6.3	16.82
6	Petrolia	35.6	14.0	13.1	5.2	37.4	14.7	3.34
7	Sylmar, County Hospital Parking lot	46.1	18.1	33.5	13.2	50.0	19.7	5.05

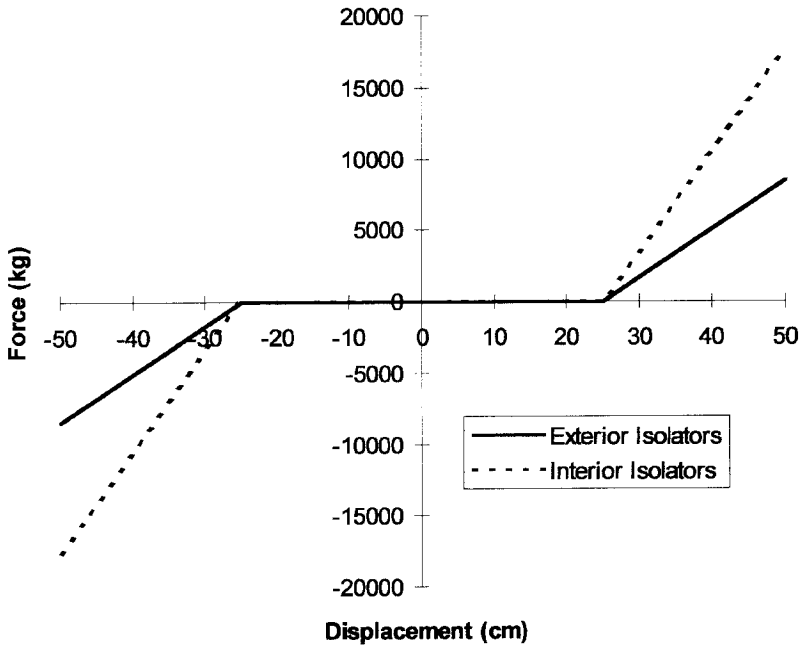

Fig. 9.21 Nonlinear gap and hook elements used to model isolator hardening.

As expected, this modification had from little to no effect on the response to the five pairs of time histories, which produced displacement components less than or slightly over 25 cm (10 in.) in each direction. The maximum resultant displacement response to the Array #6 pair, however, was reduced by 26% from 70.4 to 55.8 cm (27.72 to 22.97 in.). Surprisingly, the effect on the response to the Sylmar pair was not significant; although the isolator hardening reduced the maximum displacement in one direction, it increased it in the orthogonal direction, with the net resultant maximum displacement being almost exactly identical [49.9 cm (19.65 in.) compared to 50.0 cm (19.68 in.)].

In order to investigate the possible effects of pounding of the isolation system and a retaining wall or an adjacent building located at a distance smaller than the maximum displacement of the isolators, a third input file was generated (Example 3.s2k). This is a modification of the second input file, where additional gap and hook elements are added to the external nodes to model the very large stiffness of such an external object. The reason for adding these elements to the existing joints was to perform this exercise within the 30-node limit of the companion educational program. If this limit was not a consideration, the external walls or buildings would be explicitly modeled. The distance of the retaining wall from the isolation system was arbitrarily chosen as 45 cm (17.7 in.). The force deflection characteristics used to define the elements representing the external wall are shown in Fig. 9.22. As expected, this modification did not

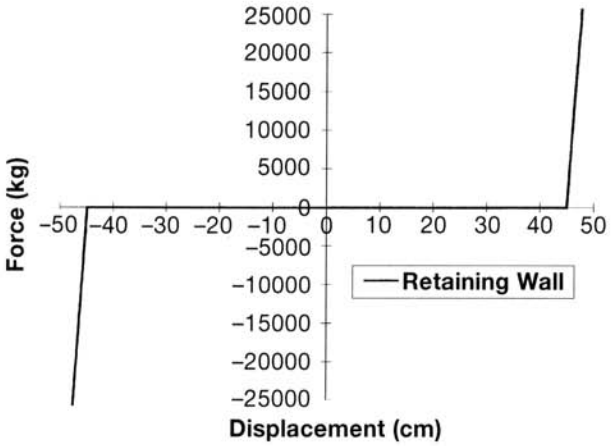

Fig. 9.22 External retaining wall stiffness as modeled by nonlinear gap and hook elements.

change the response of the system to the five pairs exhibiting displacements smaller than the assumed gap of 45 cm (17.7 in.). Impact of the isolation system against the wall, however, occurred only once in response to the Array #6 and the Sylmar pairs of ground motions generating a high-frequency spike of force as shown in Figs. 9.23 and 9.24.

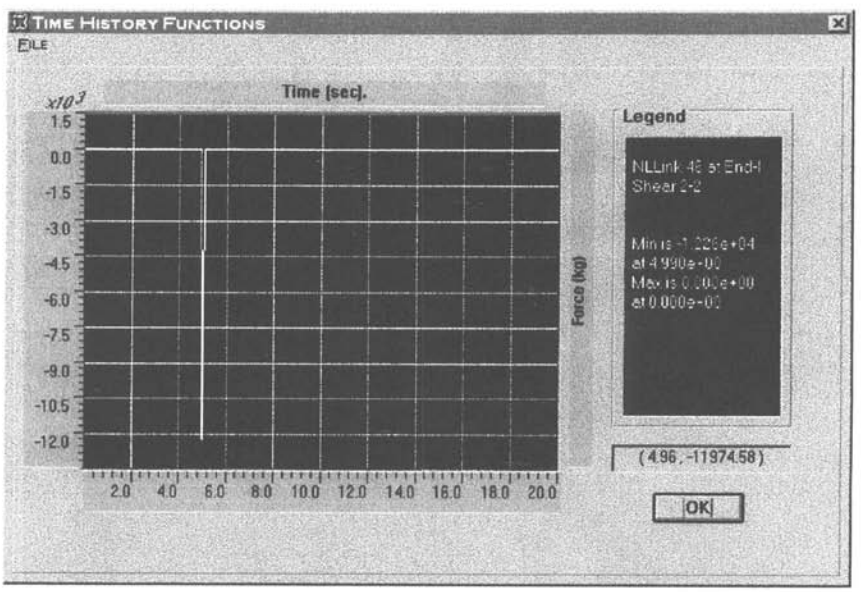

Fig. 9.23 Pounding force on the wall as modeled by a nonlinear gap element (Sylmar pair of time histories).

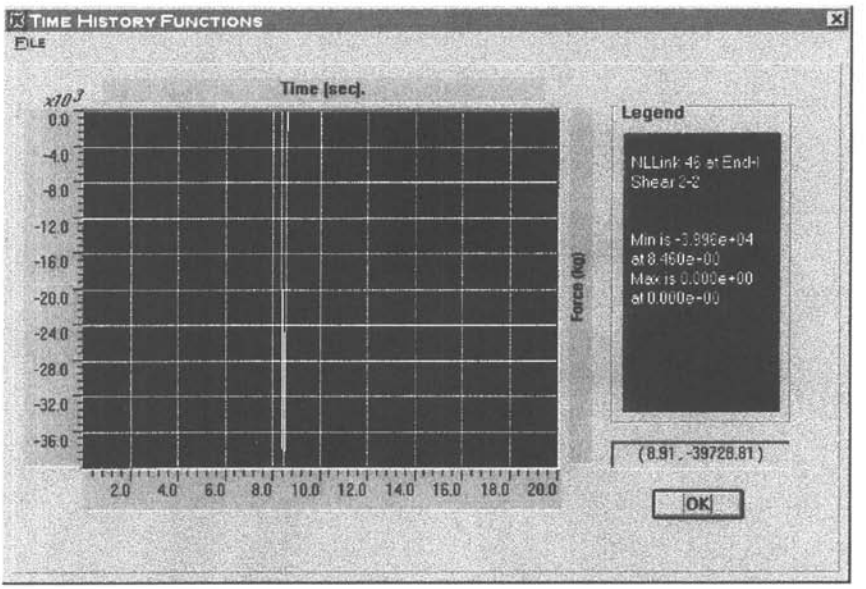

Fig. 9.24 Single impact on the wall 45 cm away from the edge of slab (Array #6 time history).

Several AVI files showing video clips of the response of the above three examples to the Array #6 and the Sylmar ground motions are contained in the SAPModels subdirectory. To watch these video clips (Fig. 9.25), simply double click on their icons.

Fig. 9.25 Snapshot of video clip showing response of the system to the 1979 Imperial Valley as recorded at the El Centro Array #6 recording station.

CHAPTER 10

SPECIFICATIONS FOR DESIGN, MANUFACTURING, AND TESTING OF ISOLATION DEVICES

10.1 INTRODUCTION

Successful implementation of any seismic-isolated project is not possible without clear specifications for design, manufacturing, and testing of the isolation devices. Furthermore, consistent provisions are needed in order to acquire and evaluate the qualifications of manufacturers and their products. Once a preliminary design of the seismic isolation system is completed, it is common practice to issue a document called the *Request for Qualifications* (RFQ). The RFQ explains the specific characteristics of the isolation system and isolation devices as envisioned by the design team and asks potential manufacturers to submit documents that demonstrate their qualifications and prior experience of manufacturing bearings with properties similar to those sought for the given project. Based on the evaluation of the RFQs and recommendations of the structural engineer of the record, a short list of manufacturers for the project is retained for further consideration.

Successful RFQ responders may offer alternative solutions to that originally envisioned. These alternatives may or may not be appropriate or feasible for the project under consideration. After careful evaluation of all possible options offered by the qualified manufacturers, the design engineers may come up with one or more alternative seismic isolation designs. For example, the designers may have originally envisioned only a high-damping rubber solution. However, the evaluation of submittals may convince them to consider other solutions such as lead–rubber bearings, friction pendulum bearings, auxiliary damping devices, or a combination of some of these systems for the project.

Once the characteristics of the acceptable isolation system are finalized, a document is produced that contains details of acceptable materials, size limitations,

Design of Seismic Isolated Structures: From Theory to Practice. F. Naeim and J. M. Kelly

performance characteristics, manufacturing processes, testing procedures, and quality assurance measures. This document, which is commonly referred to as the *Specifications for Design and Manufacturing of Isolation Devices* (SDMID), becomes the backbone of the *Request for Proposals* (RFP), which is issued to obtain competitive bids from qualified manufacturers. More importantly, this document acts as a project-specific code that governs every aspect of design, manufacturing, and construction of the isolation system from this point forward.

The key consideration in development of seismic isolation specifications is to avoid overspecification as well as underspecification. For example, in the specifications developed for a hospital in the Los Angeles area during the late 1980s, the rubber compound to be used, the manufacturing process, and the stiffness characteristics required were specified. When prototype testing of the isolators indicated stiffness characteristics that were substantially different from the required characteristics, the manufacturer claimed no fault because he used the exact rubber compound and manufacturing procedures as specified by the designers and thus could not be held responsible if the end results were different from what the specification writers had envisioned. Underspecification, on the other hand, can create even more problems. For example, if the method of calculating damping is not specified, the manufacturer may use the results obtained from small-scale tests or from smaller displacement tests that usually indicate higher damping values than those exhibited by full-scale isolators.

The following section gives a sample specification developed by Seismic Isolation Engineering for use in its isolation projects and reproduced here by permission. It contains a specification for elastomeric systems that is an attempt to cover the basic requirements of the manufacturing and testing of elastomeric isolators without encroaching on the proprietary procedures of the isolator manufacturers. It can be used with minimal modification for projects for which elastomeric isolators are intended. If alternative systems are acceptable to the engineer of record, they should be supplemented by performance specifications, testing requirements, and production quality control requirements.

It is always prudent to leave room in the specifications for alternative isolation solutions that either have not been investigated thoroughly or at the time of design did not seem feasible. With rapid changes in the technology, there is always a chance that one of these alternative systems may provide a very feasible solution for the problem at hand.

10.2 SAMPLE SPECIFICATIONS

Part 1: General

1.1 Summary

A. Section Includes

The work includes engineering design of elastomeric seismic isolation bearings, submission of technical performance data for isolation

bearings, preparation of bearing shop drawings, fabrication, testing, handling, and shipping to the job site.

1. Extent of fabricated seismic isolation bearings work of this section is indicated on the drawings and by the requirements of this section. Shipment and delivery of seismic isolation bearings shall be in accordance with the project schedule.
2. Production Bearings
   Provide high-damping rubber (HDR) or lead–rubber (LR) elastomeric seismic isolation bearings, referred to herein as "production bearings," in accordance with the specifications and the drawings.
3. Prototype Bearings
   Provide one HDR or LR bearing of each type, in accordance with these specifications and the drawings. Such bearings are referred to herein as "prototype bearings." Prototype bearings shall not be used for construction. If the bearing manufacturer's testing equipment requires that the bearings be tested in pairs, provide two prototype bearings of each type such that two independent sets of data are obtained.
4. Isolation Bearing Handling, Installation, and Long-Term Maintenance Manual
   Provide bound documentation that thoroughly describes requirements for all job site handling and installation requirements for seismic isolation bearings. Include maintenance and inspection documentation appropriate for 50 years duration. This documentation will be used for correct installation of isolation bearings and will form the basis of the building owner's long-term maintenance and inspection program for the isolation bearings.

B. Related Work
   Installation for isolation bearings is not covered in this specification document.

C. Related Sections
   1. Drawings and general provisions of contract, including general conditions and Division 1 specifications section, apply to this section.

1.2 References

A. Standards
   Comply with the applicable provisions of the current editions of the following codes and standards, unless otherwise specified herein:
   1. Uniform Building Code (UBC), 1997 Edition, Appendix to Chapter 16
   2. American Institute of Steel Construction (AISC): Specification for the Design, Fabrication, and Erection of Structural Steel for Buildings
   3. AISC: Code of Standard Practice for Steel Buildings and Bridges, except as modified herein

4. American Society for Testing and Materials (ASTM): A36—Standard Specification for Structural Steel
5. ASTM A108—Standard Specification for Steel Bars, Carbon, Cold-Finished Standard Quality
6. ASTM A325—Standard Specification for High-Strength Bolts
7. ASTM A570—Standard Specification for Structural Sheet Metal
8. ASTM A572—Standard Specification for High Strength Low Alloy Columbium-Vanadium Steels of Structural Quality
9. ASTM B29—Standard Specification for Lead
10. ASTM D395—Standard Test Methods for Rubber Property—Compression
11. ASTM D412—Standard Test Methods for Rubber Properties in Tension
12. ASTM D429—Standard Test Methods for Rubber Property—Adhesion to Rigid Substrate
13. ASTM D518—Standard Test Method for Rubber Deterioration—Surface Cracking
14. ASTM D573—Test for Rubber Deterioration—in Air Oven
15. ASTM D624—Test Method for Rubber Property—Tear Resistance
16. ASTM D1149—Standard Test Method for Rubber Deterioration—Surface Ozone Cracking in a Chamber (Flat Specimens)
17. ASTM D1229—Test Method for Rubber Property—Compression Set at Low Temperatures
18. ASTM D1457—Specification for PTFE Molding and Extrusion Materials
19. ASTM D2137—Test Method for Rubber Property—Brittleness Point
20. ASTM D2240—Standard Test Method for Rubber Property—Durometer Hardness
21. ASTM D3183—Standard Practice for Rubber—Preparation of Pieces for Test Purposes from Products
22. ASTM D4014—Standard Specification for Plain and Steel Laminated Elastomeric Bearings for Bridges
23. ASTM E4—Standard Practices for Load Verification of Testing Machines
24. ASTM E37—Standard Chemical Methods for the Analysis of Lead
25. Steel Structures Painting Council (SSPC) SP6—Commercial Blast Cleaning
26. American Welding Society (AWS) D1.1—Structural Welding Code—Steel
27. International Standards Organization (ISO): ISO-9001—Model for Quality Assurance
28. British Standards Institution—BSI (1979), "Commentary on Cor-

rosion at Bimetallic Contacts and Its Alleviation," Standard PD6484: 1979 London, UK

The bearing manufacturer shall provide appropriate specifications and standards for materials and tests that are not covered in this section, for review and approval by the owner.

1.3 System Description

A. General

The seismic isolation system design shall consist of elastomeric bearings. Elastomeric bearings may be either of the high-damping rubber (HDR) or lead–rubber (LR) type. The engineer has developed a preliminary seismic isolation system design that comprises one size of elastomeric bearing. The design assumes an effective period T_{eff} and damping of ____ seconds and ____ percent, respectively, at the DBE level design displacement D_D. The design displacement D_D and total maximum displacement D_{TM} are governed by the UBC static requirements. The preliminary isolation system design satisfies the global performance criteria defined for this project. The preliminary design is presented in the specification and shown on the drawings. The final isolation system design shall be determined by the bidding team and shall meet the requirements of the specification. Design and testing criteria for the seismic isolation system shall meet the requirements of the 1997 UBC, as modified by the additional requirements of this section.

B. Isolation System Design Data

1. Building Weight

The estimated total dead load of the building is ____ kips and the estimated live load on the building is ____ kips. The seismic live load may be taken as 0.5 times the total live load.

2. Isolation System

The seismic isolation system shall consist of elastomeric isolation bearings. Elastomeric bearings may be either of the HDR or LR type. The total numbers of elastomeric isolation bearings are shown on the drawings. Only bearing designs that satisfy the performance criteria defined in Article 1.4 shall be deemed acceptable.

3. Gravity and Seismic Loads

Dead load, live load, and seismic loads for each bearing are shown on the drawings.

1.4 Performance Criteria

A. Global Performance Requirements

1. Base Shear

The isolation system shall not transmit a base shear to the superstructure greater than ____ times the total building seismic weight, as determined from dynamic analyses using DBE site-specific ground motion time histories. The system base shear at displace-

TABLE 1 Isolation Bearing Axial Load Requirements

Quantity of Bearings	Elastomeric Bearings (HDR1 or LR1)
Range of (DL + 0.5LL)	
P1 = average of (DL + 0.5LL)	
P2 = maximum of (DL + LL)	
P3 = maximum of (1.2DL + 1.0LL + |EQMCE|)	
P4 = minimum of (0.8DL − |EQMCE|)	

ments corresponding to large shear strains shall appropriately account for the effect of elastomer strain hardening.

2. Lateral Stiffness
   a. The isolation system shall have an initial stiffness equal to the stiffness K_0 given in Table 2 times the number of elastomeric bearings given in Table 1 at a displacement of 0.5 in.
   b. The isolation system shall have an effective stiffness at the design displacement D_D equal to the stiffness K_{eff} given in Table 2 times the number of elastomeric bearings-given in Table 1.
3. Damping Properties of Isolation System
   The isolation system shall have, as a minimum, an equivalent viscous damping of ____% of critical at the design displacement D_D. The maximum equivalent viscous damping provided by the elastomeric bearings shall not be more than ____%. The final isolation system design shall provide damping within this range. The equivalent viscous damping shall be calculated as the ratio of the amount of energy dissipated per hysteretic cycle to the amount of elastic energy stored at the design displacement by an equivalent spring with a stiffness equal to the system effective stiffness. A damping modification factor may be applied to account for frequency effects.

TABLE 2 Isolation Bearing Stiffness and Damping Requirements

	Elastomeric Bearings (HDR1 or LR1)
Displacement properties	
D_0	
D_D	
D_{TM}	
Shear stiffness properties	
K_0 at D_0	
K_{eff} at D_D	
Vertical stiffness properties	
Zero shear position, K_v	
Hysteresis loop area, A_h	

If such a factor is used to adjust the equivalent damping obtained from quasi-static test methods to dynamic conditions, it shall be substantiated by appropriate static and dynamic bearing test data representative of the proposed sizes and loading conditions. Modification factors may not be based solely on coupon test results.

4. Overall Isolation System Displacement Limit
   The seismic gap, or moat, between the building and surrounding retaining structure is _____ inches. The isolation system shall limit displacements such that no contact occurs between the isolated and nonisolated portions of the building for the MCE event.
5. Dimensional Limits
   The maximum overall height of the isolation bearings, including mounting plate hardware, is _____ inches. The maximum plan dimension of elastomeric bearings, including mounting hardware, is _____ inches.
6. Gravity Load Resistance
   In the undeformed configuration, the bearings shall be capable of carrying the maximum gravity load P_2 with a factor of safety of at least 3. The minimum vertical stiffness of the elastomeric bearings, in the undeformed configuration, is given in Table 1.
7. Seismic Load Resistance
   The bearings shall provide stable hysteretic lateral force–displacement response under constant compression load P_1 when cycled to the design displacement D_D. The bearings shall be capable of withstanding, without becoming unstable, a fully reversed cyclic test under a constant compression load of P_3 to the total maximum displacement D_{TM}.
8. Bearing Connections
   Flange plates for connection of bearings to the superstructure and substructure may be either bonded directly to the bearing or bolted to an integrally bonded bearing endplate. Dowelled connections between bearings and the superstructure and substructure shall not be permitted.
9. Net Tension and Uplift
   Elastomeric bearings shall be capable of resisting a net tension of _____ psi while subjected to the total maximum displacement D_{TM} without damage and without separation of bearing components.

B. Performance Requirements for Individual Bearings
   1. Elastomeric Bearings
      a. Effective Lateral Stiffness
         Bearings shall be sized to resist the vertical load combinations described in Table 1 and shall meet all the requirements of paragraph 1.4.A. The total effective lateral stiffness at a displacement D_D for all bearings of one type under the compression load P_1 shall be within ±10% of the value specified for an individual

bearing of that type times the number of bearings of that type. The effective lateral stiffness for each individual bearing shall be within ±15% of the design lateral stiffness of the bearing type. In the case of bearings tested in pairs, the average effective lateral stiffness for each pair of bearings shall be within ±15% of the design lateral stiffness of the bearing type.

b. Rubber Properties
Required rubber properties are given in paragraph 2.2.A.1.b.

1.5 Technical Performance Data

A. General

The bearing manufacturer shall submit the following minimum documentation to demonstrate that the isolation system design satisfies the specific technical requirements for the project. A complete description of the technical characteristics of the isolation system must be submitted for approval prior to the manufacture of any bearings. This shall include:

1. Design Data—Elastomeric Bearings
   a. Load (performance) tables of allowable vertical load, effective stiffness and damping, etc., for preengineered elastomeric bearings
   b. Engineering properties—elastomeric bearings (to be submitted for each type of rubber compound used)
      (1) The bearing manufacturer shall submit the maximum shear strain corresponding to the total maximum displacement D_{TM} that should be used for the design of seismic isolation bearings fabricated from each of the rubber compounds used.
      (2) Any information that pertains to manufacturing practices and constraints that should be considered in the design of a seismic isolation system utilizing the bearing manufacturer's rubber materials.
      (3) Shear modulus of rubber at strains from 0 to 300% for cyclic loading rates of 0.5 Hz and approximately 1–2% shear strain per second
      (4) Loss angle of rubber at strains from 0 to 300% for cyclic loading rates of 0.5 Hz and approximately 1–2% shear strain per second
      (5) Decrease in shear modulus and loss angle from first to third cycle
      (6) Change in shear modulus and loss angle over the design life
      (7) Change in shear modulus and loss angle with duration of earthquake load
      (8) Design (allowable) compressive stress of bearing
      (9) Ultimate compressive stress capacity of bearing
      (10) Ultimate rubber shear strain

(11) Bond strength between rubber and steel
(12) Initial deflection of bearing under dead plus live load
(13) Long-term creep displacement under dead plus live load
(14) Bearing shear stiffness under a lateral load of 0.01–0.03 times dead load
(15) Vertical stiffness
(16) Uplift restraint capacity of bearings

c. Manufacturing procedures and specifications for bearings, including identification of applicable codes and standards
d. Mounting Requirements
Installation and mounting requirements, including any need for special techniques, methods, or equipment. Design criteria and methodology for the structural design of mounting plates and bolts shall be submitted for review and approval by the owner.
e. Product quality
(1) Product life
(2) Fire resistance rating
(3) Durability of bearings to resist the effects of aging, creep, fatigue, moisture, ozone, chemicals, and other environmental effects
f. Routine maintenance and inspection requirements
g. Inspection and replacement requirements
(1) Postearthquake inspection and replacement requirements
(2) Method to replace bearings and conceptual details to accommodate replacement

2. Test Data
a. Material Properties
Provide test results indicating various mechanical properties of the exact materials to be used in the fabrication of the bearings.
b. Structural Properties—Elastomeric Bearings
Provide detailed bearing property information for elastomeric bearings as outlined in this section. Bearing property information shall be based on test data.
(1) Submit test data for at least one elastomeric bearing fabricated from each of the compounds being proposed for this project. The smallest bearing for which data may be submitted is 24 in. in diameter or 24 in. square. Data must be submitted for tests of bearings, fabricated from each of the compounds being proposed, to the maximum shear strain corresponding to the total maximum displacement D_{TM} that is assumed in the bearing designs for this project. Data submitted must be for axial pressures on the bearing corresponding to the bearing manufacturer's recommended maximum "short-term" and maximum "long-term" design pressures. Data obtained from tests of bearings with lead plugs are

acceptable only if they are provided to support a design that includes lead plugs of comparable diameter. Data obtained from bearings without lead plugs may not be used to justify design parameters of bearings with lead plugs.

(2) A drawing of each bearing for which data are being presented shall be submitted.

(3) Submitted data shall include (at a minimum): hysteresis loops of force vs. displacement, clearly indicating the axial load (pressure) on the bearing, the shear strain and displacement of the test, the number of cycles in the test, and the rate of loading. The date of the test shall also be indicated.

(4) Submit data for virgin (unscragged) and scragged full-size bearing tests.

(5) Submit detailed stiffness and damping properties of the elastomeric bearings for which data are being submitted, including details of the calculation procedures used to establish these properties.

(6) If correction factors are used to modify stiffness and/or damping properties of the bearings or compounds, detailed information supporting these factors shall be submitted for each of the rubber compounds being proposed. This shall include, but not necessarily be limited to, data from cyclic shear coupon tests at different rates of loading, data from dynamic and static tests of reduced-scale bearings, and any available data from tests of full-size bearings. Correction factors may not be based solely on coupon test results.

3. System Performance
Submit technical data demonstrating that the seismic isolation system and individual system elements conform to all of the requirements of Article 1.4.

B. Quality Control Programs/Certifications
Provide a complete description of the bearing manufacturer's quality control/assurance programs and include all applicable certifications.

C. Product Warranty
The bearing manufacturer shall warrant the elastomeric and sliding isolation bearings for a period of at least ____ years subsequent to the date of installation of the bearings in the project. The details of the manufacturer's warranty shall be included as part of the technical performance data submittal.

1.6 Engineering Design Calculations

A. Description
Design calculations for seismic isolation bearings shall be submitted for each of the bearing designs. The design calculations shall be stamped and signed by (i) a California licensed professional engineer

experienced in the design and fabrication of seismic isolation bearings and (ii) an officer of the supplier's corporation.

B. The calculations shall include, but not necessarily be limited to:
   1. A complete summary of isolation bearing design variables, formulas, and assumptions
   2. Calculations for proportioning each type of bearing to meet the required performance parameters listed in Table 1. The dimensional constraints given in paragraph 1.4.A.5 and shown on the drawings shall be followed.
   3. Calculations for the verification of tensile integrity and stability against buckling for each type of bearing under the following load–displacement cases: in the undeformed position each bearing shall be capable of carrying the maximum gravity load P_2 for that bearing type with a safety factor of at least 3; under the total maximum displacement D_{TM} each bearing shall be stable under the maximum short-term load P_3 for that bearing type.

1.7 Submittals

A. Submit under the provisions of Section ____.

B. General: All submittals shall be made to the owner's representative.

C. Predesign Information
   Prior to commencement of design calculations, submit performance data for seismic isolation bearings, in accordance with the requirements of Article 1.5. Include sample design calculations for one bearing.

D. Design Calculations
   Calculations, as described in this section, shall be submitted in a bound volume with a comprehensive table of contents. All calculation pages shall be individually numbered and chapter dividers tabbed. Calculations shall be stamped and signed in accordance with Article 1.6 and shall be submitted for review for compliance with the drawings and specifications.

E. Shop Drawings
   Shop drawings shall include, but not be limited to, fabrication drawings, bolting templates, and schedules. Shop drawings shall be stamped and signed by a professional engineer registered in the State of California. Submit shop drawings for each elastomeric bearing size, indicating dimensions, isolator weights, and component material types.

F. Certifications
   Submit the following documents, written and signed by an independent testing agency, approved by the owner's representative:
   1. Certification that all testing equipment has been checked for accuracy by appropriate standards, (ASTM E4, etc.) for the purpose of this contract.
   2. Certified mill test reports for all steel plates and laminate plates.

G. Proposed Testing Schedule
Prior to commencement of material and bearing testing, submit the proposed schedule showing approximate dates for each stage of testing. Provide names and addresses for the proposed testing facilities. Submit updates of schedule as revisions occur.

H. Proposed Test Procedures
Prior to commencement of material and bearing testing, submit drawings of proposed test apparatus for shear tests, as defined in this section.

I. Inspection and Test Reports
Submit six copies of each of the following test reports:

1. Rubber Test Reports
Submit test reports for all rubber component samples, tested as specified in this section, prior to commencement of fabrication of prototype bearings.
2. Prototype Bearing Test Reports
Submit prototype bearing test data for review prior to commencement of fabrication of production bearings. Owner approval will be required prior to manufacture of production bearings.
3. Production Bearing Test Reports
Submit production bearing test data for each production bearing within seven calendar days after completion of testing of the subject bearing and prior to delivery to the job site.
4. Final Isolation Bearing Test Report
Submit the final isolation bearing test report, as described in this section, within 14 calendar days after completion of all production bearing testing.

1.8 Redesign and Retesting

A. The bearing manufacturer shall be obligated to provide seismic isolation bearings that conform to the requirements of the drawings and specifications. Should initial bearings as designed by the manufacturer not conform to the project requirements at the prototype testing stage, the manufacturer shall redesign and retest isolation bearings until the project requirements are satisfied, all at no additional cost to the owner.

1.9 Testing and Inspection

A. Quality Control
1. All material testing and fabrication testing shall be performed in accordance with these specifications.
2. Costs of quality control testing and inspection shall be paid for by the bearing manufacturer. Costs of all retesting and reinspection made necessary by bearings and materials that fail to meet the specification requirements shall be paid by the bearing manufacturer.

B. Quality Assurance
1. Testing and inspection will be reviewed by an inspector paid by the owner.

2. Inspections required by the owner will be in addition to those performed by the manufacturer and will be performed by an inspector experienced in elastomeric bearing manufacturing and testing and paid by the owner.
3. The inspector will observe the work assigned for conformance with the approved design drawings and specifications.
4. Inspections will be performed for the following phases and aspects of elastomeric bearing manufacture:
   a. Testing equipment
      (1) Review of testing equipment
   b. Material tests
      (1) Review of tests
   c. Prototype bearing tests
      (1) Witness and review of tests
   d. Production bearing tests
      (1) Witness and review of tests
   e. Reports
      (1) The Inspector shall provide inspection reports to the owner's representative. All discrepancies shall be brought to the immediate attention of the owner's representative for correction.
      (2) The inspector shall submit a final signed report stating whether the work requiring inspection was, to the best of the inspector's knowledge, in accordance with the approved design drawings and specifications.
5. The inspector, retained by the owner, shall be present continuously during the testing process at the discretion of the owner. If the inspector suspects any faults in the isolation bearing during testing, the inspector shall identify the isolator and suspected fault by serial number and location to the manufacturer; the isolator shall be set aside for disposition by the owner. The owner may order the isolation bearing to be vertically cut in half for examination. If the cut isolation bearing exhibits flaws or does not conform to the specification, the costs of cutting and replacement shall be borne by the bearing manufacturer. Otherwise, cutting and replacement costs shall be borne by the owner.
6. The bearing manufacturer shall provide access to the work for the purposes of the owner's inspector.

Part 2: Products

2.1 Acceptable Manufacturers

A. Subject to compliance with specified requirements, bearing manufacturers offering products that may be incorporated in the work include the following:

1. High-damping rubber bearings
2. Lead–rubber bearings

2.2 Seismic Isolation Bearings and Mounting Materials

A. HDR or LR Bearings

1. Materials

a. Inner steel laminate plates: ASTM 570, Grade 40
Outer steel plates: ASTM 572, Grade 50
Connecting bolts: ASTM A325 or ASTM 490

b. Rubber
All high-damping rubber compounds for elastomeric bearing shall satisfy the following minimum requirements:

Minimum tensile strength	1250 psi
Minimum elongation at break	600%
Minimum bond peel strength	40 lb./in.

All natural rubber compounds for elastomeric bearings shall satisfy the following minimum requirements:

Minimum tensile strength	1250 psi
Minimum elongation at break	600%
Minimum bond peel strength	40 lb./in.

c. Lead
The purity of lead shall be established by chemical analysis from a sample of that used in the bearings. This test shall confirm a minimum of 99% purity of the lead, in accordance with ASTM B29 and E37. The bearing manufacturer shall provide certification for the purity of lead.

Part 3: Execution

3.1 Fabrication

A. Elastomeric Bearings

1. General
Bearings shall be molded individually to sizes shown on the drawings. All molds shall have standard shop-practice mold finish. All bonding of elastomer to metal substrates and to external load plates shall be carried out during molding.

a. Elastomer Storage
After mixing, all elastomer parts shall be stored in an environment that is sheltered against rain, sun, wind, etc., and kept at a temperature of 70 ± 20°F until ready for molding.

b. Metal Plates
Metal plates bonded to elastomer shall be blasted and properly prepared and have the edges rounded.

c. Shop Priming and Painting
Exposed steel parts shall have one shop coat of paint. Steel surfaces shall be commercially blast cleaned in accordance with SSPC-SP6 and also in accordance with the paint manufacturer's directions. Paint shall be applied according to the paint manufacturer's directions to 2.5–3.5 mils dry thickness. The nonferrous parts shall be properly masked for protection.

d. Mounting Plates
All bolted mounting plates shall be bolted to bearings as shown on the drawings prior to packaging and delivery. If tapped holes are required, they shall be drilled using a metal template for accuracy of fit with mating plates.

3.2 Fabrication Tolerances

A. Elastomeric Bearings

1. Steel Plates
All steel mounting plates, connecting plates, and top and bottom laminate plates shall be milled to bear. Curvature offsets out of the plane of the plate in excess of $\frac{1}{16}$ in. shall be cause for rejection and replacement at the bearing manufacturer's expense. Curvature offsets shall be defined as the perpendicular distance between any point on the surface of the plate and a straight-edge laid in any orientation across the plate.

2. Rubber Layers
Rubber layers shall be of uniform thickness, in accordance with the tolerances established in ASTM D4014.

3. The tolerances on elastomeric bearing dimensions shall be as follows:

Dimension	Tolerance
Thickness of top and bottom cover rubber (if any)	$\pm\frac{1}{16}$ in.
External plan dimensions	$\pm\frac{1}{4}$ in.
Flatness of exterior top and bottom surface of completed bearing	$\pm\frac{1}{8}$ in. offset
Variation from plane parallel to theoretical surface	
Top	Slope relative to the botom of no more than 0.3 degree
Sides	$\pm\frac{1}{4}$ in.
Overall bearing height	$\pm\frac{1}{4}$ in.

3.3 Quality Control Procedure for Elastomer Compounding, Bearing Fabrication, and Molding

A detailed quality control plan shall be submitted for review and approval by the owner's representative prior to the ordering of materials and the start of work. As a minimum, the procedures shall address the items listed below:

- Incoming materials and storage
- Elastomer compound mixing
- Metals preparation
- Bearing build-up
- Vulcanization

Sliding bearings shall satisfy all of the requirements for the fabrication of elastomeric bearings in this section that are applicable to sliding bearings.

3.4 Materials Tests

A. Rubber Tests

A minimum of three samples of each rubber compound to be used shall be tested as described below prior to commencement of fabrication of prototype bearings and production bearings (these samples shall be taken from the material used to fabricate the prototype and production test bearings).

1. Tensile Stress Measurement
   Tensile stresses shall be measured and plotted at tensile strains of 100, 200, 300, 400, and 500% in accordance with ASTM D412.
2. Tensile Strength and Ultimate Elongation of Elastomer
   The minimum tensile stress at break shall be determined in accordance with ASTM D412. Minimum tensile strength and minimum ultimate elongation shall be as specified in paragraph 2.2.A.1.b.
3. Rubber-to-Metal Bond Strength
   The minimum bond peel strength shall be determined in accordance with ASTM D429 Method B. The minimum bond peel strength shall be taken as the average of the peak values of force during separation of the specimen. Failure criteria for the determination of a successful test shall be 100% rubber tearing. Delamination of the rubber from the steel plate shall be cause for rejection. The bearing manufacturer shall retest for minimum bond peel strength at his or her own expense until full compliance can be demonstrated.
4. Initial Hardness
   The initial hardness shall be determined in accordance with ASTM D2240 and shall be used as a datum for aging tests.
5. Heat Resistance (Aging Tests)
   Heat resistance shall be tested in accordance with ASTM D573.

Test samples shall be maintained at a uniform temperature of 158°F for 7 days. Maximum permissible changes in the following mechanical properties shall be:

Tensile strength	−25%
Ultimate elongation	−25%
Hardness	+10 shore A points

6. Compression Set
   The compression set shall be determined in accordance with ASTM D395 Method B. The test samples shall be maintained at a uniform temperature of 158°F for 22 hr. The maximum permissible set shall be 50%.
7. Ozone Resistance
   The ozone resistance of the outer cover rubber shall be determined by tests on rubber strips mounted in accordance with ASTM D518 Method A. The tests shall be performed in accordance with ASTM D1149 at an ozone partial pressure of 50 ± 5 MPa at 20% strain at 100 ± 4°F for 100 hr. The ozone resistance shall be regarded as satisfactory if, on conclusion of a test, no cracks are visible using a 7× magnification lens.
8. Cyclic Shear Tests
   Dynamic shear modulus and damping at shear strains of 2, 25, 50, 100, 200, and 300% shall be determined. The material characteristics in shear should be based on accepted double or quadruple test pieces, according to either ASTM D4014 or an equivalent, and should be tested at a frequency of 0.5 Hz. Details of the proposed testing procedure, including details of the test specimen size and configurations, shall be submitted for review. Three test pieces for each rubber compound utilized shall be tested as follows:
   a. Initial: Plot the shear modulus vs. strain and the damping vs. strain for tests at the strain levels noted above.
   b. Scragged: Plot the shear modulus vs. strain and the damping vs. strain for tests at the strain levels noted above conducted shortly after the initial testing has been performed (within 15 min).
   c. Recovered: Plot the shear modulus vs. strain and the damping vs. strain for tests at the strain levels noted above after the test pieces have been allowed to rest (unstrained) for 24 hr after completion of the scragged test. Temperature effects shall be quantified via dynamic testing of test pieces as noted above. Shear modulus shall be measured at a frequency of 0.5 Hz at 50% shear strain. Three temperatures shall be used: 30, 70, and 100°F. Measurements shall be made both on the rubber "as

received" and after a 12-day "soak" at the appropriate temperature. Thirty (30) cycles of loading shall be carried out on each test piece and the average value of shear modulus shall be calculated based on the first three cycles and the final three cycles.

3.5 Elastomeric Isolation Bearing Tests

A. General

1. Phases of Testing

There are two phases for testing of isolation bearings. The first phase is the testing of prototype bearings to confirm the design values for the bearings and to validate their stability under maximum loads and displacements. The second phase is a program of quality control testing during the manufacture of the production bearings.

B. Quality Control Tests

1. All bearings, including prototype, production, and extra bearings, shall be subjected to the quality control tests. For additional testing requirements for prototype bearings, see paragraph 3.5.C.
2. Connection Details

All bearings shall be tested with end-connection details that are representative of the typical connection detail for that bearing type. The connection details shall be approved by the owner's representative prior to testing.

3. Compression Tests

Each bearing shall be brought to a uniform temperature of 70 ± 10°F and shall be compression tested at that temperature. Each bearing shall first be vertically loaded to 2000 psi and the load maintained for 10 min. The load shall then be removed and the bearing "rested" for a minimum of 30 min before continuing the test. Load each bearing vertically to 1500 psi by increments of 300 psi. For each load increment, loading time shall be in the range of 1.5–3 min. After each increment of loading, the load shall be held constant for 30 sec; then the load and vertical displacement shall be measured and recorded. Unload incrementally and measure vertical displacements following the same sequence as for loading. Load shall be plotted against vertical displacement for each bearing at all load increments. The compressive stiffness shall be computed as the slope of the best-fit straight line through the load–displacement points, ignoring the zero load points. Compressive stiffness shall be recorded for each bearing. The average compressive stiffness for each bearing type shall be computed using the compressive stiffness values for all bearings of that type and shall meet the vertical stiffness requirements defined in Table 2. The bearings shall be rejected if this requirement is not satisfied. After loading to the required value of 1500 psi, increase the load to 2000 psi, then main-

tain the load for a period of not less than 1 hr. Prior to releasing the load, the bearing shall be inspected for the following faults, which, if observed, shall be cause for rejection of the bearing and replacement at the bearing manufacturer's expense:

(1) Lack of rubber-to-steel bond
(2) Laminate placement fault
(3) At least three separate surface cracks that are wider or deeper than 0.08 in.

4. Combined Compression–Shear Tests
Each bearing shall be tested in combined compression and shear subsequent to the compression tests. Each bearing shall be brought to a uniform temperature of 70 ± 10°F and shall be tested in combined compression and shear at that temperature. Each bearing shall be tested as follows:
   a. Design Displacement Test
   Each bearing shall be loaded in compression to the load of P_1 given in Table 1 for that bearing type. The compression load shall be maintained while the bearing is subjected to three fully reversed cycles at a displacement amplitude of D_D inches. At the maximum displacement of the first cycle, the bearing shear force F_m shall be recorded. A continuous plot of the shear force–displacement hysteresis loop shall be recorded. A mean shear force–displacement hysteresis loop shall be determined using the average coordinates of the three shear force–displacement cycles. The total enclosed area A_h of the mean hysteresis loop shall be computed and recorded. The effective stiffness K_{eff} of the mean curve shall be computed and recorded. The effective horizontal stiffness from the third cycle of the three fully reversed cycles shall meet the requirements of paragraph 1.4.B.1. The bearing shall be rejected if this requirement is not satisfied. Prior to releasing the axial load, the bearing shall be inspected for the following faults, which, if observed, shall be cause for rejection of the bearing and replacement of the bearing manufacturer's expense:
   (1) Lack of rubber-to-steel bond
   (2) Laminate placement fault
   (3) At least three separate surface cracks that are wider or deeper than 0.08 in.

C. Prototype Tests
1. Prototype bearings shall be new and never previously tested. Prototype bearings shall be manufactured in accordance with the specified fabrication procedures and using specified materials.
2. All prototype bearings shall be brought to a uniform temperature of 70 ± 10°F before any test and the temperature shall be maintained for all subsequent tests.

3. All prototype bearings shall be scragged before any other testing. Scragging shall consist of three fully reversed cycles of loading to a displacement of D_D inches under the compression load P_1.
4. All prototype bearings shall be tested in accordance with the Appendix to Chapter 16 of the 1997 UBC. In addition to meeting all of the UBC requirements for prototype tests, the following requirements shall also be met:
   a. Effective Stiffness
      The effective horizontal stiffness from the third cycle of the scragging test at D_D inches displacement shall meet the requirements of paragraph 1.4.B.1. No additional scragging or repetition of specified tests will be allowed on bearings that have undergone the required testing even if this will bring the stiffness within the specified range. This requirement is applicable to all elastomeric bearing types.
   b. Damping
      The total enclosed area A_h for each loop shall be computed. The effective damping ratio for each bearing type shall be computed and recorded. The effective damping of the isolation system shall be based on the test results and calculated using the formula:
      A_h^t shall be taken as the sum of the total energy dissipated by the isolation system and k_{eff}^t shall be the total stiffness of the isolation system based on the stiffness computed from the third loop of the test. The effective damping of the isolation system after corrections, as permitted in paragraph 1.4.A.3, shall meet the requirements of that paragraph. If the damping requirements are not met, the Owner's representative may reject bearings that cause the system damping to be outside the acceptable range.
5. Stability Test
   a. The stability test shall consist of one fully reversed cyclic test to D_{TM} inches displacement under a constant compressive load P_3. The load P_3 shall be the maximum specified load for a given bearing type as defined in Table 1. If the compression load on the bearing reduces from that prescribed during the shear displacement, the bearing shall be held at the first maximum displacement D_{TM} until a compression load of P_3 is reattained. At that time, the shear displacement loading may be resumed.
   b. The incremental stiffness at displacement increments of 3 in. shall be computed. The incremental stiffness shall be positive over the entire range of displacement. The test shall be repeated using the minimum downward load P_4, as defined in Table 1.
   c. For bearing test machines that are incapable of performing shear tests with a net tension load on the bearing, this test shall be performed with the minimum possible axial load.

D. Test Documentation
All test data from rubber tests and isolation bearing tests specified in this section shall be documented in a bound report entitled "Final Seismic Isolation Bearing Test Report," following completion of all production bearing tests. The final seismic isolation bearing test report shall be signed by an officer in the supplier's corporation and the responsible testing engineer.

3.6 Identification

A. Elastomeric Bearings

1. General
The bearing identification shall be stenciled in 3-in.-high characters at two (2) equally spaced locations on the outer vertical faces of the bearings and on each face of the package and shall be stamped in $\frac{1}{2}$-in.-high characters on the outer surface of the upper mounting plate.

2. Production Bearings
Each approved production bearing shall be identified by a letter and number as illustrated in the following example:

HDRB Type A	Type of bearing, as shown on drawings, for HDR bearings
(or LRB Type A	Type of bearing, as shown on drawings, for LR bearings)
027	Fabrication sequence number

B. Extra Bearings
Each approved extra bearing shall be marked "EXTRA" with the corresponding bearing type designation letter. The extra bearings shall be located on the job site as directed by the owner's representative. The extra bearings shall be set in reaction frames with loads as specified.

3.7 Delivery, Storage, and Handling

A. The bearing manufacturer shall provide written handling, lifting, and installation instructions for the bearings.

B. Deliver production bearings and extra bearings in protective packaging to the job site. Any damaged bearings or components shall not be delivered. Any damaged or scratched bearings shall be replaced by new bearings of the same type. Delivery of bearings shall be at the bearing manufacturer's expense.

C. Bearings shall be stored on wood pallets provided by the bearing manufacturer to allow for transport by forklift around the job site. Store bearings in a clean place and protect from dirt, fumes, construction debris, and physical damage.

D. Care shall be exercised in the handling of the bearings at all times to prevent damage, breaking, denting, or scoring.

E. Comply with bearing manufacturer's rigging and installation instructions for unloading isolation bearings and moving them to their final location.

F. Deliver bolting templates to the job site for use by the design/build contractor. Package templates to prevent damage, bending, or denting.

APPENDIX

COMPANION SOFTWARE AND EARTHQUAKE DATA FILES

The CD-ROM attached to the back cover of this book contains the following:

1. the educational version of the SAP-2000 Nonlinear software system including a complete set of user manuals, verification manuals, and multimedia tutorials;
2. SAP-2000 input files and AVI earthquake response animation files for examples presented in Chapter 9;
3. a selected set of 14 earthquake time histories (two horizontal components and one vertical component for each) and the corresponding Fourier and response spectra information; and
4. the ISOSEL bearing optimization program illustrated in Chapter 9, including the example data file used in that chapter.

The companion CD-ROM has an auto-start feature. Once you place the disc in your CD-ROM drive, the SAP-2000 demonstration program automatically starts. Follow the directions on your screen to install SAP-2000 and to view tutorials or view/print selected pages of the user manuals.

To install ISOSEL, you need to exit from the SAP-2000 demonstration program by clicking the cross on the top right-hand corner of the SAP-2000 window. Then, use Windows Explorer from the Windows 95 (or NT) Start menu and double click on the Setup icon contained in the \ISOBOOK\SETUP folder of the CD-ROM. The setup program will guide you through the rest of the installation process. The ISOSEL setup program also installs the SAP-2000 data files and the earthquake time histories that are used as examples in the book.

The selected earthquake records are placed in the \ISOBOOK\TIMEHIS folder of the disc. Each three-component record is represented by two files. The

acceleration, velocity, and displacement time histories of all three components (channels) for each record are contained in a single file with a .V2 extension. The Fourier and response spectra for the three channels are contained in files with a .V3 extension. These earthquake records have been selected to represent a wide range of ground motion characteristics that need to be considered in the design of seismic-isolated structures. Several of these records represent near-fault effects and large ground velocities and are specifically suggested by CDMG for design of seismic-isolated structures. These include:

- the El Centro Array #6 station record of the 1979 Imperial Valley earthquake (ARRAY06.V*);
- the Hollister and Lexington Dam station records of the 1989 Loma Prieta earthquake (HOLLISTE.V*, LEXINGT.V*);
- the Petrolia station record of the 1992 Petrolia earthquake (PETROLIA.V*);
- the Lucerne Valley and Yermo station records of the 1992 Landers earthquake (LUCERNE.V*, YERMO.V*); and
- the Sylmar (County Hospital Building Parking Lot) and the Newhall Fire Station records of the 1994 Northridge earthquake (SYLMARFF.V*, NEWHALL.V*)

Other files included in the selection compliment the above records by presenting high-frequency, large ground accelerations with less significant long-period content. These include:

- the Corralitos Station record of the 1989 Loma Prieta earthquake (CORRALIT.V*) and
- the Santa Monica City Hall Grounds record of the 1994 Northridge earthquake (S_MONICA.V*).

The rest of the files are intended to represent more moderate ground shaking at various site conditions. These are:

- the Oakland Outer Harbor Wharf station record of the 1989 Loma Prieta earthquake (OAK_WHAF.V*);
- the Pomona (4th and Locust) station record of the 1990 Upland earthquake (POMONA.V*);
- the Altadena (Eaton Canyon Park) station record of the 1991 Sierra Madre earthquake (ALTADENA.V*); and
- the Century City (LACC North) station record of the 1994 Northridge earthquake (LACC_NOR.V*).

The format and contents of typical time history and response spectra data files and plots of acceleration, velocity, and displacement time histories for the horizontal components of the selected records are included in this appendix.

Sample CDMG Time-Series File Contents (*.V2)

Channel Header Information

```
CORRECTED ACCELEROGRAM   24514-S5254-94017.03       CHAN  1:  90 DEG      FROM
UNCORRECTED ACCELEROGRAM DATA                PROCESSED: 01/31/94, CDMG QN94A514
NORTHRIDGE EARTHQUAKE
JANUARY 17, 1994 04:31 PST                 (ORIGIN(CIT): 01/17/94, 12:30:55.4 GMT)
24514-S5254-94017.03                  TRIGGER TIME: 01/17/94, 12:31:00.2 UTC
STATION NO. 24514   34.326N, 118.444W      SMA-1  S/N 5254
SYLMAR - COUNTY HOSP. PARKING LOT
CHAN  1:  90 DEG
NORTHRIDGE EARTHQUAKE      JANUARY 17, 1994 04:31 PST
HYPOCENTER(CIT): 34.215N, 118.538W, H=18KM. ML=6.6, MW=6.7(CIT); MS=6.7(NEIC)
INSTR PERIOD =  .0368 SEC,  DAMPING =  .600,  SENSITIVITY = 1.70 CM/G.
                           RECORD LENGTH = 59.980 SEC.
```

```
4.080   592.639     6.480   -76.936     6.760   -15.217    -2.103      .120
   23.000      .020      .020     -.466      .000      .000      .000      .000
     .000      .000      .000      .000      .000      .000      .000      .000
     .000      .000      .000      .000      .000      .000      .000      .000
     .000      .000      .000      .000
```

Acceleration Data for the First Channel

```
3000 POINTS OF ACCEL DATA EQUALLY SPACED AT  .020 SEC.  (UNITS: CM/SEC/SEC)
    6.631     3.507     1.628     1.105      .426      .239     -.268    -1.836
   -1.490     1.413    -1.058     1.669    11.676    11.498     -.292   -16.718
  -12.282    -3.280   -12.029    -6.913     6.389     2.310    -5.904     9.685
   32.806    23.401   -15.683   -15.219     8.594     3.664   -15.019   -12.219
```

```
    -.695      .401     -.830    -2.854    -3.932    -3.534    -2.915    -3.531
   -3.262    -4.258    -3.325    -3.853    -2.297     -.784     1.047     2.926
    2.383     2.819     2.886     3.155     2.011     1.594     2.842     1.425
     .093    -1.018    -1.129      .220     1.364     2.051     3.077     3.217
```

Velocity Data for the First Channel

```
3000 POINTS OF VELOC DATA EQUALLY SPACED AT  .020 SEC.  (UNITS: CM/SEC)
   -2.103    -2.001    -1.949    -1.921    -1.905    -1.897    -1.897    -1.917
   -1.949    -1.949    -1.946    -1.938    -1.802    -1.568    -1.454    -1.622
   -1.910    -2.064    -2.215    -2.402    -2.407    -2.317    -2.349    -2.308
   -1.880    -1.314    -1.234    -1.539    -1.602    -1.476    -1.590    -1.857
```

```
    -.123     -.127     -.131     -.168     -.237     -.312     -.377     -.441
    -.510     -.585     -.661     -.734     -.795     -.826     -.823     -.784
    -.731     -.679     -.622     -.561     -.510     -.474     -.429     -.387
    -.372     -.381     -.402     -.412     -.396     -.362     -.310     -.248
```

Displacement Data for the First Channel

```
3000 POINTS OF DISPL DATA EQUALLY SPACED AT  .020 SEC.  (UNITS: CM)
    -.466     -.507     -.546     -.585     -.623     -.661     -.699     -.737
    -.775     -.814     -.853     -.892     -.929     -.963     -.992    -1.022
```

```
     .329      .314      .302      .290      .279      .270      .261      .253
     .245      .238      .230      .222      .214      .206      .200      .194
```

End of First-Channel Data and Beginning of Data for Next Channel

```
/&  ----------  END OF DATA FOR CHANNEL  1  ----------
CORRECTED ACCELEROGRAM   24514-S5254-94017.03       CHAN  2: UP          FROM
UNCORRECTED ACCELEROGRAM DATA                PROCESSED: 01/31/94, CDMG QN94A514
NORTHRIDGE EARTHQUAKE
JANUARY 17, 1994 04:31 PST                 (ORIGIN(CIT): 01/17/94, 12:30:55.4 GMT)
24514-S5254-94017.03                  TRIGGER TIME: 01/17/94, 12:31:00.2 UTC
STATION NO. 24514   34.326N, 118.444W      SMA-1  S/N 5254
SYLMAR - COUNTY HOSP. PARKING LOT
CHAN  2: UP
```

Sample CDMG Response Spectra File Contents (*.V3)

File Header Information

```
RESPONSE AND FOURIER AMPLITUDE SPECTRA (88 PERIODS,  .04 - 12.0 SEC)   FOR
CORRECTED ACCELEROGRAM   24514-S5254-94017.03       CHAN  1:  90 DEG     FROM
UNCORRECTED ACCELEROGRAM DATA                 PROCESSED: 01/31/94, CDMG QN94A514
NORTHRIDGE EARTHQUAKE
JANUARY 17, 1994 04:31 PST                (ORIGIN(CIT): 01/17/94, 12:30:55.4 GMT)
24514-S5254-94017.03                 TRIGGER TIME: 01/17/94, 12:31:00.2 UTC
STATION NO. 24514   34.326N, 118.444W     SMA-1  S/N 5254
SYLMAR - COUNTY HOSP. PARKING LOT
CHAN  1:  90 DEG
                                    .....
                                    .....
                                    .....
                                    .....
```

Units identifier line

```
UNITS FOR SPECTRA ARE INCHES AND SEC, EXCEPT SA IS IN FRACTION OF G.
                                    .....
                                    .....
                                    .....
                                    .....
```

Damping values line
vibration periods
reported (sec)

```
      .000      .020      .050      .100      .200
      .040      .042      .044      .046      .048      .050      .055      .060
      .065      .070      .075      .080      .085      .090      .095      .100
                                    .....
                                    .....
                                    .....
                                    .....
     7.500     8.000     8.500     9.000     9.500    10.000    11.000    12.000
    13.000    14.000    15.000      .000      .000      .000      .000      .000
      .000      .000      .000      .000
```

End-of-periods line

Fourier Amplitude Spectra

```
FOURIER AMPLITUDE SPECTRA IN IN/SEC.
  .517E-01  .427E-02  .644E+00  .189E+00  .584E+00  .456E+00  .830E+00  .319E+00
  .175E+01  .244E+01  .154E+01  .485E+01  .249E+01  .877E+00  .185E+01  .734E+01
                                    .....
                                    .....
                                    .....
                                    .....
  .000E+00  .000E+00  .000E+00  .000E+00
```

Response Spectra for Various Damping Levels

```
DAMPING =  .00. DATA OF SD,SV,SA,PSSV,TTSD,TTSV,TTSA :
  .952E-02  .110E-01  .136E-01  .128E-01  .157E-01  .149E-01  .262E-01  .275E-01
  .339E-01  .480E-01  .516E-01  .860E-01  .698E-01  .668E-01  .907E-01  .123E+00
                                    .....
                                    .....
                                    .....
                                    .....
DAMPING =  .20. DATA OF SD,SV,SA,PSSV,TTSD,TTSV,TTSA :
  .948E-02  .105E-01  .115E-01  .126E-01  .138E-01  .150E-01  .185E-01  .223E-01
  .262E-01  .306E-01  .357E-01  .420E-01  .491E-01  .567E-01  .653E-01  .732E-01
                                    .....
                                    .....
                                    .....
                                    .....
.000E+00  .000E+00  .000E+00  .000E+00
```

End of First-Channel Data and Beginning of Data for Next Channel

```
/&  ----------  END OF SPECTRAL DATA FOR CHANNEL  1  ----------
RESPONSE AND FOURIER AMPLITUDE SPECTRA (88 PERIODS,  .04 - 12.0 SEC)   FOR
CORRECTED ACCELEROGRAM   24514-S5254-94017.03       CHAN  2: UP          FROM
UNCORRECTED ACCELEROGRAM DATA                 PROCESSED: 01/31/94, CDMG QN94A514
NORTHRIDGE EARTHQUAKE
                                    .....
                                    .....
                                    .....
                                    .....
                                    .....
                                    .....
                                    .....
                                    .....
```

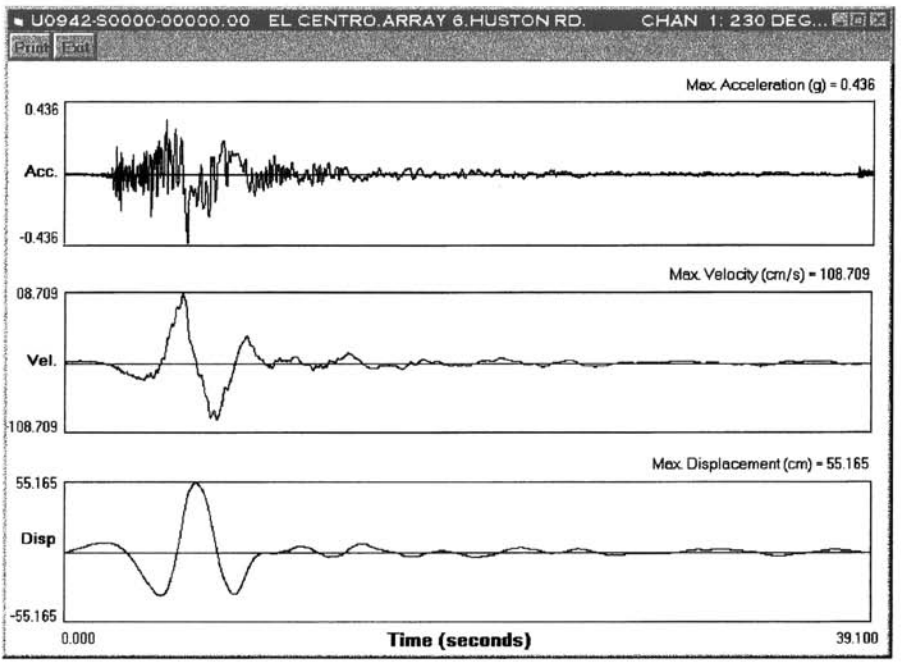
U0942-S0000-00000.00 EL CENTRO.ARRAY 6.HUSTON RD. CHAN 1: 230 DEG...
Print
Exit
Max. Acceleration (g) = 0.436
0.436
Acc.
-0.436
Max. Velocity (cm/s) = 108.709
08.709
Vel.
108.709
Max. Displacement (cm) = 55.165
55.165
Disp
-55.165
0.000
Time (seconds)
39.100

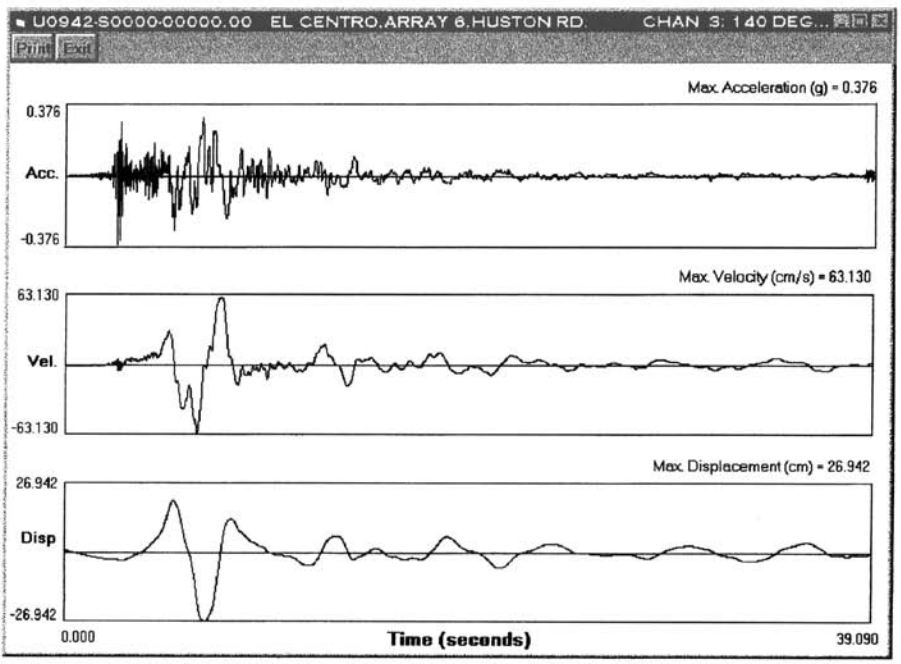
U0942-S0000-00000.00 EL CENTRO.ARRAY 6.HUSTON RD. CHAN 3: 140 DEG...
Print
Exit
Max. Acceleration (g) = 0.376
0.376
Acc.
-0.376
Max. Velocity (cm/s) = 63.130
63.130
Vel.
-63.130
Max. Displacement (cm) = 26.942
26.942
Disp
-26.942
0.000
Time (seconds)
39.090

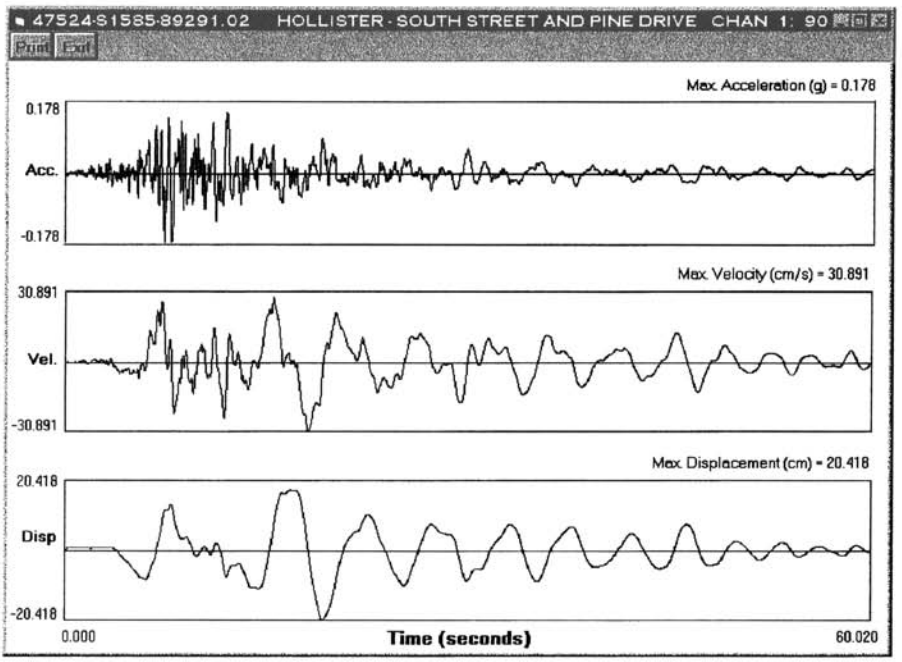
47524-S1585-89291.02 HOLLISTER - SOUTH STREET AND PINE DRIVE CHAN 1: 90
Print Exit
Max. Acceleration (g) = 0.178
0.178
Acc.
-0.178
Max. Velocity (cm/s) = 30.891
30.891
Vel.
-30.891
Max. Displacement (cm) = 20.418
20.418
Disp
-20.418
0.000
Time (seconds)
60.020

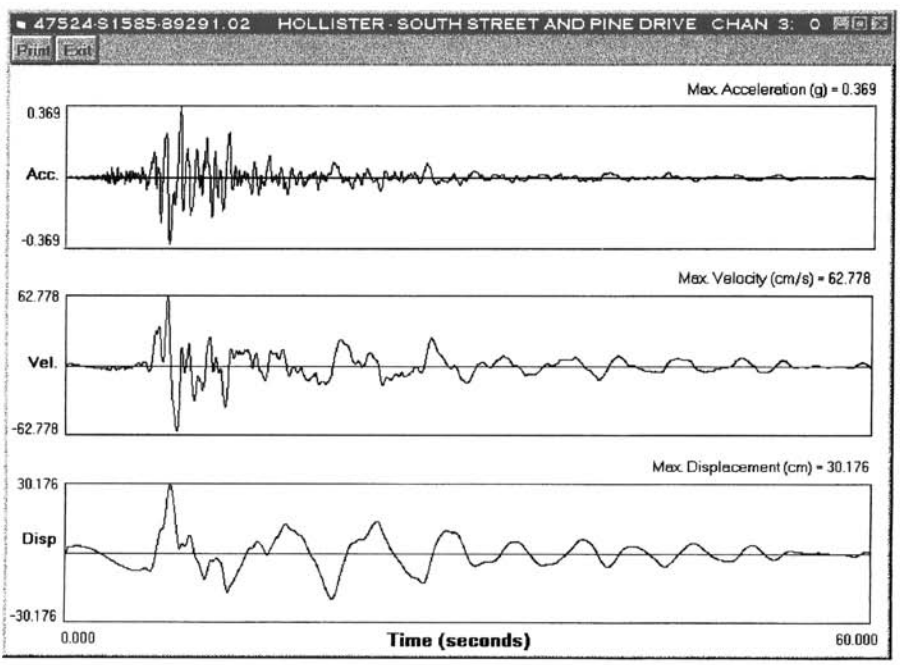
47524-S1585-89291.02 HOLLISTER - SOUTH STREET AND PINE DRIVE CHAN 3: 0
Print Exit
Max. Acceleration (g) = 0.369
0.369
Acc.
-0.369
Max. Velocity (cm/s) = 62.778
62.778
Vel.
-62.778
Max. Displacement (cm) = 30.176
30.176
Disp
-30.176
0.000
Time (seconds)
60.000

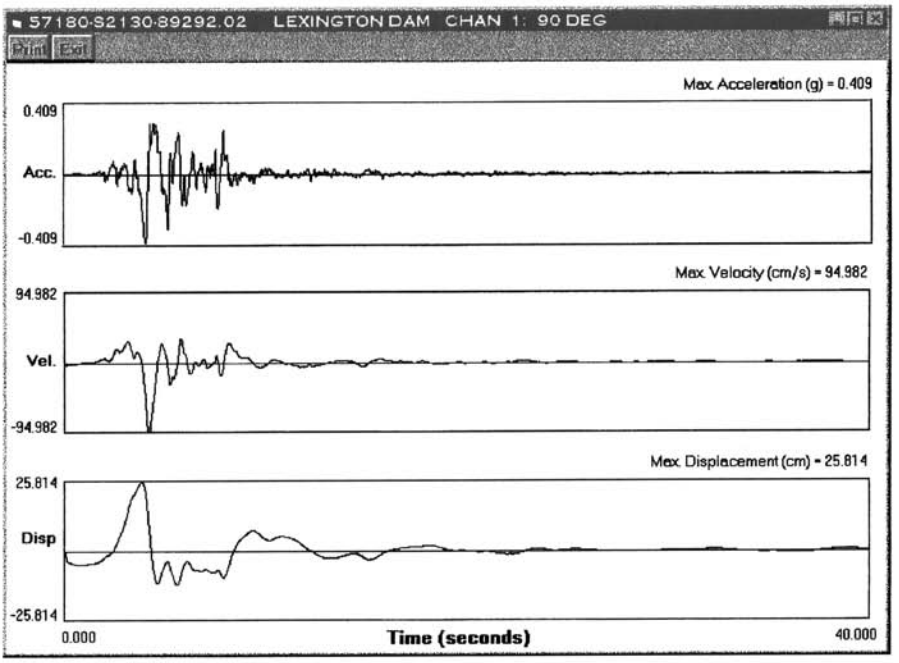
57180-S2130-89292.02 LEXINGTON DAM CHAN 1: 90 DEG
Print
Exit
Max. Acceleration (g) = 0.409
0.409
Acc.
-0.409
Max. Velocity (cm/s) = 94.982
94.982
Vel.
-94.982
Max. Displacement (cm) = 25.814
25.814
Disp
-25.814
0.000
Time (seconds)
40.000

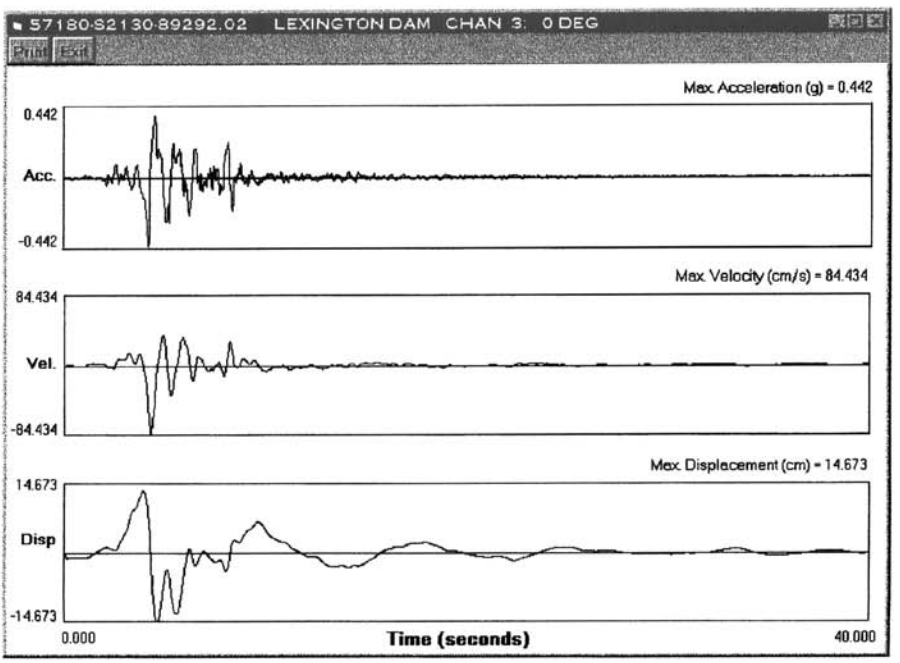
57180-S2130-89292.02 LEXINGTON DAM CHAN 3: 0 DEG
Print
Exit
Max. Acceleration (g) = 0.442
0.442
Acc.
-0.442
Max. Velocity (cm/s) = 84.434
84.434
Vel.
-84.434
Max. Displacement (cm) = 14.673
14.673
Disp
-14.673
0.000
Time (seconds)
40.000

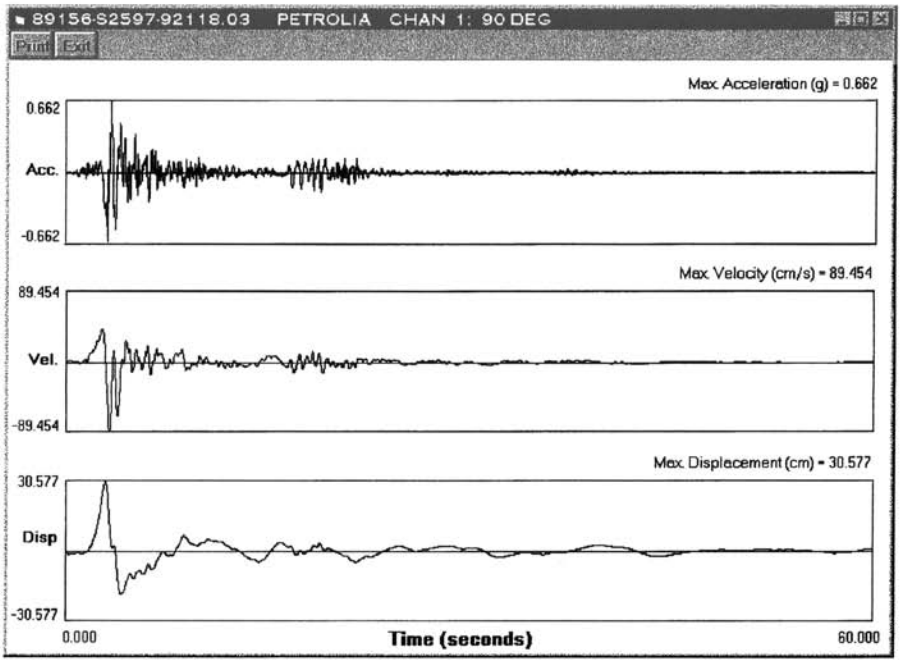
89156-S2597-92118.03 PETROLIA CHAN 1: 90 DEG
Print
Exit
Max. Acceleration (g) = 0.662
0.662
Acc.
-0.662
Max. Velocity (cm/s) = 89.454
89.454
Vel.
-89.454
Max. Displacement (cm) = 30.577
30.577
Disp
-30.577
0.000
Time (seconds)
60.000

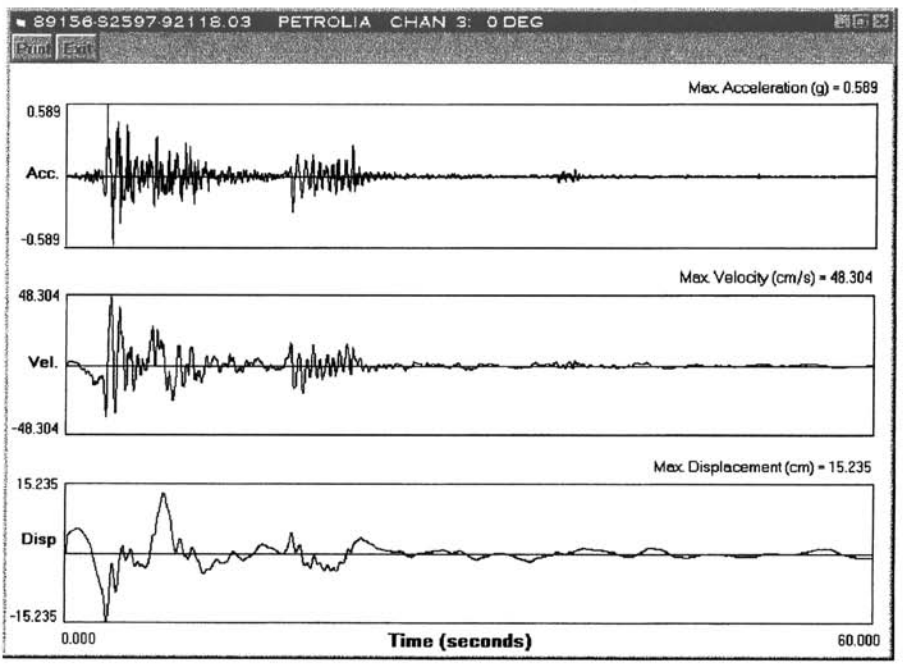
89156-S2597-92118.03 PETROLIA CHAN 3: 0 DEG
Print
Exit
Max. Acceleration (g) = 0.589
0.589
Acc.
-0.589
Max. Velocity (cm/s) = 48.304
48.304
Vel.
-48.304
Max. Displacement (cm) = 15.235
15.235
Disp
-15.235
0.000
Time (seconds)
60.000

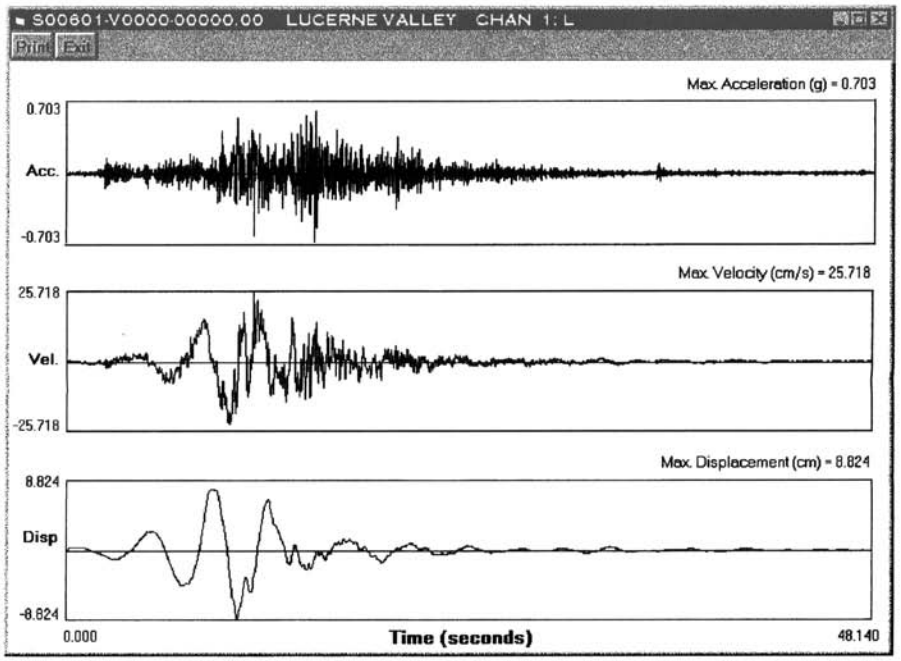
S00601-V0000-00000.00 LUCERNE VALLEY CHAN 1: L
Print Exit
Max. Acceleration (g) = 0.703
0.703
Acc.
-0.703
Max. Velocity (cm/s) = 25.718
25.718
Vel.
-25.718
Max. Displacement (cm) = 8.824
8.824
Disp
-8.824
0.000
Time (seconds)
48.140

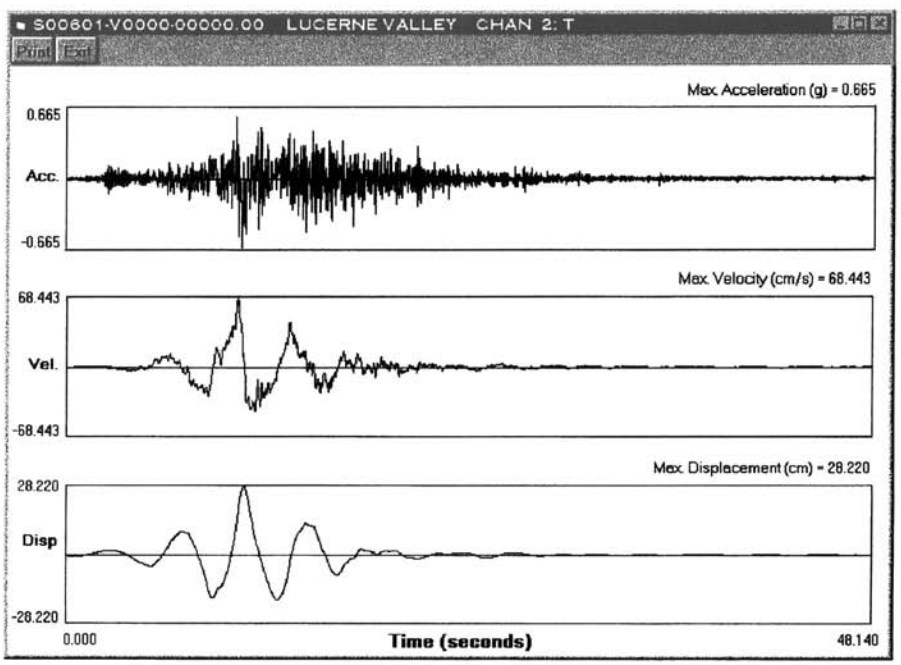
S00601-V0000-00000.00 LUCERNE VALLEY CHAN 2: T
Print Exit
Max. Acceleration (g) = 0.665
0.665
Acc.
-0.665
Max. Velocity (cm/s) = 68.443
68.443
Vel.
-68.443
Max. Displacement (cm) = 28.220
28.220
Disp
-28.220
0.000
Time (seconds)
48.140

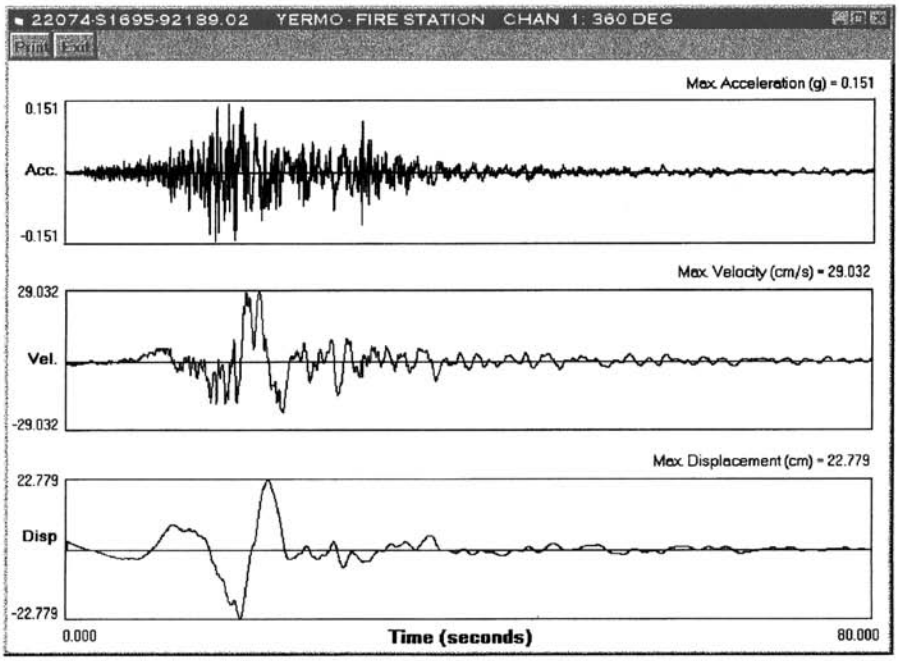
22074-S1695-92189.02 YERMO - FIRE STATION CHAN 1: 360 DEG
Print
Exit
Max. Acceleration (g) = 0.151
0.151
Acc.
-0.151
Max. Velocity (cm/s) = 29.032
29.032
Vel.
-29.032
Max. Displacement (cm) = 22.779
22.779
Disp
-22.779
0.000
Time (seconds)
80.000

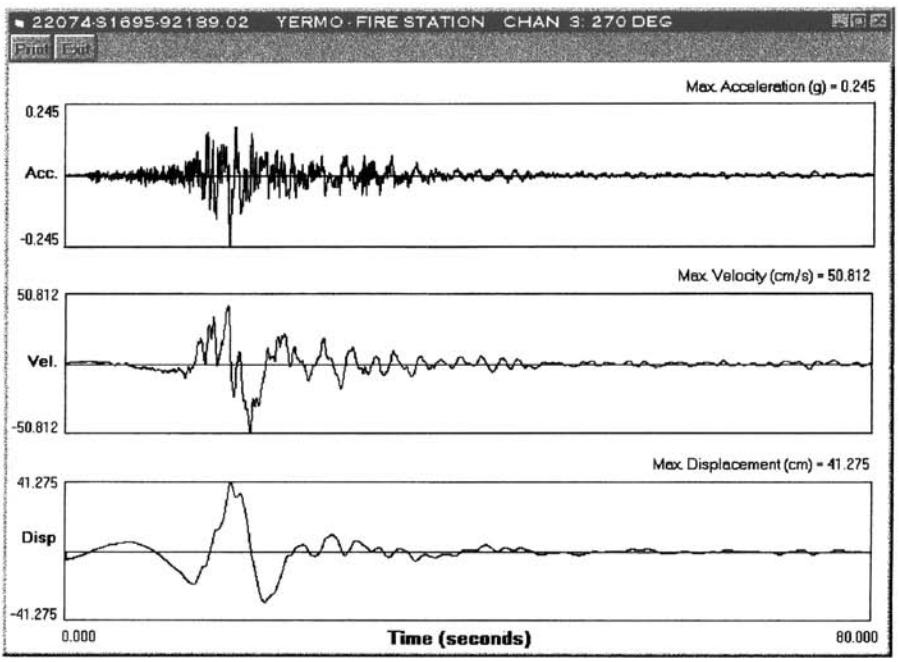
22074-S1695-92189.02 YERMO - FIRE STATION CHAN 3: 270 DEG
Print
Exit
Max. Acceleration (g) = 0.245
0.245
Acc.
-0.245
Max. Velocity (cm/s) = 50.812
50.812
Vel.
-50.812
Max. Displacement (cm) = 41.275
41.275
Disp
-41.275
0.000
Time (seconds)
80.000

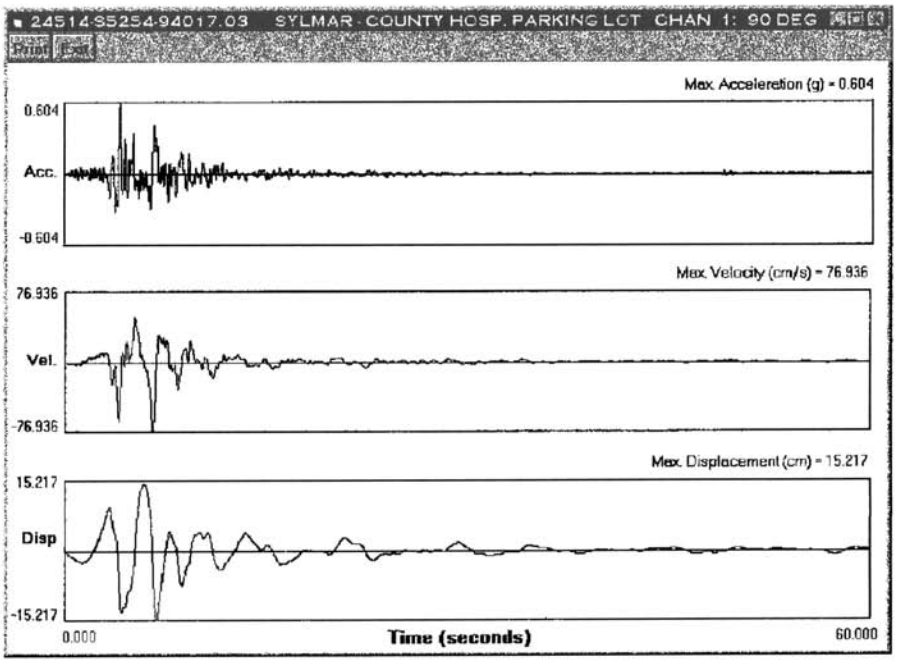
24514-S5254-94017.03 SYLMAR - COUNTY HOSP. PARKING LOT CHAN 1: 90 DEG
Print
Exit
Max. Acceleration (g) = 0.604
0.604
Acc.
-0.604
Max. Velocity (cm/s) = 76.936
76.936
Vel.
-76.936
Max. Displacement (cm) = 15.217
15.217
Disp
-15.217
0.000
Time (seconds)
60.000

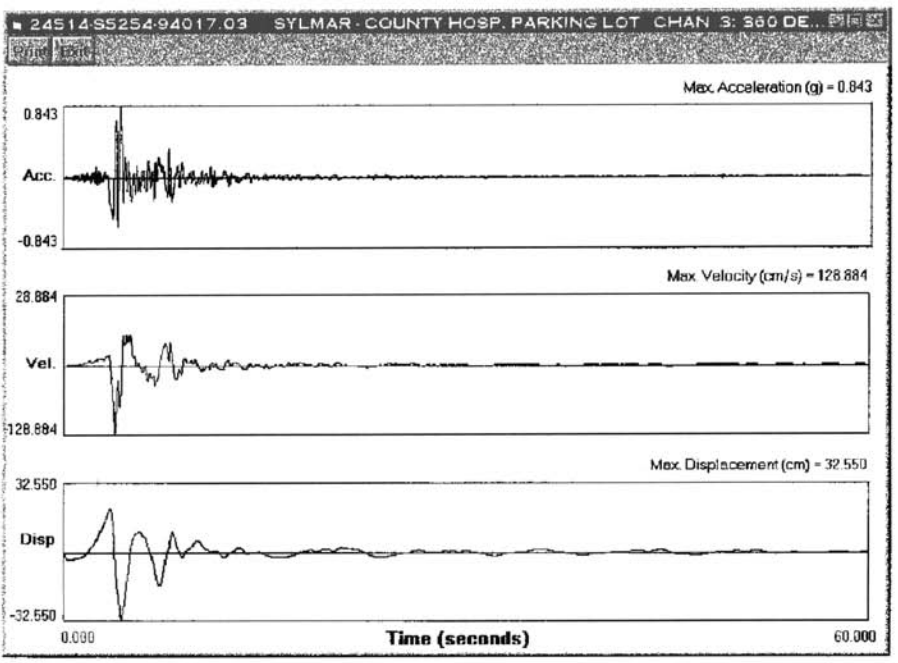
24514-S5254-94017.03 SYLMAR - COUNTY HOSP. PARKING LOT CHAN 3: 360 DE...
Print
Exit
Max. Acceleration (g) = 0.843
0.843
Acc.
-0.843
Max. Velocity (cm/s) = 128.884
28.884
Vel.
-128.884
Max. Displacement (cm) = 32.550
32.550
Disp
-32.550
0.000
Time (seconds)
60.000

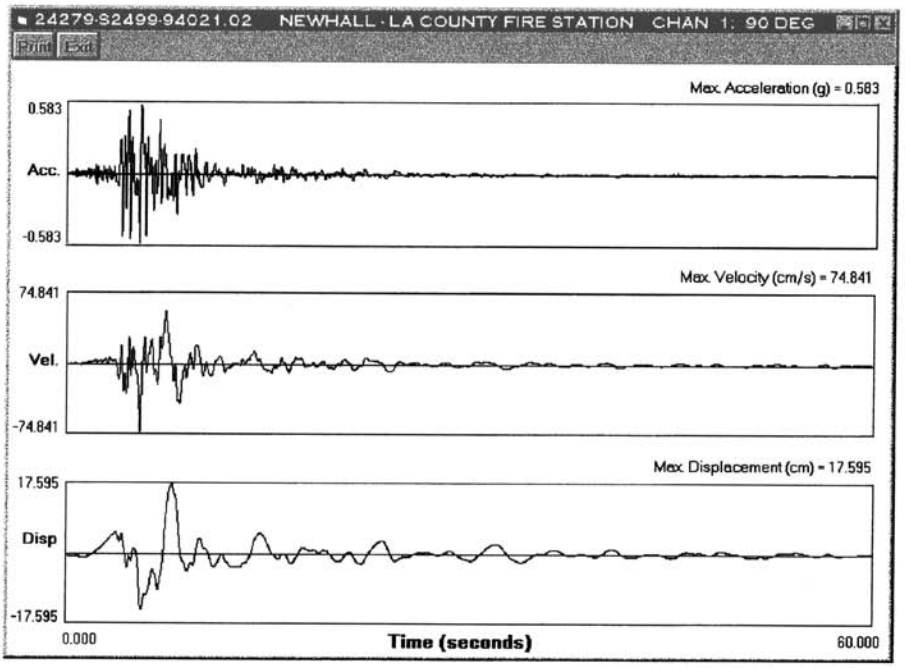
24279-S2499-94021.02 NEWHALL - LA COUNTY FIRE STATION CHAN 1: 90 DEG
Print
Exit
Max. Acceleration (g) = 0.583
0.583
Acc.
-0.583
Max. Velocity (cm/s) = 74.841
74.841
Vel.
-74.841
Max. Displacement (cm) = 17.595
17.595
Disp
-17.595
0.000
Time (seconds)
60.000

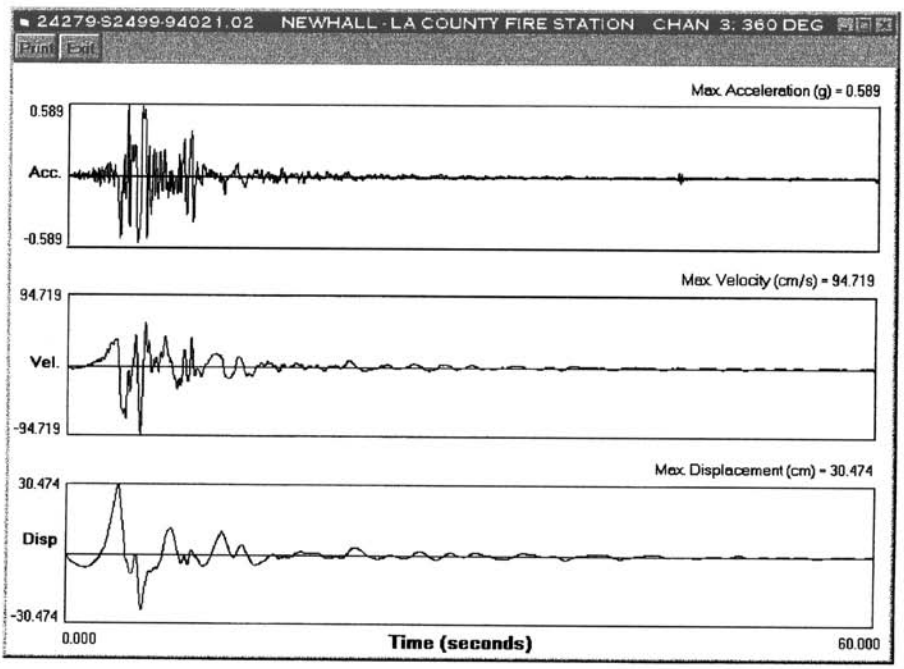
24279-S2499-94021.02 NEWHALL - LA COUNTY FIRE STATION CHAN 3: 360 DEG
Print
Exit
Max. Acceleration (g) = 0.589
0.589
Acc.
-0.589
Max. Velocity (cm/s) = 94.719
94.719
Vel.
-94.719
Max. Displacement (cm) = 30.474
30.474
Disp
-30.474
0.000
Time (seconds)
60.000

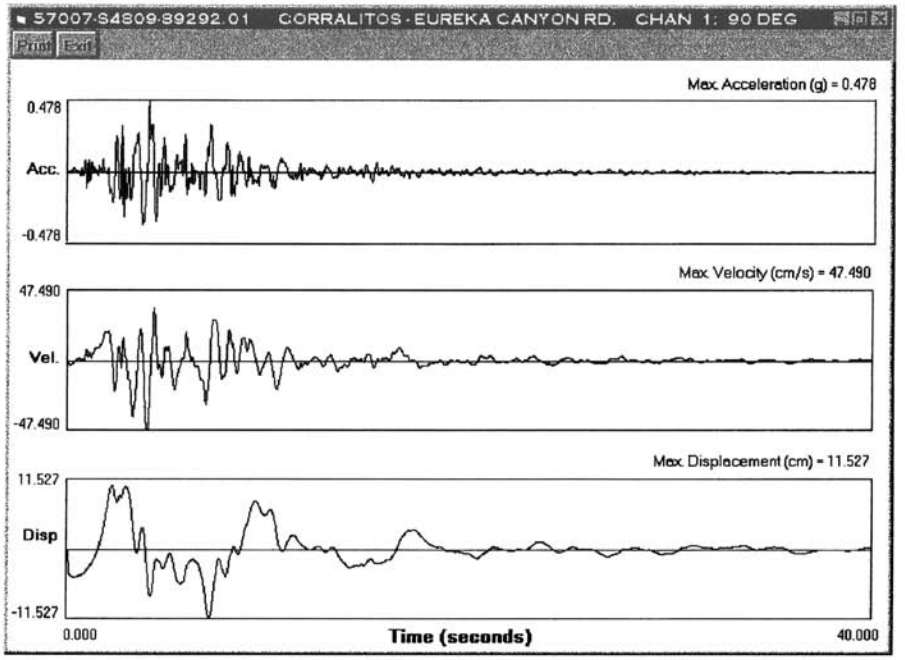
57007-S4809-89292.01 CORRALITOS - EUREKA CANYON RD. CHAN 1: 90 DEG
Print
Exit
Max. Acceleration (g) = 0.478
0.478
Acc.
-0.478
Max. Velocity (cm/s) = 47.490
47.490
Vel.
-47.490
Max. Displacement (cm) = 11.527
11.527
Disp
-11.527
0.000
Time (seconds)
40.000

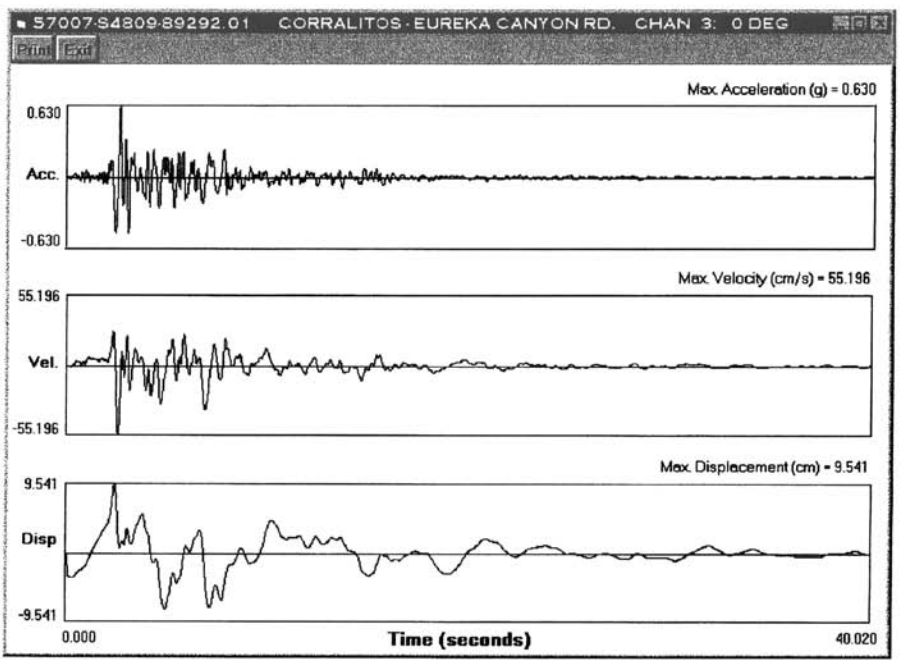
57007-S4809-89292.01 CORRALITOS - EUREKA CANYON RD. CHAN 3: 0 DEG
Print
Exit
Max. Acceleration (g) = 0.630
0.630
Acc.
-0.630
Max. Velocity (cm/s) = 55.196
55.196
Vel.
-55.196
Max. Displacement (cm) = 9.541
9.541
Disp
-9.541
0.000
Time (seconds)
40.020

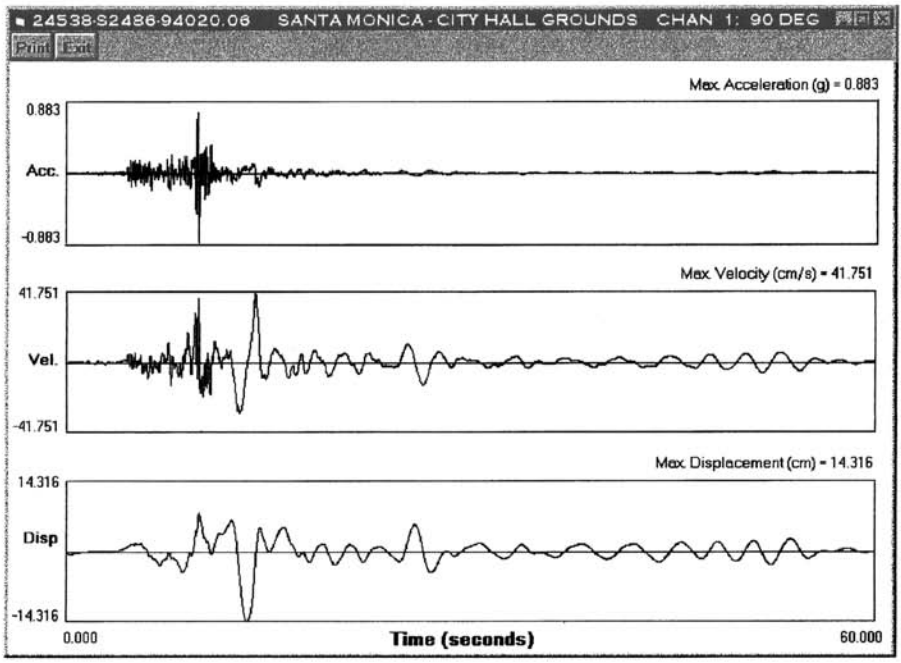
24538-S2486-94020.06 SANTA MONICA - CITY HALL GROUNDS CHAN 1: 90 DEG
Print
Exit
Max. Acceleration (g) = 0.883
0.883
Acc.
-0.883
Max. Velocity (cm/s) = 41.751
41.751
Vel.
-41.751
Max. Displacement (cm) = 14.316
14.316
Disp
-14.316
0.000
Time (seconds)
60.000

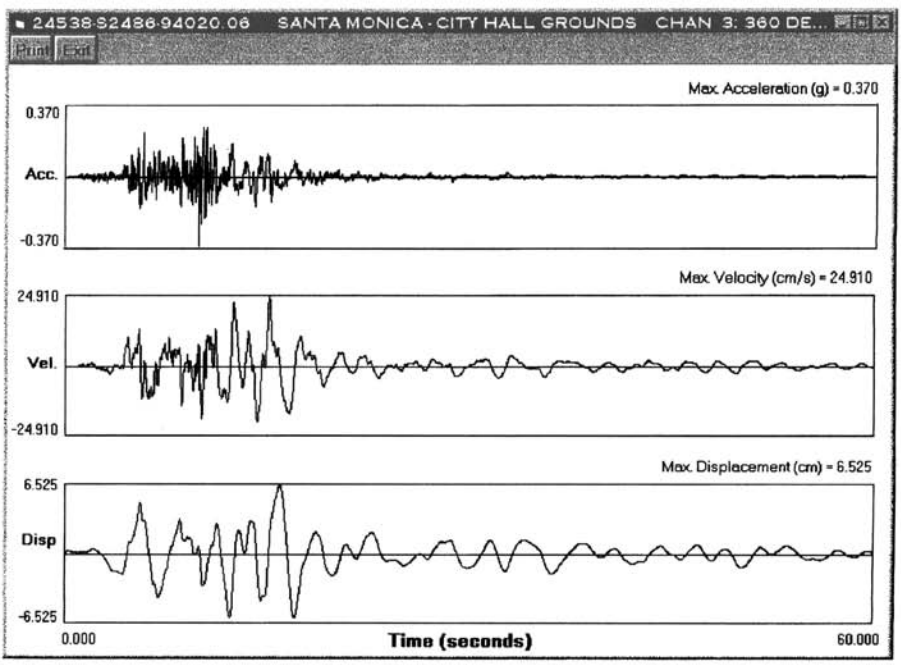
24538-S2486-94020.06 SANTA MONICA - CITY HALL GROUNDS CHAN 3: 360 DE...
Print
Exit
Max. Acceleration (g) = 0.370
0.370
Acc.
-0.370
Max. Velocity (cm/s) = 24.910
24.910
Vel.
-24.910
Max. Displacement (cm) = 6.525
6.525
Disp
-6.525
0.000
Time (seconds)
60.000

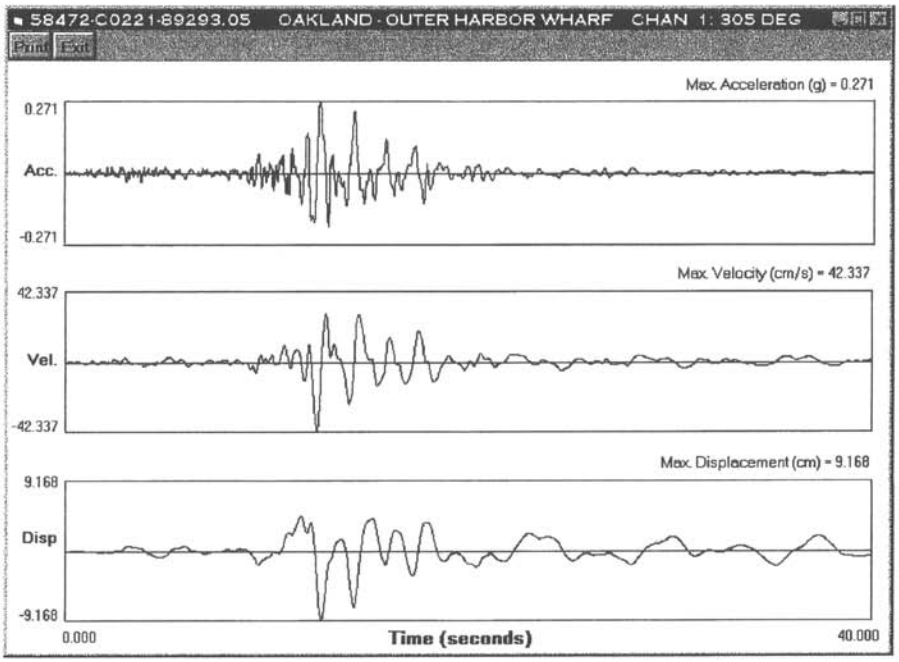
58472-C0221-89293.05 OAKLAND - OUTER HARBOR WHARF CHAN 1: 305 DEG
Print
Exit
Max. Acceleration (g) = 0.271
0.271
Acc.
-0.271
Max. Velocity (cm/s) = 42.337
42.337
Vel.
-42.337
Max. Displacement (cm) = 9.168
9.168
Disp
-9.168
0.000
Time (seconds)
40.000

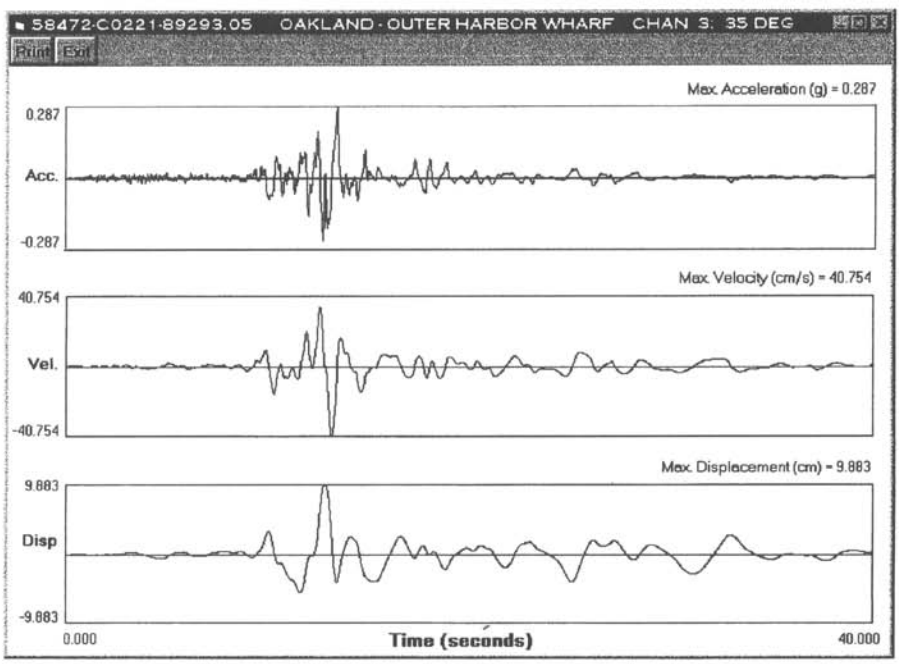
58472-C0221-89293.05 OAKLAND - OUTER HARBOR WHARF CHAN 3: 35 DEG
Print
Exit
Max. Acceleration (g) = 0.287
0.287
Acc.
-0.287
Max. Velocity (cm/s) = 40.754
40.754
Vel.
-40.754
Max. Displacement (cm) = 9.883
9.883
Disp
-9.883
0.000
Time (seconds)
40.000

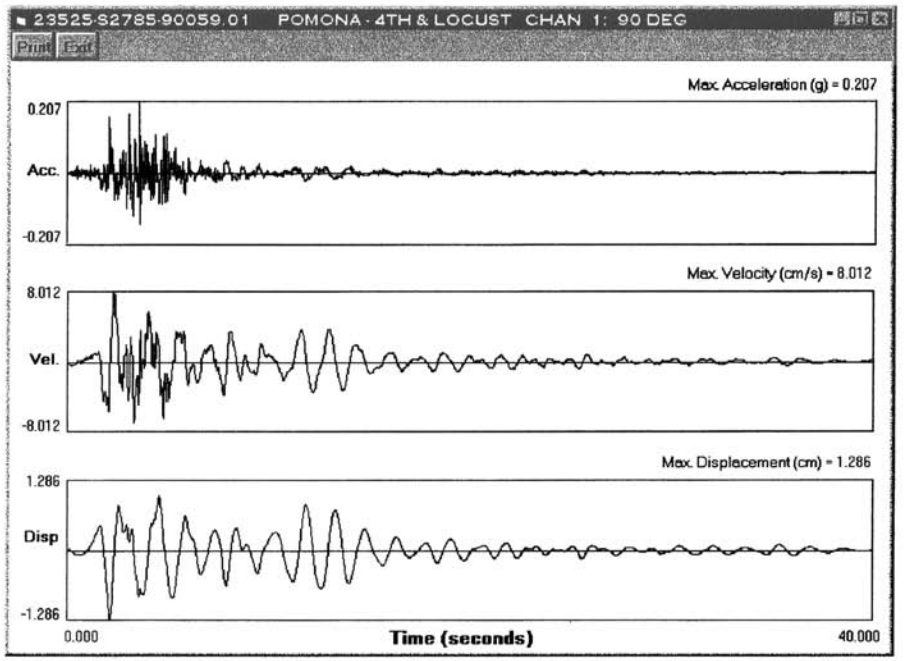
23525-S2785-90059.01 POMONA - 4TH & LOCUST CHAN 1: 90 DEG
Print
Exit
Max. Acceleration (g) = 0.207
0.207
Acc.
-0.207
Max. Velocity (cm/s) = 8.012
8.012
Vel.
-8.012
Max. Displacement (cm) = 1.286
1.286
Disp
-1.286
0.000
Time (seconds)
40.000

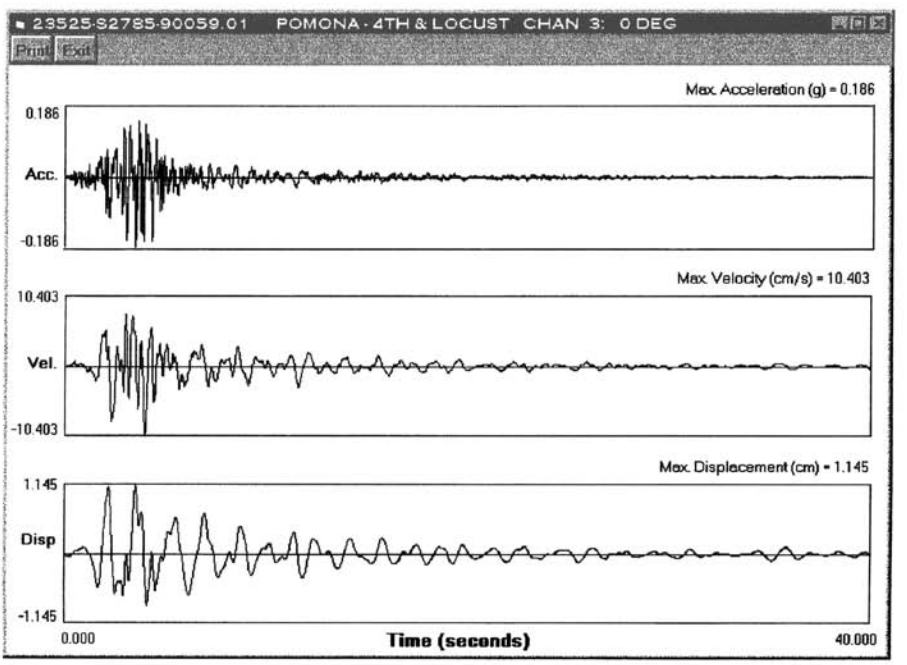
23525-S2785-90059.01 POMONA - 4TH & LOCUST CHAN 3: 0 DEG
Print
Exit
Max. Acceleration (g) = 0.186
0.186
Acc.
-0.186
Max. Velocity (cm/s) = 10.403
10.403
Vel.
-10.403
Max. Displacement (cm) = 1.145
1.145
Disp
-1.145
0.000
Time (seconds)
40.000

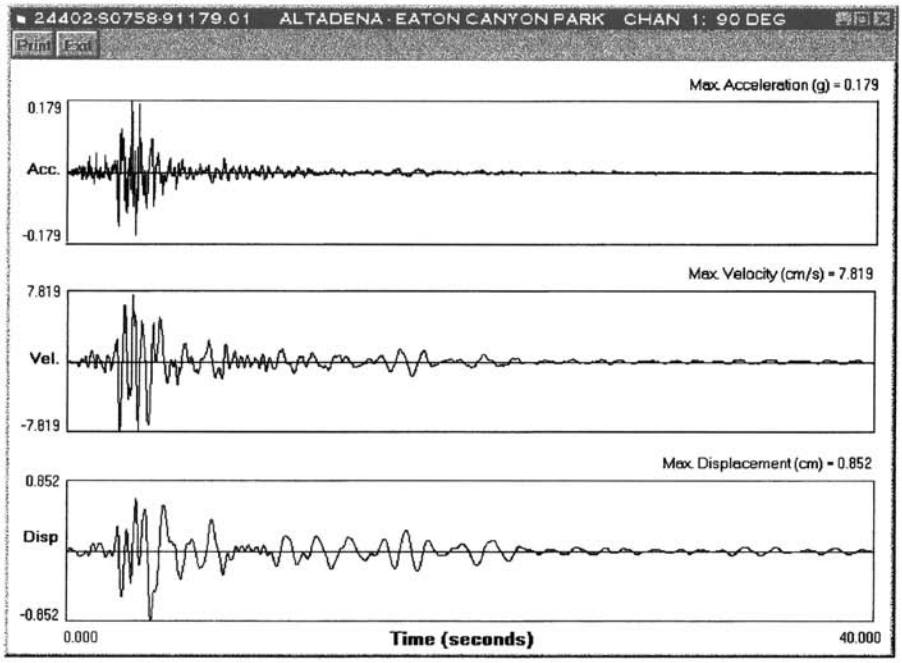
24402-S0758-91179.01 ALTADENA - EATON CANYON PARK CHAN 1: 90 DEG
Print
Exit
Max. Acceleration (g) = 0.179
0.179
Acc.
-0.179
Max. Velocity (cm/s) = 7.819
7.819
Vel.
-7.819
Max. Displacement (cm) = 0.852
0.852
Disp
-0.852
0.000
Time (seconds)
40.000

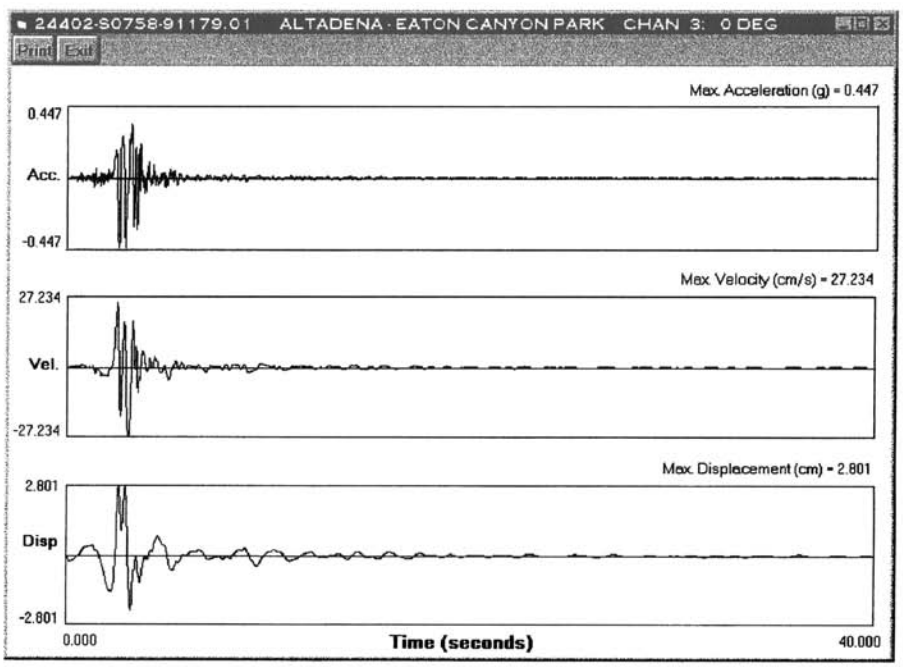
24402-S0758-91179.01 ALTADENA - EATON CANYON PARK CHAN 3: 0 DEG
Print
Exit
Max. Acceleration (g) = 0.447
0.447
Acc.
-0.447
Max. Velocity (cm/s) = 27.234
27.234
Vel.
-27.234
Max. Displacement (cm) = 2.801
2.801
Disp
-2.801
0.000
Time (seconds)
40.000

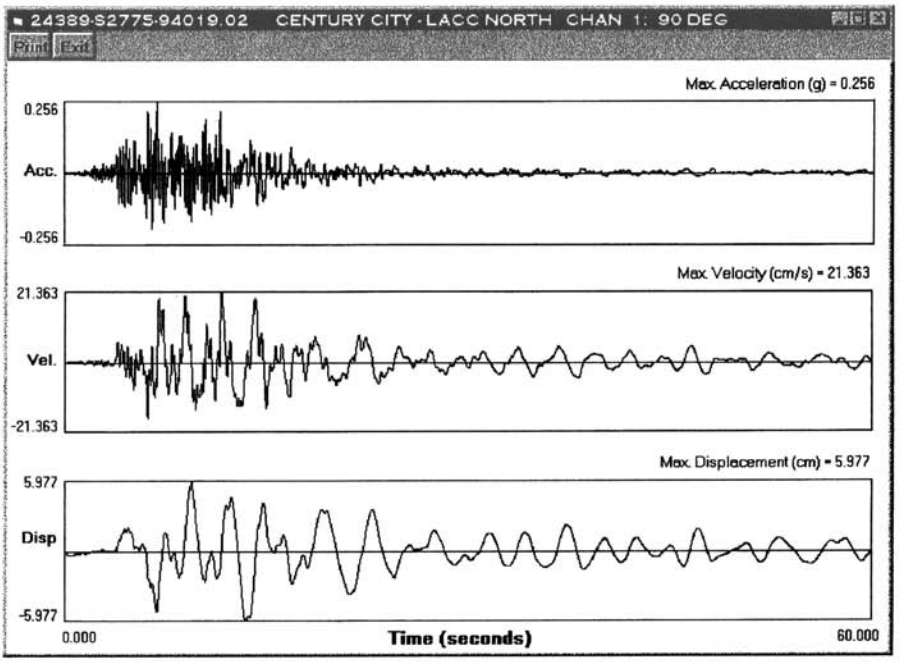
24389-S2775-94019.02 CENTURY CITY - LACC NORTH CHAN 1: 90 DEG
Print
Exit
Max. Acceleration (g) = 0.256
0.256
Acc.
-0.256
Max. Velocity (cm/s) = 21.363
21.363
Vel.
-21.363
Max. Displacement (cm) = 5.977
5.977
Disp
-5.977
0.000
Time (seconds)
60.000

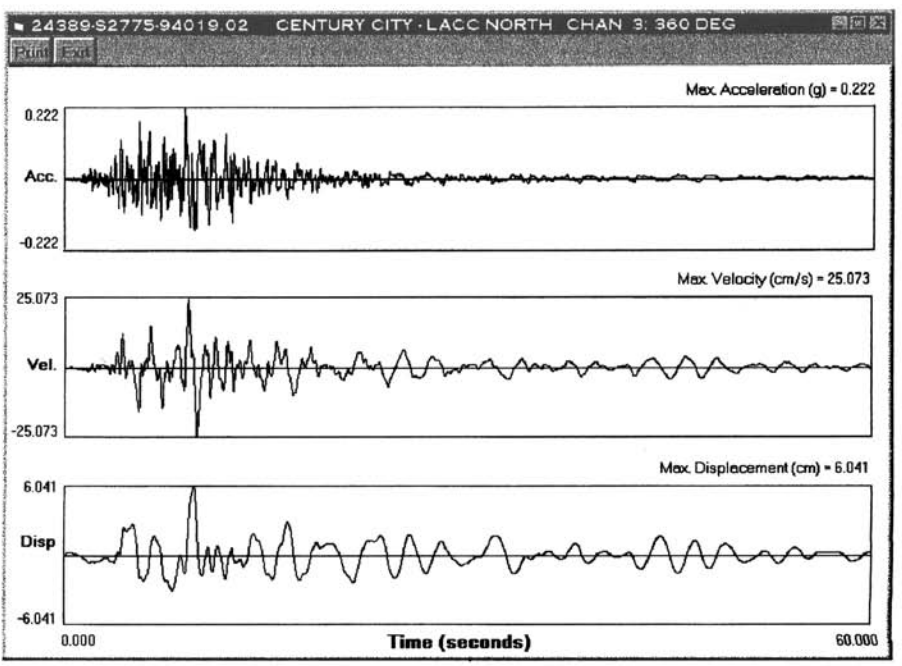
24389-S2775-94019.02 CENTURY CITY - LACC NORTH CHAN 3: 360 DEG
Print
Exit
Max. Acceleration (g) = 0.222
0.222
Acc.
-0.222
Max. Velocity (cm/s) = 25.073
25.073
Vel.
-25.073
Max. Displacement (cm) = 6.041
6.041
Disp
-6.041
0.000
Time (seconds)
60.000

REFERENCES

[1] Abrahamson, N. A., and Shedlock, K. M. (1997), "Overview," *Seismol. Res. Lett.*, Vol. 68, No. 1, pp. 9–23.

[2] Accademia dei Lincei (1909), "Relazione della Commissione Reale Incaricata di Designare le Zone piu Adatte per la Recostruzione degli Abitati Colpiti dal Terremoto del 28 Dicembre 1908 o da Altri Precedenti," Rome, Italy.

[3] Aiken, I. D., Kelly, J. M., and Tajirian, F. F. (1989), "Mechanics of Low Shape Factor Elastomeric Seismic Isolation Bearings," Report No. UCB/EERC-89/13, Earthquake Engineering Research Center, University of California, Berkeley, CA.

[4] Aiken, I. D., Kelly, J. M., Clark, P. W., Tamura, K., Kikuchi, M., and Itoh, T. (1992), "Experimental Studies of the Mechanical Characteristics of Three Types of Seismic Isolation Bearings," *Proceedings of the 10WCEE*, Madrid, Spain.

[5] Al-Hussaini, T. M., Zayas, V. A., and Constantinou, M. C. (1994), "Seismic Isolation of a Multi-Story Frame Structure Using Spherical Sliding Isolation Systems," Technical Report NCEER-94-0007, National Center for Earthquake Engineering Research, Buffalo, NY.

[6] Allahabadi, R., and Powell, G. H. (1988), "DRAIN-2DX User Guide," Report No. UCB/EERC-88/06, Earthquake Engineering Research Center, Berkeley, CA.

[7] Allen, E. W., and Bailey, J. S. (1988), "Seismic Rehabilitation of the Salt Lake City and County Building Using Base Isolation," *Proc. 9th World Conf. Earthq. Eng.*, Vol. 5, pp. 633–638, Tokyo–Kyoto, Japan.

[8] Amin, N., and Mokha, A. (1995), "U.S. Court of Appeals Building: Seismic Isolation Implementation," *Proc. Joint ASME/JSME Pressure Vessels and Piping Conf., Seismic, Shock, and Vibration Isolation*, Vol. PVP 319, pp. 229–240, Honolulu, HI.

[9] Anderson, J. C., and Bertero, V. V. (1987), "Uncertainties in Establishing Design Earthquakes," *J. Struct. Eng.* ASCE, Vol. 113, No. 8, pp. 1709–1724.

[10] Anderson, J. C., and Naeim, F. (1984) "Design Criteria and Ground Motion Effects on the Seismic Response of Multistory Buildings," Critical Aspects of

Earthquake Ground Motion and Building Damage Potential, ATC-10-1, Applied Technology Council, Palo Alto, CA.

[11] Anderson, T. L. (1989), "Seismic Isolation for the Los Angeles County Fire Command and Control Facility," Proc. ASCE Structures Congress, Vol. 1, pp. 615–624, San Francisco, CA.

[12] Applied Technology Council (1974), *An Evaluation of a Response Spectrum Approach to Seismic Design of Buildings*, ATC-2, Palo Alto, CA.

[13] Applied Technology Council (1978), *Tentative Provisions for the Development of Seismic Regulations for Buildings*, ATC-3-06, Palo Alto, CA.

[14] Applied Technology Council (1997), *Seismic Evaluation and Retrofit of Concrete Buildings*, ATC-40, Redwood City, CA.

[15] Arya, A. S. (1984), "Sliding Concept for Mitigation of Earthquake Disaster to Masonry Buildings," *Proc. 8th World Conf. Earthq. Eng.*, Vol. 5, San Francisco, CA.

[16] Arya, A. S., Chandra, B., and Qamarruddin, M. (1978), "A New Building System for Improved Earthquake Performance," *Symp. Earthq. Eng.*, Vol. 1, pp. 499–504, University of Roorkee, Roorkee, India.

[17] Arya, A. S., Chandra, B., and Qamarruddin, M. (1981), "A New Concept for Resistance of Masonry Buildings in Severe Earthquake Shocks," *J. Inst. Eng. (India)*, Vol. 61, No. 6, pp. 302–308.

[18] Asher, J. W., Hoskere, S. N., Ewing, R. D., Van Volkingburg, D. R., Mayes, R. L., and Button, M. (1995), "Seismic Performance of the Base-Isolated USC University Hospital in the 1994 Northridge Earthquake," *Proc. Joint ASME/JSME Pressure Vessels and Piping Conf., Seismic Shock and Vibration Isolation*, Vol. PVP, No. 319, pp. 147–154, Honolulu, HI.

[19] Berg, G. V. (1983), *Seismic Design Codes and Procedures*, Earthquake Engineering Research Institute Oakland, CA.

[20] Blake, T. F. (1996), *EQSEARCH—A Computer Program for the Estimation of Peak Horizontal Acceleration from California Historical Earthquake Catalogs, User Manual*, Newbury Park, CA.

[21] Blake, T. F. (1995a), *EQFAULT—A Computer Program for the Deterministic Prediction of Peak Horizontal Acceleration from Digitized California Faults, User Manual*, Newbury Park, CA.

[22] Blake, T. F. (1995b), *FRISKSP—A Computer Program for the Probabilistic Estimation of Peak Acceleration and Uniform Hazard Spectra using 3-D Faults as Earthquake Sources, User Manual*, Newbury Park, CA.

[23] Blakeley, R. W. G. (1982), "Code Requirements for Base Isolated Structures," *Proc. Int. Conf. on Natural Rubber for Earthq. Protection of Bldgs. and Vibration Isolation*, pp. 292–311, Kuala Lumpur, Malaysia.

[24.] Boardman, P. R., Wood, B. J., and Carr, A. J. (1983), "Union House—a Cross-Braced Structure with Energy Dissipators," *Bull. New Zealand Nat. Soc. Earthq. Eng.*, Vol. 16, No. 2, pp. 83–97.

[25] Bolt, B. A. (1969), "Duration of Strong Motion." *Proc. 4th World Conf. Earthq. Eng.*, pp. 1304–1315, Santiago, Chile.

[26] Boore, D. M., Joyner, W. B., and Fumal, T. E. (1997), "Equations for Estimating Horizontal Response Spectra and Peak Acceleration from Western North Ameri-

can Earthquakes: A Summary of Recent Work," *Seismol. Res. Lett.*, Vol. 68, No. 1, pp. 128–153.

[27] Built, S. M. (1982), "Lead Rubber Dissipators for the Base Isolation of Bridge Structures," Report 289, School of Engineering, Department of Civil Engineering, University of Auckland, Auckland, New Zealand.

[28] Campbell, T. I., and Kong, W. L. (1987), "TFE Sliding Surfaces in Bridge Bearings," Technical Report MF-87-06, Ontario Ministry of Transportation and Communications, Ontario, Canada.

[29] Chalhoub, M. S., and Kelly, J. M. (1990), "Earthquake Simulator Testing of a Combined Sliding Bearing and Rubber Bearing Isolation System," Report No. UCB/EERC-87/04, Earthquake Engineering Research Center, University of California, Berkeley, CA.

[30] Chalhoub, M. S., and Kelly, J. M. (1991), "Analysis of Infinite-Strip-Shaped Base Isolator with Elastomer Bulk and Compression," *J. Eng. Mechan.*, Vol. 117, No. 8, pp. 1792–1805.

[31] Charleson, A. W., Wright, P. D., and Skinner, R. I. (1987), "Wellington Central Police Station, Base Isolation of an Essential Facility," *Proc. Pacific Conf. on Earthq. Engrg.*, Vol. 2, pp. 377–388, New Zealand Nat. Soc. for Earthq. Engrg., Wairekei, New Zealand.

[32] Clark, P. W., Aiken, I. D., Kelly, J. M., Gluckler, E. L., and Tajirian, F. F. (1995), "Tests of Reduced-Scale Seismic Isolation Bearings for the U.S.-Advanced Liquid Metal Reactor (ALMR) Program," *Proc. Joint ASME/JSME Pressure Vessels and Piping Conf., Seismic Shock and Vibration Isolation*, Vol. PVP 319, pp. 303–308, Honolulu, HI.

[33] Clough, R. W., and Hucklebridge, A. A. (1977), "Preliminary Experimental Study of Seismic Uplift of a Steel Frame," Report No. UCB/EERC-77/22, Earthquake Engineering Research Center, University of California, Berkeley, CA.

[34] Computers and Structures, Inc. (1996), *ETABS Building Analysis System*, Version 6.13, Berkeley, CA.

[35] Computers and Structures, Inc. (1997), *SAP2000 Analysis Reference Manual*, Version 6.13, Berkeley, CA.

[36] Cormack, L. G. (1988), "The Design and Construction of the Major Bridges on the Mangaweka Rail Deviation," *Trans. IPENZ*, I/CE, Vol. 15, pp. 16–23.

[37] Cornell, C. A. (1968), "Engineering Seismic Risk Analysis," *Bull. Seism. Soc. Am.*, Vol. 58, No. 5.

[38] Derham, C. J., Learoyd, S. B. B., and Wootton, L. R. (1975), "Buildings on Springs to Resist Earthquakes," *Proc. 5th European Conf. on Earthq. Eng.*, Istanbul, Turkey.

[39] Derham, C. J., Kelly, J. M., and Thomas, A. G. (1985), "Nonlinear Natural Rubber Bearings for Seismic Isolation," *Nuclear Eng. Design*, Vol. 84, No. 3, pp. 417–428.

[39a] Kelly, J. M., and Derham, C. J. (1985), "Combined Earthquake Protection and Vibration Isolation of Structures," *Natural Rubber Tech.*, Vol. 16, pp. 3–11.

[40] Dowrick, D. J., Babor, J., Cousins, W. J., and Skinner, R. I. (1991), "Design of Seismically Isolated Printing Press," *Proc. Pacific Conf. on Earthq. Eng.*, Vol. 3, pp. 35–44, New Zealand Nat. Soc. for Earthq. Engrg., Auckland, New Zealand.

[41] Federal Emergency Management Agency (1998), *National Earthquake Hazards Reduction Program Guidelines for Seismic Rehabilitation of Buildings*, FEMA-273, Washington, DC.

[42] Federal Emergency Management Agency (1998), *Commentary on the National Earthquake Hazards Reduction Program Guidelines for Seismic Rehabilitation of Buildings*, FEMA-274, Washington, DC.

[43] Federal Emergency Management Agency (1997), *NEHRP Provisions for the Development of Seismic Regulations for Buildings—Working Draft*, NEHRP-97, Washington, DC.

[44] Gent, A. N. (1964), "Elastic Stability of Rubber Compression Springs," *J. Mech. Eng.*, Vol. 6, No. 4, pp. 318–326.

[45] Gent, A. N., and Lindley, P. B. (1958), *Proc. Roy. Soc. Lond. Ser. A*, Vol. 249, pp. 195–205.

[46] Giuliani, G. C. (1991), "Design and Construction of Prefabricated Isolated Buildings," *Proc. Int. Meeting on Earthq. Protection of Bldgs.*, pp. 191/C-202/C, Ancona, Italy.

[47] Gutenberg, B., and Richter, C. F. (1956), *Seismicity of the Earth*, Princeton University Press, Princeton, NJ.

[48] Hanks, T. C., and Kanamori, H. (1979), "A Moment Magnitude Scale," *J. Geophys. Res.*, Vol. 84, No. B5.

[49] Haringx, J. A. (1948), "On Highly Compressible Helical Springs and Rubber Rods, and Their Application for Vibration-Free Mounting," *III Philips Res. Rep.*, Vol. 4, pp. 206–220.

[50] Husid, R., Median, H., and Rios, J. (1969), "Analysis de Terremotos Norteamericanos y Japonesses," *Rivista del IDIEM 8*, No. 1.

[51] Idriss, I. M. (1985), "Evaluating Seismic Risk in Engineering Practice," *11th Int. Conf. Soil Mechan. Found. Eng.*, Vol. 1, pp. 255–320.

[52] Inaudi, J. A., and De la Llera, J. C. (1992), "Dynamic Analysis of Nonlinear Structures Using State-Space Formulation and Partitioned Integration Schemes," UCB/EERC-92/18, Earthquake Engineering Research Center, University of California.

[53] International Conference of Building Officials (1991), "Earthquake Regulations for Seismic-Isolated Structures," *Uniform Building Code*, Chapter 23, Whittier, CA.

[54] International Conference of Building Officials (1994), "Earthquake Regulations for Seismic-Isolated Structures," *Uniform Building Code*, Appendix Chapter 16, Whittier, CA.

[55] International Conference of Building Officials (1997), "Earthquake Regulations for Seismic-Isolated Structures," *Uniform Building Code*, Appendix Chapter 16, Whittier, CA.

[56] Jeng, V. (1984), "Dynamic Analysis of Base Isolation System," Ph.D. Dissertation, University of California, Berkeley.

[57] Jolivet, J., and Richli, M. H. (1977), "Aseismic Foundation System for Nuclear Power Stations," *Proc. 4th Int. Conf. on Struc. Mech. in Reactor Technology*, San Francisco, CA.

[58] Kannan, A. M., and Powell, G. H. (1975), "DRAIN-2D: A General Purpose Computer Program for Two-Dimensional Nonlinear Analysis of Structures," Structural Engineering, Mechanics and Materials, Department of Civil Engineering, University of California, Berkeley.

[59] Kariotis, J. C., Waqfi, O. M., and Ewing, R. D. (1992), "LPM/II: A Computer Program Using Beam Elements for the Nonlinear Dynamic Analysis of Lumped Parameter Models," Report 2.3-5, U.S.-Japan Coordinated Program for Masonry Building Research, Kariotis & Associates, South Pasadena, CA.

[60] Kawashima, K., and Aizawa, K. (1986). "Modification of Earthquake Response Spectra with Respect to Damping Ratio," *Proc. Third U.S. National Conf. on Earthquake Engineering*, pp. 1107–1116, Earthquake Engineering Research Institute, Charleston, SC.

[61] Kelly, J. M. (1982), "Aseismic Base Isolation," *Shock Vib. Dig.*, Vol. 14, No. 5, pp. 17–25.

[62] Kelly, J. M. (1988), "Base Isolation in Japan, 1988," Report No. UCB/EERC-88/20, Earthquake Engineering Research Center, University of California, Berkeley, CA.

[63] Kelly, J. M. (1990), "Base Isolation: Linear Theory and Design," *J. Earthq. Spectra*, Vol. 6, No. 2, pp. 223–244.

[64] Kelly, J. M. (1991), "Dynamic and Failure Characteristics of Bridgestone Isolation Bearings," Report No. UCB/EERC-91/04, Earthquake Engineering Research Center, Berkeley, CA.

[65] Kelly, J. M. (1996), *Earthquake-Resistant Design with Rubber*, 2nd ed., Springer-Verlag, London.

[66] Kelly, J. M., Skinner, R. I., and Heine, A. J. (1972), "Mechanisms of Energy Absorption in Special Devices for Use in Earthquake Resistant Structures," *Bull. New Zealand Nat. Soc. Earthq. Eng.*, Vol. 5, No. 3, pp. 63–88.

[67] Kelly, J. M., and Tsztoo, D. F. (1977), "Earthquake Simulation Testing of a Stepping Frame with Energy-Absorbing Devices," Report No. UCB/EERC-77/17, Earthquake Engineering Research Center, University of California, Berkeley, CA.

[68] Kelly, J. M., and Quiroz, E. (1992), "Mechanical Characteristics of Neoprene Isolation Bearings," Report No. UCB/EERC-92/11, Earthquake Engineering Research Center, Berkeley, CA.

[69] Kircher, C. G., Delfosse, G. C., Schoof, C. C., Khemici, O., and Shah, H. C. (1979), "Performance of a 230 K V ATB 7 Power Circuit Breaker Mounted on Gapec Seismic Isolators," John A. Blume Earthquake Engineering Center, Stanford University, Stanford, CA.

[70] Krinitzsky, E. L. (1993). "The Hazard in Using Probabilistic Seismic Hazard Analysis," *Civil Eng. ASCE*, Nov., Vol. 66, pp. 60–61.

[71] Langenbach, R. (1996), personal communication to James M. Kelly.

[72] Li, L. (1984), "Base Isolation Measure for Aseismic Buildings in China," *Proc. 8th World Conf. on Earthq. Engrg.*, Vol. 5, San Francisco, CA.

[73] Lindley, P. B. (1966), "Load-Compression Relationships of Rubber Units," *J. Strain Anal.* Vol. I, No. 3, pp. 190–195.

[74] Lindley, P. B. (1978), "Engineering Design with Natural Rubber," NR Technical

Bulletin, Malaysian Rubber Producers' Research Association, Brickendonbury, England.

[75] Mahin, S. A., and Lin, J. (1983), "Construction of Inelastic Response Spectra for Single Degree of Freedom Systems," Earthquake Engineering Research Center, University of California, Report No. UCB/EERC-83/17, Berkeley, CA.

[76] Makris, N., and Deoskar, H. S. (1996), "Prediction of Observed Response of Base-Isolated Structure," *J. Struct. Eng.*, Vol. 122, No. 5, pp. 485–493.

[77] McCann, W. M., and Shah, H. C. (1979), "Determining Strong Motion Duration of Earthquakes," *Bull. Seism. Soc. Am.*, Vol. 69, No. 4, pp. 1253–1265.

[78] Malaysian Rubber Producers' Research Association (1988), *Natural Rubber Science and Technology*, A. J. Roberts, Ed., Oxford University Press, Oxford, England.

[79] Mayes, R. L. (1995), "Seismic Isolation: When Content Protection Is as Important as the Structure," *Proc. 3rd Natl. Concrete and Masonry Eng. Conf.*, Vol. 2, pp. 561–582, San Francisco, CA.

[80] Ministry of Works and Development (1983), *Design of Lead-Rubber Bearings*, Civil Division Publication CDP 818/A, Wellington, New Zealand.

[81] Miyazaki, M. (1995), private communication with James M. Kelly.

[82] Mohraz, B., and Elghadamsi, F. E. (1989), "Earthquake Ground Motion and Response Spectra," in *The Seismic Design Handbook*, F. Naeim, Ed., Van Nostrand Reinhold, New York.

[83] Mondkar, D. P., and Powell, G. H. (1975), "ANSR-1—General Purpose Program for Analysis of Nonlinear Structural Response," Report No. UCB/EERC 75-37, Earthquake Engineering Research Center, University of California, Berkeley.

[84] Mostaghel, N. (1984), "Resilient-Friction Base Isolator," Report No. UTEC 84-097, Department of Civil Engineering, University of Utah, Salt Lake City, UT.

[85] Mostaghel, N., and Tanbakuchi, J. T. (1983), "Response of Sliding Structures to Earthquake Support Motion," *J. Earthq. Eng. Struct. Dynam.*, Vol. 11, pp. 729–748.

[86] Mostaghel, N., and Flint, B. F. (1986), "Preliminary Experimental Evaluation of R-FBI Bearings," Report No. UTEC 86-089, Department of Civil Engineering, University of Utah, Salt Lake City, UT.

[87] Mostaghel, N., Hejazi, M., and Tanbakuchi, J. T. (1983), "Response of Sliding Structures, to Harmonic Support Motion," *J. Earthq. Eng. Struct. Dynam.*, Vol. 11, pp. 355–366.

[88] Mostaghel, N., and Kelly, J. M. (1987), "Design Procedures for R-FBI Bearings," Report No. UCB/EERC-87/18, Earthquake Engineering Research Center, University of California, Berkeley, CA.

[89] Mostaghel, N., Kelly, J. M., and Clark, P. W. (1992), "Stability of R-FBI Bearings: Analysis and Experiment," *J. Earthq. Spectra*, Vol. 8, No. 2, pp. 259–277.

[90] Naaseh, S. (1995), "Seismic Retrofit of San Francisco City Hall: The Role of Masonry and Concrete," *Proc. 3rd Natl. Concrete Masonry Eng. Conf.*, Vol. 2, pp. 769–795, San Francisco, CA.

[91] Naeim, F., and Anderson, J. C. (1993), "Classification and Evaluation of Earthquake Records for Design," Report No. CE 83-08, Department of Civil Engineering, University of Southern California, July.

[92] Naeim, F., and Anderson, J. C. (1996), "Design Classification of Horizontal and Vertical Earthquake Ground Motion (1933–1994)," Report No. 7738.68/96, John A. Martin and Associates, Los Angeles, CA.

[93] Naeim, F., and Sommerville, P. G. (1998), *Earthquake Records and Design (95% Draft)*, EERI Monograph Series, submitted to Earthquake Engineering Research Institute, Oakland, CA.

[94] Naeim, F., and Lew, M. (1993), "Design Ground Motion Criteria for Seismic-Isolated California Hospitals—Evaluations and Recommendations," Report No. 6980.68/93, John A. Martin and Associates, Los Angeles, CA, October.

[95] Naeim, F., and Lew, M. (1995), "On the Use of Design Spectrum Compatible Time Histories," *Earthq. Spectra EERI*, Vol. 11, No. 1, pp. 111–127.

[96] Nagarajaiah, S., Reinhorn, A. M., and Constantinou, M. C. (1991), "3D-BASIS—Nonlinear Dynamic Analysis of Three-Dimensional Base Isolated Structures: Part II," Report No. NCEER-91-0005, National Center for Earthquake Engineering Research, Buffalo, NY.

[97] Nagarajaiah, S., Li, C., Reinhorn, A. M., and Constantinou, M. C. (1993), "3D-BASIS-TABS: Computer Program for Nonlinear Dynamic Analysis of Three Dimensional Base Isolated Structures," Report No. NCEER-93-0011, National Center for Earthquake Engineering Research, Buffalo, NY.

[98] Nagarajaiah, S., and Ferrell, K. (1998), "Stability of Elastomeric Isolation Bearings: Analytical Modeling," to appear in the *ASCE J. Struct. Eng.*

[99] Nagarajaiah, S., Reinhorn, A. M., and Constantinou, M. C. (1993) "Nonlinear Dynamic Analysis of Three Dimensional Base Isolated Structures (3D-BASIS-ME)," National Center for Earthquake Engineering Research, Bufallo, NY.

[100] National Earthquake Hazard Reduction Program (1997), *NEHRP Provisions for the Development of Seismic Regulations for Buildings—Working Draft*, NEHRP-97, Washington, DC.

[101] Newmark, N. M., and Hall, W. J. (1973), "Procedures and Criteria for Earthquake Resistant Design, Building Practices for Disaster Mitigation," National Bureau of Standards, U.S. Department of Commerce, Building Research Series, pp. 209–236.

[102] Newmark, N. M., and Hall, W. J. (1982), *Earthquake Spectra and Design*, Earthquake Engineering Research Institute, Berkeley, CA.

[103] Office of Statewide Health Planning and Development (Draft revised 1991), "An Acceptable Procedure for the Design and Review of California Hospital Buildings Using Base Isolation," State of California, Sacramento, CA.

[104] Office of Statewide Health Planning and Development (1996), "Division III—Earthquake Regulations for Seismic-Isolated Structures," State of California, Sacramento, CA.

[105] Page, R. A., Boore, D. M., Joyner, W. M., and Caulter, H. W. (1972), "Ground Motion Values for Use in the Seismic Design of the Trans-Alaska Pipeline System," U.S. Geological Survey, Circular 672.

[106] Prakash, V., Powell, G. H., and Campbell, S. (1994). "DRAIN-3DX: Base Program Description and User Guide, Version 1.10," Report No. UCB/SEMM-94/07, Structural Engineering, Mechanics and Materials, Department of Civil Engineering, University of California, Berkeley, Aug. 1994.

[107] Poole, R. A., and Clendon, J. E. (1991), New Zealand Parliament Buildings: Seismic Protection by Base Isolation. *Proc. Pacific Conf. on Earthq. Eng.*, New Zealand Nat. Soc. for Earthq. Engrg., Vol. 3, pp. 13–34, Auckland, New Zealand.

[108] Reaveley, L. R., Mayes, R. L., and Sveinsson, B. I. (1988), "Seismic Isolation of a Four-Story Flight Simulator Manufacturing Facility," *Proc. 9th World Conf. on Earthq. Eng.*, Poster Session Paper P2A-10, p. 79, Tokyo–Kyoto, Japan.

[109] Robinson, W. H., and Greenbank, L. R. (1975), "An Extrusion Energy Absorber Suitable for the Protection of Structures during an Earthquake," *Bull. New Zealand Natl. Soc. Earthq. Eng.*, Vol. 8, No. 3, pp. 187–191.

[110] Robinson, W. H., and Tucker, A. G. (1977), "A Lead-Rubber Shear Damper," *Bull. New Zealand Natl. Soc. Earthq. Eng.*, Vol. 10, No. 3, pp. 151–153.

[111] Robinson, W. H., and Tucker, A. G. (1983), "Test Results for Lead-Rubber Bearings for the William M. Clayton Building, Toe Toe Bridge, and Waiotukupuna Bridge," *Bull. New Zealand Natl. Soc. Eng.*, Vol. 14, No. 1, pp. 21–33.

[112] Schwartz, D. P., and Coppersmith, K. J. (1984), "Fault Behavior and Characteristic Earthquakes: Examples from Wasatch and San Andreas Fault Zones, *J. Geophys. Res.*, Vol. 89, pp. 5681–5698.

[113] Sharpe, R. D., and Skinner, R. I. (1983), "The Seismic Design of an Industrial Chimney with Rocking Base," *Bull. New Zealand Natl. Soc. Earthq. Eng.*, Vol. 16, No. 2, pp. 98–106.

[114] Sparacio, R., Cavuto, F., Martelli, A., Pugliese, A. and Sano, T. (1991), "Report on a First Experience on Seismic Retrofitting by Use of Base Isolation," *Proc. Int. Meeting on Earthq. Protection of Bldgs.*, pp. 243/C-253/C, Ancona, Italy.

[115] State of California (1996), "Earthquake Regulations for Seismic-Isolated Structures," Administrative Code, Title 24, Part 2, Division III.

[116] Staudacher, E., Habacher, C., and R. Siegenthaler (1970), "Erdbebensicherung in Baum," Neue Zürcher Zeitung, Technikbeilage, Zurich, Switzerland.

[117] Staudacher, K. (1982), "Integral Earthquake Protection of Structures IV: Full Base Isolation and Seismic Mass Analogy," Eidgenossische Technische Hochschule (Zurich), Inst. für Baustatik und Konstruktion, Bericht 134, Birkhauser Verlag, Basel, Switzerland.

[118] Stevenson, A. (1985), "Longevity of Natural Rubber in Structural Bearings," *Plastics Rubber Process. Applicat.*, Vol. 5, p. 253.

[119] Structural Engineers Association of California (1989), *General Requirements for the Design and Construction of Seismic-Isolated Structures*, Ad Hoc Base Isolation Subcommittee of the Seismology Committee, Appendix to Chapter 1 of the SEAOC Blue Book.

[120] Structural Engineers Association of California (1995), *Performance Based Engineering*, Vision 2000 Committee, Sacramento, CA.

[121] Structural Engineers Association of Northern California (1986), "Tentative Seismic Isolation Design Requirements," Yellow Book, San Francisco, CA.

[122] Taniwangsa, W., Clark, P. W., and Kelly, J. (1995), "Natural Rubber Isolation Systems for Earthquake Protection of Low-Cost Buildings," Report UCB/EERC-95/12, Earthquake Engineering Research Center, University of California, Berkeley, CA.

[123] Tarics, A. G., Way, D., and Kelly, J. M. (1984), "The Implementation of Base

Isolation for the Foothill Communities Law and Justice Center," Technical Report No. RTA-84, San Francisco, CA.

[124] Taylor, A. W., Lin, A. N., and Martin, J. W. (1992), "Performance of Elastomers in Isolation Bearings: A Literature Review," *J. Earthq. Spectra*, Vol. 8, No. 2, pp. 279–304.

[125] Tsopelas, P. C., Constantinou, M. C., and Reinhorn, A. M. (1994), "3D-BASIS-ME: Computer Program for Nonlinear Dynamic Analysis of Seismically Isolated Single and Multiple Structures and Liquid Storage Tanks," Report No. NCEER-94-0010, National Center for Earthquake Engineering Research, Buffalo, NY.

[126] Tyler, R. G. (1977a), "Dynamic Tests on PTFE Sliding Layers under Earthquake Conditions," *Bull. New Zealand Natl. Soc. Earthq. Eng.*, Vol. 10, No. 3, pp. 129–138.

[127] Tyler, R. G. (1977b), "Damping in Building Structures by Means of PTFE Sliding Joints," *Bull. New Zealand. Natl. Soc. Earthq. Eng.*, Vol. 10, No. 3, pp. 139–142.

[128] Tyler, R. G. (1991), "Rubber Bearings in Base-Isolated Structures: A Summary Paper," *Bull. New Zealand Natl. Soc. Earthq. Eng.*, Vol. 24, No. 3, pp. 251–274.

[129] Tyler, R. G., and Robinson, W. H. (1984), "High-Strain Tests on Lead-Rubber Bearings for Earthquake Loadings," *Bull. New Zealand Natl. Soc. Earthq. Eng.*, Vol. 17, pp. 90–105.

[130] Vestroni, F., Capecchi, D., Meghella, M., Mazza, G., and Pizzigalli, E. (1992), "Dynamic Behavior of Isolated Buildings," *Proc. 10th World Conf. on Earthq. Eng.*, Vol. 4, pp. 2473–2478, Madrid, Spain.

[131] Walters, M. T., Honeck, B., and Elsesser, E. (1995), "Use of Seismic Isolation in New and Retrofit Construction," *Proc. Joint ASME/JSME Pressure Vessels and Piping Conf., Seismic, Shock, and Vibration Isolation*, Vol. PVP 319, pp. 31–38, Honolulu, HI.

[132] Way, D., and Jeng, V. (1989), "N-PAD—A Three-Dimensional Program for the Analysis of Base-Isolated Structures," *Proceedings of Structures Congress 89*, ASCE, San Francisco, CA.

[133] Way, D., and Howard, J. (1990), "Seismic Rehabilitation of the Mackay School of Mines with Base Isolation," *J. Earthq. Spectra*, Vol. 6, No. 2, pp. 297–308.

[134] Wells, D. L., and Coppersmith, K. J. (1994), "New Empirical Relationships among Magnitude, Rupture Length, Rupture Width, Rupture Area, and Surface Displacement," *Bull. Seism. Soc. Am.*, Vol. 84, No. 9, pp. 974–1002.

[135] Wesnousky, S. G. (1994), "The Gutenberg-Richter or Characteristic Earthquake Distribution, Which Is It?" *Bull. Seism. Soc. Am.*, Vol. 84, No. 6, pp. 1940–1959.

[136] Westermo, B., and Udwadia, F. (1983), "Periodic Response of a Sliding Oscillator System to Harmonic Excitation," *J. Earthq. Eng. Struct. Dynam.*, Vol. 11, pp. 135–146.

[137] Yim, C. S., Chopra, A. K., and Penzien, J. (1980), "Rocking Response of Rigid Blocks to Earthquakes," Report No. UCB/EERC-80/02, Earthquake Engineering Research Center, University of California, Berkeley, CA.

[138] Youssef, N., Nuttal, B., Rahman, A., and Hata, O. (1995), "The Role of Reinforced Concrete in the Stiffening and Strengthening above Base Isolation for a Tall Historic Landmark: Los Angeles City Hall," *3rd Nat. Concrete and Masonry Eng. Conf.*, Vol. 2, pp. 729–735, San Francisco, CA.

INDEX

A

ABAQUS computer program, 220
ADINA computer program, 220
ANSR computer program, 220
ANSYS computer program, 220
Attenuation relations, 138, 155–158

B

Balls, 1–2. *See also* Bearings, elastomeric; Bearings, natural rubber
Base isolation
  acceptance of concept, 2
  application priority, 2
  description of concept, 3
  early examples, 1–2
  earthquake experience, 18, 22
  experience in Italy, 20–21
  experience in Japan, 18–20
  first building to be isolated on lead-rubber bearings, 21
  first considered as seismic-resistant design strategy, 1–2, 53
  first seismically isolated building in U.S., 5, 6–8, 207
  first use of rubber, 3
  and flexibility, 3
  future research, 23
  Kobe earthquake experience, 18, 50
  largest building in world, 18
  load-carrying component, 3
  new construction projects, 8–11
  problems in application of technology, 22
  project costs, 7, 8, 11
  project examples, 6–22
  research programs, 5–6
  retrofitting projects, 11–17
  shake table experiments, 6
  specific buildings
    Caltrans Traffic Management Center, 9
    Foothill Communities Law and Justice Center, San Bernardino, California, 5, 6–8, 207
    Los Angeles City Hall, California, 13–14, 15
    Los Angeles County Emergency Operations Center, 8–9
    Los Angeles County Fire Command and Control Facility, 8
    M. L. King/C. R. Drew Diagnostics Trauma Center, Willowbrook, California, 9–10, 55
    Memphis, Tennessee project, 10–11
    National Telephone Company (SIP), Ancona, Italy, 20
    New Zealand printing press building, 22
    Oakland City Hall, California, 11–12
    Salt Lake City, Utah project, 10, 11
    San Francisco City Hall, California, 12–13
    Union House, Auckland, New Zealand, 21, 59–60

William Clayton building, Wellington, New Zealand, 21
theoretical work, 6
three-dimensional, 58
types of systems
elastomeric-based systems, 47–52
rocking systems, 61–62
sleeved-pile system, 21–22, 58–61
sliding systems, 52–58
spring-type systems, 58, 59
and Uniform Building Code, 6, 63, 64
United States experience, 6–17
use of sliding elements, 14–16
Bearings, elastomeric. *See also* Isolation devices
buckling-type instability, 121–133
circular, 131–133
combined with sliding isolation systems, 55–56
dowelled, 133–135
enhanced stability, 125
history of use for earthquake protection of buildings, 47–48
lead-plug, 5, 18, 49–50
low-damping versus high-damping, 48–49
mechanical characteristics
bending stiffness, 94, 97–100
buckling behavior, 94
horizontal stiffness, 3, 94, 125–126
studying, 93
vertical stiffness, 3, 94–97
multilayer development, 2
natural versus synthetic rubber, 47, 48–49
overview, 47
rollout-type instability, 133–135
Skopje, Yugoslavia example, 3, 4, 47–48
square, 127–131
widespread use of, 48
Bearings, natural rubber
early example, 3
energy dissipation, 111–115
first use for seismic protection of buildings, 3, 4, 47–48
high-damping, 18, 50–52, 111–115, 185–198, 220–231
low-damping, 3, 5, 48–49
with mechanical dampers, 18
multilayer elastomeric, 2, 3, 5, 48
overview, 47
versus synthetic, 47, 48–49
use in Japan, 18
with and without steel reinforcing plates (shims), 3, 48
Bending stiffness, 94, 97–100
Bihar, India earthquake (1934), 53–54
Bilinear modeling
adjustments for high-strain stiffening, 115–116
comparisons with experimental data, 117–119
energy dissipation in high-damping natural rubber bearings, 111–115
implications for isolation designers, 107–111
isolation bearings, 104–107
Bridges
first elastomeric bearings, 2
and rocking base isolation systems, 61–62
South Rangitikei River Bridge, New Zealand, 61–62
Buckling analysis, 121–133
Buildings
early earthquake-resistant designs, 1–2
earthquake experience with base-isolated structures, 22, 50
first example of seismic isolation in U.S., 5, 6–8, 207
first to be isolated on lead-rubber bearings, 21
floor accelerations, 2–3
interstory drift, 2, 3, 77–78
Kobe earthquake experience, 18, 50
Memphis, Tennessee project, 10–11
retrofitting projects
California, 11–17
Italy, 20–21
Japan, 20
New Zealand, 22
Salt Lake City, Utah project, 10, 11
seismic isolation examples
Caltrans Traffic Management Center, 9
Foothill Communities Law and Justice Center, San Bernardino, California, 5, 6–8, 207
Los Angeles City Hall, California, 13–14, 15
Los Angeles County Emergency Operations Center, 8–9
Los Angeles County Fire Command and Control Facility, 8
M. L. King/C. R. Drew Diagnostics Trauma Center, Willowbrook, California, 9–10, 55
National Telephone Company (SIP), Ancona, Italy, 20
New Zealand printing press building, 22
Oakland City Hall, California, 11–12
San Francisco City Hall, California, 12–13
Union House, Auckland, New Zealand, 21, 59–60
William Clayton building, Wellington, New Zealand, 21

C

Calantarients, Johannes Avetican, 1, 52, 53, 54
California
  Caltrans Traffic Management Center, 9
  earthquakes in, 22, 50, 58, 169
  example of Foothill Communities Law and Justice Center, San Bernardino, 5, 6–8, 207
  Los Angeles City Hall, 13–14, 15
  Los Angeles County Emergency Operations Center, 8–9
  Los Angeles County Fire Command and Control Facility, 8
  M. L. King/C. R. Drew Diagnostics Trauma Center, Willowbrook, 9–10, 55
  Oakland City Hall, 11–12
  retrofitting projects, 11–17
  San Francisco City Hall, 12–13
California Building Code, 173
California Code of Regulations (OSHPD)
  dynamic analysis requirements, 65
  hospital design requirements, 82–83
  OSHPD-96 defined, 63
  OSHPD-96 vs. UBC-97, 63
  static analysis formulas, 65–66
  time history analysis provisions, 176
California Department of Mines and Geology, 82–83, 171
Caltrans Traffic Management Center, 9
CD-ROM
  auto-start feature, 255
  ISOSEL computer program, 203, 207–216, 255
  list of contents, 255
Characteristic earthquake model, 160–161
China, experience with sliding isolation systems, 54
Codes. *See also* California Code of Regulations (OSHPD); Uniform Building Code (UBC)
  California hospital design requirements, 82–83
  design method requirements, 65
  dynamic analysis requirements, 65, 78–80
  isolator design and testing requirements, 81–82
  overview, 63–64
  peer review requirements, 80
  sample reference list, 235–237
  seismic hazard level criteria, 64
  static analysis formulas, 65–78
  UBC-97 regulations for seismic-isolated structures, 84–92
  Yellow Book, 64, 83
Computer programs
  ABAQUS, 220
  ADINA, 220
  ANSR, 220
  ANSYS, 220
  COSMOS, 220
  DRAIN-2D and DRAIN-3D, 115, 220
  EQFAULT, 163
  EQSEARCH, 163
  ETABS, 218
  FRISKSP, 163
  IDARC-2D and IDARC-3D, 220
  INADEL, 220
  ISOSEL, 203, 207–216, 255
  LPM, 115, 220
  MATLAB, 220
  NASTRAN, 220
  N-PAD, 217
  SAP-2000, 218–220, 222, 224–231, 255
  3D-BASIS, 115, 217–218
Construction, building, 1–3. *See also* Buildings
COSMOS computer program, 220

D

Damped-sway foundation system, 60
Dampers, mechanical, 5
Damping. *See also* High-damping rubber bearings; Low-damping rubber bearings
  absence of, 48–49
  basic concept, 3, 5
  design example, 188–189
  and Foothill Communities Law and Justice Center, San Bernardino, 5, 6–8
  and Los Angeles County Fire Command and Control Facility, 8
Damping coefficients, 71–73
Design basis earthquake (DBE), defined, 64
Design codes. See codes
Design forces, 75–76, 78
Design ground motion criteria. *See also* Earthquake ground motions
  code interpretations, 172–173
  criteria for defining, 137–139
  determining, 155–158
Design spectra, 78, 137, 138, 146–149
Deterministic seismic hazard evaluations, 158–159
Dhubai, India earthquake (1930), 53–54
Displacements
  and bearing stability, 126–133
  changes in UBC, 66–67, 92
  design example, 187, 195–198
  in dynamic analysis, 78–80
  factors in calculating, 66–67
    damping coefficients, 71–73
    design forces, 75–76
    drift limits, 77–78

effective system vibration periods, 73–74
MCE response coefficient, 70
near-source factors, 68–69
seismic source type, 68
seismic zone factor, 67
site soil profile type, 68
spectral seismic coefficients, 70–71
total design displacements, 74–75
vertical distribution of force, 76–77
and sliders, 14–15
in static analysis, 67, 74–75
UBC-97 minimum requirements, 92
Dowelled bearings, 133–135
DRAIN-2D and DRAIN-3D computer programs, 115, 220
Drift limits. See interstory drift
Ductility factor, 75–76
Dynamic analysis. *See also* Response spectra; Time history analysis
and building codes, 65, 78–80
scaling, 78–80
versus static analysis, 65, 67

E

Earthquake ground motions. *See also* Design ground motion criteria
attenuation relations, 138, 155–158
and base isolation concept, 2–3
characterizing with spectral values, 140, 142, 144–149
characterizing with time-domain parameters, 140–142
energy attributes, 142, 149–150
estimating, 138, 150–158
impulse-type versus sinusoidal, 142
predictive formulations, 138, 150–158
source characterizations, 150–155
Earthquake records
growth in number and availability, 139
list of files on CD-ROM, 255–256
overview, 174
and response spectra, 146, 147
sample CD-ROM contents, 257–272
and time history analysis, 137–138, 174
Earthquakes. *See also* Earthquake records; Seismic hazard evaluation
applying time histories, 174–184
in California, 22, 50, 58, 169
code hazard level criteria, 64
DBE versus MCE, 64
early building design responses, 1–2
estimating magnitude, 151–155
experience with base-isolated buildings, 22, 50
historical data, 169
in India, 53–54
Kobe, Japan (1995), 18, 50
Messimo-Reggio, Italy (1908), 53
Tangshan, China (1976), 54
Elastic response spectra, 146
Elastomeric bearings. *See* Bearings, elastomeric
Electricité-de-France sliding system, 55
Energy
hysteretic, 112, 113, 118–119, 142, 149–150
input, 142, 149
Energy dissipation, 62, 111–115
Enhanced stability bearings, 125
EQFAULT computer program, 163
EQSEARCH computer program, 163
ETABS computer program, 218
Europe, experience with base isolation, 20–21

F

Father of Modern Seismology, 2
Faults, 68–69, 156
FCLJC. *See* Foothill Communities Law and Justice Center (FCLJC)
FEMA (Federal Emergency Management Agency), 64, 172, 173
Floating-point operations (FLOPs), 206, 216
Floor accelerations, 2–3
Foothill Communities Law and Justice Center (FCLJC), San Bernardino, California, 5, 6–8, 207
FPS. *See* Friction pendulum system (FPS)
Frequency-domain scaling of time histories, 180–183
Friction. *See* Friction pendulum system (FPS); Resilient-friction base isolation (R-FBI) system
Friction pendulum system (FPS)
bilinear modeling of bearings, 104–107
examples in U.S., 16–17
as isolation system based on sliding, 57–58
mechanical characteristics, 101–104
overview, 16–17
FRISKSP computer program, 163

G

GERB system, 58, 59
GLIS (Gruppo de Lavoro Isolamento Sismico), 20
Ground motions. *See* Earthquake ground motions
Gruppo de Lavoro Isolamento Sismico (GLIS), 20
Gutenberg–Richter model, 160–161

H

Hazard. *See* Seismic hazard evaluation
High-damping rubber bearings
  bilinear modeling of energy dissipation, 111–115
  California building examples, 6–10
  and Caltrans Traffic Management Center, 9
  characteristics, 50–52
  design example, 18, 185–198
  and Foothill Communities Law and Justice Center, San Bernardino, 5, 6–8
  and Los Angeles County Emergency Operations Center, 8–9
  and Los Angeles County Fire Command and Control Facility, 8
  nonlinear dynamic time history analysis, 220–231
  overview, 50
  use in Japan, 18
Horizontal stiffness, 3, 94, 125–126
Hospitals
  California design requirements, 82–83
  M. L. King/C. R. Drew Diagnostics Trauma Center, Willowbrook, California, 9–10, 55
Hyogo-Ken Nanbu (Kobe) earthquake, Japan, 18, 50
Hysteretic energy, 112, 113, 118–119, 142, 149–150

I

IDARC-2D and IDARC-3D computer programs, 220
INADEL computer program, 220
Inelastic response spectra, 148–149
Input energy, 142, 149
Internal lead-plugs, as dampers, 5
International Conference of Building Officials. *See* Uniform Building Code (UBC)
Interstory drift, 2, 3, 77–78
Isolation. *See* Base isolation
Isolation devices. *See also* Bearings, elastomeric
  bilinear modeling of bearings, 104–107
  determining design loads, 203–206
  determining number and size, 203–204
  mechanical characteristics
    elastomeric bearings, 93–100
    friction pendulum system, 101–104
    lead-plug bearings, 100–101
  nonlinear dynamic time history analysis, 220–231
  optimizing distribution using ISOSEL, 206–207
  sample specifications, 234–254
    bearing delivery, storage, and handling, 253–254
    bearing identification, 253
    engineering design calculations, 242–243
    fabrication, 246–247
    list of standards references, 235–237
    manufacturers, 245
    materials tests, 248–250
      elastomeric isolation bearing tests, 250–253
      rubber tests, 248–249
    overview, 233–234
    performance criteria, 237–240
    products, 245–246
    quality control procedure for elastomer compounding, bearing fabrication, and molding, 248
    redesign and retesting, 244
    seismic isolation bearings and mounting materials, 246
    submittals, 243–244
    system description, 237
    technical performance data, 240–242
    testing and inspection, 244–245
  stability under large lateral displacement, 126–133
  UBC design and testing requirements, 81–82
ISOSEL computer program
  application to design of FCLJC, 207–216
  installing, 255
  optimizing isolator distribution, 206–207
  overview, 203
Italy
  examples of base-isolated buildings, 20–21
  experience with base isolation, 20–21
  first consideration of isolation as seismic-resistant design strategy, 53
  Gruppo de Lavoro Isolamento Sismico (GLIS), 20
  Messimo-Reggio earthquake, 53
  National Telephone Company (SIP), Ancona, 20
  retrofitting projects, 20–21

J

Japan
  early earthquake-resistant building designs, 2
  examples of base-isolated buildings, 18, 19
  Kobe earthquake, 18, 50
  TASS system, 56

use of high-damping rubber bearings, 18
use of low-damping rubber bearings, 48, 49

K

King (M.L.)/C. R. Drew Diagnostics Trauma Center, Willowbrook, California, 9–10, 55
Kobe earthquake, 18, 50
Kobe Prefecture, Japan, West Japan Postal Company Center, 18, 19

L

Laminated elastomeric bearings. *See* Bearings, elastomeric
Lead-plug bearings
bilinear modeling, 104–107
California building examples, 11, 13
design example, 198–202
mechanical characteristics, 100–101
overview, 5, 49–50
Least-squares analysis, determining bearing design loads, 204–206
Linear regression, determining bearing design loads, 204–206
Linear theory
extension to building examples, 31–35
seismic isolation, 25–31
Los Angeles City Hall, California, 13–14, 15
Los Angeles County Emergency Operations Center, 8–9
Los Angeles County Fire Command and Control Facility, 8
Low-damping rubber bearings, 3, 5, 48–49
LPM computer program, 115, 220

M

Malaysian Rubber Producers' Research Association, United Kingdom, 50
Maps, seismic zones, 170–172
Masonry buildings, and sliding isolation systems, 53–54
MATLAB computer program, 220
Matsumura-Gumi Technical Research Building, Kobe, Japan, 18, 19
Maximum capable earthquake (MCE), 64, 70, 173
Maximum considered earthquake (MCE), 173
Maximum credible earthquake (MCE), 173
Maximum probable earthquake (MPE), 172
MDOF. *See* Multi-degree-of-freedom (MDOF) systems
Memphis, Tennessee, base isolation project, 10–11
Messimo-Reggio earthquake, Italy, 53
Milne, John, 2
Models
bilinear modeling, 104–119
characteristic earthquake model, 160–161
Gutenberg–Richter model, 160–161
probabilistic seismic hazard evaluation, 159–161
time history analysis using SAP-2000, 222–231
Moment magnitude, 151
Multi-degree-of-freedom (MDOF) systems, 149
Multilayer elastomeric bearings. *See* Bearings, elastomeric

N

NASTRAN computer program, 220
National Telephone Company (SIP), Ancona, Italy, 20
New Zealand
Central Police Station, Wellington, 22, 60
examples of base-isolated buildings, 21–22, 59–60
experience with lead-plug bearings, 49
National Museum of New Zealand, Wellington, 22
printing press building in Petone, 22
South Rangitikei River Bridge, 61–62
Union House, Auckland, 21, 59–60
Northridge earthquake, California, 22, 50, 58
N-PAD computer program, 217
Nuclear power plants, 48–49, 55, 58

O

Oakland City Hall, California, 11–12

P

Peer review, 80
Piles
damped-sway foundation system, 60–61
example of Central Police Station, Wellington, 22, 60
example of Union House, Auckland, New Zealand, 21, 59–60
sleeved-pile isolation system, 58–61
Power plant applications, 125
Predictive relations. *See* Attenuation relations
Probabilistic seismic hazard evaluations, 159–166

Programs. *See* Computer programs
Public housing, 2

R

Resilient-friction base isolation (R-FBI) system, 56–57
Response spectra
  versus design spectra, 146
  earthquake record example, 146, 147
  elastic response, 146
  ground motion parameters, 142
  inelastic, 148–149
  limitations of analysis, 138, 146
  and probabilistic seismic hazard analysis, 166, 170
  SDOF systems, 143–146
  smoothed, 146
  versus time history, 65
Retrofitting buildings
  Italian example, 20–21
  Japan experience, 20
  Los Angeles City Hall, California, 13–14, 15
  New Zealand example, 22
  Oakland City Hall, California, 11–12
  San Francisco City Hall, California, 12–13
Richter law of magnitudes, 160
Rocking base isolation systems, 61–62
Rollout stability, 133–135
Rubber, 2, 3, 50. *See also* Bearings, natural rubber

S

Salt Lake City, Utah, base isolation project, 10, 11
San Andreas Fault, and Foothill Communities Law and Justice Center, San Bernardino, 6–7
Sand, 1
San Francisco City Hall, California, 12–13
SAP-2000 computer program, 218–220, 222, 224–231, 255
Scaling
  in dynamic analysis, 78–80
  frequency-domain time histories, 180–183
  time-domain time histories, 176–180
  time histories, 78, 84–85, 139, 142, 176–183
SDOF. *See* Single-degree-of-freedom (SDOF) systems
SEAONC. *See* Structural Engineers Association of Northern California (SEAONC)
Seismic capacity, defined, 137
Seismic coefficients, 66–67
Seismic demand, defined, 137
Seismic fuzes, 3, 4
Seismic hazard evaluation
  and design code interpretation, 158, 172–173
  deterministic
    examples, 166, 167–168
    limitations of, 166, 169–170
    procedures for, 158–159
  examples, 163–166, 167–168, 169, 170
  limitations of, 166, 169–170
  overview, 139, 158
  probabilistic
    examples, 166, 169, 170
    limitations of, 166, 169–170
    models for, 159–161
    procedures for, 161–163
Seismic isolation. *See also* Base isolation
  code overview, 63–64
  code provisions, 63–92
  extending linear theory model to examples
    analysis of coupled dynamic equations, 36–45
    modal analysis, 33–35
    uncoupled equations of motion, 31–32
  linear theory, 25–31
  theoretical basis, 25–45
  two-mass structural model, 25–31
Seismic response coefficients, 70–71, 72
Seismic sources, 68–69
Seismic zone factors, 66
Seismic zone maps, 170–172
Seismology. *See* Earthquakes; Seismic isolation
Shear strain, 96–97, 98
Shims, 48
Single-degree-of-freedom (SDOF) systems
  response to general excitation, 143
Site soil profiles, UBC static analysis calculations, 68
Skopje, Yugoslavia, 3, 4, 47–48
Sleeved-pile isolation system
  example of Central Police Station, Wellington, New Zealand, 22, 60
  example of Union House, Auckland, New Zealand, 21, 59–60
  overview, 58–59
Sliding isolation systems
  combined with elastomeric bearings, 15, 55–56
  examples in U.S., 14–16
  and friction pendulum system, 16–17
  friction pendulum system (FPS), 57–58
  materials for bearings, 55
  nuclear power plant applications, 55, 58
  overview and background, 52–54
  resilient-friction base isolation (R-FBI) system, 56–57
  restoring force capability, 15–16

talc in, 52
TASS system, 56
theoretical analysis, 54–55
types of systems, 55–58
Software. *See* Computer programs
Soil types, UBC static analysis calculations, 68
Spectra. *See* Design spectra; Response spectra
Springs, in base isolation systems, 58, 59
Static analysis
changes in Uniform Building Code, 65–67
versus dynamic analysis, 65, 67
factors in calculating displacement, 67–78
damping coefficients, 71–73
design forces, 75–76
drift limits, 77–78
effective system vibration periods, 73–74
MCE response coefficient, 70
near-source factors, 68–69, 92
seismic source type, 68
seismic zone factor, 67
site soil profile type, 68
spectral seismic coefficients, 70–71
total design displacements, 74–75
vertical distribution of force, 76–77
and seismic isolation design, 65–78
Stiffness
basic concept, 3
bending, 94, 97–100
bilinear modeling adjustments for high-strain stiffening, 115–116
design example, 186, 188, 189–190
horizontal, 3, 94, 125–126
vertical, 3, 94–97
Structural Engineers Association of California, 172, 173
Structural Engineers Association of Northern California (SEAONC), 64
Swiss Full Base Isolation (FBI-3D), 3
System vibration periods, 73–74

T

Tangshan, China earthquake (1976), 54
TASS system, 56
3-D BASIS computer program, 115, 217–218
Time-domain parameters, 140–142, 176
Time history analysis
frequency-domain scaling, 180–183
modeling using SAP-2000, 222–231
OSHPD-91 provisions, 176
OSHPD-96 provisions, 176
problems of use, 183–184
versus response spectrum analysis, 65
role of earthquake records, 137–138, 174
scaling, 78, 84–85, 139, 142, 174, 176–183
time-domain scaling, 176–180
UBC-94 provisions, 174–175
UBC-97 provisions, 175
when to use, 184

U

UBC. *See* Uniform Building Code (UBC)
Uniform Building Code (UBC)
changes in static analysis formulas, 65–78
code interpretations of design ground motions, 172–173
compliant design example, 89–92
compliant design steps, 85–89
definition of MCE, 173
design method requirements, 65
dynamic analysis requirements, 65, 78–80
as impediment to use of base isolation technology, 6
isolator design and testing requirements, 81–82
minimum displacement requirements, 92
overview, 63, 64
peer review, 80
seismic hazard level criteria, 64
seismic zone map in, 170–172
and time history analysis, 65, 78, 174–175
UBC-97 vs. OSHPD-96, 63
Union House, Auckland, New Zealand, 21, 59–60
United Kingdom, 48–49
United States, base isolation work in, 6–17
United States Geological Survey (USGS), 171
University of Nevada at Reno, Mackay School of Mines building, 15–16, 55

V

Vertical stiffness, 3, 94–97
Vibration isolation, 2

W

West Japan Postal Company Center, 18, 19
World Wide Web, 139–140, 171, 172

Y

Yellow Book, 64, 83
Yugoslavia, first use of rubber base isolation, 3, 4, 47–48

For information about the CD, refer to pages 255–272.

System Requirements

Windows 3.x or Windows 95/NT
4X Speed CD-ROM drive or better
Sound card